

https://dspace.org/

Ferrocene conjugates as potential anticancer agents

Dago N'Da, David

2006-02-10
http://hdl.handle.net/10539/179

Downloaded from a DSpace repository. https://dspace.org/

SYNTHESIS OF METHOTREXATE AND FERROCENE CONJUGATES AS POTENTIAL ANTICANCER AGENTS

David Dago N'Da

A thesis submitted to the faculty of Science, University of the Witwatersrand, in fulfilment of the requirements for the degree of Doctor of Philosophy of Science.

Johannesburg, 2004

Declaration

I declare that this thesis in my own, unaided work. It is being submitted for the degree of Doctor of Philosophy of Science in the University of the Witwatersrand, Johannesburg, South Africa. It has not been submitted before for any degree or examination in any other University.

_____

David Dago N'Da

_____*day of* _____*, 2005*

ABSTRACT

Methotrexate (MTX) is a highly potent drug against leukemia and other neoplasias. The drug is notorious, however, for exerting toxic side effects and inducing drug resistance in the target cells as a result of deficiencies in the active carrier-mediated membrane-crossing mechanism. The bioreversible binding to a water-soluble and biocompatible carrier polymer is an advanced technology designed to circumvent critical pharmacological hurdles the drug must clear for efficacious biological action.

The present project aimed at the anchoring of MTX and other drugs to various primary amine-functionalized polymeric carriers and the evaluation of the cytotoxic performance of the resulting conjugates in cell culture tests.

The polymeric carriers used were polyaspartamides, prepared by an aminolytic ring-opening process of polysuccinimide, and poly(amidoamines), on the other hand, obtained by the copolymerization of methylenebisacrylamide with mono-N-*tert*-butoxycarbonyl-protected primary diamine and bifunctional amines.

The anchoring was achieved through formation of biofissionable amide bonds. The *in vitro* biological evaluation against various human cell lines revealed the polymer-MTX conjugates to be more active than the clinically used parent drug.

In order to demonstrate the multidrug-binding capacity of the polyaspartamide-type carriers, and at the same time ensuring target-specific drug delivery, folic acid, a potential cell entry facilitator, was co-conjugated to selected polymeric conjugates containing MTX or ferrocene.

The *in vitro* inhibition of cell growth by the folate-drug co-conjugates was also evaluated against the same human cell lines.

DEDICATION

I dedicate this thesis to my brothers and sister

ACKNOWLEGMENTS

The author expresses his sincere gratitude to the following people for their contribution in the accomplishment of this thesis.

Prof. E. W. Neuse, my supervisor, for his extreme kindness, helpfulness and tireless guidance.

Prof. Connie Medlen, Department of Pharmacology, University of Pretoria, and her research team members; Neil Margo and Suzaan Visser, for all the cell culture testing experiments.

Prof. Karel Ulbrich, Department of biomedical chemistry, Institute of Macromolecular Chemistry, Czech Republic, for the kind acceptance in his laboratory in the framework of the UNESCO-IUPAC postgraduate polymer course; Dr. Vladimir Súbr, my project supervisor, for the GPC characterization of both the polymers and conjugates; and all the research team members of this laboratory for their help and support during my stay.

Prof. E. Cukrowska, Analytical laboratory, School of Chemistry, for the atomic absorption analysis.

Dr. B. J. Ximba, for the proof reading of this thesis.

Mr. Richard Mampa, for the NMR spectroscopy.

Dr. M. Labrouche and J. M. Dumortier, for their unforgettable support, help and advice.

My friends, E. Ayemon, A. E. Mocket and S. Drissa for their encouragements.

All my laboratory colleagues, especially Dr. Osman for her advice.

Ms. T. Ginka, my UNESCO-IUPAC postgraduate colleague for her help.

CONTENTS

LIST OF FIGURES……..x

LIST OF SCHEMES……..xii

LIST OF TABLES……xiii

LIST OF ABBREVIATIONS……...xvi

CHAPTER 1- INTRODUCTION

1.1 Cancer Problem……1

1.2 Cancer and HIV-AIDS…….2

1.3 Objectives of the Study……3

CHAPTER 2-OVERVIEW OF CANCER TREATMENT MODALITIES

2.1 Surgery

2.1.1 Prophylactic surgery…….6

2.1.2 Diagnostic and staging surgery……6

2.1.3 Curative surgery……...6

2.1.4 Cytoreductive and palliative surgery……...6

2.1.5 Supportive and restorative surgery……...7

2.2 Radiation Therapy……7

2.3 Chemotherapy

2.3.1 Anticancer drugs

2.3.1.1 Alkylating drugs…….11

2.3.1.2 Antibiotics……..12

2.3.1.3 Antimetabolites……...15

2.3.1.8 Other chemotherapeutic drugs……...26

2.3.2 Deficiencies of chemotherapy……30

2.3.3 Combination therapy……..31

2.4 Immunotherapy……..32

2.5 Antiangiogenesis Therapy……..32

2.6 Gene Therapy…….33

2.7 Photodynamic Therapy……..33

CHAPTER 3- POLYMERIC ANTICANCER DRUG CONJUGATES

BACKGROUND AND LITERATURE REVIEW

3.1 Polymers as Drug Carriers

3.1.1 Requirements for polymeric drug carriers

3.1.1.1 Hydrosolubility……...35

3.1.1.2 Biodegradability…….35

3.1.1.3 Biocompatibility…….36

3.1.1.4 Chemical composition……36

3.1.2 Natural polymers as drug carriers……..37

3.1.3 Synthetic polymers as drug carriers.

3.1.3.1 Amino acid polymers and copolymers……...39

3.1.3.2 Poly (amidoamines)……...40

3.1.4 Pharmacokinetic benefits of macromolecular prodrugs……41

3.1.5 Mechanism of cellular uptake of polymeric conjugates……43

3.1.6 Polymer-drug Conjugation

3.1.6.1 Polymer-MTX conjugation…….46

3.1.6.2 Polymer-folic acid anchoring……46

3.1.6.3 Polymer-ferrocene conjugation……47

3.1.7 Anticancer drug co-conjugation……47

CHAPTER 4- RESULTS AND DISCUSSION

4.1 Polymeric Carriers

4.1.1 Introduction……49

4.1.2 Polyaspartamide carriers (PAsA)

4.1.2.1 Synthesis of polysuccinimide (PSI)……....52

4.1.2.2 Preparation of homopoly (α,β-DL-aspartamides)……. ...53

4.1.2.3 Preparation of copolyaspartamides (PAsA)……..54

4.1.3 Poly(amidoamine) carriers (PAA)

4.1.3.1 Preparation of mono-N-Boc-protected primary diamine..70

4.1.3.2 Synthesis of primary amine-functionalized poly(amidoamine) carriers……74

4.2 Polymer Drug Conjugation

4.2.1 Polymer-methotrexate conjugates

4.2.1.1 Preparation of polyaspartamide-MTX conjugates……...84

4.2.1.2 Preparation of poly(amidoamine)-MTX conjugates……96

4.2.1.3 Cell culture testing……104

4.2.2 Preparation of polymer-ferrocene conjugates

4.2.2.1 Polymer-ferrocene conjugation by HBTU-mediated coupling method…….....119

4.2.2.2 Polymer-ferrocene conjugation by active ester coupling method…….....127

4.2.3 Polymer multidrug conjugation

4.2.3.1 Preparation of polyaspartamide-co-drug conjugates…..141

4.2.3.2 Cell culture testing……...149

CHAPTER 5- EXPERIMENTALE SECTION

5.1 General Procedures……..156

5.2 Reagents, Reactants and Solvents……158

5.3 Experimental Procedures

5.3.1 Preparation of polymeric carriers

5.3.1.1 Polyaspartamide (PAsA) carriers……...158

5.3.1.2 Poly(amidoamine) (PAA) carriers……..167

5.3.2 Polymer-MTX conjugates

5.3.2.1 Polyaspartamide-MTX conjugates……...173

5.3.2.2 Poly(amidoamine)-MTX conjugates……183

5.3.3 Polymer-ferrocene conjugates

5.3.3.1 Synthesis of ferrocenylbutanoic acid derivatives…….186

5.3.3.2 Preparation of polymer-ferrocene conjugates…….188

5.3.4 Polyaspartamide conjugates with two drug systems……202

CHAPTER 6-CONCLUSION AND PERSPECTIVE……...209

REFERENCES……..214

APPENDIX: ^{1}H-NMR Spectra……...224

LISTS OF FIGURES

Figure 2.1: Cell cycle phases……..8

Figure 2.2: Structures of two DNA alkylating agents……..12

Figure 2.3: Structure of dactinomycin: antitumor antibiotic……13

Figure 2.4: Structures of anthracycline antibiotics……..14

Figure 2.5: Structure of mitoxantrone……..15

Figure 2.6: Structure of methotrexate……..16

Figure 2.7 (a)**:** Structure of some classical MTX-analogs drugs……...20

Figure 2.7 (b)**:** Structure of some non-classical antitumor antifolate Drugs……..21

Figure 2.8: Structure of folic acid…….21

Figure 2.9: Two-step conversion of folic acid to the active tetrahydrofolate by the enzyme folate reductase and its inhibition by methotrexate…22

Figure 2.10: Structures of purine analogs antimetabolites…….24

Figure 2.11: Structures of pyrimidine antimetabolites……...26

Figure 2.12: Proposed mechanism of ferrocene activity……30

Figure 3.1: General model of macromolecule-drug conjugates……...42

Figure 3.2: Schematic representation of endocytotic pathways and intracellular fate of polymer-drug conjugates……45

Figure 4.1: Structure of polyamide-type carrier……...49

Figure 4.2: Inherent viscosity (η_{inh}) versus M_w of PAsA…….69

Figure 4.3: Antiproliferative activity of PAsA-MTX and free MTX against HeLa…….111

Figure 4.4: Antiproliferative activity of PAsA-MTX and free MTX against Colo Cells……112

Figure 4.5: Antiproliferative activity of PAA-MTX conjugates and free MTX against HeLa cells……116

Figure 4.6: Antiproliferative activity of PAA-MTX conjugates and free MTX against Colo cells……117

Figure 4.7: Antiproliferative activity of PAsA co-conjugates, free MTX and free cisplatin against HeLa cells……..154

Figure 4.8: Antiproliferative activity of PAsA co-conjugates, free MTX and free cisplatin against Colo cells……155

LISTS OF SCHEMES

Scheme 2.1: Reactions of ferrocene complex in biological environment……..29

Scheme 4.1: Synthesis of polysuccinimide (PSI)……...53

Scheme 4.2: Preparation of homopoly (α, β-DL-aspartamides)…….54

Scheme 4.3: Preparation of copolyaspartamides (PAsA)……...55

Scheme 4.4: Synthesis of mono-N-Boc-protected primary diamines….....71

Scheme 4.5: Synthesis of poly(amidoamines) bearing extrachain hydrosolubilizing groups……75

Scheme 4.6: Synthesis of poly(amidoamines) bearing intrachain hydrosolubilizing groups……76

Scheme 4.7: Preparation of polyaspartamide-MTX conjugates……..85

Scheme 4.8: Preparation of poly(amidoamine)-MTX conjugates.....97

Scheme 4.9: Synthesis of *para*-nitrophenyl 4-ferrocenylbutanoate…….119

Scheme 4.10: Preparation of ferrocene conjugates by HBTU-mediated coupling method……..120

Scheme 4.11: Preparation of ferrocene conjugates by ONp active ester coupling method……..128

Scheme 4.12: Preparation of poly(amidoamine)-ferrocene conjugate in methanol……...130

Scheme 4.13: Preparation of polyaspartamide-FA/MTX co-conjugates……143

LISTS OF TABLES

Table 4.1: Composition of PAsA containing tertiary amine-terminated side chain……...56

Table 4.2: Summary of preparative data for PAsA containing tertiary amine-terminated side chain…..……59

Table 4.3: ^{1}H NMR and viscometric results for PAsA containing tertiary amine-terminated side chain…..……....60

Table 4.4: Composition of PAsA containing hydroxyl- or methoxy-terminated side chain…….…….....61

Table 4.5: Summary of preparative data for PAsA containing hydroxyl- or methoxy-terminated side chain…….…….....64

Table 4.6: ^{1}H NMR and viscometric results for PAsA containing hydroxyl- or methoxy-terminated side chain…….…….....66

Table 4.7: GPC characterizatics of PAsA……...68

Table 4.8: Summary of preparative data for H_2N-R´-NH-Boc compounds…72

Table 4.9: ^{1}H NMR data for H_2N-R´-NH-Boc compounds……73

Table 4.10: Composition of primary amine-functionalized PAAs……77

Table 4.11: Summary of preparative data for PAA carriers……..79

Table 4.12: ^{1}H NMR and viscometric data for PAA drug carriers……..…….80

Table 4.13: GPC characteristics of poly(amidoamine) carriers…….82

Table 4.14: Composition of PAsA-MTX conjugates……86

Table 4.15: Reaction variables for PAsA-MTX conjugates……..88

Table 4.16: ^{1}H NMR and viscometric results for the PAsA-MTX conjugates……...90

Table 4.17: Summary of analytical results for all PAsA-MTX conjugates…..92

Table 4.18: Composition of PAA-MTX conjugates……....98

Table 4.19: Experimental variables for all PAA-MTX conjugates…….100

Table 4.20: ^{1}H NMR and viscometric results for the PAA- MTX conjugates……101

Table 4.21: Analytical results of PAA-MTX conjugates……102

Table 4.22: Antiproliferative activity of PAsA-MTX conjugates against CEM/E and CEM/S cell lines …….106

Table 4.23: Antiproliferative activity of PAsA-MTX conjugates against HeLa and CoLo cell lines……..110

Table 4.24: Antiproliferative activity of PAA-MTX conjugates……115

Table 4.25: Composition of polymer-ferrocene conjugates prepared by HBTU coupling method……..122

Table 4.26: Reaction conditions for ferrocene conjugates prepared by HBTU mediated coupling method……...123

Table 4.27: ^{1}H NMR and viscometric results for Fc (HBTU) conjugates …..124

Table 4.28: Summary of analytical data for all Fc (HBTU) conjugates……..125

Table 4.29: Composition of ferrocene conjugates prepared by the ONp active ester method…….131

Table 4.30: Reaction conditions for ferrocene conjugates prepared by active ester coupling method……..133

Table 4.31: ^{1}H NMR and viscometric results for all Fc (ONp) conjugates…135

Table 4.32: Summary of analytical results for all Fc (ONp) conjugates…….137

Table 4.33: Composition of PAsA co-drug conjugates……...144

Table 4.34: Reaction conditions for all PAsA co-conjugates…….145

Table 4.35: ^{1}H NMR and viscometric results for PAsA co-conjugates……..146

Table 4.36: Summary of analytical data for all PAsA co-conjugates…….147

Table 4.37: Antiproliferative activity of polyaspartamide-co-drug conjugates…….153

LISTS OF ABBREVIATIONS

AEE: Aminoethoxyethanol

Boc: *tert*-butoxycarbonyl

Calcd: Calculated

DAP: 1, 3-Diamino-2-propanol

DCC: Dicyclohexylcarbodiimide

DCM: Dichloromethane

DET: Diethylenetriamine

DHFR: Dihydrofolate reductase

DMF: N,N-Dimethylformamide

DMP: 3-(N,N-Dimethylamino)propylamine

DMSO: Dimethyl sulfoxide

DNA: Deoxyribonucleic acid

EA: Ethanolamine

EDA: Ethylenediamine

EDDA: 2, 2 ′-(ethylenedioxy) diethylamine

EPR: Enhanced permeability and retention

EtAc: Ethyl acetate

FA: Folic acid

FAO: Food and agriculture organization

FR: Folate receptor

GPC: Gel permeation chromatography

HBTU: 2-(1H-benzotriazol-1-yl)-1,1,3,3-tetramethyluronium hexafluorophosphate

Hex: Hexane

HMP: Hexamethylphosporamide

HONp: *para*-nitrophenol

HSU: N-hydroxysuccinimide

ICP-OES: Inductively coupled plasma-optical emission spectroscopy

Inh: Inherent

IR: Infrared

LTR: Long term repeat

MBA: Methylenebisacrylamide

MDR: Multi-drug resistance

MEA: Methoxyethylamine

MTX: Methotrexate

NMP: N-Methylpyrrolidone

NMR: Nuclear magnetic resonance

PAA: Poly(amidoamine)

PAsA: polyasapartamide

PDA: 1,3-propylenediamine

PDT: Photodynamic therapy

PEO: Poly (ethylene oxide)

PSI: polysuccinimide

RFC: Reduced folate carrier

RNA: Ribonucleic acid

RT: Room temperature

TEA: Triethylamine

TFA: Trifluoroacetic acid

TRIA: 4,7,10-trioxa-1,13-tridecanediamine

UV-Vis: Ultraviolet-visible

WHO: World health organization

C H A P T E R 1

INTRODUCTION

1.1 Cancer Problem

Cancer presents one of the most formidable health problems worldwide. More than 10 million people are diagnosed with cancer every year. The world health organization (WHO) estimated that there will be 15 million new cases every year by 2020. Cancerous diseases cause 6 million deaths every year, almost 12% of worldwide mortality. Lung, colorectal and stomach cancer are among the five most common cancers in the world for both men and women. Lung and stomach cancers are most common among men worldwide, while for women, the most common forms are breast and cervical cancer. The incidence and mortality rates of certain types of cancer have wide geographical differences, which are attributed to racial, cultural, and especially environmental influences.

In South Africa, cancer poses a lifetime risk to one in four South African men and one in five women, and strikes population groups differently. The age, race, gender and socio-economic status also play an important part in determining the prevalence of particular cancers.

The cancers affecting South African women, in order of prevalence, are: cervical, breast, colorectal, lung, and oesophageal cancer. The risk of cervical cancer is one in 29, while that of breast cancer is one in 31. The significant trend is that cervical cancer has overtaken breast cancer. Cervical cancer comprises 13.4% of all cancers among women from 15 to 29 years old, with young black women being particularly vulnerable.

Prostate, lung, oesophageal, bladder and colorectal cancer rate among the top five cancers affecting all South African men. The leader, prostate cancer, has risen from a risk of one in 31 to one in 24. Statistics for lung cancer and oesophageal

cancer, both fuelled by smoking, show a slight increase, with the incidence of lung cancer much higher among men than women, and among white and coloured men than black men.

1.2 Cancer and HIV-AIDS

The immunodeficiency state in HIV infection predisposes one to the development of both opportunistic infections and neoplasms. In the latter case, lymphoma is usually a late manifestation. The incidence of different types of lymphoma (Hodgkin's disease, non-Hodgkins lymphoma (NHL) and T-cell lymphoma) is increased in HIV-infected individuals, though only immunoblastic and primary central nervous system lymphoma are increased significantly. Three kinds of HIV-associated lymphoma (Burkitt's, immunoblastic and primary central nervous system lymphoma) are classified as AIDS-related illnesses.

In its latest report, the National Cancer Registry (NCR) of South Africa emphasized the increasing rate of cancers associated with HIV nationwide, *e.g.*, soft tissue cancer (Kaposi's sarcoma) which is a threat to the youth. Kaposi's sarcoma which mostly affects the skin, is now the third and fourth most common cancer in men and women aged 15 to 29 years, respectively. More scaring is the rapid risk of expansion. Kaposi's sarcoma, which is classified as an "Aids-defining" disease, almost doubled within five years (1993-1997) [1]. Given the alarming rate of HIV-AIDS in the South-African youth, the report appears as a warning. Indeed, at the end of 1999 there were an estimated 4.2 million adults and children in South Africa living with HIV and AIDS. The adult rate of infection was 19.94%, meaning nearly one in five South Africans was living with HIV and AIDS. Of these, 2.3 million were women, and 95 000 children.

In light of these statistics, it stands to reason that the burden imposed on the National Health Services in controlling neoplasias or, at least, alleviating their impact on human suffering, is staggering.

1.3 Objectives of the Study

The worldwide incidence of neoplasias, in conjunction with the increasing prevalence at the national level in each country, renders the cancer control a public health and economic issue. It should, therefore, be regarded as a high priority. The fight against cancer has always been a priority for the scientific community involved in medical research since the first cancer case was discovered two centuries ago.

Chemotherapy constitutes one of the modalities of cancer treatment, either *per se* or in conjunction with other treatment regimens. However, despite much progress in the chemotherapy of cancerous diseases, antitumor drugs in current clinical use generally suffer from a series of deficiencies, including excessive organ toxicity, lack of cell specificity, short circulation half lives, and a pronounced tendency to induce resistance in the target cells. As a consequence, complete cures by chemotherapy are still rare indeed.

The primary objective of the research project was to address the problem of the lacking drug efficaciousness by providing a vehicle for improved pharmacokinetic utilization of anticancer agents. The bioreversible conjugation of selected anticancer drug models with water-soluble macromolecular carriers designed in accordance with specific biomedical requirements was the route of accomplishment of this objective. The conjugates were to be constructed so as to act as prodrugs delivering the monomeric bioactive agent at the site of action in intracellular space for interaction with nuclear DNA or proteinaceous constituents.

The second objective was the biological activity evaluation of the synthesized polymer-drug conjugates against various human cancer cell lines. These included the human adenocarcinoma of the cervix (HeLa), the colorectal adenocarcinoma, (Colo 320 DM), the human leukemic lymphoblast (CEM/S) and its resistant sub-line (CEM/E). The motivation was to compare the potency of these conjugates with the parent drugs presently in clinical use.

The principal drug system chosen was based on the antifolate agent, methotrexate (MTX). Other drug systems, including ferrocene compounds, and the vitamin B, folic acid (FA), were identified for co-conjugation with MTX in an effort to provide macromolecular drugs for combination therapy.

After an overview of the modalities for cancer treatment in Chapter 2, the background of the polymeric anticancer drug conjugates will be reviewed in Chapter 3, followed by Chapter 4, where the results leading to the achievement of the objectives of this project will be discussed. The conclusion and future prospects will be stressed in Chapter 5 while Chapter 6 will cover the experimental efforts of this study.

C H A P T E R 2

OVERVIEW OF CANCER TREATMENT MODALITIES

There are many modalities for cancer treatment. They are highly variable and dependent on a number of factors such as the type, location and amount of disease and the health status of the patient. The treatments are designed to directly kill or remove the cancer cells or to lead to their eventual death by depriving them of signals needed for cell division or to stimulate the host immune system after kill or removal of theses cells. However, some are effectively utilized whereas others are still in their infancy. The four principal modalities utilized are surgery, radiation, chemotherapy, and immunotherapy. They will be reviewed in this chapter with more emphasis on chemotherapy as it is the impetus of this study, and so will be some new therapies which are still in their infancy.

The cancers treatments may be divided into different categories based on their goal, mode of action, and are often used in combination, either simultaneously or sequentially.

2.1 Surgery

Surgery, the oldest modality, consisting of removing the primary tumor, is by far the most effective treatment of cancer. It also has an important role in diagnosing and staging of cancer.

Although offering the greatest chance to cure many types of cancer by removing the primary tumors, surgery is ineffective for metastasized or disseminated tumors. There are many types of surgery, and they are highly goal-oriented.

2.1.1 Prophylactic surgery

Prophylactic surgery, also called preventive surgery, aims at removing a body tissue likely to become malignant. Sometimes it is used to remove an entire organ when an individual has an inherited condition that makes development of cancer likely. A typical case is when a human female with a very strong family history of breast cancer is found to have a mutation in her DNA in a breast cancer gene (*BRCA1* or *BRCA2*). These genes, accounting for approximately 5-10% of all breast cancer cases [2] and 80% of familial breast cancer cases [3, 4], make her a candidate for prophylactic mastectomy (breast removal).

2.1.2 Diagnostic and staging surgery

Diagnostic surgery is used to get a tissue sample to identify a specific cancer and make a diagnosis, which is often confirmed only by cellular microscopy, and staging surgery [5], a tool to determine the extent and the amount of disease.

2.1.3 Curative surgery

Curative surgery is the mostly known. Thought as primary treatment of cancer, it involves the removal of a tumor when it appears to be confined to one area. Curative surgery is performed when the hope of taking out all of the cancerous tissue still exists. It may be used along with chemotherapy or radiation therapy, which can be given before or after the operation. In some cases, radiation therapy is used during an operation, and is therefore termed intraoperative radiation therapy.

2.1.4 Cytoreductive and palliative surgery

Cytoreductive surgery, also known as debulking surgery, is performed in some cases when removing a tumor entirely would cause too much damage to an organ or surrounding areas. In these cases, the surgeon may remove as much of the tumor as possible and then try to treat the remaining portion with radiation

therapy or chemotherapy. Debulking surgery is commonly used for advanced cancer of the ovary.

Palliative surgery refers to the treatment of complications of advanced disease. It is not intended to cure the cancer. It can also be used to correct a problem that is causing discomfort or disability. For example, some cancers in the abdomen may grow large enough to obstruct (block off) the intestine. This may require surgery for effective relief. Palliative surgery may also be used to treat pain when it is hard to control by other means.

2.1.5 Supportive and restorative surgery

Supportive surgery is used in combination with other modalities. Typically, a vascular access device such as a catheter port can be placed into a vein to help deliver chemotherapy treatments, thus reducing the number of needle sticks needed.

Restorative reconstructive surgery [6, 7] is used to restore a person's appearance or the function of an organ or body part after primary surgery. Typical examples are breast reconstruction after mastectomy or the use of tissue flaps, bone grafts, or prosthetic (metal or plastic) materials after surgery for oral cavity cancers.

2.2 Radiation Therapy

Radiation, which constitutes the second modality in cancer treatment, is often administered in attempts to eliminate and halt the development of secondary tumors resulting from residual and undetectable cancer cells that frequently remain in the body after surgery. It may also be used in early stages to cure or control the disease, or to shrink the tumor before surgery. Radiation alters the genetic code which controls the cell growth and division. Thus, radiation functions as a treatment by interference with the normal life cycle of a cell in the body, exclusively in the mitotic phase, M.

Ionizing radiation is the common radiation used in cancer treatment. In principle, the radiation forms ions on passing through tissues and dislodges electrons from

atoms. These species, in turn, cause cell death or a genetic change by interfering with the cell M phase. The efficacy of the therapy is radiation energy-dependent, and the higher the energy the more deeply the radiation can penetrate into the tissues. Thus, ionizing radiation can be divided into two major types, *viz*, photons (x- and γ-rays) and particulate radiations (electrons, protons, neutrons, α, and β particles). Of these, neutron radiation is used for some cancer of the head, neck, and prostate. Figure 2.1, below, depicts the cell cycle phases.

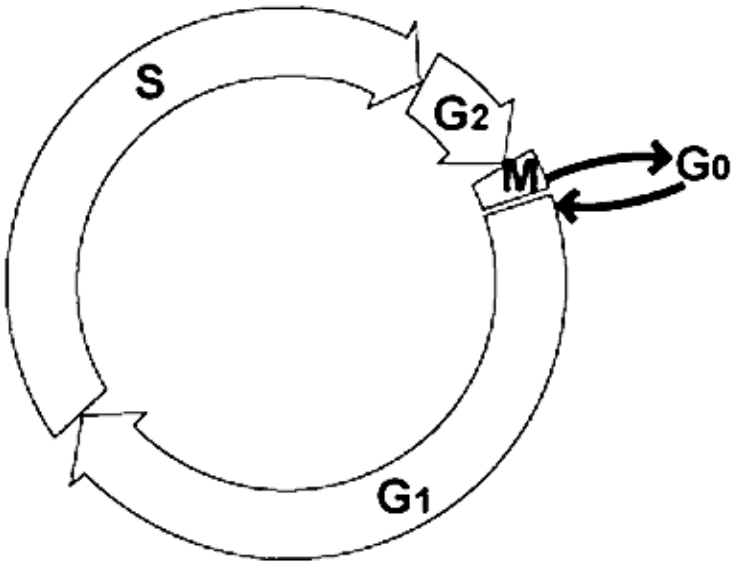


Figure 2.1: Cell cycle phases

G_0: Cell resting phase.

G_1: RNA and protein synthesis phase.

S: DNA replicating phase.

G_2: Cell pre-splitting phase.

M or mitosis phase: The cell has actually split into two new cells.

Other forms of radiation include stereotactic radiation (or therapy), which delivers a large precise radiation dose to a small tumor area. It is mostly used for brain cancer therapy. Iintraoperative radiation therapy (IORT), more often employed in

abdominal or pelvic cancers, delivers radiation at the time of surgery directly to the area of cancer, thus reducing the amount of tissue exposed to radiation as normal tissues can be moved out of the way during surgery and protected, allowing a higher dose of radiation to the cancer.

2.3 Chemotherapy

Like radiation therapy, chemotherapy is administered in attempts to eliminate and halt the development of secondary tumors resulting from residual and undetectable cancer cells that frequently remain in the body after surgery.

Many anticancer agents and other chemical entities exert immune-stimulating effects on the cancer patient's immune system during chemotherapy.
The toxic effects of chemical agents on the cancerous cell for the most part involve interference with the cell's replicative mechanism and, thus, with intracellular nucleic acid synthesis and the ultimate role played by the nuclear DNA in mitosis. The effectiveness of the anticancer drugs is generally, although not exclusively, at an optimal level whenever the target tissue consists of rapidly dividing cells, as is generally the case in a malignant system. However, the human body contains a number of compartments in which normal, *i.e*., healthy cells are required to replicate at a high rate in order to fulfil their physiological role, *e.g*., the bone marrow, the linings of the gut and the urinary tract. It is, indeed, in these compartments where most of the systemically acting anticancer drugs exert their most undesirable toxic side effects, as the rapidly proliferating cells do not provide sufficiently long time intervals during which normal DNA repair mechanisms, mediated by selective repair enzymes, can remain operative [8-10].

2.3.1 Anticancer drugs

Anticancer drugs are divided into several categories based on the mechanism of cytotoxic activity and the cell cycle phase interference. Although on occasional instances, the mechanisms of cytotoxic activity associated with particular classes may loosely coincide, in general, the members within a given class function by a mechanism particular to that class. The anticancer activity is dependent on growth

fraction (fraction of cells actively dividing with respect to the entire population of viable cells), and mass doubling time (the time taken by a tumor to double in size). Tumors with a high growth fraction are more susceptible to the cytotoxic effects of anticancer drugs than those with a high percentage of dormant cells. Dividing-cells are drug sensitive. Thus, tumors with shorter mass doubling times are more amenable to treatment with drugs. As tumors get larger, the mass doubling time increases and the growth fraction decreases. Unfortunately, normal tissues with high growth fractions (bone marrow, oral and intestinal mucosa, hair follicles) are also damaged by anticancer drugs, and treatment with many of these drugs may produce bone marrow depression, gastrointestinal tract ulceration, and alopecia [11]. Tumor size is another limiting factor to successful chemotherapy in malignant disease. Drugs may not be able to penetrate into a solid tumor in amounts sufficient to kill the cells. Also, most cells in a bulky tumor may be in a nonproliferative stage at the time of treatment and thus survive to re-establish the tumor mass. Thus, the longer a tumor has been present the greater is the likelihood that it has already metastasized. Therefore, for any tumor therapy to be completely effective the most invasive metastatic cells must be killed. Moreover, the response to certain cell phase-specific drugs depends on the percent of cells in a sensitive phase during the time of exposure to pharmacologically effective concentrations of drug. In general, for cycle phase-specific agents such exposure should be for at least two cell cycle times. Cells in the G_0 phase are, for the most part, refractory to chemotherapy. These cells may re-enter the cell cycle and result in disease recurrence. Most anticancer drugs are effective against cells in one particular phase of the cycle and have their greatest activity during S phase when cells are undergoing DNA synthesis.

Drug resistance is one of the most important problems encountered with cancer chemotherapy, and several different biochemical mechanisms by which tumor cells develop resistance to anticancer drugs have been identified. These include:

(a) Decreased intracellular drug levels resulting from increased drug efflux [12] or decreased inward transport. Anthracyclines, dactinomycin, vinca alkaloids,

and epidopodophyllotoxins are among the drugs becoming ineffective by this mechanism.

(b) Increased drug inactivation. Included in this group are the alkylating agents, antimetabolites and bleomycin.

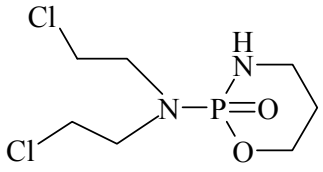
(c) Decreased conversion of drug to an active form. This mechanism is mostly common among the antimetabolites (5-FU, 6-MP, etc.) which must first be converted into nucleotide before therapeutic activity can be observed.

(d) Altered amount of target enzyme or receptor (gene amplification).

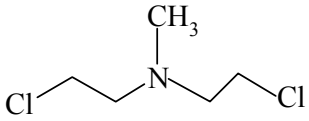
2.3.1.1 Alkylating drugs

These drugs are active against chronic leukemias, non-Hodgkin's lymphoma, Hodgkin's disease, multiple myeloma, and certain cancers of the lung, breast, and ovary. Cyclophosphamide and mechlorethamine (nitrogen mustard) are two representatives of this class. They are covalent DNA-binding drugs, and act by forming strong electrophiles through the formation of carbenium ion intermediates. This results in the formation of covalent linkages by alkylation of various nucleophilic moieties. The chemotherapeutic and cytotoxic effects are directly related to the alkylation of DNA, mainly through the N-7 atom of guanine, although other moieties are also alkylated. The formation of one covalent bond with nucleophiles can result in mutagenesis or teratogenesis, but the formation of two of these bonds through crosslinking can produce cytotoxicity. Bifunctional alkylating agents can undergo a second cyclization of the second side chain and form a covalent bond with another nucleophilic group. The second group can be N-7 of another guanine or some other nucleophilic moiety. These bifunctional alkylating agents such as nitrogen mustard react with another nucleophilic moiety resulting in the crosslinking of two nucleic acid chains or the linking of a nucleic acid to a protein. This type of alteration causes a major disruption in nucleic acid function. Cytotoxicity of bifunctional alkylators correlates very closely with interstrand crosslinkage of DNA. Some of the cellular responses produced include cell-cycle blocking, DNA repair and apoptosis. The nucleophilic groups of proteins, RNA and many other molecules are potential targets of the alkylating agents.

The alkylating agents are generally considered to be cell-cycle phase non-specific and are known to be mostly cytotoxic to rapidly proliferating cells. DNA alkylation occurs anytime in the cell cycle, but the biological consequences are more severe during the replicating S phase. The biochemical mechanisms identified as a cause of resistance to these drugs include decreased cellular uptake of the drug, increased production of nucleophiles such as glutathione and increased repair of DNA. Of these, increased inactivation and decreased uptake of drug are of clinical importance. Figure 2.2 below depicts the structures of two alkylating agents.



Cyclophosphamide



Nitrogen mustard: **Mechloroethamine**

Figure 2.2: Structures of two DNA alkylating agents

2.3.1.2 Antibiotics

The antibiotic-type drugs have evolved from natural sources, but as they are presented in small quantities in biological material, worldwide efforts have focused on the development and synthesis of analogs and relatives possessing structural entities, such as planar fused-ring systems. These analogs are capable of intercalating between nuclear bases in the DNA double helix or otherwise interfering with protein synthesis, replication or transcription. Although, all of them are noncovalent DNA-binding drugs, they differ slightly in their mechanism of action.

Antitumor antibiotics: These drugs are noncovalent DNA-binding agents. They interact with DNA in a variety of different ways including intercalation, DNA

strand breakage and inhibition of the enzyme topoisomerase II. Although isolated from natural sources and antibiotics, they lack the specificity of the antimicrobial antibiotics, and therefore produce significant toxicity.

Dactinomycin, a representative of this class, is the only antitumor antibiotic in clinical use. It functions as a drug by intercalation between guanine-cytosine base pairs in the DNA helix, inhibiting RNA and DNA polymerase. This results in the cytotoxic effect, and ultimately apoptosis, and this cytotoxicity is cell cycle phase non-specific, although more acute in the G_1 phase. Dactinomycin is used to treat Wilm's tumor, choriocarcinoma, and soft tissue sarcomas. Resistance to this anticancer agent is mediated by the expression of P-glycoprotein causing increased efflux of the drug. The major side effect from dactinomycin use is immunosuppression due to bone marrow suppression. Nausea, vomiting, and diarrhoea are other side effects related to the use of this drug. Dactinomycin is one of several drugs considered part of the multidrug resistant (MDR) complex. Figure 2.3 shows its structure.

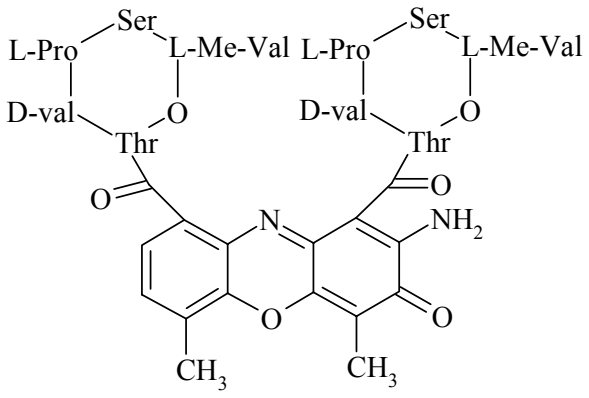
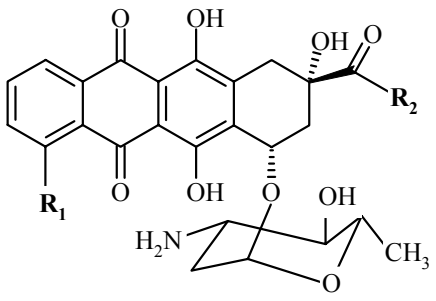


Figure 2.3: Structure of dactinomycin

Anthracycline antibiotics: The anthracyclines are among the most important antitumor drugs clinically available. Doxorubicin [13, 14], daunorubicin [14], and idarubicin are the mostly known of this class of anticancer agents. Anthracycline antibiotics (doxorubicin and daunorubicin) intercalate into DNA and inhibit DNA

and RNA synthesis, alter membrane signal transduction (phosphatidyl inositol pathway), and generate oxygen radicals. These oxygen radicals are produced by the cytochrome p450 system in the liver and are potent denaturing agents. Anthracycine antibiotics are a broad spectrum of anticancer agents that are used to treat many carcinomas, sarcomas, and leukemias. While Doxorubicin [15] is widely used for the treatment of several solid tumors (carcinomas and sarcomas), daunorubicin and idarubicin are used exclusively for the treatment of leukaemia. Resistance to anthracycine antibiotics is mediated by the expression of P-glycoprotein, which causes increased efflux of these anticancer drugs. Side effects include cardiotoxicity, myelosuppression, rash, nausea, vomiting, alopecia, and diarrhoea. The structures of these antibiotics are shown below.



	R_1	R_2
Idarubicin	-H	$-CH_3$
Daunorubicin	$-OCH_3$	$-CH_3$
Doxorubicin	$-OCH_3$	$-CH_2OH$

Figure 2.4: Structures of anthracycline antibiotics

Anthracenediones: These drugs are analogs of the anthracyclines. They lack the sugar moiety of the anthracyclines, but retain the planar polycyclic aromatic ring structure that permits intercalation into DNA. They have shown impressive clinical activity, including less cardiac toxicity, which results mostly in nonproduction of quinone-type free radicals. Mitoxantrone, a representative of this class, is an intercalating agent that is effective in treating various tumors [14]. Mitoxantrone interacts with DNA by a high-affinity intercalation. The diaminoalkyl groups present in the side chains of the antitumor drug are responsible for its ability to induce, after metabolic activation, interstrand covalent cross-links in DNA of tumor cells [16]. As for the anthracyclines, intercalation of

mitoxantrone into DNA interferes with the strand-reunion reaction of topoisomerase II, resulting in production of protein-linked double-strand DNA breaks.

Although mitoxantrone is cytotoxic to cells throughout the cell cycle, cells in late S phase are more sensitive. The structure of this drug is depicted below.

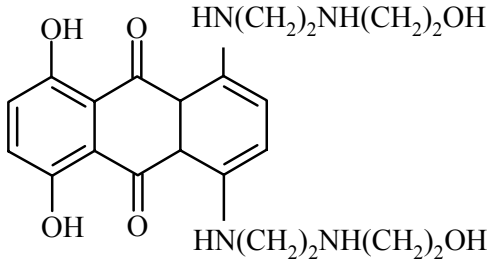


Figure 2.5: Structure of mitoxantrone

Bleomycins: The bleomycins are a group of antitumor agents isolated from Streptomyces vericillus. Clinical bleomycin is a metal-chelating water-soluble glycopeptide that interacts with DNA in the early G_2 phase of the cell cycle to cause strand breakage after oxidation from bleomycin-DNA-Fe (II) to bleomycin-Fe (III). This strand breakage induces chromosomal abnormalities and cell death. Bleomycin is highly active against squamous cell tumors of the head, neck and lungs, effective against germ cell tumors of the testis and ovary, and is also used to treat testicular carcinomas along with cisplatin and vinblastine. One of the most common resistance mechanisms is an increased degradation of drug by certain amidase enzymes. Side effects include pulmonary toxicity, alopecia, and hyperpigmentation of the hands. In contrast to many other anticancer drugs, bleomycin rarely causes myelosuppression.

2.3.1.3 Antimetabolites

Antimetabolites are structural analogs of naturally occurring compounds. They interfere with the production of nucleic acids and work through a variety of

mechanisms including competition for binding sites on enzymes and incorporation into nucleic acids. Antimetabolites inhibit the growth of the most rapidly proliferating cells in the body (*e.g.*, bone marrow, gastrointestinal tract, etc.), and are divided into three categories: antifolates, purine analogs and pyrimidine antimetabolites.

Antifolate antimetabolites: They produced both the first striking remissions in leukaemia [17] and the first cure of a solid tumor, choriocarcinoma.

(a) *Methotrexate*

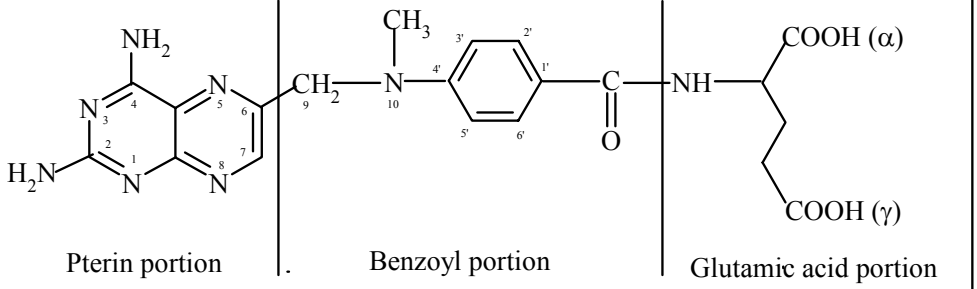


Figure 2.6: Structure of methotrexate

History of clinical use: Methotrexate (Figure 2.6), a folate antimetabolite synthesized five decades ago, has been in clinical use for more than 35 years. It has a long history of use in the treatment of various immunologic diseases. MTX began as a drug for cancer treatment, particularly childhood leukaemia, in the early 1940s [18]. In the 1960s it was used for the treatment of rheumatoid arthritis and psoriasis. In the mid-1980s [19] many rheumatologists reported their experiences with MTX use in studies of rheumatoid arthritis. Guidelines for MTX use were then developed to address dosing, liver biopsy and monitoring strategies, which were aimed at reducing the incidence of adverse affects [20]. Currently, methotrexate is indicated for the treatment of acute lymphocytic leukemia (ALL), as well as for rheumatoid arthritis and psoriasis. The drug has also been found efficacious in the treatment of other diseases, including asthma, systemic lupus erythematosus, Crohn's disease, myositis, vasculitis and ectopic pregnancy [21-23].

MTX is also used for its steroid-sparing properties in asthmatic patients and others who may have side effects related to corticosteroid use [24]. The literature reports MTX as a key component in the treatment of HIV-related lymphomas and other germ cell neoplasias [25, 26], as well as of the late MTX-induced expression of HIV-LTR (long terminal repeat), MTX being a chemotherapeutic agent that is not directly DNA damaging [27].

However, clinical MTX effectiveness is often hampered by the development of acquired resistance. In particular, in human and murine tumors an impaired cellular uptake of the drug occurs as a consequence of a defective active carrier system (reduced folate carrier (RFC)), which regulates the cell entrance of folate analogs. Several biochemical mechanisms of resistance have been demonstrated. Of these, the major ones are decreased drug uptake, amplification of the dihydrofolate reductase gene and thus an increase in the target enzyme, gene mutations, and decreased ability to form methotrexate polyglutamate inside cells [28-30].

Mode of action: The passive diffusion of MTX through cell membrane is limited, due to its hydrophilic nature. Indeed, MTX is highly polar; and owing to this polarity, at the nearly neutral pH of biological fluids, it is present mainly in the doubly anionic species form. This leads to inhibition of cell penetration. As a consequence, only a small portion of MTX successfully enters the intracellular space by passive diffusion while the major portion enters by carrier-mediated mechanism. The main pharmacological target of action of MTX is the competitive inhibition of dihydrofolate-reductase (DHFR), an intracellular enzyme which reduces folic acid to tetrahydrofolate cofactors, which are in turn key intermediates in several important biochemical pathways, among which are the *de novo* biosynthesis of purines and of thymidylate. Mathews and *al*. [31], using Raman spectra of the MTX-DHFR complex, showed that the inhibition occurs as result of ionic binding between the N-1 of the pterin portion and the enzyme. Lack of reduced folates, purines and thymine in actively proliferating cells, such as those of the tumors, leads to a blockage of DNA and RNA synthesis, and eventually to cell death.

The affinity of MTX to some folate-requiring enzymes in the biosynthetic pathways towards purines and thymidylate has been found to increase as the number of γ-glutamyl residues increases. Moreover, the increased polarity of the polyglutamylated species of MTX hampers their efflux from cells.

Medical limitations: MTX exerts its primary toxic effects against the rapidly replicating cells of the bone marrow and gastrointestinal epithelium. The severity of the clinical effects depends largely on the duration of exposure to inhibitory levels of the drug. All of the stem-cell types of the marrow can be affected to produce leucopoenia, thrombocytopenia and, with long-term administration, anaemia. Mucositis is one of the earliest signs of toxicity, and its appearance is an indication of the need for the administered dose to be reduced. Methotrexate also causes kidney damage, which is a frequent complication of high-dose therapy. It is manifested by elevated serum creatinine and decreased creatinine clearance. Crystalline deposits of methotrexate and methotrexate-derived material have been found in the renal tubule, which seems to account for most of the nephrotoxicity. Alkalinizing the urine to increase the solubility and ensuring good urine flow minimizes most of the nephrotoxicity due to high-dose methotrexate. Both low- and high-dose therapy can cause hepatotoxicity. High-dose therapy results in elevated liver enzymes and low dose therapy produces a different type of hepatotoxicity which includes cirrhosis. Methotrexate can also cause a reversible pulmonary syndrome, which has been observed primarily in children undergoing maintenance therapy. Intrathecal and high-dose administration is accompanied by several types of neurotoxicity. These range from acute manifestations to long-term delayed toxicity in the form of encephalopathy. Nausea and anorexia frequently occur as acute side effects of methotrexate therapy [32]. To overcome the dose-limiting toxicity of MTX, and to allow the use of protocols with very high doses of MTX for the treatment of resistant cell lines or to achieve cytotoxic drug concentrations across the blood-brain barrier, in clinical use, a strategy named “folinic acid rescue therapy” has been devised [33]. Although the biochemical mechanism is still debated, intravenous administration of leucovorin (a racemic mixture of isomers of folinic acid) at a scheduled time after the infusion of high-

dose MTX therapy was found to be beneficial to healthy cells, and protects them from the cytotoxic action of MTX. In a moderate-dose therapy, MTX is administered in combination with other chemotherapeutic agents for the maintenance of remissions [34].

Methotrexate-anolog drugs: The shortcomings observed with MTX, namely, the systemic toxicity and cell non-specificity, led to the development of various strategies, and the search for analogs is one of them. A number of structural analogs of MTX have been investigated as new candidate antifolate drugs [35], and raltitraxed (N-[(5-{methyl[(2-methyl-4-oxo-3,4-dihydro-6-quinazolinyl) methyl]amino}-2-thienyl)carbonyl]glutamic acid) is currently licensed for therapeutic use despite being nephrotoxic [36]. These compounds, if present in biological samples such as plasma, serum, saliva, urine, cerebrospinal fluid, and tissue specimens, can be extracted, separated and detected under a variety of chromatographic conditions. They can be classified into two broad categories: "classical" antifolates, prototyped by MTX, which retain an aryl-glutamate or a chemically equivalent group, and "non-classical" antifolates, which lack the hydrophilic portion of the molecule. Figures 2.7 (a) and (b) show the structures of these analogs.

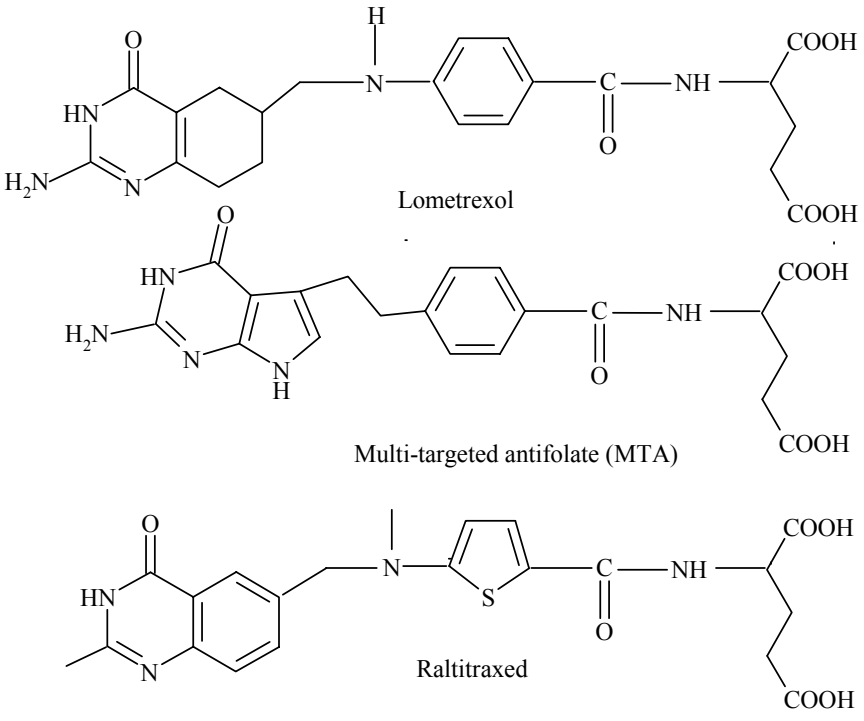


Figure 2.7 (a): Stuctures of some classical MTX-analog drugs

Certain "non-classical" DHFR inhibitors are well-established as anti-infective agents, and some are currently tested as candidate antitumor drugs. Owing to lack of the aryl-glutamate moiety, these drugs are much more lipophilic than MTX and "classical" antifolates, and can thus enter even tumor cells with impaired classical folate transport or cross the blood-brain barrier.

Trimetrexate is a highly hydrophobic, non-glutamylable analog of MTX, which carries a substituted quinazoline system in place of the pterine portions, a trimethoxyaniline group in place of the *para*-aminobenzoic acid portion [37].

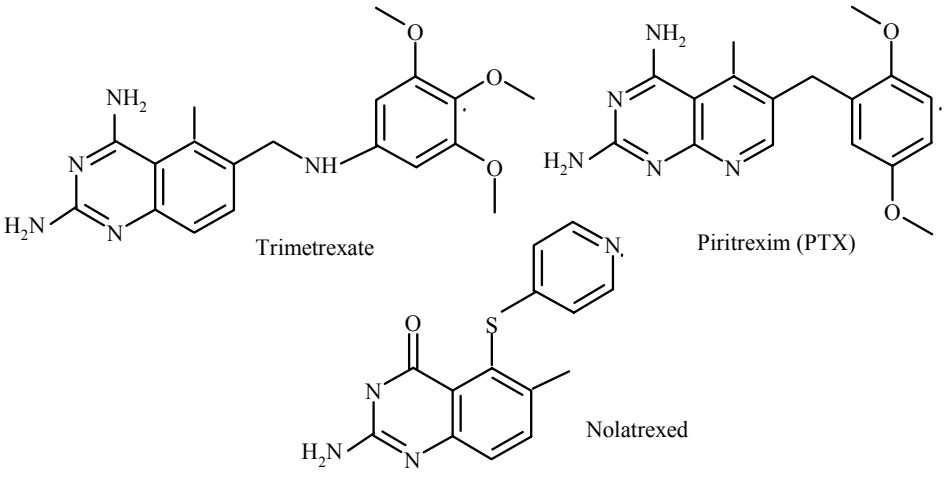


Figure 2.7 (b): Structures of some non-classical antitumor antifolate drugs

(b) Folic acid

Folic acid, or pteroylglutamic acid, consists of a pteridine that is linked to *para*-aminobenzoic acid (PABA) and glutamic acid.

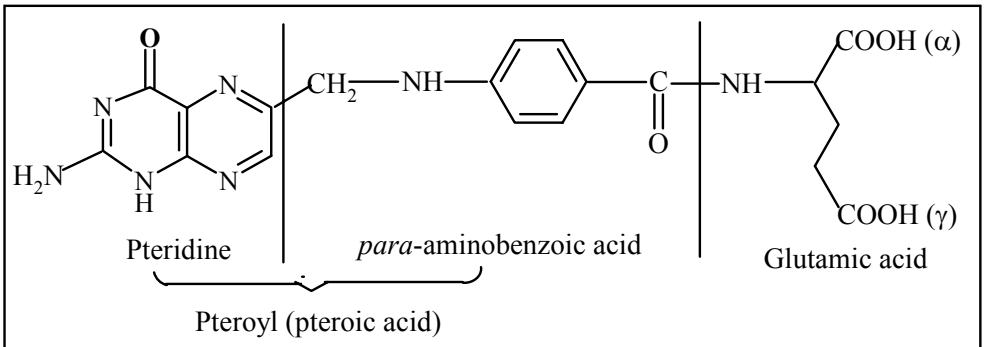


Figure 2.8: Structure of folic acid

Physiological role: As a pharmaceutical product, folic acid (FA) is a vitamin, a nutritional supplement, and a diagnostic aid in folate deficiency [38]. FA, referring to the folate form, is a well-known water-soluble vitamin of the B-complex. It is mainly evolved from natural sources, but as it is available in small quantities in biological material, worldwide efforts focused on its development and synthesis. The pharmaceutical product is chemically synthesized, and the L-enantiomer is

the biologically active form. Folic acid is involved in many metabolic mechanisms leading to the synthesis of DNA and normal erythropoiesis. In intestinal cell, FA is mostly reduced to tetrahydrofolate (H_4folate), the active form of this vitamin in a two-step reaction, which is catalyzed by the enzyme folate reductase. Inhibitors of this enzyme, like MTX, act as antifolate. Figure 2.9 depicts the fate of folic acid in the biological environment.

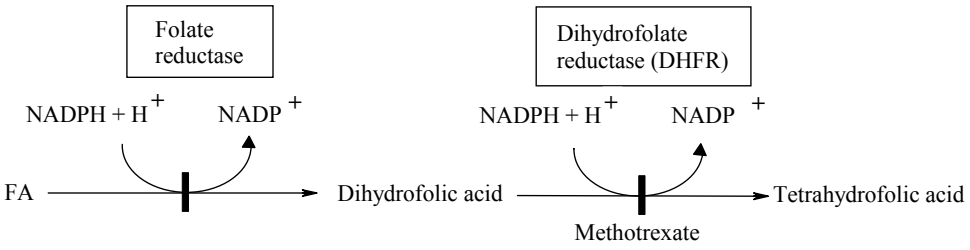


Figure 2.9: Two-step conversion of folic acid to the active tetrahydrofolate by the enzyme folate reductase and its inhibition by methotrexate

H_4folate functions as a coenzyme, a carrier of various activated one-carbon units in metabolic reactions. Folic acid and vitamin B_{12} metabolic pathways intersect at the conversion of homocysteine to methionine. FA is also proven to be completely ineffective [39] against any type of cancerous disease. However, it is also known to impact deeply on cancer development. Indeed, folate deficiency appears to play a crucial role early in cervical carcinogenesis by facilitating genetic modification at a fragile chromosomal site [40]. Also, the interest in folic acid has grown with the evidence that modest supplementation could prevent hyperhomocysteinemia, which is an independent risk factor for atherosclerotic cardiovascular disease. Folic acid plays a crucial role in DNA synthesis, where it enables cells to replicate normally. This is particularly critical during foetal development. During pregnancy, especially the first trimester, folic acid intake is important in preventing a wide range of birth defects, most notably neural tube defects. Deficiency in FA leads to anaemia. Indeed, normal physiologic changes in pregnancy affect the haemoglobin concentration, and there is a relative or absolute reduction. The most common anaemias during pregnancy are iron deficiency anaemia and folate deficiency macrocytic anaemia, which occur in women on

inadequate diets and not receiving prenatal iron and folate supplements. In an attempt to assess the effects of iron and folate supplementation on haematological and biochemical parameters and on outcome in pregnancy, Kulier and *al.* concluded that routine supplementation raises or maintains the iron, ferritin and folate levels in the serum and red cells, and results in a substantial reduction of the proportion of women with haemoglobin below 10g/dL in late pregnancy [41]. In light of its physiological key role, FAO (Food and agricultural organization) and WHO recommended folic acid intakes in terms of free folate [42].

Mechanism of intracellular uptake: Folic acid is transported into cells either through a receptor-mediated endocytosis [43] facilitated by the folate receptor, or with the help of carrier proteins, such as the reduced folate carrier (RFC). The membrane-associated folate receptor is known to be overexpressed on the surface of a variety of human tumor cells, including cancers of the ovary, colon, kidney, uterus, testis, brain, lung, breast, and myelocytic blood cells, while it is highly restricted in most normal tissues [44]. Thus, when folic acid molecules are covalently linked to proteins, the folate-protein conjugates are internalized into cells *via* the receptor-mediated mechanism [131]. In this process, the ligand (folate)-bound receptor is sequestered in caveolae, internalized into postcaveolar plasma vesicles, released from the receptor *via* an intravesicular reduction in pH, and subsequently transported into the cytoplasm. The ligand-free receptor is then recycled to the cell surface by reopening of the caveolae.

Purine analog antimetabolites: 6-Mercaptopurine (6-MP) and 6- thioguanine (6-TG) are the two major anticancer drugs in this category. These drugs are analogs of hypoxanthine and guanine, respectively. In addition to being anticancer drugs, they are also immunosuppressive and antiviral. The antipurines can both inhibit nucleotide and nucleic acid synthesis and be incorporated into nucleic acid.

They function at multiple sites and their cytotoxic activity is the result of combined effects on these different sites. Typically, 6-MP is first converted to 6-mercaptopurine ribose phosphate (6-MPRP), the nucleotide-active form that inhibits amidotransferase and dehydrogenase. Amidotransferase is the enzyme

involved in the synthesis of the purine bases (adenine and guanine) while dehydrogenase is the key enzyme in guanine nucleotide biosynthesis. Additionally 6-MPRP can be incorporated into DNA and RNA, thus forming a strand of nucleic acid with an aberrant structure. This renders the resulting modified nucleic acids unable to direct proper protein synthesis.

Therapeutically, both drugs are used primarily in the treatment of leukemias. Side effects include myelosuppression, rash, nausea, vomiting, hepatotoxicity, and diarrhoea. All of these effects are the result of the killing of rapidly dividing cells such as those found in the intestinal tract. The structures of these purine analogs are shown below.

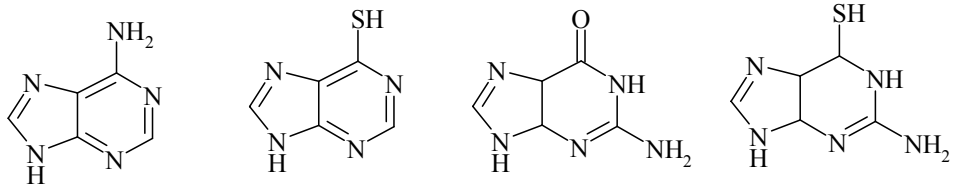


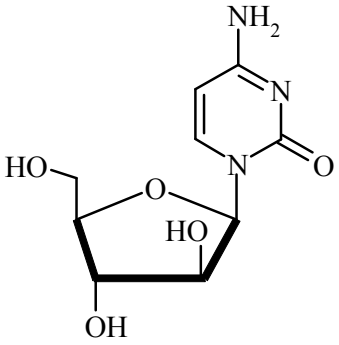
Figure 2.10: Structures of purine analog antimetabolites

Pyrimidine antimetabolites: Pyrimidine analogs have also been used in the treatment of diseases as diverse as cancer, psoriasis, fungal infections and viral infections. The best characterized and most important representatives of this class are 5-fluorouracil (5-FU) and Ara-C.

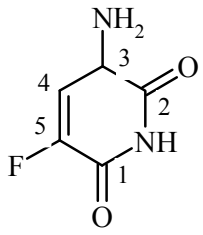
In contrast to MTX that inhibits indirectly the enzyme thymidylate synthetase through inhibition of dihydrofolate reductase, 5-FU is a direct inhibitor of this key enzyme. In this inhibition process, 5-FU is first converted to the nucleotide 5'-FUMP, which, after several different pathways, can either be incorporated into RNA or converted to the deoxynucleotide (F-dUMP). The inhibition of the enzyme thymidylate synthetase by F-dUMP leads to deletion of TTP, a necessary constituent of DNA, resulting in cell death.

The major biochemical mechanisms of resistance associated with the use of 5-FU include decreased conversion to the nucleotide form and increased breakdown of the nucleotide. 5-FU is used in the treatment of several common solid tumors. It is partially effective against metastatic carcinomas of the breast and the gastrointestinal tract. Combination with leucovorin has been very successful as the leucovorin enhances formation of the ternary complex. The toxicities of this drug are administration mode-dependent, and anorexia and nausea are among the earliest observed symptoms.

In its mechanism of action, cytosine arabinoside (Ara-C) is first converted to the monophosphate nucleotide (AraCMP) by deoxycytidine kinase. The monophosphate then reacts with appropriate kinases to form the Ara-C di- and triphosphate nucleotide (AraCTP), which, on accumulation, causes inhibition of DNA chain elongation when Ara-C is incorporated at the terminal position of a growing DNA chain. Unlike other antimetabolites, the effects of Ara-C are directed exclusively towards DNA, and it has little or no effect on RNA synthesis or function. Ara-C is primarily used either alone or in combination with daunorubicin for the treatment of acute myelocytic leukaemia due to its potent myelosuppressive action. It has occasionally been used to treat acute lymphocytic leukemia, and in high doses for non-Hodgkin's lymphoma and chronic myelocytic leukaemia. The principal toxicity is bone marrow depression, which is manifested as granulocytopenia and thrombocytopenia. Other toxicities include oral ulceration, nausea, vomiting and diarrhoea, and peripheral neurotoxicity with high dose therapy. Figure 2.11 depicts the structures of both pyrimidine antimetabolites.



Cytosine arabinoside (**Ara-C**)



5-Fluorouracil (**5-FU**)

Figure 2.11: Structures of pyrimidine antimetabolites

2.3.1.8 Other chemotherapeutic drugs

Among other numerous anticancer agents, one should cite hormonally acting or hormone-blocking agents, intercalating agents of the cisplatin-type, photochemically activated drugs, hypoxia-selective cytotoxins, radiation sensitizers, the enzyme-type agents such L-asparaginase, and the mitotic-type inhibitors such as vinblastine, vincristine, and vinorelbine. Those mitotic-type inhibitors are active specifically during the M phase of the cell cycle. Also included are the enzyme-type agents such L-asparginase as well as the organoiron drug of the ferrocene-type.

Although they vary in the mechanism of action and frequently also in their pharmacokinetic pathways, these drugs generally have in common a cytotoxic effect, which results from interaction with endocytic nuclear material.

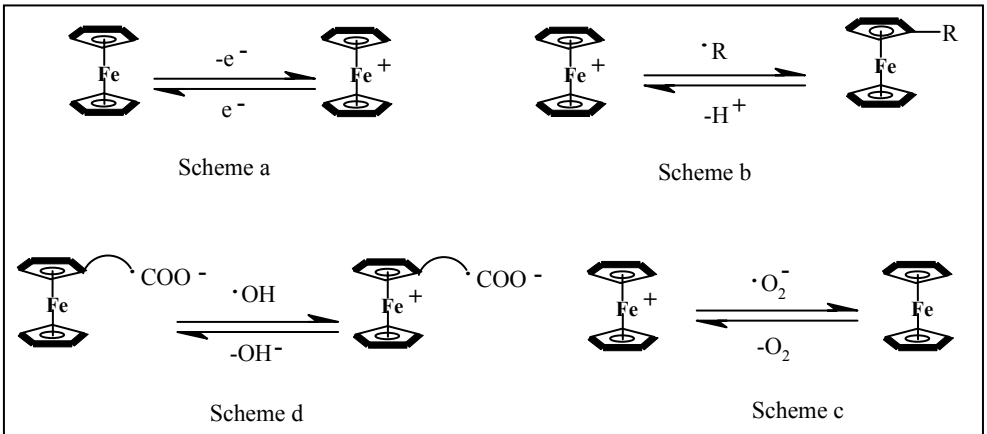
The ferrocene drug system

Over the past 30 years platinum-based drugs, notably cisplatin and carboplatin, have dominated the treatment of various cancers by chemical agents. However, these drugs cause serious side effects, including renal impairment, neurotoxicity and ototoxicity (loss of balance/hearing). Thus, there has been considerable interest and increased research activity in developing other transition metal compounds as anticancer drugs, which are less toxic than the platinum-based

drugs. Among these derivatives, metallocenes and metallocene dihalides proved to be particularly active against a number of tumors [45], and, despite the fact that their activity seems to follow mechanistic paths which differ from those of cisplatin, both drugs have a DNA intracellular target.

The first metallocene discovered was ferrocene, and its particular structure was brought out by Wilkinson [46] in the early 1950s. Ever since, there has been a rapid growth in the study of ferrocene compounds for several reasons, which include their highly promising antiproliferative activity against various murine and human cancer lines, and their unusual stability owing to the sandwich structure conferred by the binding of the iron center by the two Cp (cyclopentadienyl) rings.

Behavior in physiological environment: One of the important characteristics displayed by the ferrocene complex is its outstanding oxidation-reduction behaviour. It readily converts to the ferricenium ion, which is a free radical of high stability. This one-electron transfer reaction is reversible (Scheme a), and has some implications in the biological realm. Electron transfer and free-radical reactions play a vital role in biological processes, and therefore the ferricenium-ferrocene system should be a topic of major interest in both biochemical and biomedical research. Many investigations dealing with the biological behavior and functioning of ferrocene compounds have indeed been reported. Thus, under enzymatic control, ferrocene is oxidized by hydrogen peroxide, whereas ferricenium ion is reduced by NADH and metalloproteins (Scheme b). Besides, ferricenium ion reacts with the biologically important superoxide anion radical, leading to a regeneration of ferrocene and dioxygen (Scheme c). A reverse electron transfer reaction, resulting in oxidation of the ferrocene complex to its ferricenium salt, occurs with ferrcenylcarboxylates in their interaction with the highly reactive hydroxyl radical, transforming the latter to a harmless hydroxyl anion (Scheme d). Scheme 2.1 below gathers the different reactions of the ferrocene complex in the biological environment.



Scheme 2.1: Reactions of ferrocene complex in biological environment

Free-radical chemistry plays a vital role in cancer generation and in various phases of growth and control of neoplasia. Effective inhibition and detoxification processes in the cancerous organism may well be involved in the aforementioned superoxide and free radical-scavenging reactions. A deactivating recombination of ferrocene in its oxidized state with the free-radical form of ribonucleotide reductase, an important enzymatic link in DNA synthesis, may represent another potential contribution to the inhibition of the cell's proliferation process. The preparation of numerous ferricenium compounds and their evaluation for antiproliferative activity against ascitic murine tumors and several human tumor clonogenic cultures are reported in review articles [47, 48]. For those salts tested that were insoluble, like the ferrocene parent itself, no activity was revealed in the screens. In contrast, ferricenium salts comprising the picrate, tetrachloroferrate (III), μ-oxo-bis(trichloroferrate(III)), trichloroacetate, or chloride counter ions, were found to be active, and they all showed good water solubility with high saturation limits. Under optimal conditions, in the Ehrlich ascites screening test, best results (cure rates of 100%) were displayed by the picrate and the trichloroacetate salts. A moderate activity was even detected with ferrocenylacetic acid, a water-soluble derivative of unoxidized ferrocene. Ferricenium salts, dissolved in aqueous medium at physiological pH (~7.4), are unstable, and this would indicate too short half lives *in vivo* of such compounds in the central circulation system for effective survival *en route* to the target tissue. However, the

results drawn from ferrocenylacetic acid behavior suggest that the administration of a ferrocene compound *in vivo* in the ferricenium state may not be necessary. The oxidation-reduction equilibrium distribution of ferricenium and ferrocene species in any body compartment is likely to be solely under the control of the biological environment [49], *i.e.* pH and enzymatic activity in that compartment, and not of the oxidation state in which the ferrocene compound was initially administered. Thus, the biological effects encountered *in vitro* should also be shown *in vivo* irrespective of the compounds' initial oxidation state, the only prerequisite being water solubility of the compound, which should be highly sufficient for rapid dissolution and dissipation in the aqueous fluid system. Unlike the platinum-based compounds, the cytotoxic activity of ferrocene compounds, namely ferricenium salts, is probably not based on their direct binding to DNA, but on their ability to regenerate oxygen-active species which induce oxidative DNA damage.

Interest in the antitumor activity of ferrocene derivatives, usually associated with ferricenium compounds, recently increased when it was observed that ferrocene itself has a marked antitumor effect in experiments with tumor-bearing mice. Indeed, Kovjazin and *al.* [50], investigating the antitumor properties of ferrocene, conducted *in vivo* experiments in mice bearing established lung metastases of B-16 melanoma. The results showed unexpectedly ferrocene to possess outstanding antitumor effects resembling a bell-shaped curve. This was attributed to its immune stimulatory potential which was induced by lymphocyte activation. The Figure 4.12 below depicts the proposed mechanism of ferrocene action [50].

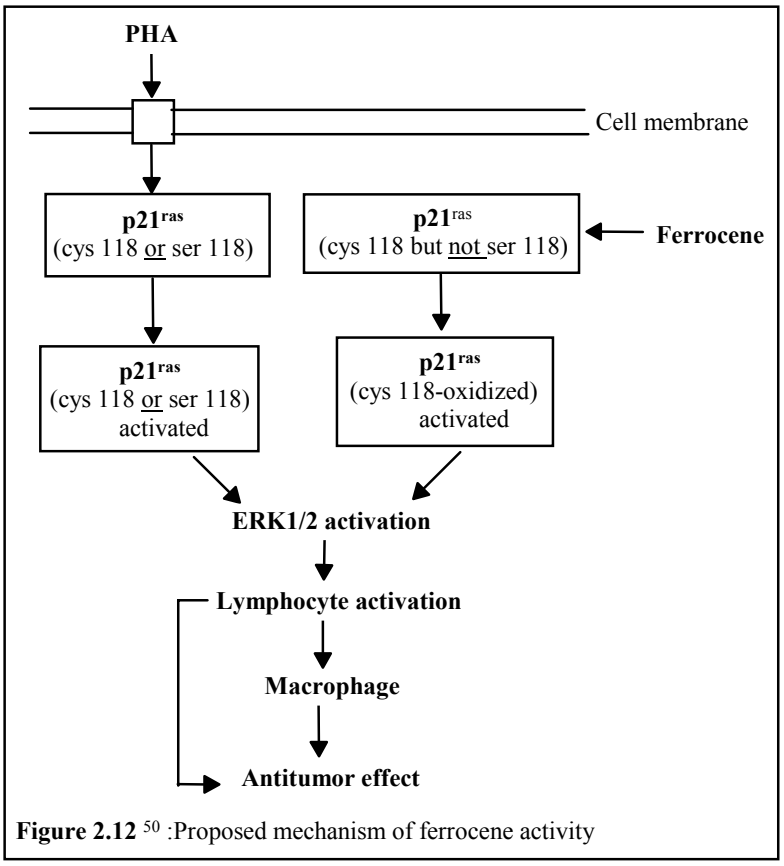


Figure 2.12 [50] :Proposed mechanism of ferrocene activity

2.3.2 Deficiencies of chemotherapy

Despite progress made in chemotherapy, either alone or in conjunction with other modalities for the treatment of cancerous diseases. However, in general, the overall success rate has remained modest and unsatisfactory. Thus, with most cancers, complete eradication is rare. Remission of limited duration and reappearance of malignant symptoms are frequent as a result of a variety of deficiencies associated with present-day anticancer drugs. Typical deficiencies include the following:

(a) *Inadequate water solubility*, which hampers swift and efficacious drug distribution in the body's aqueous fluid system, and results in enhanced exposure to macrophage activity.

(b) *Decreased serum half-life* as a consequence of catabolism, protein binding, capture by the reticuloendothelial system, or efficacious excretion mechanisms.

(c) *Excessive systemic toxicity*, which grossly diminishes therapeutic drug effectiveness and oftentimes necessitates premature termination of therapy.
(d) *Monophasic salt-like* or *charged structure*, which inhibits membrane penetration and cell entry through normal passive diffusion. As a result, only a small fraction of the medicinal agent will successfully enter intracellular space for interaction with nuclear DNA or proteinaceous constituents.
(e) *Lack of cell specificity*, with ensuing drug distribution into both normal and transformed cells. In consequence, drug application will be excessively wasteful, and healthy tissues will be exposed to toxic side effects.
(f) *Induced drug resistance*, which results in lack of long-term effectiveness. As a consequence, treatment by drug-specific therapy must be discontinued after initial promising remission, and this leads to early recurrence of cancerous lesions.

2.3.3 Combination therapy

Combination chemotherapy is a strategy of fundamental importance involving multiple drug administration to produce additive and even synergistic effects without enhancing overall drug toxicity. A specific goal of combination therapy is the broadening of the activity spectrum through the use of two or more agents functioning by different mechanisms and exerting different toxicity effects. Numerous combinations of both time-proven and novel drug models have been administered clinically. Thus, co-administration of doxorubicin, bleomycin, and vinscristine has been used as therapy for AIDS-related Kaposi's sarcoma and other germ cell neoplasm [51]. Methotrexate is commonly used in combination with 5-fluorouracil and cyclophosphamide in the adjuvant treatment of breast cancer

Although much progress has been made, cancer chemotherapy is still unsatisfactory owing to the aforementioned deficiencies. Therefore, intensive investigations of site specific polymer-drug delivery must be undertaken in order to allow the development of ultraspecific targeted macromolecular drugs. These macromolecular drugs have the advantage of increasing the potency while simultaneously reducing resistance to therapy and toxic effects of current anticancer drugs.

2.4 Immunotherapy

Immunotherapy is the fourth modality, which is still much in its infancy. Aiming at stimulating of the host's own immune system, it is described as a biologic response modifier or biologic therapy. Immunotherapy is sometimes used by itself, but it is most often used as an adjuvant (along with or after another type of therapy) to add to the anticancer effects of the main therapy. Although the thought of using one's own immune system to fight cancer is appealing, immunotherapy currently has a small role in treating the most common types of cancer. In general, immunotherapy is most likely to be effective when treating small cancers, and will probably be less effective for more advanced stages of a disease. In the presence, or after removal, of cancerous cells, the immunotherapy either stimulates the host's own immune system, and is designated as active specific immunotherapy [52] (*e.g.* cancer [53] and dendritic vaccines) or uses the immune system components such as antibodies created outside, and is known as passive immunotherapy (*e.g.* naked [54] and conjugated monoclonal antibody therapy). The most promising tumor cell vaccines are currently under study in clinical trials against several cancer malignancies including melanoma [55], kidney, ovarian, breast [56], colorectal and lung cancer, as well as leukaemia.

2.5 Antiangiogenesis Therapy

Antiangiogenesis therapy in cancer treatment refers to the use of drugs or other substances to stop tumors from developing new blood vessels, leading to tumor death [57]. Most antiangiogenic drugs work by preventing the first step in the making of new blood vessels, that is, the growth of the endothelial cells forming the inner lining of the blood vessels. They present two main advantages over chemotherapeutic drugs: Firstly, they are non toxic to normal cells, and therefore can be applied over a long period without interruption, thus leading to higher effectiveness, and secondly, since they do not lead to cell resistance, they could be active for much longer periods of time.

2.6 Gene Therapy

Gene therapy is one of the modalities for cancer malignancies treatment, which is still in its infancy. Gene therapy consists of inserting a specific gene into cells to restore a missing function, or to give the cells a new function, as cancer is the result of cell's genetic mutations. This therapy is used in a variety of ways in the clinical trials. These comprise the addition of functioning genes to cells with abnormal or missing genes, blocking genes from making cancer cells resistant to chemotherapy or adding genes to tumor cells for easy detection and elimination by the host's immune system, or adding genes to immune system cells, and stopping genes from contributing to angiogenesis (blood vessel formation), or adding angiogenesis inhibitor genes to cancer cells.

The main obstacle to the use of gene therapy is the finding of the appropriate vectors for the gene delivery. Many vectors are under investigation. Of these, one should cite the viruses, which are known to be extremely efficient in the delivery of foreign genes into cells and tissues [58], as well as the non-viral vectors such as cationic liposomes and cationic polymers [59, 60].

2.7 Photodynamic Therapy

Photodynamic therapy (PDT), also called photoradiation therapy, phototherapy, or photochemotherapy, is a treatment that combines a light source and a photosensitizing agent (a light-activated drug) to destroy cancer cells. The mechanism of action is described as follows: On exposure to light, the photosensitizing agent reacts with oxygen to form chemicals that destroy cancerous cells. The use of PDT is limited by the depth of penetration of light in the tissue. Therefore, PDT is mainly used to treat areas on or just under the skin, or in the lining of internal organs.

CHAPTER 3

POLYMERIC ANTICANCER DRUG CONJUGATES

Background and Literature review

The use of therapeutic systems to obtain a controlled drug release in cancer is a more and more exploited approach in the modern pharmaceutical technology [61, 62]. Growing interest in this field arises on the one hand from the often unsuccessful research for effective and non-toxic new drugs and on the other hand from new knowledge of the biochemical events around and inside tumor tissues. Indeed, following administration, the active agent is distributed over the entire body and reaches not only the target cells or tissues but also interacts with healthy cells. This leads to peripheral toxicities and low therapeutic efficiency, and prompts the search for novel therapeutic strategies. Many drug delivery systems have been explored, including drug-antibody conjugates (immunoconjugates), conjugates obtained by linking drugs to natural or synthetic polymers (macromolecular prodrugs) [63-65], vesicular or particulate systems (liposomes [66], nanoparticles [67], microparticles for regional therapy [68]) and polymeric implants [69]. Unfortunately some of these systems have often disappointed early expectations. In the case of immunoconjugates, the inefficacy was mainly due to the limited access of these relatively big molecules into tumor mass, the heterogeneity of tumor cells and the different humoral response among patients [70]. Therefore, a strong interest was developed in the potentially promising systems, and water-soluble carriers covalently linked to the drug through a biodegradable spacer constitute one of them.

3.1 Polymers as Drug Carriers

Modification of biologically active compounds with polymers is one of the methods for altering and controlling their pharmacokinetics, biodistribution, and toxicity [71]. Polymers chosen as drug carriers are either natural or synthetic macromolecules. They must meet certain requirements in order to maximize their potential as polymeric drug carriers by decreasing the toxicity and (or) increasing the therapeutic index of the anticancer drug.

3.1.1 Requirements for polymeric drug carrier

These include hydrosolubility, biodegradability; biocompatibility, and chemical composition.

3.1.1.1 Hydrosolubility

Solubility in aqueous media is a necessary criterion for any polymer intended to be used as a drug carrier in the biomedical field. Such polymer should be linear and highly flexible. This will have the advantage of increasing the positive entropy of the solution, and therefore favour the dissolution process, and the presence of intra- or extrachain hydrophilic entities such hydroxyl- and amino-terminals. These hydrophilic entities are of excellent utility as they are capable of undergoing effective hydration. The ability to incorporate charged species into the polymer also leads to its hydrosolubility property. Moreover, the use of poly(ethylene oxide) (PEO) in the polymer therapeutic field rose in interest owing to its numerous properties such as the solubility in both aqueous and organic media, ease of chemical modification, and biocompatibility [72, 73], which are also imparted once PEO is incorporated into a polymer.

3.1.1.2 Biodegradability

To prevent rapid excretion by kidneys observed with low molecular weight compounds, the candidate carrier must be sufficiently large. However, its

backbone must comprise segments amenable to hydrolytic and enzymatic cleavage in order to allow for the biodegradation and resultant catabolic elimination following drug release. If non-biodegradable such as the synthetic polymers with carbon-carbon backbone, the polymer should have a molecular weight not exceeding the renal threshold 30 000 - 50 000. The failure to comply with this requirement will result in deposit and accumulation in various organs. However, the biodegradability of a polymeric carbon backbone can be increased if the latter is equipped with peptide, saccharide or nucleotide sequences, as they are recognized and biodegraded by the numerous enzymes present in the lysosomal compartment of the cell.

3.1.1.3 Biocompatibility

The polymeric backbone must be non-toxic, non-immunogenic, and non-thrombogenic in order to avoid any carrier-generated toxic, immunogenic and blood-clotting side effects. Indeed, failure to meet these requirements will result in premature destruction of the carrier through attack by the host defence systems, which renders the drug delivery system useless.

PEO is found to be a promoter of cell fusion and hydration [74] as well as a chemical entity for reducing or controlling the antigenicity of immunogenic proteins [75]. An earlier review article [76] stressed the conjugation of PEO to protein or liposome as an important tool for reducing the shortcomings encountered in using these therapeutic agents, namely the degradation by proteolytic enzymes, thermal instability, and immunogenicity. More recently it has been reported that the presence of PEO segments in polyelectrolyte causes complexation with plasmids, reducing the side effects and increases the lifetime of these complexes *in vivo* [77, 78].

3.1.1.4 Chemical composition

The carrier macromolecule must comprise reactive functional groups suitable for drug anchoring and release. These groups should be separated from the principal

chain by short side chains or spacers. The presence of spacers will serve to diminish the steric inaccessibility due to the polymeric backbone. By their nature, the spacers should be stable in the blood stream [79] but susceptible to either enzymatically catalyzed or pH-dependent hydrolysis in the lysosomal compartment [80]. Likewise, polymeric carriers should display the ability to be directed to predetermined cell types. This can be achieved by the incorporation of targeting moieties such as cationic functions and antibodies [81]. The presence of cationic functions, including tertiary amino groups, is required in the carrier backbone as this will facilitate adsorptive pinocytotic cell entry [82] and therefore prevent problems related to potential ionicity or polarity of the monomeric drug, and on the other hand, increase drug selectivity for the transformed cell, given that many types of cancer cell are characterized by negative surface charge. Also the macromolecular carrier should incorporate an interposition, between the spacer-bearing units, of subunits lacking drug-binding abilities along the principal chain. This will prevent multifunctional drug binding by reducing spacer density in the molecule.

3.1.2 Natural polymers as drug carriers.

Natural polymers have the advantage of easy availability and biocompatibility, although their preparation may be restricted by the need for several purification steps, and their use is limited by their high immunogenicity. Many of them have been identified and have been or are being used as possible drugs or possess an intrinsic anticancer activity. Naturally occurring polymers such as Albumin, BSA, Chitins, and dextran have been successfully conjugated to doxorubicin [83, 84] and mitomycin [85], respectively. In general, these polymers being biodegradable owing to their natural origin, they will be excreted from the bloodstream by natural catabolic mechanisms. However, their use as drug carriers is often limited. Indeed, the substitution of natural macromolecules with covalently linked low-molecular-weight drug molecules generally results in the hampering of the host's ability to enzymatically degrade the polymeric carrier effectively [86]. The loss of biodegradation ability into easily eliminated fragments leads to inhibition of elimination from the body.

Some synthetic macromolecules, including polylysine (PLL M_w = $5x10^6$) [87], diethylaminoethyl-dextran (DEAE-dextran (M_w = $2x10^6$), and poly (Arg-Gly-Asp) (M_w =10 000) [88], have shown intrinsic anticancer activity. They are termed *polymer drugs*, and their mechanism of action is either the direct action upon the tumor cell, or the stimulation of the host's immune system [89]. Some cytokines, topoisomerase inhibitors, monoclonal antibodies, thymic hormones, cell growth inhibitors, and enzymes [90] are among the natural and biological macromolecules possessing anticancer activity. The main problem associated with the administration of such natural macromolecules is their short intravascular half-life, immunogenicity, and sometimes poor solubility [90]. Their modification with synthetic macromolecules dramatically increases their therapeutic effectiveness.

3.1.3 Synthetic polymers as drug carriers.

The synthetic polymers used as drug carriers are tailor-made in accordance with the general requirements to be fulfilled by any polymer in an attempt to serve in a biological environment (section 3.1.1), especially their entire molecular-weight distribution must be under the kidney threshold (30 000 - 50 000) if they are not biodegradable. This will have the advantage of minimizing storage. Moreover, they must be designed in such a way as to be easily internalized by fluid-phase pinocytosis in order to prevent their non-specific re-uptake after being released into the bloodstream following cell death. Indeed, the absence of non-specific interactions with plasma membranes minimizes the probability of accumulation of the carrier in nontarget cells, and thus increases its biocompatibility. These synthetic polymers are categorized according to the chemical nature (*e.g.* polysaccharides, vinylic, acrylic polymers, poly(amino acids), etc.), the stability of the backbone, and the molecular weight. More interest was developed in the use of the synthetic polymers as drug carriers since Ringsdorf [91] proposed his model of water-soluble macromolecular prodrugs in the mid-Seventies. Ever since that time, numerous carrier types have been investigated including the poly(amino acids) and poly(amidoamines).

3.1.3.1 Amino acid polymers and copolymers

In recent years, intensive studies of poly(amino acids) have been performed, motivated by the definite advantages these polymers have over other macromolecules generally used as drug carriers. Indeed, because of the proteinaceous structure imparted to them by the protein-like amide linkage, one assumes their easy cleavage to amino acids (in the body), which, being non-toxic, would be used as cellular nutrients. The first poly(amino acid) whose plasma expander property was investigated was poly(glutamic acid) [92]. However, the results were not encouraging, the compound proved to be inefficient [93] and toxic [94]. The major cause of this was that at physiological pH the net charge exhibited was too high, and this was confirmed by the lower toxicity observed with the poly(glutamic acid-*co*-lysine) [95]. Therefore, the interest for the preparation of uncharged poly(amino acids) as plasma expander rose. This was achieved by blocking the side carboxyl groups through amide linkage with an amino alcohol whose hydroxyl groups render the polymer water-soluble and at the same time eliminates the electrostatic interaction with cells and other components of the organism. The resulting poly([N^5-(2-hydroxyethyl)-L-glutamine] (PHEG) proved to be more efficient, non-toxic, and non-immunogenic on animal testing [96], but from an economic viewpoint its large-scale production was found to be costly [97]. In this respect, the synthesis of analogous derivatives of poly(aspartic acid) lent itself as an alternative. These derivatives are widely used, and exhibit special properties, such as biocompatibility, biodegradability, and non-toxicity. The potential of plasma expander properties of poly(aspartic acids) was revealed in 1974 [98] by Antoni and co-workers on their study of poly-α,β-(2-hydroxyethyl)-DL-aspartamide (PHEA), and more recently with α, β-polyasparthydrazide (PAHy) [99]. Many model polymeric drugs have been reported, such as PAHy-Ofloxacin [99], and PHEA-L-dopa [100]. The pulmonary absorption kinetics of a single molecular-weight distribution of fluorophore-labeled-PHEA, a hydrophilic and biocompatible synthetic polypeptide studied in isolated perfused rat lung [101], was also reported. Poly(aspartic acid)-derived cisplatin conjugates were prepared and in *vitro* cytotoxicity was studied [102]. More recently [103], the synthesis and

biopharmaceutical characterization of four new PHEA-based polymers, which bear PEG as pendant groups, confirmed the retention of the suitable properties previously observed with PHEA, namely, biodegradability, solubility, multifunctionality, and biocompatibility.

3.1.3.2 Poly(amidoamines)

Poly(amidoamines) (PAAs) belong to the family of polymers characterized by the regular arrangement of amido groups and secondary (or/and tertiary) amines along the macromolecular chain. Pioneered by Ferruti [104], they are synthesized by polyaddition of primary monoamines or bis(secondary amines) to bisacrylamides. Since they bind tightly to heparin, PAAs were introduced in biomedical applications, initially as a heparin-adsorbing surface for medical devices (heparin renders the device non-thrombogenic) [105]. PAAs were later proposed as particularly promising drug [105] and DNA [106] delivery carriers owing to their water solubility [105], biodegradability [107], conformation-changing ability with changing pH [108], and potentially low cytotoxicity compared with other synthetic polymers, *e.g*. poly-L-lysine [107]. Furthermore, PAAs are also known to possess structure-cytotoxicity relationships [107]. They have both aminic and amidic sites in their backbones, and the polymers prepared, in general, are selected to incorporate several different variables to reinforce the aforementioned physicochemical properties. Using the pKa values of different PAAs, Ferruti demonstrated the basicity of the aminic nitrogen atoms of each repeating unit to be independent of the degree of protonation of the whole macromolecule. Thus, the main influence on polymer basicity is governed by the aminic moiety [105]; therefore several different monoamines were incorporated. The purpose of monoamine incorporation was to ensure firstly higher basicity, as the mechanism of a macromolecule cell entry, endocytosis, exposes it to pH changes, from pH 7.4 extracellular to pH 5.5-6.5 within the endosomal-lysosomal system [109], and, secondly, increased water solubility. More recent review articles from Ferruti's laboratory cover the synthesis of primary amine-functionalized PAAs [110], the

biomedical applications [111], and the correlation between physicochemical and biological properties [112] of the PAAs.

3.1.4 Pharmacokinetic benefits of macromolecular prodrugs

Ringsdorf's model, as the possibility of drug delivery systems able to achieve both controlled release of the drug, through optimization of its pharmacokinetics, and drug targeting, through a moiety able to drive the carrier-bound drug to specific organs and tissues, rapidly became a primary goal, especially in cancer chemotherapy. Since then, polymers with varying chemical and biological properties have been investigated. These included polymer carrier-bound drugs, where a physiologically active substance is bonded to a polymeric chain and so becomes a macromolecular prodrug.

Most of the carriers utilized for drug anchoring are predominantly non-biodegradable polymers of the polyvinyl class, dextran, antibodies and other proteins, as well as biodegradable synthetic polyamides and polyesters. Biomedical *in vitro* and *in vivo* evaluation has generally revealed a spectrum of promising activities against a large number of murine and human cancer lines, provided that the drug species are anchored via biofissionable links, preferably oligopeptide and other spacers. An overriding finding has been a marked reduction in toxicity, frequently coupled with enhanced cancer cell specificity and extended circulation half-lives. Selected conjugates have entered clinical trials, and among these, is a highly promising neocarcinostatin derivative [113]. Some excellent review articles [114, 115], which cover the observed benefits of drug anchoring to polymeric carriers, the polymer-drug conjugation technology, and the drug anchoring concept, are available, as well as a large number of related reports [116-118] dealing with the polymer anchoring of *doxorubicin*, *methotrexate, mitoxantrone* and other "classical" anticancer agents.

The main function of the conjugate resulting from the chemical (generally, reversibly covalent) bonding of bioactive agent to the carrier is seen to be a successful drug transport to the endoplasmic space (site of action in the chemotherapy of cancer), where the bioactive drug exerts its biological action

after release ensured either by passive hydrolysis or caused by a more specific mode including enzymatic or reductive or pH-controlled cleavage. Figure 3.1 below illustrates a general scheme showing the principal configurations of a macromolecule-drug conjugate system.

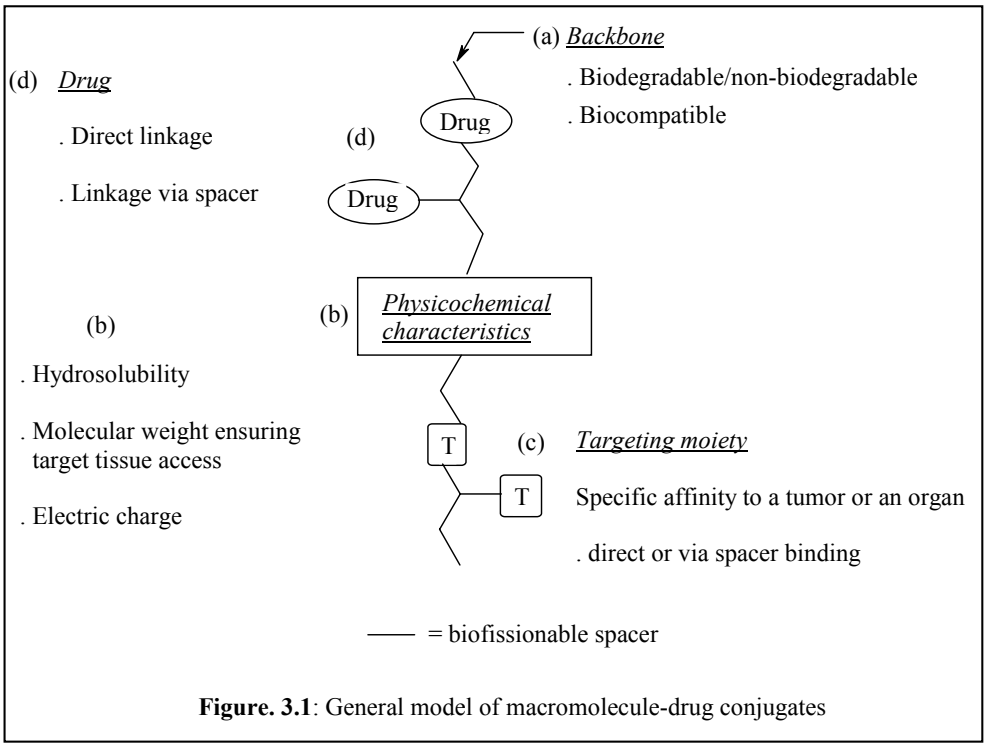


Figure. 3.1: General model of macromolecule-drug conjugates

A water-soluble polymer conjugate designed in full compliance with a variety of biomedical specifications will furnish some or all of the following pharmacokinetic advantages:

(1) Efficacious drug distribution in the aqueous fluid system is ensured even for an intrinsically water-insoluble drug as the intravenously or intraperitoneally administered drug conjugate is carried immediately into the aqueous phase of the vasculature or the intraperitoneal cavity. Smooth drug dissipation serves to enhance bioavailability while reducing the risk of interception by the reticuloendothelial system.

(2) Easier endocytotic [119] (especially, pinocytotic) cell entry will be experienced by the water-soluble conjugate irrespective of the structural peculiarities of the drug, such as ionicity, polarity or electrical charge. Many common drug molecules are polar or salt-like, and thus encounter difficulties in membrane penetration and cell entry by the usual passive diffusion mechanism generally available to exogenous molecules. Unless associated with a specialized carrier-mediated transport system, such polar or salt-like molecules, therefore, fail to reach intracellular space effectively, and most of them will be wasted as medicinal agents.

(3) Temporary protection from enzymatic attack, serum protein binding and other deleterious depletion mechanisms will be provided to the conjugate while circulating in the vascular system. As a result, premature drug losses through renal clearance and catabolic processes will be substantially reduced, and serum circulation life time will be extended with beneficial effects on the drug's bioavailability.

(4) In common with macromolecules in general, polymeric conjugates tend to accumulate in solid tumors as a consequence of the *enhanced permeability and retention (EPR)* [120]*effect*, and thus benefit from a tumoritropic driving force. This effect results from enhanced intratumoral vascular permeability, which allows for considerable leakage of the polymeric molecules into the tumor tissue. Moreover, whereas in normal tissues, macromolecules in interstitial space are efficiently recovered by the lymphatic system, this lymphatic clearance is strongly retarded in tumorous tissue, adding to polymer accumulation in such tissue.

3.1.5 Mechanism of cellular uptake of polymeric conjugates

While low-molecular-weight drugs enter the cell interior by passive diffusion, macromolecules, on the other hand, get into the intracellular space by endocytosis, a common term encompassing phagocytosis and pinocytosis. Phagocytosis refers to the internalization of vesicular material by specialized cells (macrophages and monocytes), and pinocytosis involves the internalization of all solutes dissolved in

the extracellular fluid and any material adherent to the infolding cell surface [121]. The polymer conjugate molecules are internalized by pinocytosis involving membrane invagination with concomitant capture of macromolecules, followed by transfer into the endosomal compartment of the cell. After a series of vesicle fusion events, most of molecules are directed into a secondary lysosomal compartment, thus ensuring continued exposure to acidic environment. However, because of its low permeability, the lysosomal membrane only allows the escape into the cytoplasm of low-molecular-weight compounds (including free drug) that are released from the polymeric conjugates as a consequence of lysosomal degradation. This renders the biodegradability of the spacer by lysosomal enzymes a prerequisite for lysosomotropic drug delivery. Endocytosis (pinocytosis) is macromolecule-structure-dependent. Thus, three types of endocytosis occur. These are:

(a) Fluid-phase endocytosis. This mechanism takes place when the macromolecules do not interact with the cell surface; consequently, they are taken up slowly, depending on their concentration in the extracellular fluid.

(b) Adsorptive endocytosis is specific to the macromolecule imparted with hydrophobic [122] and positively charged [82] moieties. Indeed, for this type of macromolecules, non-specific interactions with plasma membranes of different cells occur, resulting in concomitant increase in the rate of macromolecular uptake.

(c) Receptor-mediated endocytosis, the rationale for the design of targetable polymeric carriers, occurs when moieties such antibody, antigens, and viruses are incorporated into the macromolecular structure. These moieties, which are complementary to cell surface receptors or antigens of a subset of cells, render the macromolecule biorecognizable [81]. In the receptor-mediated endocytosis the macromolecule is specifically internalized by a select subset of cells, and the rate of uptake, as well as the body distribution, is substantially altered.

Non-biodegradable macromolecules accumulate within lysosomes, and are released slowly by exocytosis or as a consequence of cell death. Figure 3.2 summarises the endocytic pathways.

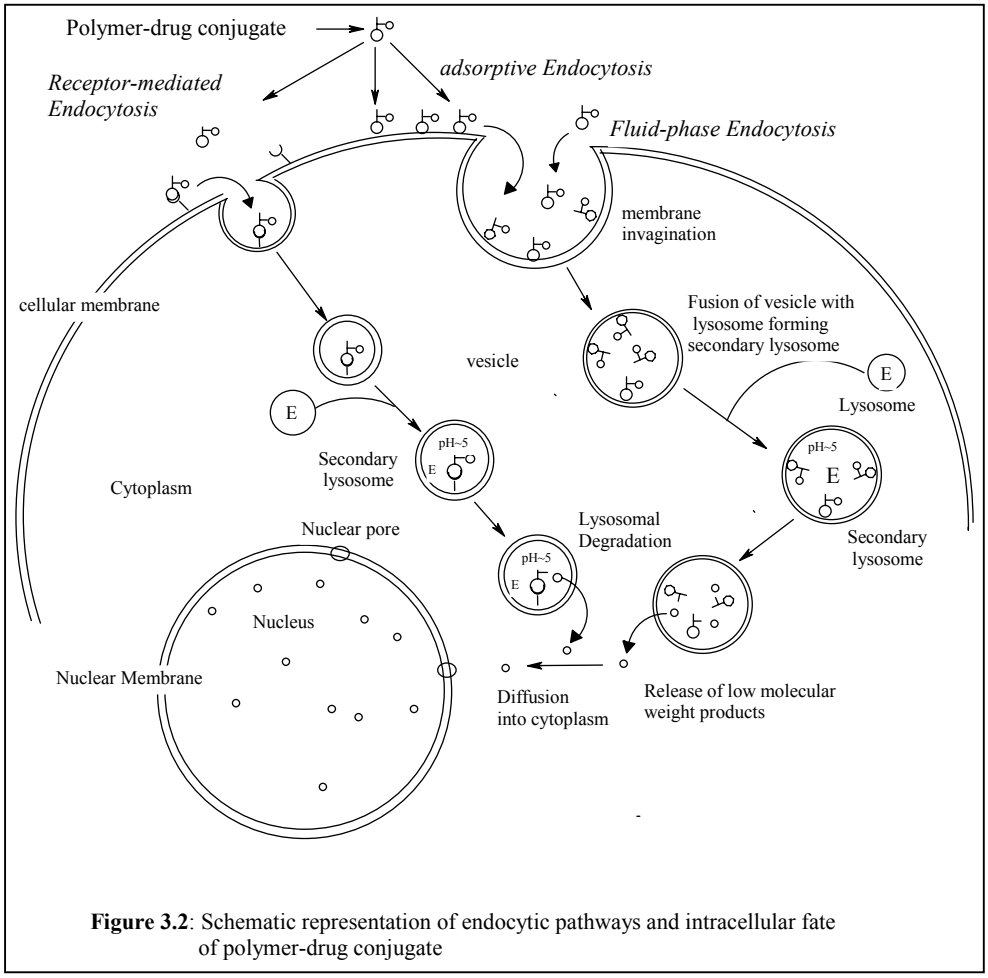


Figure 3.2: Schematic representation of endocytic pathways and intracellular fate of polymer-drug conjugate

3.1.6 Polymer-drug conjugation

The drug systems submitted to investigation in the framework of this project have been conjugated to various polymeric carriers and the conjugation which is achieved by formation of either ester or amide biocleavable bond is extensively reported.

3.1.6.1 Polymer-MTX conjugation

In an attempt to improve its therapeutic index, including the site-specific targeting or providing controlled release, MTX has been conjugated to biopolymers like mono- and polyclonal antibodies [123, 124], serum albumins [125, 126], neoglycoproteins [127], chitosan [128]. The conjugation of MTX to synthetic polymers has been extensively reported [129-131]. These reports include investigation from this laboratory. Indeed, following Ringsdorf's model of macromolecular prodrugs, MTX was conjugated to various polymeric carriers. In earlier project [130] polyaspartamides were conjugated with MTX through tethers containing an ester group as the biofissionable site, and in a recent study [129] we prepared a series of related conjugates with biocleavable carboxamide links in the connecting spacer.

3.1.6.2 Polymer-folic acid anchoring

The potential use of cellular nutrients as mediators of macromolecular and colloidal particle uptake is appealing, since receptor-mediated endocytosis is a cellular process designed for transporting critical molecules across the plasma membrane into the cytoplasm [132]. Rapidly-dividing cells express high affinities for folic acid because folate is an essential factor in purine, nucleotide, and DNA synthesis. Hence, the possibility exits of utilizing this pathway for promoting folate-linked molecules or colloidal particles to enter gastrointestinal (GI) epithelia. And, by virtue of its ability to be taken up by folate receptor overexpressed on certain tumor cells, folic acid has been widely investigated as a targeting molecule for active anticancer drug delivery. Proper synthesis procedures have been pointed out to link folic acid to drug carriers to produce targeting drug delivery systems. The folic acid molecule possesses two carboxyl groups, termed α- and γ-, which can act as handles for covalent attachment. However, according to literature, there is a stronger affinity of folate toward its receptor when linked *via* the γ-carboxyl group, whereas its α-carboxyl derivatives are not readily recognized [133].

Folate-induced receptor-mediated endocytosis has been extensively exploited to facilitate entry of anchored drugs [134], antibodies [135], imaging agents [136], liposomes [137] or macromolecules [138], and proteins into cells. Folate-conjugated proteins present the advantages of conceivably contacting and binding to all cells in a culture medium simultaneously. This avoids membrane damage or alteration as the macromolecular uptake occurs through a natural vitamin endocytosis pathway. Unlike hormone- or virus-mediated endocytosis, folate uptake occurs in all dividing cells, at reasonably rates, and folate is deposited into cytosolic rather than lysosomal compartments.

3.1.6.3 Polymer-ferrocene conjugation

The aforementioned considerations (Section 3.2.1.8) led to the strategy of conjugating the inherently hydrophobic ferrocene complex reversibly to water-soluble macromolecular carriers. The reversible anchoring of the complex to the polymeric carrier can lead to considerably enhanced therapeutic effectiveness of the therapeutic agent, as crucially important factors combined to increase bioavailability at the target site while reducing toxicity and risk of resistance build-up. Following Ringsdorf's model of macromolecular prodrugs, the ferrocene complex was conjugated to various polymeric carriers in Neuse's laboratory. Conjugation was achieved with ferrocenylcarboxylic acids and either amine-functionalized carriers leading to amide-bonded [139] ferrocene conjugates, or hydroxyl-functionalized carriers affording ester-bonded [140] ferrocene conjugates. A more recent article from the same laboratory reported the cytotoxic activity of macromolecular ferrocene conjugates against Colo 320 DM human colon cancer line [141]. In the present study, 4-ferrocenylbutanoic acid was anchored to polymers, using various approaches.

3.1.7 Anticancer drug co-conjugation

During the past decade, many research projects have focused on the sequential and simultaneous delivery of drug combinations to reduce the side effects

associated with the systemic delivery of anticancer agents [142]. Several drugs have been found to amplify the anticancer activity of others [143]. This synergistic effect can potentially lead to reduced doses for each drug administered [144]. Hence, the simultaneously administration of several drugs could reduce the side effects caused by the high doses of single drug, and could prevent the development of multi-drug resistance (MDR) [145].

An alternative approach to systemic delivery of antineoplastic agents is the localized release from a polymer. Various strategies can lead to the simultaneous and targeted delivery of a combination of anticancer drugs, and the use of hydrogels constitutes one of them. Bouchir et *al.*[116] incorporated three model drugs, namely, methotrexate (antimetabolite), doxorubicin (anthracycline antibiotic), and mitoxantrone (anthracenedione antibiotic) into cross-linked oxidized alginate hydrogel and successfully released them from the polymer. The model antineoplastic agents were loaded into the hydrogel *via* three differents mechanisms. Methotrexate was incorporated within the pores of the hydrogel and was released by diffusion into the surrounding medium. Doxorubicin was covalently attached to the polymer backbone *via* hydrolytically labile linker and was released following the chemical hydrolysis of the linker. Mitoxantrone was ionically complexed to the polymer and was released after dissociation of the complex. Rao and co-worker [146] also reported the simultaneous incorporation and controlled release of methotrexate and cisplatin using the hydrogel approach.

Another possible route for the simultaneous delivery of anticancer compounds is the co-conjugation of two or more of these agents to a single polymeric carrier *via* biofissionable linkages. Reports covering this approach are rare. However, the literature extensively reported the targeted delivery of a drug system in which a targeting moiety together with a drug is anchored to the same polymer backbone *via* biofissionable linkages [147, 148].

CHAPTER 4

RESULTS AND DISCUSSION

4.1 Polymeric Drug Carriers

4.1.1 Introduction

In fulfilment of the two objectives of this study, the synthesis by bioreversible conjugation of selected anticancer drug models with water-soluble macromolecular carriers and the biological activity evaluation of the resulting conjugates, and in accordance with the necessary prerequisites for any macromolecule intended to serve in the biomedical field (Section 3.1.1), an attempt was made to afford tailor-made drug carriers through the design and derivation of several synthetic polymeric structures. This was additionally motivated by the non-abundance of the naturally occurring counterparts and the possibility to impart the desired functions leading to the accomplishment of the goals. The polymeric carriers used for the anchoring of the selected drug models fell into the wide aliphatic polyamide type (schematized below) with subunits randomly distributed along the chain.

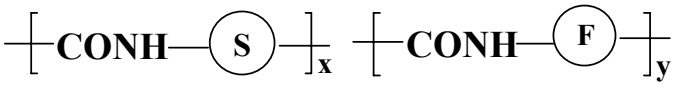


Figure 4.1: Structure of polyamide-type carrier

In this scheme, **S** represents an extra- or intra-chain hydrosolubilizing group required to impart water-solubility to the ultimate polymer-drug conjugate. **S** is a tertiary amine, hydroxyl or methoxy functionality.

F stands for an extra- or intra-chain functional group capable of reversible-drug anchoring. In this study, the primary amino group was adopted as the functional group of choice. This amino group leads to polymer-drug binding *via* amide bond formation. The amide bond has the ability to undergo biofission, which results in enzymatic activity in the intracellular lysosomal compartment, and causes drug release from the cytoplasmic space. Additional subunits of predetermined structures may be incorporated, if required, to afford tailor-made polymers that are equipped with all necessary functions. This allows efficacious administration and enhanced pharmacokinetics of the anticancer drug.

All the drug systems used in the framework of this project are hydrophobic. Hence, the polymeric carriers were designed to provide a balance between the load of these inherently hydrophobic drugs and the solubilizing moieties on the polymer, because hydrophilic polymer-drug conjugates are required at varying concentration. The carriers designed were linear polyamides of different side chains but with similar drug anchoring capacity, the primary amino group. The side chains were tertiary amine-, hydroxyl- or methoxy-terminated. The choice of these structures was based on the following considerations:

(a) The weight-average molecular weight, generally in the range of 20 000 - 30 000, is sufficiently low to suppress (chain length-dependent) inherent polymer toxicity, but still high enough to retard renal clearance. The conjugates, therefore, enter cells easily owing to the *enhanced permeability retention (EPR) effect*.

(b) The intrachain amide groups assist in gradual backbone cleavage for ease of catabolic elimination of the polymer in the “spent” state. The stereoisomeric “scrambling” of any peptide units in the backbone chain impedes unduly rapid α-peptidase-mediated “unzipping”, ensuring this fragmentation to be an appropriately retarded process.

(c) Properly selected polyamides are essentially non-toxic, and immunogenicity of these synthetic polymers is expected to be appreciably lower in

comparison with that commonly occurring with high-molecular-weight proteinaceous biopolymers.

(d) The **S**-modified subunits can be easily introduced as majority components (x > y), thus ensuring effective insulation of the **F**-modified subunits from each other. This will reduce the risk of intramolecular interaction of adjacent conjugated drug species.

(e) Tertiary amine functions can be introduced as side groups to provide the special functions of adsorptive pinocytotic cell entry and target cell affinity.

(f) While inherently water-soluble, with **S** comprising selected amine or hydroxyl functions, the polyamides can be made to acquire additional solubility in methanolic medium. This can be achieved by incorporation of poly(ethylene oxide) (PEO) side chains as additional solubilizing groups. This added solubility feature will be advantageous in follow-up reactions in alcoholic media.

(g) When synthesized from amino acid monomers, the polyamide carrier will provide vitally required nutrients for the rapidly growing cell tissue, and hence may be preferentially taken up by the cancerous cell.

The option of a polymeric carrier bearing extra-chain functional groups for drug species anchoring was adopted in this project. The adoption was based on a commonly observed phenomenon that fissionable groups as main chain components are generally less prone to cleavage than the same type of groups located more accessibly in side chains.

Two classes of polyamide conforming to the basic carrier model (Figure 4.1), namely, polyaspartamide (PAsA) and poly(amidoamines) (PAAs) were used for drug conjugation by amide bond formation between the carriers and the carboxylic acid-functionalized drugs. The primary amine functional groups of these polymers were introduced as terminals in component **F**.

The subunits incorporating this binding site form 10 to 20 mol-% of the chains, leaving 90 and 80 mol-% of **S**-labelled subunits of the *tert*-amine, hydroxyl or methoxy types for hydrosolubilization. The choice of the compositional specification was based on the necessity to restrict drug loading to levels commensurate with retention of water solubility of the resulting conjugates. Indeed, experiments with carrier containing larger mole percentages of **F**-labelled subunits had previously demonstrated the need for utilization of a disproportionately large excess of drug in the feed for complete drug incorporation. In addition, the coupling products so obtained had displayed a propensity for branching and crosslinking with concomitantly decreasing solubility once they had been isolated in the solid state. All polymeric carriers were fractionated by dialysis to remove constituents with molecular weight substantially below 25 000.

4.1.2 Polyaspartamide carriers (PAsA)

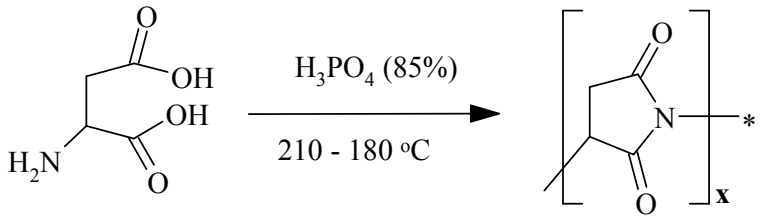
The potential value of polysuccinimide-derived aspartamide polymeric carriers for biomedicinal agents was revealed by Drobnik [149], and his proposal was subsequently translated, in this laboratory, to the reality of a class of eminently functional carriers for a variety of antineoplastic drug systems that include those submitted to our investigation. The polyaspartamides were prepared from polysuccinimide.

4.1.2.1 Synthesis of polysuccinimide (PSI)

The literature reported two different methods for the synthesis of polysuccinimide (PSI). These are the polymerization of N-carboxyanhydride of α-amino acid in general (NCA method) [150] and the thermal phosphoric acid- catalyzed polycondensation of aspartic acid (Neri method) [151]. The NCA method was found to be disadvantageous both in cost and production as the pendent reactive groups carried by the amino acid had to be protected before polymerization, and then deprotected under harsh conditions to give poly (amino acid). In addition, the

management of large amounts of phosgene, diphosgene or triphosgene, a reagent widely used for the synthesis of N-carboxyanhydride, raised complex safety problems in a large-scale plant. On contrary, the Neri method is reported to deliver high molecular weight PSI in one step [152].

In light of these considerations, the Neri method was the approach adopted for the synthesis of poly-DL-succinimide from DL- aspartic acid as shown in Scheme 4.1. The crude polymer was treated with dicyclohexylcarbodiimide (DCC) coupling agent for further chain extension purposes. A representative polymer had a relative viscosity of 35 mL g^{-1} in DMF at 30 ^{o}C, which corresponds to a weight-average molecular weight of 32 000.



DL-aspartic acid Poly-DL-succinimide

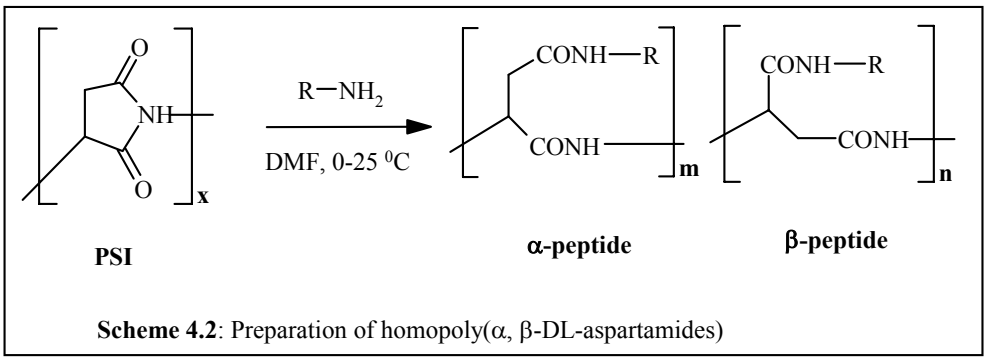
Scheme 4.1: Synthesis of polysuccinimide (PSI)

The ^{1}H NMR spectrum of PSI in DMSO-d_6 showed a large resonance at 5.2 ppm corresponding to the methine proton (NCO-*CH*). The methylene protons (*CH_2*CH) are seen as two peaks of roughly equal intensity at 3.3 and 2.6 ppm.

4.1.2.2 Preparation of homopoly (α, β-DL-aspartamides)

In general, polyaspartamides are readily prepared from poly DL-succinimide by an aminolytic ring-opening process in anhydrous, dipolar aprotic medium, such as N,N-dimethylformamide (DMF) at 0-25 ^{o}C. The product is racemic and possesses both α- and β-peptidic repeat units. Scheme 4.2 shows the preparation of homopoly(α,β-DL-aspartamides) by the poly-DL-succinimide aminolytic ring-

opening process using one type of amine reactant. For convenience, only the α-forms of polyaspartamide will be depicted in further schematic diagrams.

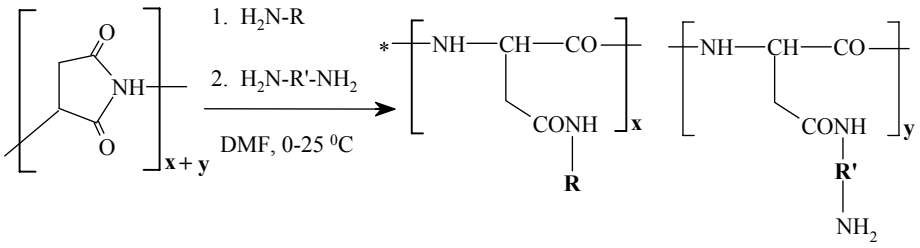


Scheme 4.2: Preparation of homopoly(α, β-DL-aspartamides)

While D-type polymers are resistant to enzymatic cleavage, L-type polymers are more prone to rapid enzymatic degradation. Therefore, a backbone structure of the DL-racemic mixture will ensure retarded enzymatic cleavage and ultimate backbone degradation as a result of hydrolytic cleavage.

4.1.2.3 Preparation of copolyaspartamides (PAsA)

Aminolytic ring-opening of polysuccinimide can lead to the generation of copolyaspartamides through a stepwise process which involves utilization of two or more different amine reactants in given stoichiometric feed ratios. Thus, H_2N-R and H_2N-R´-NH_2 were used sequentially to form polyaspartamides, in which the subunits featured R and R´-NH_2 in predetermined ratios along the chain. In the framework of this project, a series of random copolyaspartamides of the general type depicted in Scheme 4.3 were prepared as drug carriers. In this scheme and the subsequent schemes, the end groups (generally of the amine- and carboxyl-types) were neglected. The methods of synthesis were adopted from the literature. In some cases, unpublished procedures developed previously in this laboratory were used. In the schematic copolyaspartamide model, the group R (tertiary amine, hydroxyl or methoxy) has a hydrosolubilizing function while the primary amino group that is covalently attached to the R´ group has a drug-anchoring function, and is also used as a spacer segment.



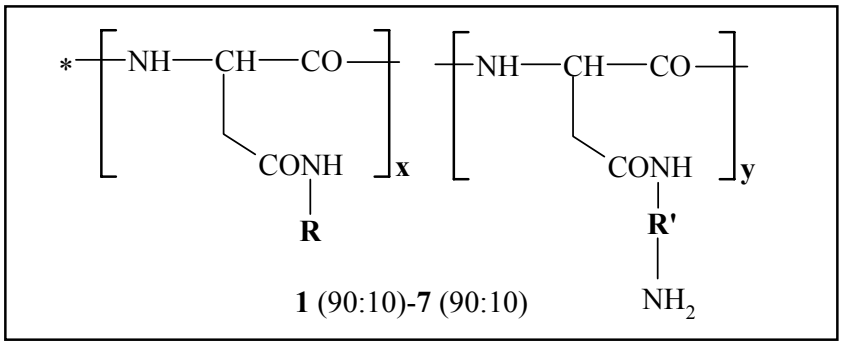
Scheme 4.3: Preparation of copolyaspartamide (**PAsA**)

The diamine (H_2N-R´-NH_2) could, by its nucleophilic difunctionality, lead to irreversible crosslinking during the aminolytic ring opening process. However, the operational conditions developed in this laboratory led to complete PSI ring opening with no evidence of irreversible crosslinking.

The adsorptive endocytotic cell entry of a prodrug [63] is influenced deeply by its ability to undergo protonation in physiological conditions (pH~7.4). Therefore, the copolyaspartamides synthesized in this study were classified into two categories, based on their protonation potential. Thus, the first category comprises the copolyaspartamides containing tertiary amine-terminated side chains, and the second category those bearing hydroxyl- or methoxy-terminated side chains.

Copolyaspartamides containing tertiary amine-terminated side chain: Their composition is shown in Table 4.1. The ratios in parentheses denote the molar percentage (x: y) of the respective constituents in the chains of these polymers and all subsequent carriers and conjugates.

Table 4.1: Composition of PAsA containing tertiary amine-terminated side chain



Carriers	R	R´	x/y
1 (90:10)	$-(CH_2)_3N(CH_3)_2$	$-(CH_2)_3-$	9
2 (80:20)	$-(CH_2)_3N(CH_3)_2$	$-(CH_2)_3-$	4
3 (90:10)	$-(CH_2)_3N(CH_3)_2$	$-(CH_2)_2NH(CH_2)_2-$	9
4 (80:20)	$-(CH_2)_3N(CH_3)_2$	$-(CH_2)_2NH(CH_2)_2-$	4
5 (90:10)	$-(CH_2)_3N(CH_3)_2$	$-(CH_2)_2O(CH_2)_2O(CH_2)_2-$	9
6 (80:20)	$-(CH_2)_3N(CH_3)_2$	$-(CH_2)_2O(CH_2)_2O(CH_2)_2-$	4
7 (90:10)	$-(CH_2)_3N(CH_3)_2$	$-CH_2CHOHCH_2-$	9

As can be seen in Table 4.1, these copolyaspartamides are all 3-(N,N-dimethylamino)propylamine (DMP)-based. The tertiary amine group acts as both hydrosolubilizing and cell-selecting group. Many considerations supported the choice of this group from all those investigated in this laboratory [153]. First, as a strong base *per se*, it is readily protonated even under weakly basic conditions. Secondly, in this protonated state, the amino group, more cationic and positively charged, will preferentially approach surfaces of certain types of cancer cells that are negatively charged. This will favor the adsorptive pinocytotic cellular uptake of the macromolecules as reported by Shen [154].

In accordance with the general principle stressed in section 4.1.1, DMP was used as a major reactant (x > y) in the two-step preparative process of these polymers. The first step is the reaction in anhydrous conditions between a given amount of polysuccinimide and its corresponding R-NH_2 counterpart. This reaction, based on the desired x/y feed ratio, is performed at room temperature.

In the second step, the resulting mixture is added to a large excess of a solution NH_2-R´-NH_2, and the reaction is continued for 24h. This was a comparatively long enough time to ensure full reactivity of the diamine. The relative amount of NH_2-R´-NH_2 (3-fold stoichiometric amount) was necessary to achieve the desired percentage incorporation with complete ring opening and substitution of the remaining succinimide units of the substrate polymer without causing crosslinking through involvement of the terminal amino group. The diamine nucleophiles NH_2-R´-NH_2 used throughout this project are exemplified by 1,3-propylenediamine (PDA); diethylenetriamine (DET); 2,2´-(ethylenedioxy)diethylamine (EDDA) and 1,3-diamino-2-propanol (DAP). EDDA introduced a relatively long spacer between the main chain and the drug-anchoring site.

In order to avoid unwanted hydrolytic ring opening resulting in the generation of free carboxylic acid side groups, both steps were performed under strictly anhydrous conditions.

The polymeric products were isolated as completely water-soluble solids by a series of operations which involved precipitation with an adequate non-solvent, aqueous dialysis (in tubing with 25 000 molecular weight cut-off limit), and freeze-drying. As a consequence of the crude fractionation achieved by this dialysis step, yields did not exceed 75%, generally ranging from 52% to 72% (Table 4.2). The inherent viscosities (η_{inh}) ranged from 10 to 20 mL g^{-1}, with small differences when compared with each another (Table 4.3).

The solid-state IR spectra of polymers **1-7** revealed a tertiary amine band at 1400-1340 cm^{-1} as well as a weak methyl band at 1460 cm^{-1} corresponding to N(CH_3)$_2$. The amide I band is remarkable in the region 1680-1610 cm^{-1}, and the band at 1580 cm^{-1} corresponds to amide II. Both spectra of **5** and **6** exhibited a strong

asymmetric band at 1060 cm^{-1} corresponding to ether band of EDDA. The OH band of DAP is also visible as a broad band in the region 3400-3200 cm^{-1}.

The ^{1}H NMR spectra of polymers **1-7** measured in D_2O, and recorded at pH 10-11 for elimination of protonation effects, showed characteristic band groups, some of them containing overlapping signals. Thus, the *CH* (methine) signal of aspartic appeared in the region of 4.75-4.5 ppm; CH_2-O (methylene) and *CH*-OH (methine) signals were grouped in the region of 3.7-3.6 ppm. The methylene protons of CONH-CH_2 were found in the region of 3.5-3.0 ppm. Proton signals of CO-CH_2, CH_2-N $(CH_3)_2$, CH_2-NH, and CH_2-NH_2 groups were superposed in the region of 2.9-2.0 ppm. Methylene protons of $CH_2CH_2CH_2$ groups were in the 1.8-1.5 ppm region.

Table 4.2: Summary of preparative data for PAsA containing tertiary amine-terminated side chain

Reactants in feed (mol-%) [a]			**Reaction conditions** [c]	**PAsA carriers**	
R-NH_2	**H_2N-R´-NH_2**	**Mole ratio x/y** [b]		**Yield** (%) [d]	**Designation**
DMP (90)	PDA (30)	9	(1) 10h, RT; (2) 4h-0^oC then 24h, RT	52	**1** (90:10)
DMP (80)	PDA (60)	4	´´	72	**2** (80:20)
DMP (90)	DET (30)	9	´´	52	**3** (90:10)
DMP (80)	DET (60)	4	´´	59	**4** (80:20)
DMP (90)	EDDA (30)	9	´´	61	**5** (90:10)
DMP (80)	EDDA (60)	4	´´	57	**6** (80:20)
DMP (90)	DAP (30)	9	´´	54	**7** (90:10)

Parenthetic numbers indicate the number of moles of amino compound per 100 base moles of poly-DL-succinimide.
DMP = 3-(N, N-dimethylamino)propylamine, PDA = 1,3-propylenediamine, DET = Diethylenetriamine, EDDA = 2,2´-(ethylenedioxy)diethylamine, DAP = 1,3-diamino-2-propanol.
[b] Mole ratio (used) of hydrosolubilizing to drug-anchoring groups.
[c] RT= room temperature; reaction step sequence in parentheses.
[d] Polymer yield after ultimate (25 000 molecular weight cut-off) dialysis.

Table 4.3: ^{1}H NMR and viscometric results for PAsA containing tertiary amine-terminated side chain

PAsA carriers				**Number of protons counted** [d] (expected) [e] **chemical shift** (ppm)				
Designation	η_{inh} (mL g^{-1}) [a]	**x/y** [b]	**Base molecular weight** [c]	δ 4.75-4.4 [f]	δ 3.7-3.5	δ 3.5-3.0	δ 2.9-2.0	δ 1.8-1.5
1 (90:10)	11.61	9	1964.5	10(10)		20(20)	94(94)	20(20)
2 (80:20)	14.47	4	968.2	5(5)		10(10)	44(44)	10(10)
3 (90:10)	10.24	9	1993.5	10(10)		20(20)	98(98)	18(18)
4 (80:20)	16.99	4	997.2	5(5)		10(10)	48(48)	8(8)
5 (90:10)	10.57	9.1	2038.5	9(10)	9(8)	20(20)	94(94)	18(18)
6 (80:20)	20.14	4.2	1042.3	4(5)	7(8)	11(10)	43(44)	8(8)
7 (90:10)	13.25	9	1980.5	10(10)	1(1)	21(20)	95(94)	18(18)

[a] At 30.0 ± 0.5 °C, in deionized H_2O; concentration c = 2 mg/mL.

[b] Mole ratio (found) of hydrosolubilizing to drug-anchoring groups after ^{1}H NMR integration.

[c] Molecular weight of the simplest recurring unit (normalized to y=1) rounded off to the nearest integer.

[d] In D_2O, pH 10-11, chemical shifts, δ/ppm, referenced against internal sodium 3-trimethylsilyl-2,2,3,3-d_4-propionate; integration error limits ± 12%.
Protons are calculated (figures rounded off to the nearest integer) on basis of found x/y ratios.

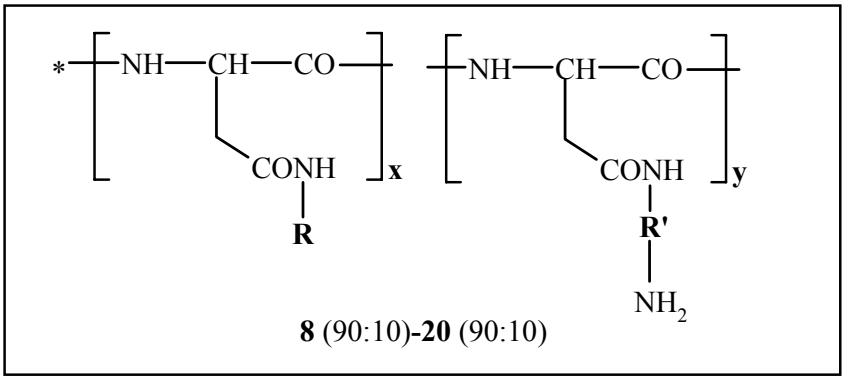
[e] Expected count for composition in accordance with recurring unit (see b).

[f] Assignment: δ/ppm: 4.75-4.5 (*CH* Asp); δ 3.7-3.6 (*CH*$_2$-OH; *CH*-OH); 3.5-3.0 (CONH-*CH*$_2$); 2.9-2.0 (CO-*CH*$_2$, *CH*$_2$-N(*CH*$_3$)$_2$, *CH*$_2$-NH, *CH*$_2$-NH$_2$), 1.8-1.5 (CH$_2$*CH*$_2$CH$_2$).

From the ^{1}H NMR data of the polymers **1-7** (compiled in Table 4.3), we deduced that the x/y ratios of hydrosolubilizing to drug-binding groups were in excellent in agreement with the proposed structures. This proves the efficacy of the preparative procedure.

Copolyaspartamides containing hydroxyl- or methoxy-terminated side chain: Table 4.4 shows the composition of the copolyaspartamides with hydroxyl- or methoxy-terminated side chain acting as hydrosolubilizing groups.

Table 4.4: Composition of PAsA containing hydroxyl- or methoxy-terminated side chain



8 (90:10)-**20** (90:10)

Carriers	R	R´	x/y
8 (90:10)	$-(CH_2)_2OH$	$-(CH_2)_2NH(CH_2)_2-$	9
9 (80:20)	$-(CH_2)_2OH$	$-(CH_2)_2NH(CH_2)_2-$	4
10 (90:10)	$-(CH_2)_2OH$	$-CH_2CHOHCH_2-$	9
11 (90:10)	$-(CH_2)_2OH$	$-(CH_2)_3-$	9
12 (90:10)	$-(CH_2)_2OH$	$-(CH_2)_2O(CH_2)_2O(CH_2)_2-$	9
13 (90:10)	$-(CH_2)_2O(CH_2)_2OH$	$-(CH_2)_2NH(CH_2)_2-$	9
14 (80:20)	$-(CH_2)_2O(CH_2)_2OH$	$-(CH_2)_2NH(CH_2)_2-$	4
15 (90:10)	$-(CH_2)_2O(CH_2)_2OH$	$-(CH_2)_3-$	9

Table 4.4 continued

Carriers	R	R´	x/y
16 (90:10)	$-(CH_2)_2O(CH_2)_2OH$	$-CH_2CHOHCH_2-$	9
17 (90:10)	$-(CH_2)_2OCH_3$	$-(CH_2)_2NH(CH_2)_2-$	9
18 (80:20)	$-(CH_2)_2OCH_3$	$-(CH_2)_2NH(CH_2)_2-$	4
19 (90:10)	$-(CH_2)_2OCH_3$	$-(CH_2)_3-$	9
20 (90:10)	$-(CH_2)_2OCH_3$	$-(CH_2)_2O(CH_2)_2O(CH_2)_2-$	9

The major components of these polymers (x > y) are either hydroxyl- or methoxy-functionalized. These components are unable to undergo protonation under physiological conditions, and will rather favor a fluid-phase pinocytotic cell entry of the macromolecules as opposed to the adsorptive-pinocytosis observed with the tertiary amine-terminated polymers. This enables a comparison of cytotoxic activity of the ultimate prodrugs *via* these different hydrosolubilizing groups as the spacer segments are identical in both categories of copolyaspartamides.
The hydroxyl- and methoxy-terminated amines used as reactants are represented by ethanolamine (EA), aminoethoxyethanol (AEE), and methoxyethylamine (MEA), respectively.

The aminolysis of polysuccinimide leading to the formation of these copolyaspartamides occurred in two steps as depicted in the general Scheme 4.3. In the first step, PSI was allowed to react with $R\text{-}NH_2$ in a selected feed molar ratio (x/y) for 24h period. The longer reaction period, in comparison with that for DMP-based copolymers, was motivated by the influence of the basicity on the rate of PSI aminolysis [155]. The $R\text{-}NH_2$ reactants being weakly acidic, are expected to react more slowly, therefore, a longer period is required to ensure PSI ring-opening to the desired extent. In the second step, the resulting mixture was added to a solution of $NH_2\text{-}R´\text{-}NH_2$ (3-fold stoichiometric amount) and the reaction was continued in the same conditions as for the first category of polyaspartamides. These copolyaspartamides, worked up similarly to preceding polymeric carriers,

were obtained in yields ranging from 50 to 70% and possessed inherent viscosities in the range of 11 to 18 mL g^{-1}.

The solid-state IR spectra of polyaspartamides **8-16** revealed a broad band in the region 3400-3200 cm^{-1}, which is attributable to the OH group. Polymers **8-20** showed a broad amide I band in the region 1680-1610 cm^{-1}. The presence of an amide II band is also noticeable at 1530 cm^{-1}. Polymers **13-20** showed a strong asymmetric ether band at 1060 cm^{-1}.

The ^{1}H NMR spectra (400 MHz) of these polymers, measured in D_2O solutions, were recorded at pH 10-11 in order to preclude any protonation effects. They showed several groups of bands, which were occasionally superimposed upon each other. Prominent band groups were in the regions of 4.75-4.5 ppm (*CH* Asp), 3.7-3.6 ppm (*CH*$_2$-O, *CH*-OH, O*CH*$_3$), 3.5-3.0 ppm (CONH*CH*$_2$), 2.9-2.0 ppm (CO*CH*$_2$, *CH*$_2$NH, *CH*$_2$NH$_2$), 1.8-1.5 ppm (CH_2*CH*$_2$$CH_2$).

From ^{1}H NMR data of the polymers **8-20** (complied in Table 4.6); we deduced that the x/y ratios of hydrosolubilizing to drug-binding groups correlated with the proposed structures.

Table 4.5: Summary of preparative data for of PAsA containing hydroxyl- or methoxy-terminated side chain

Reactants in feed (mol-%) [a]			**Reaction conditions** [c]		
R-NH_2	**H_2N-R´-NH_2**	**Mole ratio x/y** [b]		**Yield** (%) [d]	**Designation**
EA (90)	DET (30)	9	(1) 24h, RT; (2) 4 h-0^oC then 24h, RT	65	**8** (90:10)
EA (80)	DET (60)	4	´´	68	**9** (80:20)
EA (90)	DAP (30)	9	´´	68	**10** (90:10)
EA (90)	PDA (30)	9	´´	69	**11** (90:10)
EA (90)	EDDA (30)	9	´´	74	**12** (90:10)
AEE (90)	DET (30)	9	´´	68	**13** (90:10)
AEE (80)	DET (60)	4	´´	70	**14** (80:20)
AEE (90)	PDA(30)	9	´´	62	**15** (90:10)
AEE (90)	DAP (30)	9	´´	63	**16** (90:10)

Table 4.5 continued

Reactants in feed (mol-%) [a]			**Reaction conditions** [c]		
R-NH_2	**H_2N-R´-NH_2**	**Mole ratio x/y** [b]		**Yield** (%) [d]	**Designation**
MEA (90)	DET (30)	9	(1) 24h, RT; (2) 4 h-0^oC then 24h, RT	54	**17** (90:10)
MEA (80)	DET (60)	4	´´	66	**18** (80:20)
MEA (90)	PDA (30)	9	´´	71	**19** (90:10)
MEA (90)	EDDA (30)	9	´´	55	**20** (90:10)

[a] Parenthetic numbers indicate the number of moles of amino compound per 100 base moles of poly-DL-succinimide. PDA = 1,3-propylenediamine, DET = diethylenetriamine; EA = ethanolamine, MEA = 2-methoxyethylamine, DAP = 1,3-diamino-2-propanol, EDDA = 2,2´–(ethylenedioxy)diethylamine.

[b] Mole ratio (used) of hydrosolubilizing to drug-anchoring groups.

[c] RT= room temperature; reaction step sequence in parentheses.

[d] Polymer yield after ultimate (25 000 molecular weight cut-off) dialysis.

T**able 4.6**: ^{1}H NMR and viscometric results for PAsA containing hydroxyl- or methoxy-terminated side chain

PAsA carriers				**Number of protons counted** [d] (expected) [e] **chemical shift** (ppm)				
Designation	η_{inh} (mL g^{-1}) [a]	**x/y** [b]	**Base molecular weight** [c]	δ 4.75-4.4 [f]	δ 3.7-3.6	δ 3.5-3.0	δ 2.9-2.0	δ 1.8-1.5
8 (90:10)	16.2	9	1623.7	10(10)	18(18)	20(20)	26(26)	
9 (80:20)	15.5	4	832.9	5(5)	8(8)	10(10)	16(16)	
10 (90:10)	12.75	9	1610.7	10(10)	20(19)	20(20)	22(22)	
11 (90:10)	12.05	9	1594.6	10(10)	18(18)	20(20)	22(22)	2(2)
12 (90:10)	13.45	9	1668.7	10(10)	24(24)	20(20)	22(22)	
13 (90:10)	14.02	9	2020.1	10(10)	54(54)	20(20)	26(26)	
14 (80:20)	12.08	4	1009.1	5(5)	37(36)	10(10)	16(16)	
15 (90:10)	11.54	9	1991.1	9(10)	55(54)	20(20)	22(22)	2(2)
16 (90:10)	11.28	9	2007.7	10(10)	54(55)	20(20)	22(22)	

Table 4.6 continued

PAsA carriers				Number of protons counted [d] (expected) [e] chemical shift (ppm)				
Designation	η_{inh} (mLg^{-1}) [a]	**x/y** [b]	**Base molecular weight** [c]	δ 4.75-4.4 [f]	δ 3.7-3.6	δ 3.5-3.0	δ 2.9-2.0	δ 1.8-1.5
17 (90:10)	18.43	9	1750	10(10)	45(45)	20(20)	25(26)	
18 (80:20)	17.31	4	889	5(5)	20(20)	10(10)	16(16)	
19 (90:10)	15.45	9	1720.9	10(10)	45(45)	20(20)	22(22)	2(2)
20 (90:10)	14.85	9	1795	10(10)	53(53)	20(20)	22(22)	

[a] At 30.0 ± 0.5 °C, in deionized H_2O; concentration c= 2 mg/mL.

[b] Mole ratio (found) of hydrosolubilizing to drug-anchoring groups after ^1H NMR integration.

[c] Molecular weight of the simplest recurring unit (normalized to y=1) rounded off to the nearest integer.

[d] In D_2O, pH 10-11, chemical shifts, δ/ppm, referenced against internal sodium 3-trimethylsilyl-2,2,3,3-d_4-propionate; integration error limits ± 12 %. Protons are calculated (figures rounded off to the nearest integer) on basis of found of x/y ratios.

[e] Expected count for composition in accordance with recurring unit (see b).

[f] Assignment: δ/ppm: 4.75-4.5 (*CH* Asp); 3.7-3.6 (CH_2O; *CH*OH; OCH_3); 3.5-3.0 (CONHCH_2); 2.9-2.0 (COCH_2, CH_2NH, CH_2NH_2), 1.8-1.5 ($CH_2CH_2CH_2$).

Characterization data of a dozen of copolyaspartamide carriers by gel permeation chromatography (GPC) (performed generously by an outside institution) are compiled below.

Table 4.7: Gel permeation chromatography [a] characteristics of PAsA

Designation	η_{inh} (mL g^{-1})	M_w [c] $x10^{-3}$	M_n [b] $x10^{-3}$	I_n [d]
1 (90:10)	11.61	25.28	12.33	2.05
2 (80:20)	14.47	27.64	12.23	2.26
3 (90:10)	10.24	22.56	12.19	1.85
4 (80:20)	16.99	28.36	11.34	2.5
5 (90:10)	10.57	24.48	11.54	2.12
6 (80:20)	20.14	54.85	30.47	1.8
7 (90:10)	13.25	17.86	12.85	1.39
8 (90:10)	16.2	28.28	23.56	1.2
9 (80:20)	14.02	54.0	25.71	2.1
10 (90:10)	18.43	31.07	20.99	1.48
13 (90:10)	11.54	54.48	20.3	2.71
14 (80:20)	17.31	29.4	15.55	1.89

[a] Performed using sepharose 6 gel, at a flow rate of 0.5ml/min, in a buffer solution of 0.3 M sodium acetate and 0.5 g NaN_3, pH 6.5.

[b] M_w= weight-average molecular weight.

[c] M_n = number-average molecular weight.

[d] I_n= M_w/ M_n, polydispersity index.

These results showed that the weight-average molecular weight of the copolyaspartamides was, for the most part, in the 20 000 - 30 000 range. This was in accordance with the biomedical requirement that the average molecular weight of the polymeric carrier should be sufficiently low to suppress inherent polymer toxicity, as well as high enough to retard renal clearance (Section 4.1).

The polydispersity indices were in the range of 1.2 to 2.7. The relation between inherent viscosity and molecular weight (Figure 4.2) revealed large differences in the stiffness of these copolyaspartamides. The trend of increasing viscosities did not always match an increase in M_w. Typically, polymer **7** (M_w = 17 860) displayed a higher viscosity (13.25 mL g^{-1}) than polymer **13** (M_w = 54 480, and viscosity = 11.54 mL g^{-1}). The difference in the stiffness could be explained either by hydrolytic cleavage or aggregation in the polymeric chain. However, no further investigation was performed to elucidate these peculiar differences.

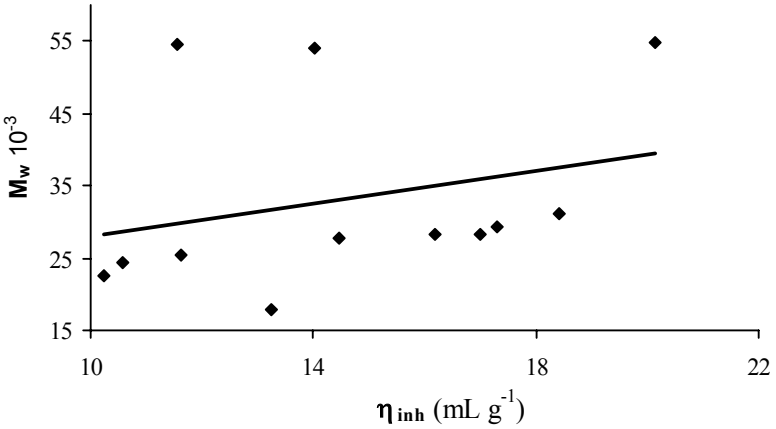


Figure 4.2: Inherent viscosity (η_{inh}) versus M_w of PAsA

4.1.3 Poly(amidoamine) carriers (PAAs)

Interest in the study of poly(amidoamines), pioneered by Ferruti [104, 105, 107-109, 110-112] was prompted by the need for polymeric carriers that provide primary amino groups as side chain terminal for drug anchoring while possessing complete

solubility in both aqueous and organic media, and more critically in methanolic media. This led to the synthesis, by a Michael addition mechanism, of bisacrylamide-derived polymers that contain various solubilizing groups as side-chain or main-chain components in addition to short side chains which possess primary amine functionality as the drug conjugation site.

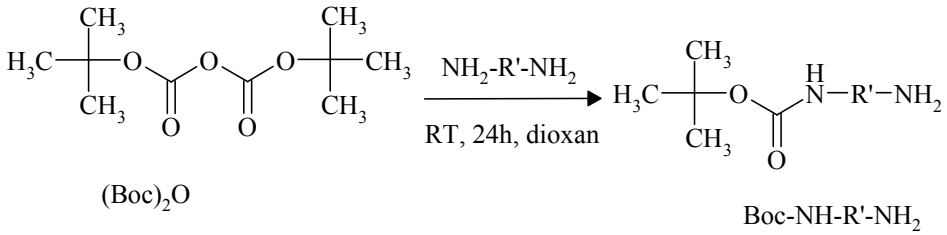
Methylenebisacrylamide (MBA), used in earlier [109, 156] and more recent [157] investigations from this laboratory, was chosen as the bifunctional acrylic acid derivative, which had to be copolymerized in various feed ratios with functionalized monoamines and diamines mono-N-protected by *tert*-butoxycarbonyl (Boc) substituent. Deprotection of the primary amino groups with trifluoroacetic acid afforded the target polymers.

4.1.3.1 Preparation of mono-N-Boc-protected primary diamine

Ethylenediamine (EDA), 1,3-propylenediamine (PDA), diethylenetriamine (DET), and 2,2´-(ethylenedioxy)diethylamine (EDDA) are four diamine derivatives selected to be mono-N-protected with *tert*-butoxycarbonyl substituent. They were chosen as short-chain aliphatic spacers designed to provide spacing between main chain and the drug. Moreover, the choice of the protecting group, Boc, was motivated by its easy removal by trifluoroacetic acid [158] in a short period that is enough to avoid hydrolytic cleavage of the ultimate polyamidoamine.

As an example, Boc-PDA, compound **22**, was prepared in a pure state by reacting di-*tert*-butyl dicarbonate, $(Boc)_2O$, with a large excess of PDA dissolved in dioxan, followed by filtration of disubstitued-diamine upon addition of water. This was followed by extraction of the filtrate with dichloromethane, and evaporation of the combined extracts to dryness in *vacuo*. Scheme 4.4 depicts the preparation of the mono-N-Boc-protected primary diamines used in this study, and the experimental conditions are summarized in Table 4.8. The yields ranged from 85 to 93%. The ^{1}H NMR data of the mono-N-Boc-protected primary

diamines (Table 4.9) satisfactorily confirmed the assigned structures of these compounds.



$(Boc)_2O$

Boc-NH-R'-NH_2

21-24

21 R': -CH_2-CH_2- **Boc-EDA**

22 R': -CH_2-CH_2-CH_2- **Boc-PDA**

23 R': -CH_2-CH_2-NH-CH_2-CH_2- **Boc-DET**

24 R': -CH_2-CH_2-O-CH_2-CH_2-O-CH_2-CH_2- **Boc-EDDA**

Scheme 4.4: Synthesis of mono-N-Boc-protected primary diamines

Table 4.8: Summary of preparative data for H_2N-R´-NH-Boc compounds

Reactants in feed (mol-%)				**Reaction conditions** [c]	**H_2N-R´-NH-Boc**	
Diamine [a]	**$(Boc)_2O$** [b]	**Mole ratio diamine: $(Boc)_2O$**	**Medium**		**Yield** (%)	**Designation**
EDA	$(Boc)_2O$	9	dioxan	24h, RT	93	**21**
1,3-PDA	´´	9	´´	´´	85	**22**
EDDA	´´	7	´´	´´	92	**23**
DET	´´	7	´´	´´	92	**24**

[a] EDA = ethylenediamine; PDA = 1,3-propylenediamine, EDDA = 2,2´-(ethylenedioxy)diethylamine; DET = diethylenetriamine.

[b] $(Boc)_2O$ = di-*tert*-butyl dicarbonate.

[c] RT= room temperature.

Table 4.9: ^{1}H NMR data for H_2N-R´-NH-Boc compounds

H_2N-R´-NH-Boc compounds	**Number of protons counted** [a] (expected) [b] **chemical shift** (ppm)				
designation	δ 3.8-3.6 [c]	δ 3.5-3.1	δ 3.0-2.5	δ 1.8-1.6	δ 1.5-1.3
21		2 (2)	2 (2)		9 (9)
22		2 (2)	2 (2)	2 (2)	9 (9)
23		2 (2)	5 (6)		9 (9)
24	8 (8)	2 (2)	2 (2)		9 (9)

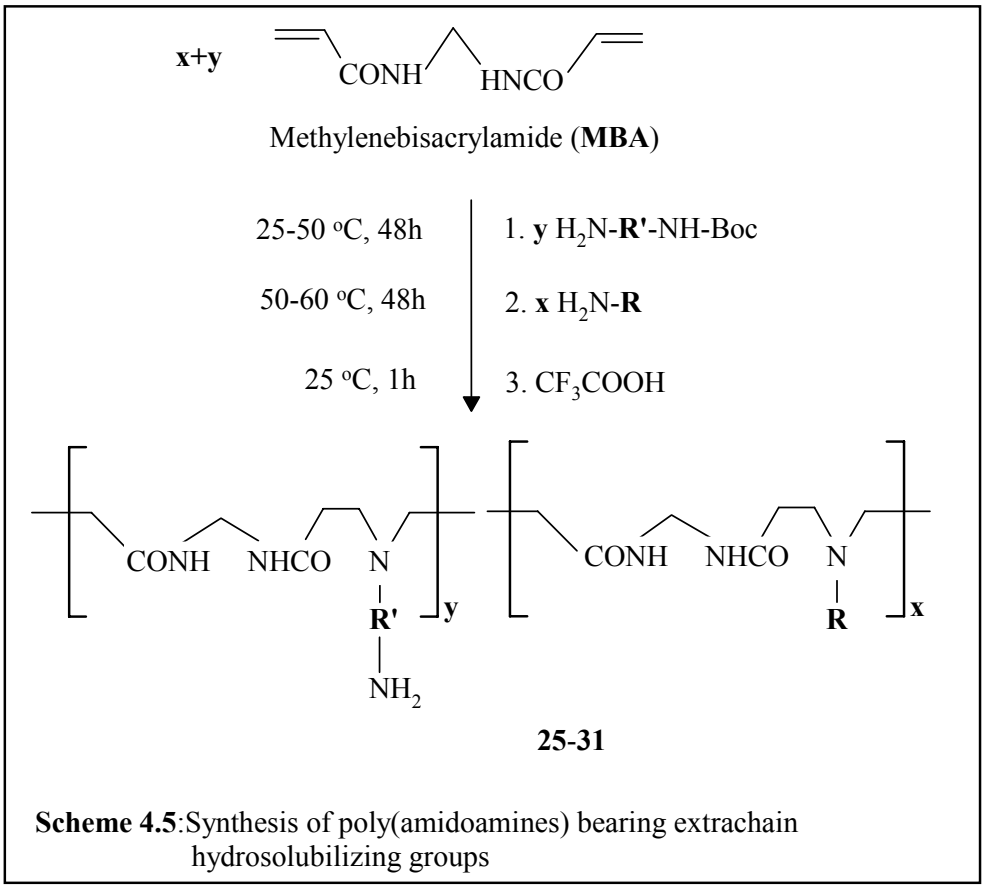
[a] In D_2O, pH 7, chemical shifts, δ/ppm, referenced against internal sodium 3-trimethylsilyl-2,2,3,3-d_4-propionate, integration error limits ± 12 %. Protons are calculated (figures rounded off to the nearest integer).

[b] Expected count for composition in accordance with recurring unit.

[c] Proton assignment, δ/ppm: 3.7-3.6 ($OCH_2\mathit{CH_2}O$, $NCH_2\mathit{CH_2}O$); 3.5-3.1 ($CONH\mathit{CH_2}$); 3.0-2.5 ($\mathit{CH_2}NH_2$); 1.8-1.6 ($CH_2\mathit{CH_2}CH_2$); 1.5-1.3 ($\mathit{CH_3}$).

4.1.3.2 Synthesis of primary amine-functionalized poly(amidoamine) carriers

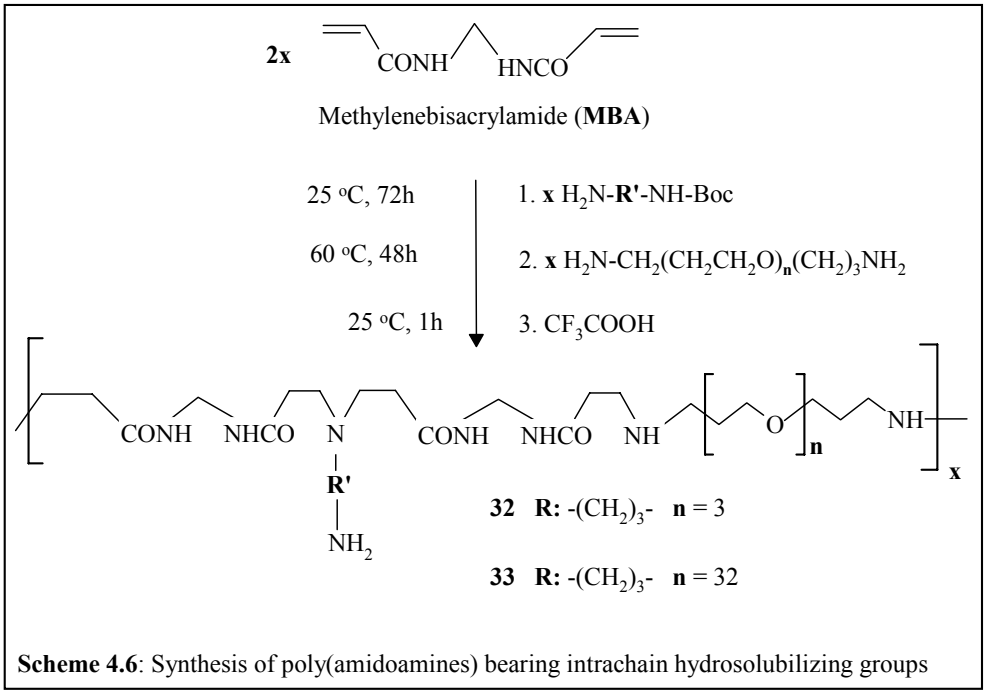
PAAs bearing extrachain hydrosolubilizing groups: The primary amine-functionalized poly(amidoamine) carriers containing hydrosolybilizing side chains were obtained by polymerization conducted in aqueous medium, performed in two steps. In the first, methylenebisacrylamide (MBA), served as the key monomer. It was allowed to react with the respective amount of proteted amine (H_2N-R´-NH-Boc), based on the desired x/y feed ratio. Such protection was necessary to prevent grafting-type side reactions from proceeding during the propagation step. Upon the addition of the second amine comonomer (H_2N-R) the experiments were continued. In the propagation sequence of this scheme, the terminal amino groups of the amine co-reactants act as bifunctional sites, undergoing double addition with resultant formation of *tert*-amine functionality in the main chain, precluding three-dimensional crosslinking. Therefore, considerably higher reactant (H_2N-R) concentrations (1.5-3 M) could be used. A brief treatment with ethanolamine (EA) to eliminate any terminal unsaturation was followed by solvent removal, treatment with trifluoroacetic acid for N-deprotection, and acid removal under reduced pressure. The crude target polymers were worked up by aqueous dialysis in tubing with 12 000 - 14 000 and 25 000 molecular weight cut-off tubing, and were isolated in the solid state upon freeze-drying. The products possessed complete solubility in water and, as required, in methanol. They were structurally characterized by comparison of the CONH*CH*$_2$NHCO methylene proton resonance near 4.5 ppm with other prominent bands in the ^{1}H NMR spectra. The preparation is depicted in the Scheme 4.5 below.



Scheme 4.5:Synthesis of poly(amidoamines) bearing extrachain hydrosolubilizing groups

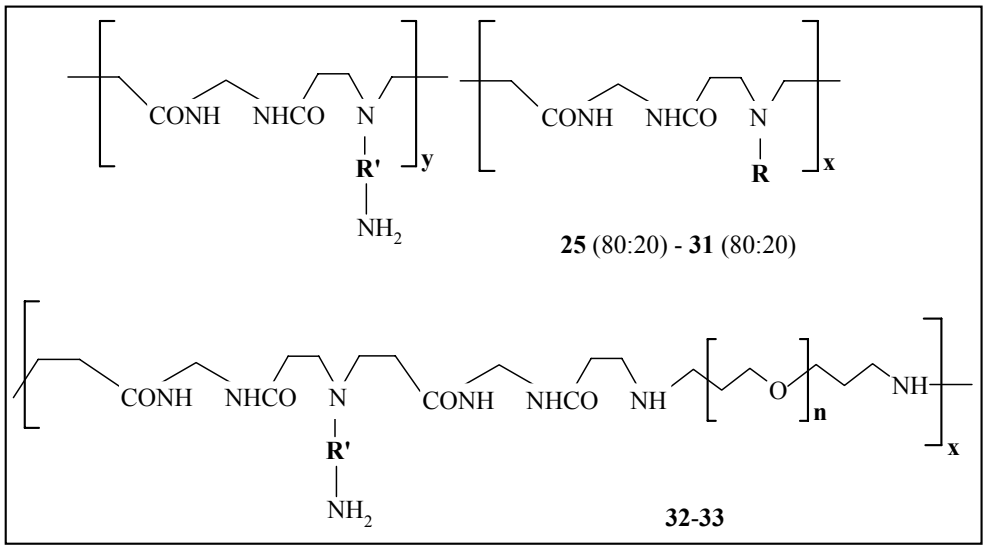
PAAs bearing intrachain hydrosolublizing groups: Contrasting with Scheme 4.5 which shows the synthesis of poly(amidoamines) (**25-31**) in which the side groups serve as solubilizing entities, Scheme 4.6 depicts PAAs comprising the solubilizing units as main chain segments. The synthesis is also a two-step process. In the first step, MBA was reacted with 0.5 equivalents of a mono-N-protected diamine in aqueous isopropanol medium. The bis(acrylamido)-terminated macromonomer so generated was allowed in the second step to copolymerized with primary diamines of the poly(ethylene oxide)-type H_2N-$CH_2(CH_2CH_2O)_{\mathbf{n}}(CH_2)_3NH_2$, where **n** = 3 and 32, thus giving polymers **32** and **33**, respectively. The polymerization and work-up conditions were slightly different to those leading to **25-31**. These monomers bearing two primary amino groups would be expected to react tetrafunctionally in the polyaddition reactions, as the intermediary secondary amino groups, although inherently less reactive, are prone to further addition. The ultimate products would come out as gels generated

by three-dimensional crosslinking, as already experienced earlier by Ferruti [159] and co-workers. In our work, in order to circumvent such crosslinking, we applied more selective conditions, including low reactant concentrations and low initial temperature, were required in order to ensure monofunctional reactivity of the $-NH_2$ terminals in the diamine. Thus, reactions were typically carried out by allowing MBA and diamine, 0.2-0.4 M each, to copolymerize. The temperature was maintained at 0-5°C during the first 24h of the reaction and the water-soluble product was thoroughly purified and crudely fractionated by exhaustive aqueous dialysis in a membrane tubing with a molecular weight cut-off limit of 25 000. It was isolated in the solid state by freeze-drying, with water and methanol solubility retained



Scheme 4.6: Synthesis of poly(amidoamines) bearing intrachain hydrosolubilizing groups

Table 4.10: Composition of primary amine-functionalized PAAs



Carriers	R	R´	x/y	n
25 (80:20)	$-(CH_2)_2N(CH_3)_2$	$-(CH_2)_3-$	4	
26 (80:20)	$-(CH_2)_3N(CH_3)_2$	$-(CH_2)_3-$	4	
27 (80:20)	$-(CH_2)_3N(CH_3)_2$	$-(CH_2)_2\,NH(CH_2)_2-$	4	
28 (80:20)	$-(CH_2)_2N(CH_3)_2$	$-(CH_2)_2\,O(CH_2)_2O(CH_2)_2-$	4	
29 (80:20)	$-(CH_2)_3N(CH_3)_2$	$-(CH_2)_2\,O(CH_2)_2O(CH_2)_2-$	4	
30 (80:20)	$-(CH_2)_2O(CH_2)_2OH$	$-(CH_2)_3-$	4	
31 (80:20)	$-(CH_2)_2O(CH_2)_2OH$	$-(CH_2)_2\,O(CH_2)_2O(CH_2)_2-$	4	
32		$-(CH_2)_3-$		**3**
33		$-(CH_2)_3-$		**32**

The constituent R, represented by a dimethylaminoalkyl residue in polymers **25**-**29**, imparts cationic behaviour to the molecule under physiological pH conditions. This feature entails potential pharmacokinetic benefits which afford facilitated

pinocytotic cell entry of the molecule in biomedical applications [111, 159]. When introduced into related polyamide-based drug conjugates, the dimethylaminoalkyl functionality has generally been found to provide superior cytotoxic activity in cell culture tests against cancer lines [141, 160].

For comparison a hydroxyl-terminated side chain incapable of adding to the polymers' cationic behaviour has been incorporated in **30** and **31**. The R´ segment represents various short-chain aliphatic spacers designed to provide spacing between the main chain and the drug.

As already mentioned, the PEO chains were introduced into MBA by virtue of their numerous properties, namely, high hydrophilic character, nontoxicity, blood compatibility, lower immunogenicity and antigenicity. Therefore, the presence of the PEO segments in the chain of polyamidoamines **32** and **33** is expected to improve both the physico-chemical and pharmacokinetic properties of these polymeric carriers.

Experimental variables and viscometric and ^{1}H NMR data are summarized in Table 4.11 and 4.12, respectively.

Table 4.11: Summary of preparative data for PAA carriers

Reactants in feed (mol-%) [a]			**Reaction conditions** [c]	**PAA carriers**	
R-NH_2	**H_2N-R´-NH-Boc**	**Mole ratio x/y** [b]		**Yield** (%) [d]	**Designation**
DME (80)	Boc-PDA (20)	4	(1) 48h, 25-50^{0}C ; (2) 48h, 60^{o}C then 1h, RT	22.1	**25** (80:20)
DMP (80)	Boc-PDA (20)	4	´´	16.8	**26** (80:20)
DMP (80)	Boc-DET (20)	4	´´	16.8	**27** (80:20)
DME (80)	Boc-EDDA (20)	4	´´	15.5	**28** (80:20)
DMP (80)	Boc-EDDA (20)	4	´´	18.4	**29** (80:20)
AEE (80)	Boc-PDA (20)	4	´´	15.7	**30** (80:20)
AEE (80)	Boc-EDDA (20)	4	´´	18.4	**31** (80:20)
TRIA (50)	Boc-PDA (50)		(1) 72h, 25^{o}C; (2) 24h, 0^{o}C then 48h, 50^{o}C and 1h at RT	16	**32**
PEO_{1500} (50)	Boc-PDA (50)		´´	23.19	**33**

[a] Parenthetic numbers indicate the number of moles of amino compound per 100 base moles of MBA (methylenebisacrylamide).

DME = 3-(N,N-dimethylamino)ethylamine, TRIA = 4,7,10-trioxa-1,13-tridecanediamine; PEO = O,O´-bis(3-aminopropyl)poly(ethylene glycol) 1500.

[b] Mole ratio (used) of hydrosolubilizing to drug-anchoring groups.

[c] RT= room temperature; reaction step sequence in parenthesis.

[d] Polymer yield after ultimate (25 000 molecular weight cut-off) dialysis.

Table 4.12: ^{1}H NMR and viscometric data for PAA carriers

PAA carriers				**Number of protons counted** [d] (expected) [e] **chemical shift** (ppm)				
Designation	η_{inh} (mL g^{-1}) [a]	**x/y** [b]	**Base molecular weight** [c]	δ.4.8-4.5 [f]	δ 3.7-3.5	δ 3.0-2.8	δ 2.7-2.0	δ 1.8-1.5
25 (80:20)	24.29	4	1197.6	10(10)		21(20)	65(66)	2(2)
26 (80:20)	17.5	4	1253.7	10(10)		21(20)	66(66)	10(10)
27 (80:20)	16.86	4	1281.7	10(10)		22(20)	68(70)	7(8)
28 (80:20)	20.98	4	1271.7	10(10)	8(8)	22(20)	66(66)	
29 (80:20)	18.45	4	1327.8	10(10)	8(8)	21(20)	64(64)	8(8)
30 (80:20)	20.10	4	1265.5	10(10)	24(24)	20(20)	33(32)	2(2)
31 (80:20)	16.98	4	1339.6	10(10)	31(32)	20(20)	33(32)	
32	15.58		602.8	4(4)	12(12)	8(8)	15(16)	6(6)
33	14.17		1880.4	4(4)	130(128)	9(8)	16(16)	5(6)

[a] At 30.0 ± 0.5 °C, in deionized H_2O; concentration c= 2 mg/mL.

[b] Mole ratio (found) of hydrosolubilizing to drug-anchoring groups after ^{1}H NMR integration.

[c] Molecular weight of the simplest recurring unit (normalized to y=1 for 25-31) rounded off to the nearest integer.

[d] In D_2O, pH 10-11, chemical shifts, δ/ppm, referenced against internal sodium 3-trimethylsilyl-2,2,3,3-d_4-propionate; integration error limits ± 12 %.

Protons are calculated (figures rounded off to the nearest integer) on basis of found x/y ratios.

[e] Expected count for composition in accordance with recurring unit (see b).

[f] Proton assignment, δ/ppm: 4.6-4.5 (CONH*CH*$_2$HNCO), 3.8-3.5 (O*CH*$_2$*CH*$_2$O), 3.0-2.8 (CO*CH*$_2$), 2.7-2.0 (*CH*$_2$N(*CH*$_3$)$_2$, *CH*$_2$NH$_2$, *CH*$_2$N(CH$_2$CH$_2$)), 1.8-1.5 (CH$_2$*CH*$_2$CH$_2$).

As indicated in Table 4.11, the experimental yields for the PAAs were quite low (15-23%). This was in accordance with previous reports from diverse laboratories [104, 109, 111]. Indeed, polymerization reactions involving Michael additions are inherently inefficient, because, while requiring an aqueous or partially aqueous solvent system for efficacious propagation, the growing polymer chains are susceptible to hydrolytic fission at the labile amide link constituents of the bisacrylamide monomers. Hence, the two reaction sequences militate against each other, and any polymerization will invariably provide a compromise between propagation and depropagation. As a result, the molecular weight distribution of the polymer products will be unduly wide. In order to collect polymers in the desired molecular weight range of 20 000 and higher, which are required for acceptably extended serum residence times, one has to resort to fractionation techniques, which cut off all material that is substantially below the stated limit. Since this material constitutes the bulk of the polymerization product, the ultimate yields of the desired fractions, depending critically on the relative hydrolytic stability of the monomers used, are generally quite low. However, these low yields were accepted in this study as the price to be paid for obtaining material in the proper molecular size.

Some properties of the PAAs are compiled in Table 4.13. According to this table the weight-average molecular weight and the polydispersity indices are in the 11 000 - 65 000, and 1.4-2.7 range, respectively. The inherent viscosities (Table 4.12) for all the polymers are in the 14-24 mL g^{-1} range. The average-molecular-weights were very variable among them. In accordance with the biomedical requirements already mentioned (section 4.1), only polymers **25**, **28**, **32** and **33** characterized (M_w = 65 360; 52 000; 28 830 and 23 000, respectively) could be used as drug carriers. Although the increasing molecular-weight of polymers **33**, **32**, **28** and **25** corresponds to an increase in inherent viscosity, one could not correlate the trend of viscosity with that of the molecular-weight in general. For example, polymer **29** (M_w =14 880; viscosity, 18.45 mL g^{-1}) has lower-molecular-weight than polymer **32** (M_w = 28 830; viscosity, 15.58 mL g^{-1}).

Moreover, the polymers: **26**, **27**, and **29**, have molecular-weight of 11 000; 13 000; and 14 880 respectively; this is well below the cut-off limit of 25 000 used in dialysis. These low molecular-weight could be explained by the well-established fact that ionic and branched polymers act as rigid, comb-like structures in solution, for that reason, their hydrodynamic volume is greater compared to their linear and neutral analogs [161]. It just means that they appear bigger than their normal size in the dialysis tube, and therefore do not go through the membrane.

Table 4.13: GPC characteristics of poly(amidoamine) carriers

Designation	η_{inh} (mL g^{-1})	M_w x10^{-3}	M_n x10^{-3}	I_n
25 (80:20)	24.29	65.36	23.99	2.73
26 (80:20)	17.5	11.02	6.24	1.72
27 (80:20)	16.86	13.21	6.3	2.09
28 (80:20)	20.98	52.00	24.76	2.1
29 (80:20)	18.45	14.88	5.59	2.66
32 (**n** = 3)	15.58	28.83	20.74	1.39
33 (**n** = 32)	14.17	23.44	11.32	2.07

The solid-state IR spectra of all polymers **25-33** showed a broad amide I band in the region 1680-1610 cm^{-1}, a tertiary amine band at 1400-1340 cm^{-1} as well as a strong methyl band at 1460 cm^{-1} corresponding to $N(CH_3)_2$. The band at 1060 cm^{-1}, corresponding to the ether bond was noticeable in polymers **28-33**, and was particularly remarkable in **33** owing to the presence of the PEO segment (**n** = 32). The *OH* band was also visible as a broad band in the region 3400-3200 cm^{-1} of the spectra of polymers **30** and **31**.

The ^1H NMR spectra (400 MHz measured in D_2O solutions) were recorded at pH 10-11 (adjusted with NaOH) in order to preclude any protonation effects. These spectra showed several groups of bands which were occasionally superimposed upon each other. Thus, the methylene protons of $CONHCH_2HNCO$ group were prominent in the 4.6-4.5 ppm region. The methylene protons of OCH_2CH_2O were

grouped in the 3.8-3.5 ppm region and those of CO*CH*$_2$ in 3.0-2.8 ppm region. The band appearing in the 2.7-2.0 ppm region was assigned to the methylene and methyl protons of *CH*$_2$N (*CH*$_3$)$_2$, *CH*$_2$-NH$_2$, and CH$_2$-N (*CH*$_2$) (CH$_2$) groups. The band in the 1.8-1.5 ppm region was assigned to methylene protons of the CH$_2$*CH*$_2$CH$_2$ group.

The mol-% of drug binding primary amino groups in polymers **25** and **30** was found to be 20% by comparing the integral of the signal in the 1.8-1.5 ppm region, assigned to the methylene protons of CH$_2$*CH*$_2$CH$_2$ group originating exclusively from PDA monomer, with the integral of the signal near 4.5 ppm assigned to MBA. As indicated in Table 4.12, in a similar fashion, polymers **28** and **29** were found to possess 20 mol-% NH$_2$ groups by considering the methylene protons of O*CH*$_2$*CH*$_2$O originating exclusively from the EDDA monomer. This method was not applicable to other PAAs, as the characteristic protons of the spacers were also found either in both the main chain and the side chain of the hydrosolubilizing group or in one of them. However, the number of protons derived from the ^{1}H NMR spectra of these PAAs and those provided by the recurring units coincide. Thus, polymers **26**, **27** and **31** were found to contain 20 mol-% NH$_2$, while **32** and **33** possess 100 mol -% NH$_2$.

4.2. Polymer Drug Conjugation

The numerous carriers of polyaspartamide and poly(amidoamine)-type, which featured primary amino side groups, were used to anchor drug systems *via* the formation of biofissionable amide groups between the carrier and the drugs.

The first drug investigated was methotrexate. Investigation of the ferrocene-type drug followed. Finally, each of these drugs was co-conjugated with folic acid.

4.2.1 Polymer-methotrexate conjugates

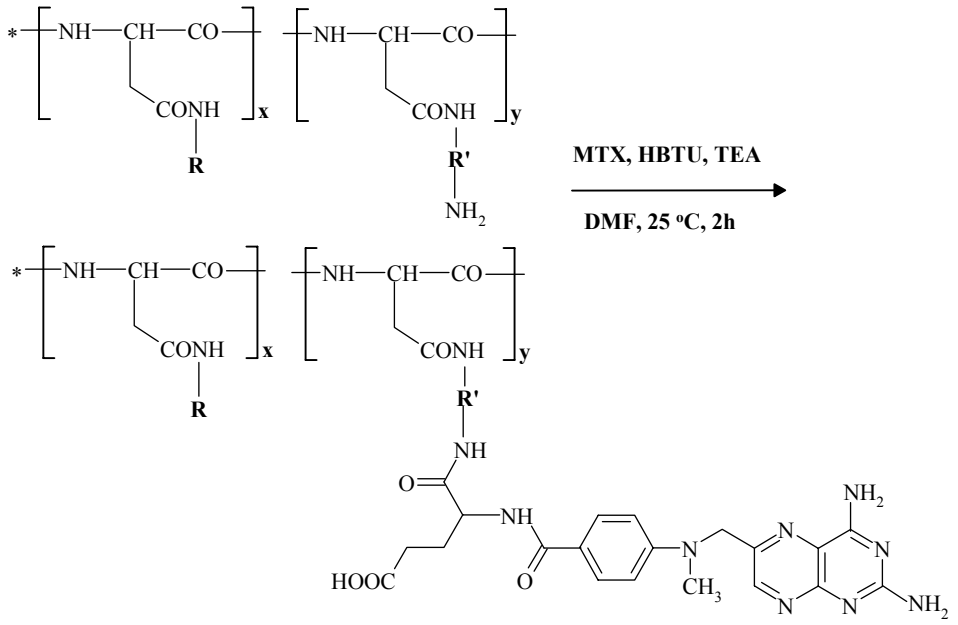
The literature provides numerous examples of MTX anchoring, which involves the covalent reversible attachment of the carrier through amide bond formation. Anchoring of MTX by coupling with the aid of water-soluble carbodiimides such

as 1-ethyl-3-(3´-dimethylaminopropyl)carbodiimide hydrochloride has been the preferred technique in these studies [127, 162]. Proteinaceous carriers have been used in the coupling process and these reactions were conducted in aqueous phase.

Coupling in anhydrous media such as N,N-dimethylformamide (DMF) has generally been brought about through the intermediacy of *in situ* presynthesized, active N-succinimide esters. In this laboratory, these active esters, especially if applied in higher mole ratios, tended to cause gradual crosslinking of the ultimate conjugates, presumably because of the presence of bifunctionally active drug molecules. The preferred method herein adopted therefore involved the direct acid-amine coupling, which was mediated by the HBTU coupling agent, 2-(1H-benzotriazol-1-yl)-1,1,3,3-tetramethyluronium hexafluorophosphate. The coupling reactions were performed by treatment of the carrier with MTX, an organic base, and HBTU for 2 hours at ambient temperature in DMF solution. MTX: NH_2 molar reactant ratios typically employed were 1.2 or 1.3. Under these conditions, MTX binding in most experiments approached the 100% level. However, in polymer-homologous reactions, such as carrier-drug conjugation, one commonly observes greater variability than in analogous non-polymeric processes. Accordingly, coupling experiments occasionally failed to achieve an extent of conjugation larger than 70-90%, with corresponding proportions of the drug binding left intact in the conjugates. These required a retreatment with drug, base, and coupling agent, and in the resulting conjugates essentially complete anchoring was generally achieved. The actual binding site on the glutamyl constituent of the drug in these reactions is unknown. In the conjugate structures shown in the project, binding has been ascribed to the α-carboxyl group. The arbitrary choice was corroborated by a literature report, which gave preference to that group as the more reactive one in coupling reactions with polylysine [163]. It may be recalled, parenthetically, that MTX-dihydrofolate reductase binding likewise involves the drug's α-carboxyl group [164], although steric factors in the complex may contribute to this regiospecific binding.

4.2.1.1 Preparation of polyaspartamide-MTX conjugates

The target conjugates **1**(90:10)-**MTX** to **18**(80:20)-**MTX** were prepared from polyaspartamides **1-18** by amide bond formation with MTX. As described above, the amidation reactions are depicted in Scheme 4.7.



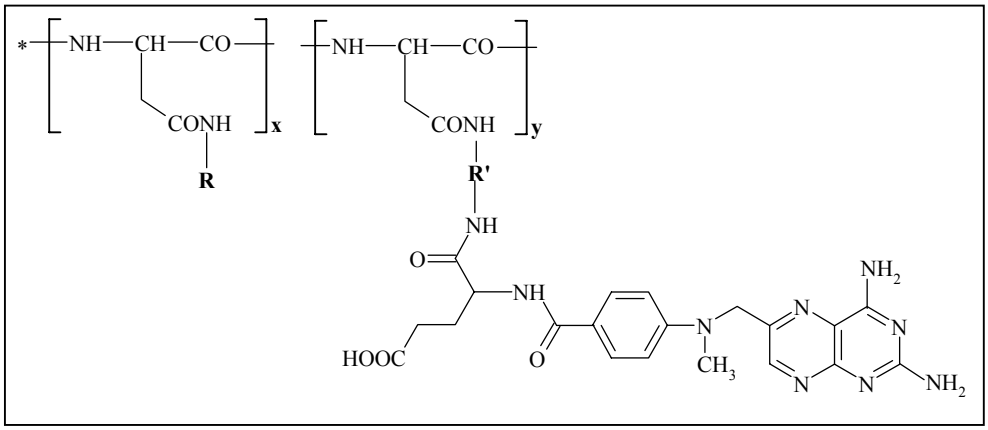
Scheme 4.7: Preparation of polyaspartamide-MTX conjugates

In the case of DAP spacer-type carriers, the hydroxyl group, by virtue of its position, could provoke steric hindrance, thus reducing the accessibility to the primary amino drug-binding group. Therefore, the reaction period was extended to 3h.

The polymer-MTX conjugates, after precipitation, were isolated upon centrifugation, and subjected to size exclusion chromatography with Sephadex gel G-25. The gel has a molecular weight cut-off limit in the 1 000 - 5 000 range. Thus, the unreacted drug (M_w 454.45) and by-products were removed by this process. The resulting eluates were ultimately subjected to staged aqueous dialysis in 25 000 cut-off membrane tubing under carefully controlled pH conditions. The aim was to remove lower-molecular-weight products that are inadequate for biomedical applications. The ultimate product yields typically ranged from 41 to 80%. The efficiency of the purification process was confirmed by thin layer

chromatography (TLC). Indeed, TLC of an aqueous solution of conjugates (acidified to pH~3-4 with addition of hydrochloric acid) revealed an R_f value of zero (0.9 for free MTX) when eluted with methanol-water-ammonia (40:10:1, v/v/v).

Table 4.14: Composition of PAsA-MTX conjugates



Carriers	R	R´	Conjugates designation
1 (90:10)	$-(CH_2)_3N(CH_3)_2$	$-(CH_2)_3-$	**1** (90:10)-**MTX**
2 (80:20)	$-(CH_2)_3N(CH_3)_2$	$-(CH_2)_3-$	**2** (80:20)-**MTX**
3 (90:10)	$-(CH_2)_3N(CH_3)_2$	$-(CH_2)_2NH(CH_2)_2-$	**3** (90:10)-**MTX**
4 (80:20)	$-(CH_2)_3N(CH_3)_2$	$-(CH_2)_2NH(CH_2)_2-$	**4** (80:20)-**MTX**
5 (90:10)	$-(CH_2)_3N(CH_3)_2$	$-(CH_2)_2O(CH_2)_2O(CH_2)_2-$	**5** (90:10)-**MTX**
6 (80:20)	$-(CH_2)_3N(CH_3)_2$	$-(CH_2)_2O(CH_2)_2O(CH_2)_2-$	**6** (80:20)-**MTX**
7 (90:10)	$-(CH_2)_3N(CH_3)_2$	$-CH_2CHOHCH_2-$	**7** (90:10)-**MTX**
8 (90:10)	$-(CH_2)_2OH$	$-(CH_2)_2NH(CH_2)_2-$	**8** (90:10)-**MTX**
9 (80:20)	$-(CH_2)_2OH$	$-(CH_2)_2NH(CH_2)_2-$	**9** (80:20)-**MTX**
10 (90:10)	$-(CH_2)_2OH$	$-CH_2CHOHCH_2-$	**10** (90:10)-**MTX**
13 (90:10)	$-(CH_2)_2O(CH_2)_2OH$	$-(CH_2)_2NH(CH_2)_2-$	**13** (90:10)-**MTX**
15 (90:10)	$-(CH_2)_2O(CH_2)_2OH$	$-(CH_2)_3-$	**15** (90:10)-**MTX**

Table 4.14 continued

Carriers	R	R´	Conjugates designation
16 (90:10)	$-(CH_2)_2O(CH_2)_2OH$	$-CH_2CHOHCH_2-$	**16** (90:10)**-MTX**
17 (90:10)	$-(CH_2)_2OCH_3$	$-(CH_2)_2NH(CH_2)_2-$	**17** (90:10)**-MTX**
18 (80:20)	$-(CH_2)_2OCH_3$	$-(CH_2)_2NH(CH_2)_2-$	**18** (80:20)**-MTX**

Pertinent reaction variables and conjugate yields are summarized in Table 4.15, while the ^{1}H NMR and viscometric results of the PAsA-MTX conjugates are shown in Table 4.16. The MTX contents (mass percentage) were determined by ^{1}H NMR spectroscopy by assessing the relative intensities of the aromatic resonances in the 8.5-6.5 ppm region against prominent bands in the spectra. Table 4.17 summarizes all analytical results including GPC characteristics of these conjugates.

Table 4.15: Reaction variables for PAsA-MTX conjugates

Reactants in feed				**Reaction conditions** [b]	**PAsA-MTX conjugates**	
Carriers	**Coupling agent**	**Carrier : drug : coupling agent ratio** (mol-%) [a]	**Medium**		**Yield** (%) [c]	**Designation**
1 (90:10)	HBTU	1:1.2:1.1	DMF	2h, RT	61	**1** (90:10)-**MTX**
2 (80:20)	,,	,,	,,	,,	53	**2** (80:20)-**MTX**
3 (90:10)	,,	1:1.2:1.1 then 1:0.8:0.5	,,	2h then 4h, RT	41	**3** (90:10)-**MTX**
4 (80:20)	,,	,,	,,	,,	48	**4** (80:20)-**MTX**
5 (90:10)	,,	,,	,,	,,	43	**5** (90:10)-**MTX**
6 (80:20)	,,	,,	,,	,,	42	**6** (80:20)-**MTX**
7 (90:10)	,,	1:1.2:1.1	,,	3h, RT	73	**7** (90:10)-**MTX**
8 (90:10)	,,	,,	,,	2h, RT	63	**8** (90:10)-**MTX**
9 (80:20)	,,	,,	,,	,,	55	**9** (80:20)-**MTX**
10 (90:10)	,,	,,	,,	3h, RT	74	**10** (90:10)-**MTX**

Table 4.15 continued

Reactants in feed				Reaction conditions [b]	PAsA-MTX conjugates	
Carriers	**Coupling agent**	**Carrier : drug : coupling agent ratio** (mol-%) [a]	**Medium**		**Yield** (%) [c]	**Designation**
13 (90:10)	HBTU	1:1.2:1.1	DMF	2h, RT	71	**13** (90:10)-**MTX**
14 (80:20)	,,	1:1.2:1.1 then 1:0.8:0.5	,,	2h then 4h, RT	54	**14** (80:20)-**MTX**
15 (90:10)	,,	1:1.2:1.1	,,	2h, RT	67	**15** (90:10)-**MTX**
16 (90:10)	,,	,,	,,	3h, RT	80	**16** (90:10)-**MTX**
17 (90:10)	,,	,,	,,	2h, RT	77	**17** (90:10)-**MTX**
18 (80:20)	,,	,,	,,	,,	66	**18** (80:20)-**MTX**

[a] Molar ratio of carrier repeating unit to MTX to coupling agent.

[b] RT= room temperature.

[c] Conjugate yield after size exclusion chromatography and ultimate (25 000 molecular weight cut-off) dialysis.

Table 4.16: ^{1}H NMR and viscometric results for the PAsA-MTX conjugates

Conjugates designation	**η_{inh}** (mL g^{-1}) [a]	**x/y** [b]	**Base molecular weight** [c]	**% MTX** Calcd [d]	**% MTX** NMR [e]	**Protons counted** [g] (expected) [h] **chemical shift** (ppm)		
						δ 8.5-6.5 [f]	δ 3.7-3.6	δ 1.8-1.5
1 (90:10)-**MTX**	16.15	9.2	2392.2 (2400.9)	18.93	18.6	4.90 (5)		20 (20)
2 (80:20)-**MTX**	19.95	4.2	1391.6 (1404.6)	32.36	31.68	4.85 (5)		10 (10)
3 (90:10)-**MTX**	16.75	9	2429.9 (2429.9)	18.7	18.7	5 (5)		18 (18)
4 (80:20)-**MTX**	20.18	4.2	1416.3 (1433.7)	31.7	30.81	4.80 (5)		8 (8)
5 (90:10)-**MTX**	15.42	9.2	2461.9 (2475)	18.36	17.91	4.85 (5)		18 (18)
6 (80:20)-**MTX**	21.08	4.1	1465.7 (1478.8)	30.7	30.08	4.85 (5)		8 (8)
7 (90:10)-**MTX**	15.94	9.2	2408.2 (2416.9)	18.8	18.5	4.90 (5)		18 (18)
8 (90:10)-**MTX**	18.66	9.4	2042.7 (2060.1)	22.06	21.36	4.80 (5)	18 (18)	
9 (80:20)-**MTX**	17.5	4.2	1247.6 (1269.3)	35.8	34.61	4.75 (5)	8 (8)	
10 (90:10)-**MTX**	16.5	9.4	2025.3 (2047.0)	22.2	21.31	4.75 (5)	19 (19)	

Table 4.16 continued

Conjugates designation	η_{inh} (mL g^{-1}) [a]	**x/y** [b]	**Base molecular weight** [c]	% **MTX** Calcd [d]	% **MTX** NMR [e]	**Protons counted** [g] (expected) [h] **chemical shift** (ppm) δ 8.5-6.5[f]	δ 3.7-3.6
13 (90:10)-**MTX**	16.25	9	2456.6 (2456.5)	18.5	18.5	5 (5)	54 (54)
14 (80:20)-**MTX**	15.95	4	1445.6 (1445.5)	31.4	31.4	5 (5)	24 (24)
15 (90:10)-**MTX**	12.35	9.5	2405.8 (2427.5)	18.72	17.95	4.75 (5)	54 (54)
16 (90:10)-**MTX**	14.87	9.1	2439.2 (2443.5)	18.6	18.45	4.95 (5)	55 (55)
17 (90:10)-**MTX**	19.85	9.4	2169.0 (2186.3)	20.79	20.12	4.80 (5)	45 (45)
18 (80:20)-**MTX**	21.98	4	1321.1 (1325.4)	34.3	34.06	4.95 (5)	20 (20)

[a] At 30.0 ± 0.5 °C, in deionized H_2O; concentration c = 2 mg/mL.
[b] Mole ratio (found) of hydrosolubilizing to drug-anchoring groups after ^1H NMR integration.
[c] Molecular weight, actual (in parenthesis, calculated for 100% acylation).
[d] Derived from 100% acylation.
[e] Derived from ^1H NMR spectrum (error limit ± 12%).
[f] In D_2O, pH 10-11, chemical shifts, δ/ppm, referenced against internal sodium 3-trimethylsilyl-2,2,3,3-d_4-propionate; integration error limits ± 12 %. Protons are calculated for the structural representations in Table 4.14.
[g] Expected count for composition in accordance with recurring unit (see b).
[h] Assignment: δ/ppm: 8.6-6.6 (aromatic and heteroaromatic *CH* of MTX); 3.8-3.5 (CH_2O; *CH*-OH; OCH_3); 1.8-1.5 ($CH_2CH_2CH_2$).

Table 4.17: Summary of analytical results for all PAsA-MTX conjugates

Conjugates designation	η_{inh} (mL g^{-1})	$M_w x10^{-3}$	$M_n x10^{-3}$	I_n	% MTX Calcd [a]	% MTX UV-ε_{370} [b]	% MTX NMR [c]	NH_2 acylation (%) UV [d]	NH_2 acylation (%) NMR [e]
1 (90:10)-**MTX**	16.15	26.35	17.0	1.55	18.93	18.30	18.6	97	98
2 (80:20)-**MTX**	19.95	32.2	18.68	1.74	32.36	30.75	31.68	95	97
3 (90:10)-**MTX**	16.75	28.25	14.49	1.95	18.7	18.36	18.7	98	100 [f]
4 (80:20)-**MTX**	20.18	33.03	15.3	2.17	31.7	29.8	30.81	94	96 [f]
5 (90:10)-**MTX**	15.42	25.2	15.27	1.65	18.36	18.05	17.91	98	98 [f]
6 (80:20)-**MTX**	21.08	35.03	18.07	1.94	30.7	29.75	30.08	97	97 [f]
7 (90:10)-**MTX**	15.94	* [g]	*	*	18.8	18.2	18.5	~97	98
8 (90:10)-**MTX**	18.66	31.86	18.21	1.75	22.06	20.85	21.36	95	96
9 (80:20)-**MTX**	17.5	*	*	*	35.8	33.02	34.61	92	95 [f]
10 (90:10)-**MTX**	16.5	*	*	*	22.2	20.65	21.31	93	95

Table 4.17 continued

Conjugates designation	η_{inh} (mL g^{-1})	$M_w x10^{-3}$	$M_n x10^{-3}$	I_n	% **MTX** Calcd [a]	% **MTX** UV-ε_{370} [b]	% **MTX** NMR [c]	**NH_2 acylation** (%) UV [d]	**NH_2 acylation** (%) NMR [e]
13 (90:10)-**MTX**	16.25	*	*	*	18.5	18.25	18.5	99	100
14 (80:20)-**MTX**	15.95	*	*	*	31.14	30.95	31.4	99	100 [f]
15 (90:10)-**MTX**	12.35	*	*	*	18.72	17.65	17.95	94	95
16 (90:10)-**MTX**	14.87	*	*	*	18.6	18.04	18.45	97	99
17 (90:10)-**MTX**	19.85	31.9	17.06	1.87	20.79	19.65	20.12	95	96
18 (80:20)-**MTX**	21.98	66.17	31.88	2.08	34.3	33.6	34.06	98	99

[a] Mass percentage calculated for 100% acylation.

[b] From UV-vis absorbance of bound MTX in H_2O at 370 nm using $\varepsilon = 6500\ cm^{-1}M^{-1}$.

[c] Derived from ^1H NMR spectrum (error limit ± 12%).

[d] Ratio of b to a.

[e] Ratio of c to a.

[f] In parallel experiments conducted under identical or modified conditions, percentage acylation ranged from 66-85%, requiring retreatment.

[g] Non-determined.

As can be seen from Table 4.16, the inherent viscosities of the polyaspartamide-MTX conjugates are in the 14-22 mL g^{-1} range. For those determined, the average molecular weights range from 25 000 to 66 000, and the polydispersity indices are in the 1.5-2 range. These conjugates show an increase in both molecular weights and inherent viscosities compared to the derived polymeric carriers, thus indicating incorporation of drug molecules into the polymer chain to proceed without major chain cleavage during the conjugation process. There is a fair match between the trend of molecular weight and inherent viscosity, the molecular weight increasing with increase in the inherent viscosity for these conjugates. One could speculate that since such relation was not observed in the parent carriers, the ultimate dialysis process of the conjugates in the 25 000 cut-off membrane tubing might have eliminated lower-molecular-weight fractions However, these results should be considered cautiously since the observations were made on small numbers of conjugates.

The solid-state IR spectra of polyaspartamide-MTX conjugates commonly revealed a broad amide I band in the region 1680-1610 cm^{-1}, and the band at 1580 cm^{-1} is attributable to amide II band. The spectra of conjugates **1**(90:10)-**MTX** to **7**(90:10)-**MTX** retained the majority of bands present in the spectra of the parent polymeric carriers **1**-**7**. Thus, the tertiary amine band as well as the weak methyl band assigned to N(CH_3)$_2$ were present in the region 1400-1340 cm^{-1} and at 1460 cm^{-1}, respectively. The spectra of conjugates **5**(90:10)-**MTX** and **6**(80:20)-**MTX** exhibited a strong asymmetric band at 1060 cm^{-1}, which is attributable to –CH_2-O-CH_2- of EDDA. The *OH* band of DAP was also visible as a broad band in the region 3400-3200 cm^{-1} of the spectrum of **7**(90:10)-**MTX** conjugate.
The spectra of conjugates **8**(90:10)-**MTX** to **16**(90:10)-**MTX** showed a broad *OH* band in the 3400-3200 cm^{-1} region. The ether *CH-O-CH* stretching mode to which the band at 1060 cm^{-1} is attributable was also seen in the spectra of conjugates **13**(90:10)-**MTX** to **18**(80:20)-**MTX**.

MTX contents (mass percentage) were determined from the ^{1}H NMR spectra of the conjugates. This was achieved by assessing the relative intensities of the aromatic resonances in the 8.5-6.5 ppm region, characteristic of the drug, against

other prominent bands assigned to the polymeric carriers. Thus, in spectra of conjugates **1**(90:10)-**MTX** to **7**(90:10)-**MTX**, the methylene $CH_2CH_2CH_2$ proton peak was chosen as it did not overlap with other signals. The MTX contents were in the range of 18-31% by mass. UV-visible spectroscopy was also used to assess MTX content in these conjugates. This was achieved using the molar extinction coefficient, $\varepsilon = 6500\ mol^{-1}cm^{-1}$ and the absorbance at $\lambda = 370$ nm in H_2O. The determined values also ranged from 18 to 31%. These drug contents indicated the extent of primary amino group acylation, calculated either by ^1H NMR or UV spectroscopy, to be in the range of 94-100%. Conjugates **3**(90:10)-**MTX** to **6**(80:20)-**MTX**, having initially achieved an extent of conjugation lower than 90%, were retreated with 0.8 equivalents of the drug, 0.5 equivalents of HBTU coupling agent, and 1 equivalent of the organic base. The reaction was conducted at room temperature for a period of 4h. A 96-100% extent of conjugation was attained as shown in Table 4.17.

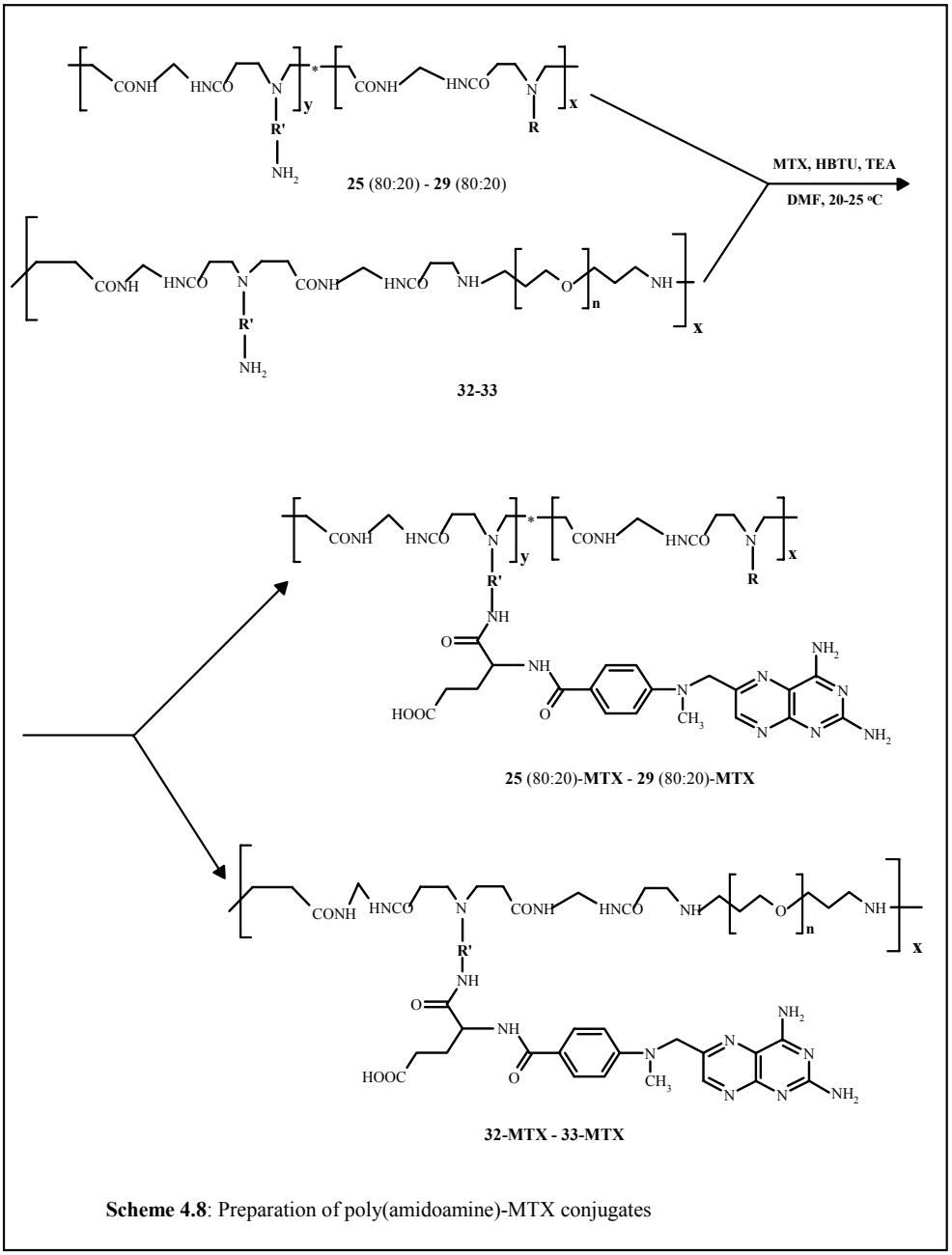
For conjugates **8**(90:10)-**MTX** to **18**(80:20)-**MTX**, the drug contents were assessed by using the integral of the signals in the 3.7-3.6 ppm region. The signals in this region are assigned to methine (*CH*-OH), methylene (CH_2O) and methyl (OCH_3) protons, and are characteristic of the polymeric carriers with hydroxyl- or methoxy-terminated side groups. The drug contents were in the range of 17 to 34% by mass. This corresponds to an extent of conjugation of 92-100%. These values were in a fair agreement with those found by UV spectroscopy.

On balance, for the polyaspartmide-MTX conjugates, the drug contents determined either by ^1H NMR or UV spectroscopy wa in excellent agreement with those provided by the proposed structures. This led to two pertinent deductions: Firstly, the purification process (combination of size exclusion chromatography and exhaustive dialysis) was efficient as it afforded conjugates devoid of free drug. The presence of free drug in the conjugates would distort the biological evaluation of these conjugates, resulting in erroneous data. Secondly, the conjugates did not undergo molecular association in aqueous solution under the conditions of NMR experiments; such self-assembly would cause MTX signal

attenuation in the NMR spectra as observed with MTX conjugates based on poly(ethylene oxide)-terminated block-copolymers [165].

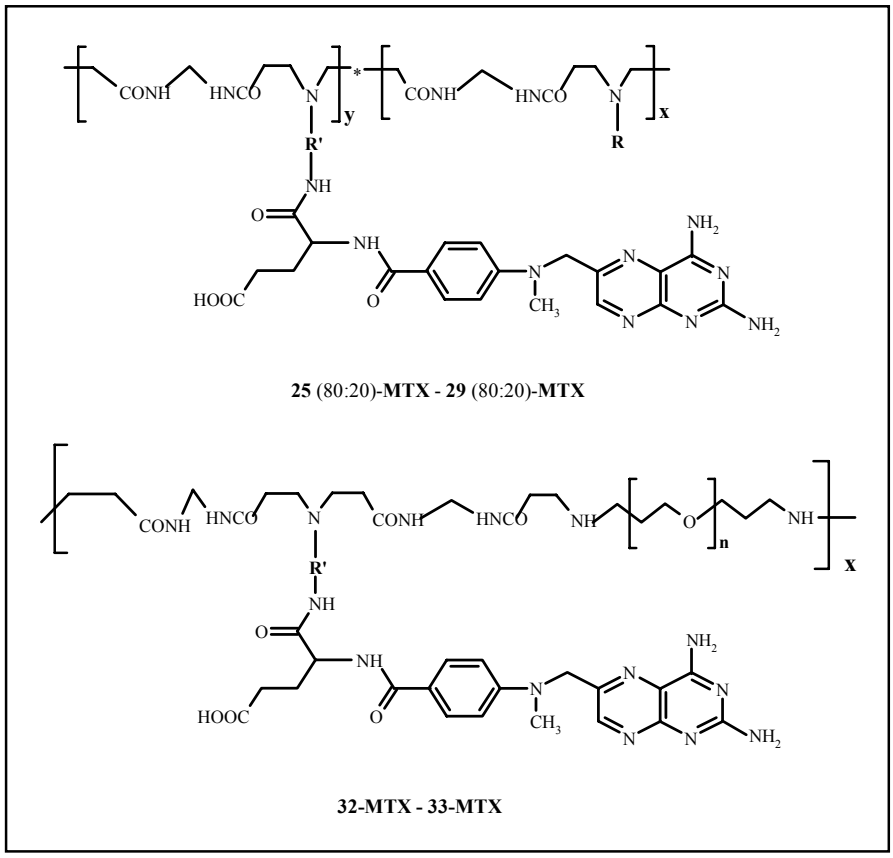
4.2.1.2 Preparation of poly(amidoamine)-MTX conjugates

The method of synthesis was the same as that for polyaspartamide-MTX conjugates. The coupling reactions were performed by treatment of the poly(amidoamine)-type carriers with MTX, an organic base, and HBTU as shown in Scheme 4.8. MTX: NH_2 molar reactant ratios typically employed were 1.2 or 1.3.



Scheme 4.8: Preparation of poly(amidoamine)-MTX conjugates

Table 4.18: Composition of PAA-MTX conjugates



Carriers	**R**	**R´**	**Conjugate designation**
25 (80:20)	$-(CH_2)_2N(CH_3)_2$	$-(CH_2)_3-$	**25** (80:20)-**MTX**
26 (80:20)	$-(CH_2)_3N(CH_3)_2$	$-(CH_2)_3-$	**26** (80:20)-**MTX**
27 (80:20)	$-(CH_2)_3N(CH_3)_2$	$-(CH_2)_2\,NH(CH_2)_2-$	**27** (80:20)-**MTX**
28 (80:20)	$-(CH_2)_2N(CH_3)_2$	$-(CH_2)_2\,O(CH_2)_2O(CH_2)_2-$	**28** (80:20)-**MTX**
29 (80:20)	$-(CH_2)_3N(CH_3)_2$	$-(CH_2)_2\,O(CH_2)_2O(CH_2)_2-$	**29** (80:20)-**MTX**
32 (**n** = 3)		$-(CH_2)_3-$	**32-MTX**
33 (**n** = 32)		$-(CH_2)_3-$	**33-MTX**

The conjugates, after precipitation from solution by adding non-solvent and isolation by centrifugation, were subjected to purification by both size exclusion

chromatography on Sephadex gel G-25 and exhaustive dialysis in ultimate 25 000 cut-off membrane tubing. Yields of the conjugates isolated in the solid state by freeze-drying of the dialysis retentates were in the 44-60% range.

Tables 4.19, 4.20, and 4.21 show the experimental variables, the viscometric and ^{1}H NMR data, and the summary of analytical data, respectively.

Solid-state IR spectra of all conjugates retained the prominent bands of the parent polymeric carriers. Thus, these conjugates showed a broad amide I band in the 1680-1610 cm^{-1} region. The spectra of conjugates **25**(80:20)**-MTX** to **29**(80:20)-**MTX** retained the tertiary amine band at 1400-1340 cm^{-1} as well as a strong methyl band at 1460 cm^{-1}, which corresponds to N(CH_3)$_2$. The band at 1060 cm^{-1}, corresponding to CH_2-O-CH_2, was noticeable in conjugates **25**(80:20)**-MTX**, **29**(80:20)-**MTX**, and **32-MTX**. This band is particularly strong in **33-MTX** due to the presence of the PEO segment (**n** = 32).

These conjugates were characterized by weight-average molecular weights ranging from 15 000 to 86 000. The polydispersity indices were in the range of 1.3 to 2.5. An increase in molecular weight of conjugates was observed as compared to those of the parent polymeric carriers. The inherent viscosities, found in the range of 20 - 25 mL g^{-1}, were increased compared to those of the carriers. In overall, the trend of increasing molecular weight matched the increase in viscosity, thus confirming the incorporation of drug molecules into the polymeric carrier chains.

Table 4.19: Experimental variables for all PAA-MTX conjugates

Reactants in feed				**Reaction conditions** [b]	**PAA-MTX Conjugates**	
Carriers	**Coupling agent**	**Medium**	**Carrier : drug : coupling agent ratio** (mol-%) [a]		**Yield** (%) [c]	**Designation**
25 (80:20)	HBTU	DMF	1:1.2:1.1	2h, RT	45	**25** (80:20)-**MTX**
26 (80:20)	,,	,,	,,	,,	50	**26** (80:20)-**MTX**
27 (80:20)	,,	,,	,,	,,	49	**27** (80:20)-**MTX**
28 (80:20)	,,	,,	,,	,,	44	**28** (80:20)-**MTX**
29 (80:20)	,,	,,	,,	,,	48	**29** (80:20)-**MTX**
32 (**n** = 3)	,,	,,	,,	3h, RT	47	**32**-**MTX**
33 (**n** = 32)	,,	,,	1:1.2:1.1 then 1:0.8:0.5	3h then 4h, RT	60	**33**-**MTX**

[a] Molar ratio of carrier repeating unit to MTX to coupling agent.

[b] RT= room temperature.

[c] Conjugate yield after size exclusion chromatography and ultimate (25 000 molecular weight cut-off) dialysis.

Table 4.20: ^{1}H NMR and viscometric results for the PAA- MTX conjugates

Conjugates designation	η_{inh} (mL g^{-1}) [a]	**x/y** [b]	**Base molecular mass** [c]	% **MTX** Calcd. [d]	% **MTX** NMR [e]	**Protons counted** [f] (expected) [g] **chemical shift** (ppm) δ 8.5-6.5 [h]	δ 4.8-4.5
25 (80:20)-**MTX**	25.09	4	1634.1 (1634).1	27.8	27. 8	5 (5)	10 (10)
26 (80:20)-**MTX**	19.35	4.1	1681.5 (1690.2)	26.89	26.35	4.9 (5)	10 (10)
27 (80:20)-**MTX**	20.65	4	1713.9 (1719.2)	26.4	26.17	4.95 (5)	10 (10)
28 (80:20)-**MTX**	22.05	4.2	1683.8 (1708.2)	26.6	25.38	4.77 (5)	10 (10)
29 (80:20)-**MTX**	21.08	4	1764.3 (1764.3)	25.76	25.76	5 (5)	10 (10)
32-MTX	21.95		1004.4 (1039.3)	43.73	40.24	4.6 (5)	4 (4)
33-MTX	21.8		2229.5 (2316.8)	19.62	15.69	4 (5)	4 (4)

[a] At 30.0 ± 0.5 °C, in deionized H_2O; concentration c = 2 mg/mL.
[b] Mole ratio (found) of hydrosolubilizing to drug-anchoring groups after ^{1}H NMR integration.
[c] Molecular weight, actual. (in parenthesis, calculated for 100% acylation).
[d] Derived from 100% acylation.
[e] Derived from ^{1}H NMR spectrum (error limit ± 12%).
[f] In D_2O, pH 10-11, chemical shifts, δ/ppm, referenced against internal sodium 3-trimethylsilyl-2,2,3,3-d_4-propionate; integration error limits ± 12 %. Protons are calculated for the structural representations in Table 4.20.
[g] Expected count for composition in accordance with recurring unit (see b).
[h] Proton assignment, δ/ppm: 8.6-6.6 (aromatic and heteroaromatic *CH* of MTX); 4.8-4.5 (CONH*CH*$_2$HNCO).

Table 4.21: Analytical results of PAA-MTX conjugates

Conjugates designation	η_{inh} (mL g^{-1})	**M_w x10^{-3}**	**M_n x10^{-3}**	**I_n**	**% MTX** Calcd. [a]	**% MTX** UV- ε_{370} [b]	**% MTX** NMR [c]	**NH_2 acylation (%)** UV [d]	**NH_2 acylation (%)** NMR [e]
25 (80:20)-**MTX**	25.09	86.6	67.1	1.3	27.8	27.74	27.8	~100	100
26 (80:20)-**MTX**	19.35	15.05	9.33	1.6	26.89	26.09	26.35	97	98
27 (80:20)-**MTX**	20.65	15.52	10.25	1.5	26.4	26.16	26.17	~100	99
28 (80:20)-**MTX**	22.05	60.8	45.8	1.3	26.6	25.27	25.38	95	95
29 (80:20)-**MTX**	21.08	18.66	13.61	1.4	25.76	25.28	25.76	98	100
32-**MTX**	21.95	26.09	13.44	2.5	43.73	40.1	40.24	91	92
33-**MTX**	21.8	33.02	14.49	1.8	19.62	15.3	15.69	78	80 [f]

[a] Mass percentage calculated for 100% acylation.

[b] Mass percentage found from UV absorbance of bound MTX in H_2O at 370 nm using $\varepsilon = 6500\ M^{-1}cm^{-1}$.

[c] Mass percentage derived from ^1H NMR spectrum (error limit ± 12%).

[d] Ratio of b to a.

[e] Ratio of c to a .

[f] In parallel experiments conducted under identical or modified conditions, percentage acylation ranged from 66-85%, requiring retreatment.

The MTX content (percent by mass using ^{1}H NMR spectroscopy) were determined by assessing the relative intensities of the aromatic resonances in the 8.5-6.5 ppm region characteristic of the drug against that of the methylene signal CONH*CH*$_2$HNCO near 4.5 ppm. Thus, the conjugates **25**(80:20)-**MTX** to **29**(80:20)-**MTX** show drug contents in the range of 25 to 28%. This corresponds to primary amino group acylation in the 95-100% range. These results were confirmed by quantitative UV spectroscopy of polymer solutions using the molar extinction coefficient value (ε = 6500 mol^{-1}cm^{-1}) and the absorbance at λ = 370 nm in H_2O. No excess drug was revealed in comparison with the content derived from theoretical structures. This fact confirms the efficiency of the purification procedure, as free drug was used in 20% excess.

The MTX content of conjugate **32-MTX** was found to be 40.24% and 40.1% by NMR and UV spectroscopy, respectively. This corresponds to 91% and 92% NH_2 acylation. The found drug content, hence, was lower than to the theoretical value of 43.73 %. NMR and UV spectroscopy gave MTX mass loading of 15.69% and 15.3%, respectively, for conjugate **33-MTX**, which was below the expected value of 19.62%. Therefore, the conjugate was retreated with 0.8, 0.5, and 1 equivalent of free drug, HBTU coupling agent, and organic base respectively, with an extended reaction period of 4h. The ultimate conjugate was characterized by 15.68% of drug content as determined by NMR spectroscopy. This corresponds to 80% NH_2 acylation, which is still lower than expected. **32**-**MTX** and **33**-**MTX** were derived from polymeric carriers containing intrachain hydrosolubilizing groups (PEO segment). While carrier **32** contained a short PEO segment (**n** = 3), polymer **33** comprised a long PEO segment (**n** = 32**)**. The extent of conjugation of **32**-**MTX** ranged from 91 to 92%, while the acylation of drug binding sites was observed to be 80% in the case of **33**-**MTX**, even under optimal conditions. The difference in drug conjugation extent observed with both carriers could be due to less accessibility of the drug binding site as a result of coil formation of PEO chain around the site. This could be more pronounced in polymer **33**, which is characterized by a long and highly flexible PEO chain of 32 units compared with carrier **32** in which the PEO chain length contains only 3 units.

4.2.1.3 Cell culture testing

The conjugates of both classes were evaluated in cell culture tests against various human cancer cell lines. The parenthetic attributes denoting mol-% composition in the conjugate designations will be omitted in the following text.

(a) CEM/S and CEM/E cell lines

Selected PAsA-MTX conjugates were tested *in vitro* by established procedure [166] against human CEM/S leukemic lymphoblasts, a drug-sensitive cell line and, in parallel, against the derived multidrug-resistant CEM/E subline. Free MTX was tested under the same conditions for comparison. The cytotoxic activities determined for the individual samples are listed in Table 4.22, expressed in terms of IC_{50} values, (drug concentration required to retain 50% cell viability relative to drug-free control). The table also contains entries for the resistance factor, RF, defined here as the ratio of IC_{50} [CEM/E] over IC_{50} [CEM/S].

A cursory comparison of the results tabulated in the two CEM columns immediately reveals the expected trend of lowered activity on going from CEM/S to CEM/E, with the resistance factors generally in the vicinity of 15-20, and the same trend obtains for free MTX (RF = 20.5). Against the two CEM lines, then, the carrier-bound drug, on balance, exhibits no selective ability to circumvent resistance. For conjugates **2-MTX** and **7-MTX** resistance factors below 5 are apparent from the tabulation. These are exceptional, however, and a larger number of repetitively synthesized conjugates will be required to confirm and rationalize this deviating behaviour.

Comparing now performance data of individual conjugate structures, we detect only minor differences on going from type to type. Significantly, against CEM/S, the overall IC_{50} range (~0.02 – 0.2) for polymers with tertiary amine side functionalities (**1-MTX** to **7-MTX**) does not substantially differ from that (~0.01 – 0.3) determined for the conjugates featuring hydroxyl-terminated side groups (**8-MTX** to **15-MTX**). The same argument holds for IC_{50} data determined against CEM/E. (The only outstanding case is conjugate **17-MTX**, which shows poor

performance relative to all other samples; this may be an artefact, however, which will be reinvestigated). Evidently, realistic structure-performance relationships can only be derived on the basis of an increased sample number for each structural type, and future investigations will focus on this topic.

The most striking aspect of the here described series of tests emerges as we compare for each CEM column the data derived for the carrier-drug conjugates with those pertaining to unconjugated MTX. With just one exception (conjugate **17-MTX**), the conjugate-derived IC_{50} values are considerably lower than the respective values for the free drug. This indicates the cytotoxic activities of the polymer-bound drug to exceed monomeric MTX activity by a large factor (40- to 50-fold in about one-third of all tested samples). The tabulated figures in the activity factor column (AF = IC_{50} [MTX] /IC_{50} [conjugate]) provide the details.

In summary: methotrexate, both conjugated and unconjugated, shows essentially the same trend of decreasing antiproliferative activity on going from the sensitive to the resistant CEM lines. Conjugation thus provides no panacea for circumvention of drug resistance interests against CEM. On the other hand, vastly superior activities, up to 50-fold and higher, against both CEM/S and CEM/E are observed for the carrier-anchored MTX derivatives in relation to the unbound drug. In view of the common experience that realistic pharmacological benefits, as they arise from drug binding to carrier polymer, will manifest themselves predominantly, if not solely, in the living organism [167, 168], these findings are highly significant and warrant ongoing studies involving further synthetic work and extensive *in vitro*/*in vivo* screens.

Table 4.22: Antiproliferative activity of polyaspartamide-MTX conjugates against CEM/E and CEM/S cell lines

Polyaspartamide-MTX Conjugates			CEM/S		CEM/E		
Designation	Base molecular weight	% MTX by mass	IC_{50} (μg MTX/mL)	AF [a]	IC_{50} (μg MTX/mL)	AF	RF [b]
1-MTX	2392.2	18.6	0.107	7.8	1.556	11.0	14.5
2-MTX	1391.6	31.68	0.137	6.1	0.542		4.0
3-MTX	2429.9	18.7	0.121	6.9	1.773	9.6	14.7
4-MTX	1416.3	31.7	0.02	41.7	0.467	36.5	23.4
5-MTX	2461.9	18.36	0.163	5.1	2.12	8.1	13.0
7-MTX	2408.2	18.8	0.145	5.8	0.633	27.0	4.4
8-MTX	2042.7	22.06	0.273	3.1	6.433	2.7	23.6
13-MTX	2456.6	18.5	0.013	64.1	0.281	60.7	21.6
15-MTX	2405.8	18.72	0.011	75.8	0.228	74.9	20.7
17-MTX	2169.0	20.79	>20	-	>20	-	-
MTX	-	-	0.834	-	17.07	-	20.5

[a] Activity factor defined here as IC_{50} [free MTX] : IC_{50} [conjugate].

[b] Resistance factor defined as IC_{50} [CEM/E] : IC_{50} [CEM/S].

(b) HeLa and Colo cell lines

The conjugates of both classes were evaluated in cell culture tests for antiproliferative activity against a refractory *.i.e.* less drug-responsive cell line derived from the Colo 320 DM human colorectal adenocarcinoma. For comparison, the samples of both classes were separately screened for activity against the HeLa human cervical epitheloid adenocarcinoma line generally found to be drug-sensitive and frequently used as a standard. Activities were determined in triplicate by the earlier described procedure, and the findings, expressed as IC_{50} values were averaged for each sample. In order to obtain a measure of the drug activity of the conjugates relative to unconjugated drug, free MTX was also included in these test series, and the results derived from five determinations against each cell line, averaged for each line, were used for this comparison. It is convenient to present and discuss the test results separately for the two classes of conjugates.

Polyaspartamide-MTX conjugates

For the polyaspartamide-based conjugates **1-MTX** to **18-MTX**, the IC_{50} values were derived from plots of cell growth relative to control versus conjugate concentration (Fig. 4.3 and 4.4). They are expressed in terms of μg MTX/mL and are listed in Table 4.23 for the tests against both cell lines. The table also contains the averaged results shown by free MTX for each cell line. Also included are the activity factors, AF, here defined as the ratio of conjugate activities over MTX activity and expressed in terms of IC_{50} (MTX)/ IC_{50} (conjugate).

It is instructive to consider first the data in the HeLa column. A superficial examination reveals that IC_{50} values for the first one-half of the listed conjugates are lower than that for MTX. For these first 4 tested samples (conjugates **1-MTX**, **3-MTX**, **5-MTX**, and **7-MTX**) an averaged activity factor of 4.15 can be calculated from the averaged IC_{50} value (0.0123 μg MTX/mL). These conjugates as a group, hence, are some 4-fold more active than the free drug. It must be

recalled that these samples are characterized by *tert*-amine side chain terminals in the hydrosolubilizing groups R.

The situation is different for the second one-half of the tabulated samples (conjugates **8-MTX** to **16-MTX**) identified by hydroxyl chain terminals in R. For the first 5 tested samples, the averaged IC_{50} value, 2.0176 μg MTX/mL, suggests an average activity factor of 0.025, thus reflecting a reverse behavior, with free MTX now some forty-times more active than the samples as a group. Conjugate **18-MTX** identified by methoxy side chain terminal in R, with IC_{50} value, 8.414 μg MTX/mL corresponding to an activity factor of 0.006, is 167-fold less active than free MTX. It is clear that, against the HeLa line, the *tert*-amine functionality in conjugates **1-MTX** to **7-MTX** exerts a positive influence on the *in vitro* cytotoxic data. In the biological environment, this functionality is partially protonated, which renders the polymer moderately basic and may thus facilitate pinocytic cell entry with resultant activity enhancement. Larger sample numbers will be required, however, to corroborate this explanation.

Let us proceed now to the Colo column. To the unconjugated drug, the Colo line proves to be some 50-times more refractory than HeLa, which clearly identifies that Colo variant as a strongly drug-resistant line. Here, for the first four samples listed in this column (conjugates **1-MTX**, **3-MTX**, **5-MTX** and **7-MTX**) the averaged IC_{50} value (0.2875 μg MTX/mL) leads to an average activity factor of 9.61, showing these *tert*-amine functionalized polymers as a group to be over 10-fold more active than free MTX. In this first one-half of samples, conjugates **5-MTX** and **3-MTX**, which show a reverse behavior, can possibly be artifacts. The lower performance observed can be due to poor solubility. Indeed, poor solubility would result in aggregation, and ultimately in the delivery of a small portion of the drug in the intracellular compartment. Among the seven samples in the category of hydroxyl-functionalized, the conjugates **10-MTX**, **14-MTX** and **16-MTX** are distinctly less active as a group against this strongly resistant line. With an activity ratio of 0.34, derived from the averaged IC_{50} value (8.1253 μg MTX/mL), the hydroxyl-functionalized conjugates are even less active than the free drug. This average AF value is misleading, however, being strongly affected

by the three outsiders (possibly artifacts), the conjugates **10-MTX**, **14-MTX** and **16-MTX**. If these are omitted from the calculations, an activity factor of 3.18 results from the averaged IC_{50} value (0.8693 μg MTX/mL). This indicates that even these hydroxyl-functionalized conjugates for the most part are three-times as active as the unconjugated drug.

Table 4.23: Antiproliferative activity of polyaspartamide-MTX conjugates against HeLa and Colo cell lines

Polyaspartamide-MTX conjugates			HeLa		CoLo		
Designation	Base molecular weight	% MTX by mass	IC_{50} (µg MTX/mL)	AF [d]	IC_{50} (µg MTX/mL)	AF	RF
1-MTX	2392.2	18.6	0.013	3.9	0.196	14	15.08
2-MTX	1391.6	31.68	-	-	2.82	0.98	-
3-MTX	2429.9	18.7	0.0075	6.8	0.032	86.4	4.27
4-MTX	1411.9	30.81	-	-	2.872	0.96	-
5-MTX	2466.3	17.91	0.0037	13.8	0.432	6.4	11.68
7-MTX	2408.2	18.5	0.025	2.0	0.49	5.6	19.6
8-MTX	2042.7	21.36	0.379	0.14	1.214	2.3	3.2
9-MTX	1234.5	34.61	-	-	0.044	62.8	-
10-MTX	2025.3	21.31	4.918	0.01	12.965	0.21	2.64
13-MTX	2456.6	18.5	0.536	0.1	1.712	1.6	3.19
14-MTX	1445.6	31.4	-	-	24.069	0.12	-
15-MTX	2401.4	17.95	0.027	1.9	0.507	5.5	18.78
16-MTX	2439.4	18.45	4.228	0.01	16.366	0.17	3.87
17-MTX	2168.4	20.12	8.414	0.006	>50	> 0.06	5.94 >
18-MTX	1321.1	34.06	-	-	46.286	0.06	-
MTX	-	-	0.051	-	2.764	-	54

[a] Activity factor defined here as IC_{50} [free MTX] : IC_{50} [conjugate]

[b] Resistance factor defined as IC_{50} [Colo] : IC_{50} [HeLa].

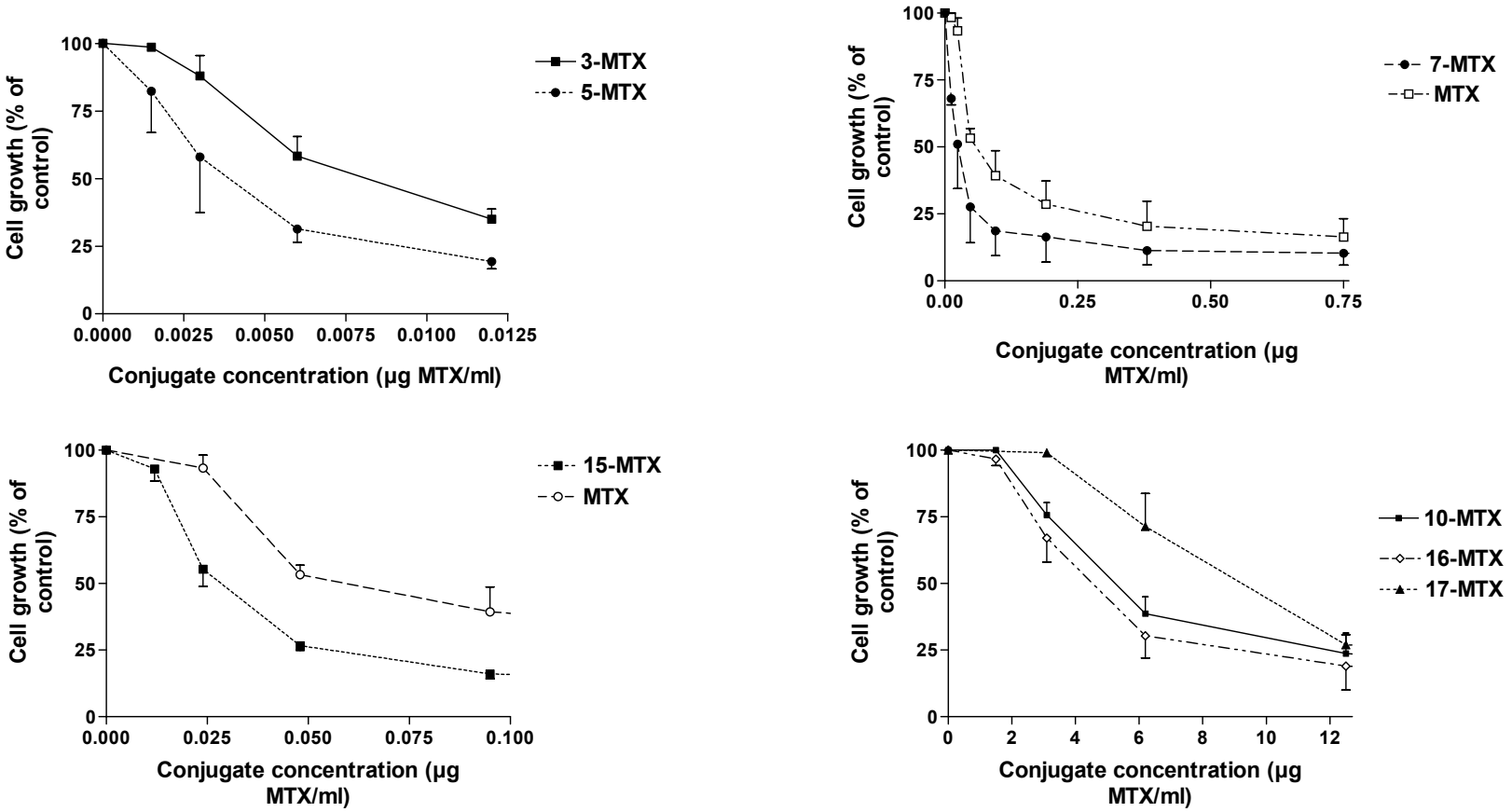


Figure 4.3: Antiproliferative activity of PAsA-MTX and free MTX against HeLa cells

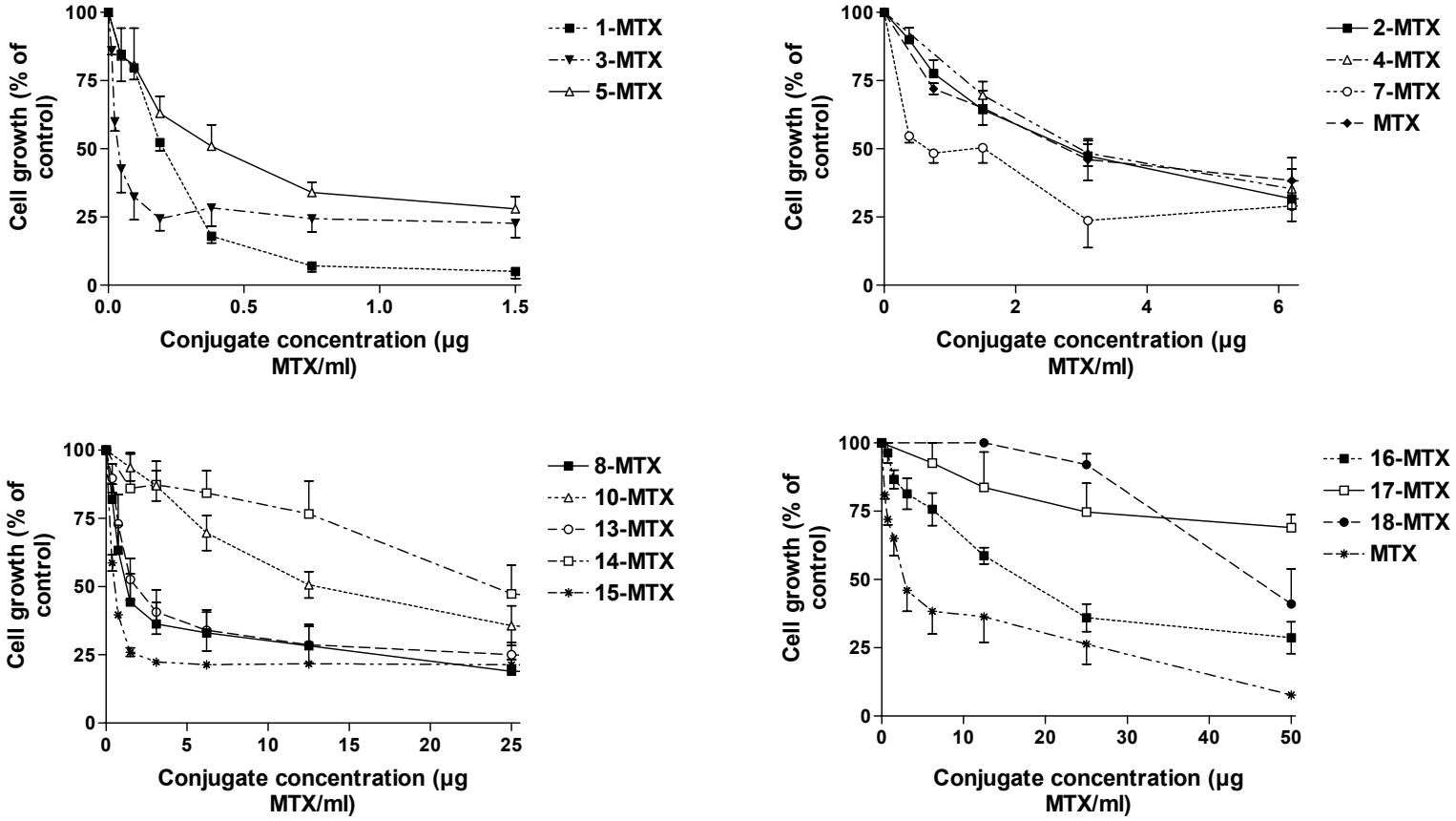


Figure 4.4: Antiproliferative activity of PAsA-MTX and free MTX against Colo cells

Poly(amidoamine)-MTX conjugates

This class comprises a small number of conjugates (**25-MTX** to **33-MTX**; one sample per conjugate) made available for a very preliminary evaluation of activities against the HeLa and Colo lines. The results in terms of IC_{50} values derived from plots (Figures 4.5 and 4.6) and activity factor are presented in Table 4.24, which includes data obtained in this test series for unconjugated MTX.

Let us first inspect the data in the HeLa column. For the first five conjugates **25-MTX** to **29-MTX**; characterized by the presence of *tert*-amine terminals on short side chains functioning as hydrosolubilizing moieties, the IC_{50} values approximate that of free MTX. The average activity factor, 1.34, derived from the averaged IC_{50} data (0.053 μg MTX/mL), identifies this group of conjugates as slightly more active than MTX proper. Conjugates **32-MTX** and **33-MTX**, in contrast, containing a solubilizing intrachain oligo(ethylene oxide) segment, provide AF of 0.05 and 0.03, respectively. The activities of these two conjugates are thus considerably lower than that of MTX.

The same basic trend is apparent for all conjugates from the Colo data. While conjugates **25-MTX** to **29-MTX** as a group are four-times more active than free MTX, with averaged IC_{50} = 1.2266 μg MTX/mL and resultant AF: 3.67, the remaining two conjugates turn out to be less active than free MTX, with activity factors of 0.47 and 0.29, respectively. The oligo(ethylene oxide) segment in **32-MTX** and **33-MTX** possesses protein-repellent characteristics, and this may lead to inhibition of intracellular enzymatic cleavage of the drug-binding carboxamide links and resultant lower bioavailability.

Based on the IC_{50} values, **27-MTX** is more effective than **25-MTX**. However, the cell-killing efficaciousness is more pronounced with **25-MTX** than it is with **27-MTX**. Indeed, Fig. 4.6 (a) shows **25-MTX** to maintain its trend of cell growth inhibitory activity at the concentration of 0.75 μg MTX/mL, while at the same concentration **27-MTX** forms a plateau with about 25% of cells surviving. The same phenomenon was observed with conjugates **26-MTX** (Fig. 4.6 (b)) and **32-MTX** (Fig. 4.6 (c)). The plateau formation, which corresponds to gently enhanced

cell resistance with increasing drug concentration can be due to decreased intracellular drug levels resulting from increased drug efflux or decreased inward transport. More experiments and extended numbers of conjugates will be required for elucidation of this behavior in these cases.

Moreover, using the Tables 4.13, 4.21, and 4.23, it appears that the polydispersity indexes of polymer **25**(80:20) to **33** are relatively high: 2.73; 1.72; 2.09; 2.1; 2.66; 1.39; and 2.07 respectively.

Fortunately, these values have sensibly improved after conjugation with Methotrexate. The lowest values are for conjugates **25**(80:20)-**MTX** to **29**(80:20)-**MTX**: 1.3; 1.6; 1.5; 1.3; and 1.4 respectively. The highest are for **32**-**MTX** and **33**-**MTX** with 2.5 and 1.8 respectively.

However, the narrow polydispersity (around 1.2) of conjugates has been associated biological [169]. If we look at the results compiled in Table 4.23, the conjugates **25**(80:20)-**MTX** to **29**(80:20)-**MTX** are more effective than **32**-**MTX** and **33**-**MTX**. Even the conjugate 17(90:10)-MTX with polydispersity of 1.87 (Tables 4.17 and 4.22) showed no cytotoxicity at all. This study may have demonstrated once again that polydispersity plays a certain role in the effectiveness of drug conjugates.

In conclusion, cell culture tests performed against the drug-sensitive HeLa and the strongly resistant Colo lines reveal a vastly superior cell-killing potential for polymer-bound MTX as a class in relation to the unconjugated drug. Best performers belong to the group of polyaspartamide-based conjugates featuring *tert*-amine side chain terminals as hydrosolubilizing entities, with selected compounds some 4- to 10-times more active than free MTX. The superiority of this group of conjugates is particularly apparent in tests against the resistant Colo line. While in tests against this line all compounds show lowered cytotoxic performance, this loss of activity is much less severe with the polymeric than the monomeric drug. Polyaspartamide-bound MTX derivatives, notably those containing *tert*-amine side chain terminals, thus stand out as eminently promising candidates for further bio-evaluation work in tests against both sensitive and multidrug-resistant cancer cells.

Table 4.24: Antiproliferative activity of PAA-MTX conjugates against HeLa and CoLo cell lines.

PAA-MTX conjugates			**HeLa**		**Colo**		
Designation	M_w x 10^{-3}	% MTX by mass	IC_{50} (µg MTX/mL)	AF [a]	IC_{50} (µg MTX/mL)	AF [a]	RF [b]
25-MTX	86.6	27.8	0.086	0.83	0.675	6.7	7.48
26-MTX	15.05	26.35	0.134	0.53	1.348	3.3	10.1
27-MTX	15.52	26.17	0.014	5.1	0.087	51.7	6.2
28-MTX	60.8	25.38	0.025	2.8	3.179	1.4	127.2
29-MTX	18.66	25.76	0.0058	12.24	0.844	5.3	145.5
32-MTX	26.09	40.24	1.324	0.05	9.58	0.47	7.24
33-MTX	33.02	15.69	2.659	0.03	15.625	0.29	5.9
MTX	-	-	0.071	-	4.5	-	63.4

[a] Activity factor defined here as IC_{50} [free MTX] : IC_{50} [conjugate].

[b] Resistance factor defined as IC_{50} [Colo] : IC_{50} [HeLa].

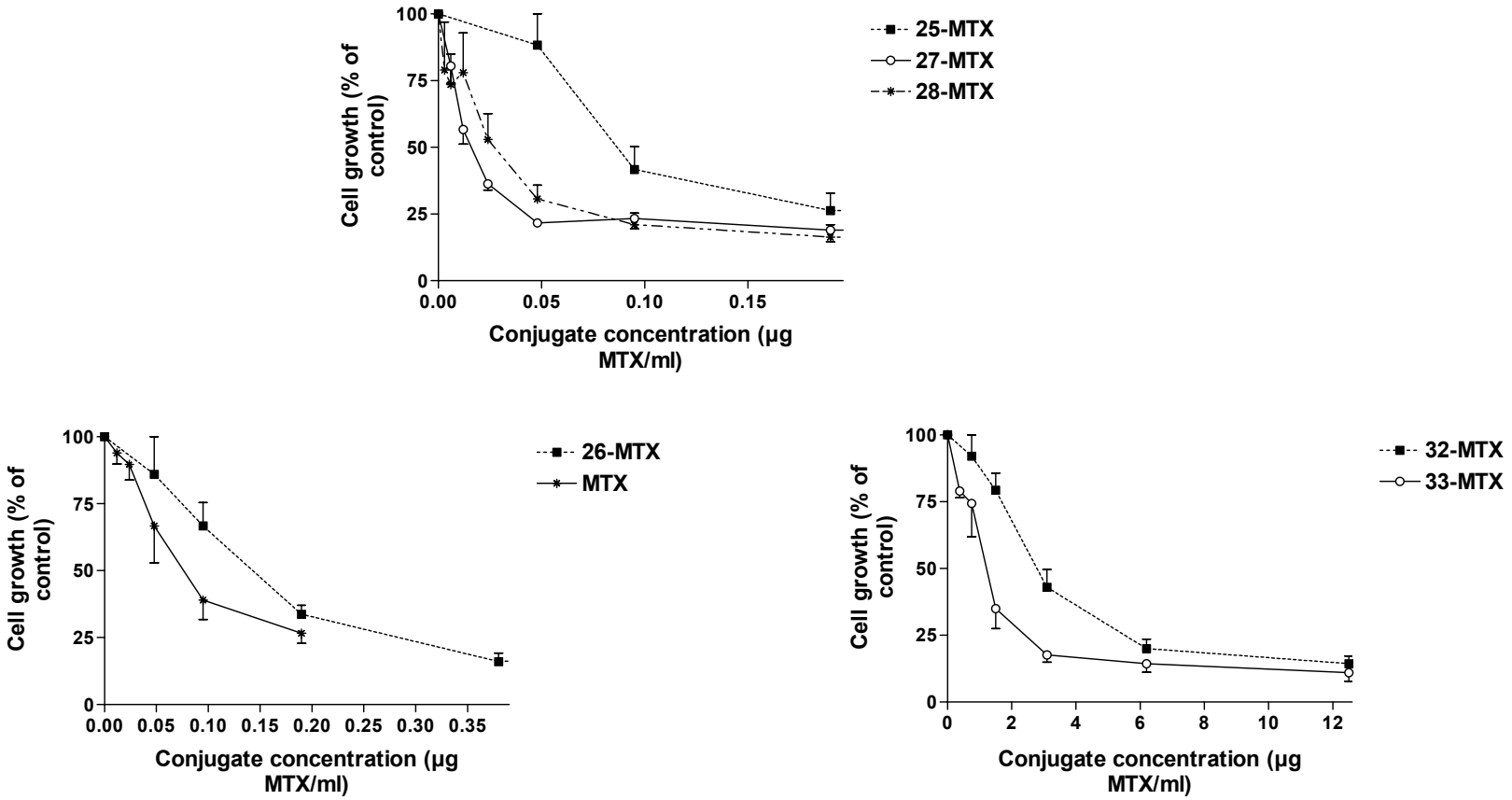


Figure 4.5: Antiproliferative activity of PAA-MTX conjugates and free MTX against HeLa cells

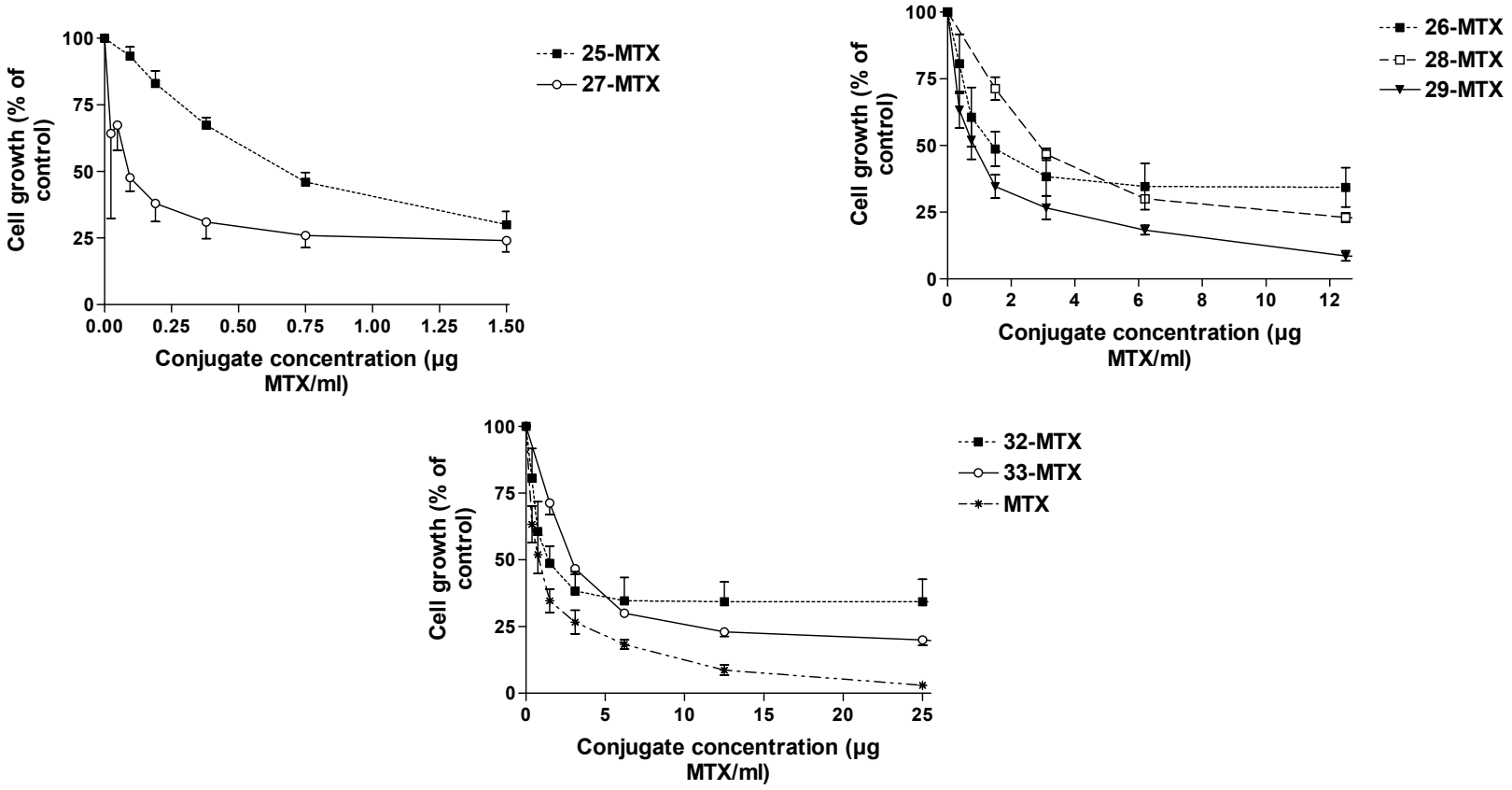


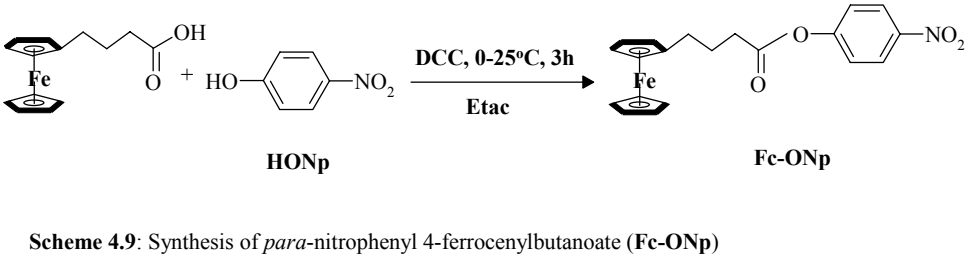
Figure 4.6: Antiproliferative activity of PAA-MTX conjugates and free MTX against Colo cells

4.2.2 Preparation of polymer-ferrocene conjugates

The ferrocene derivative involved in this study was 4-ferrocenylbutanoic acid, whose choice was motivated by its conveniently low reduction potential as reported by Swarts et *al*. [170]. It was synthesized as described in the literature [171]. Various polymers of both polyaspartamide and poly(amidoamine) types, which feature primary amino side chain terminals, were anchored to the ferrocene unit through the formation of biofissionable amide links. Two ferrocene anchoring methods have extensively been investigated in this laboratory. The first method involves direct acid-amine coupling, which is mediated by 2(1H-benzotriazol-1-yl)-1,1,3,3-tetramethyluronium fluorophosphate (HBTU), while the second involves coupling *via* the active N-succinimide ester of the ferrocene compound, N-succinimidyl 4-ferrocenylbutanoate. The active ester was prepared from the 4-ferrocenylbutanoic acid and N-hydroxysuccinimide (HSU) in the presence of dicyclohexylcarbodiimide in ethyl acetate medium. In order to assess the extent of drug conjugation of each coupling method, a series of screening experiments were performed. In these experiments, the ratio of Ferrocene/polymer repeat unit varied in the 1.3-2.5 range. In some cases, where the extent of conjugation was unsatisfactory (< 90%), the conjugates were treated with additional amount of drug and the reaction period was extended in order to achieve greater degrees of acylation ranging from 95 to 100%. The results of screening experiments indicated that the two coupling methods are essentially equivalent in efficiency [172]. The HBTU-mediated acylation, while reported in one case [170] to cause main chain fragmentation, offers the benefit of originating directly from the free butanoic acid without requiring the active ester intermediacy. The HSU ester method, on the other hand, offers the advantage of retaining main chain integrity, thus permitting long reaction periods as may be required for coupling processes involving reactants of low reactivity.

In the present project, the coupling efficiency of another type of ferrocenylbutanoic acid-based active ester was investigated for comparison with the preceding methods.

This active ester, *para*-nitrophenyl 4-ferrocenylbutanoate, was synthesized using a method adapted from literature [173] as depicted in Scheme 4.9.



Scheme 4.9: Synthesis of *para*-nitrophenyl 4-ferrocenylbutanoate (**Fc-ONp**)

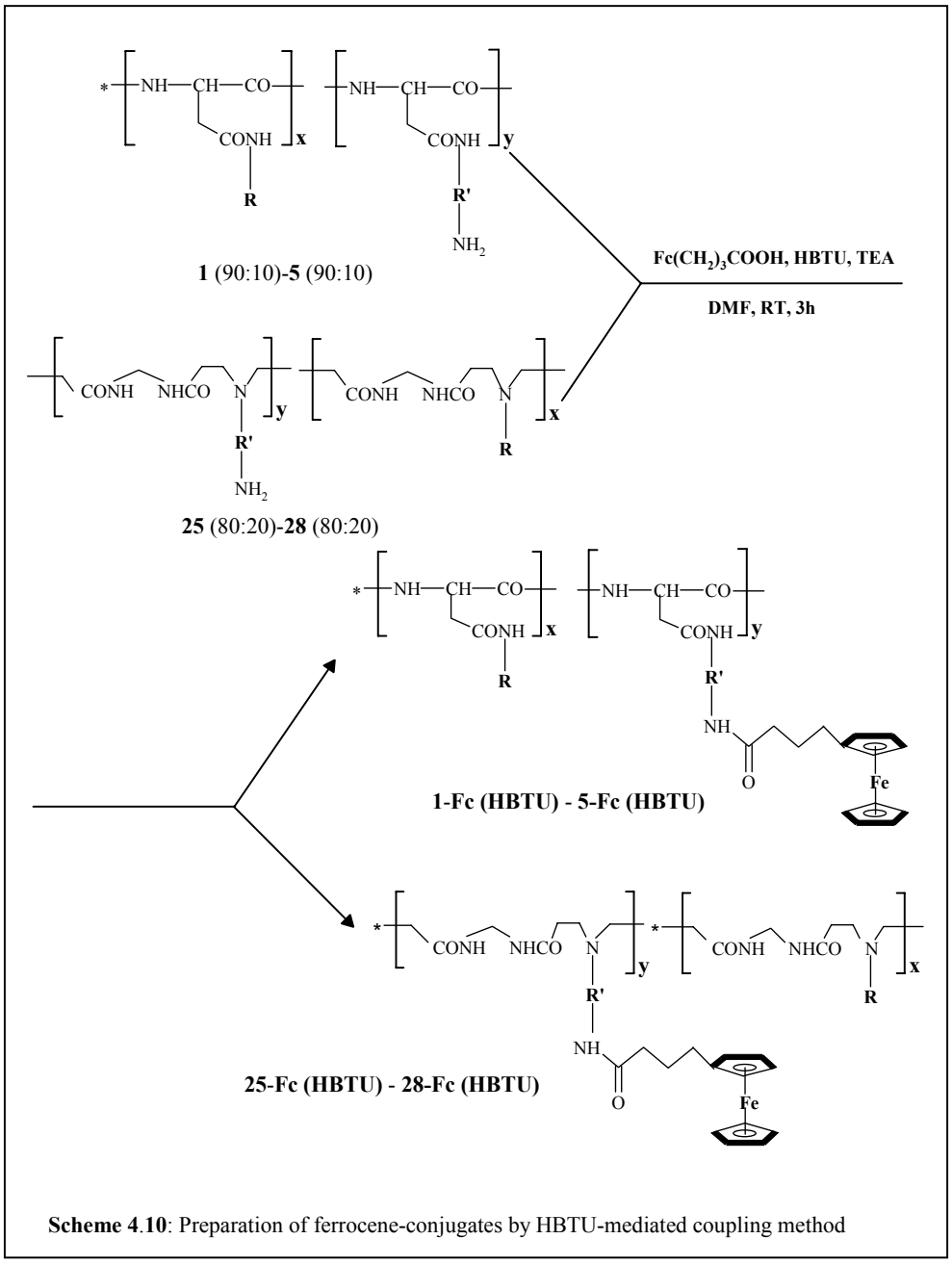
Thus, the two main drug conjugation methods herein used were the HBTU-mediated and the *para*-nitrophenyl active ester methods. However, in order to demonstrate the drug-anchoring potential of poly(amidoamine), an exemplifying polymer was allowed to react with the HSU-derived active ester of ferrocenylbutanoic acid in methanolic solution.

4.2.2.1 Polymer-ferrocene conjugation by HBTU-mediated coupling method

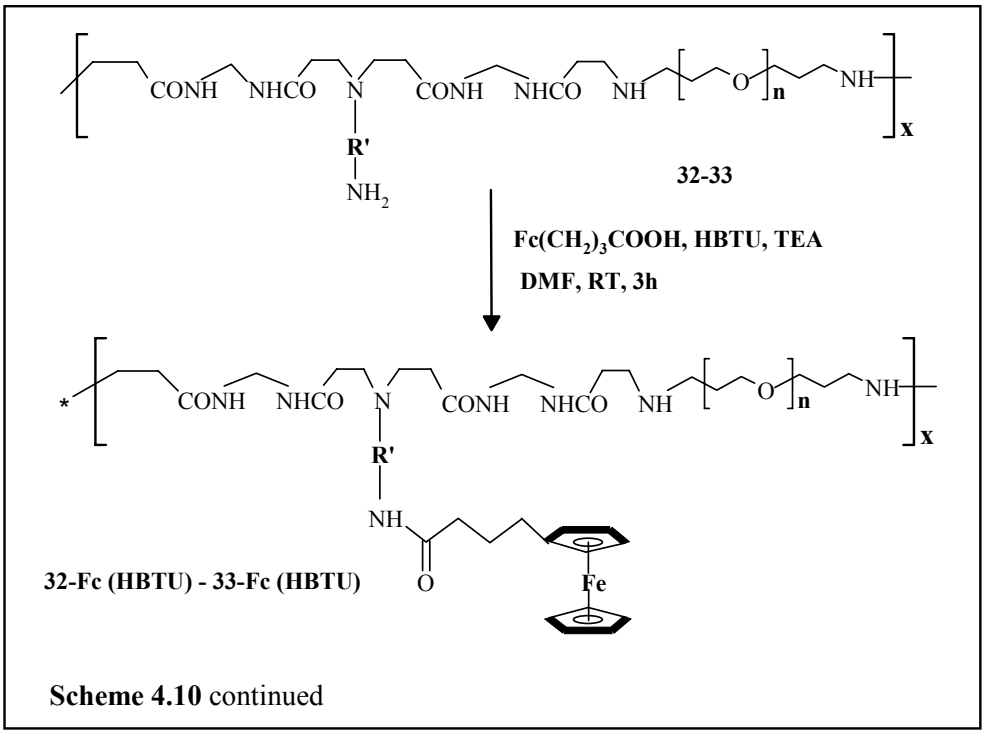
These conjugates were obtained by treating the primary amine-functionalized polymeric carriers of both polyaspartamide and poly(amidoamine) types with 1.2-1.4 molar equivalents of the ferrocenylbutanoic acid in the presence of 1.1-1.3 equivalents of HBTU and 2 equivalents of organic base (triethylamine, TEA) at pH of 7 or higher as shown in Scheme 4.10. The carriers were converted into conjugates in which complete acylation of available primary amine functions were achieved after typically 3h. The water-soluble product conjugates were precipitated from the reaction solution and, after purification by size exclusion chromatography and exhaustive dialysis, were isolated by freeze-drying in the solid state.

Table 4.25 shows the composition of these conjugates, and the reaction conditions leading to these conjugates are summarized in Table 4.26, whereas the spectroscopic and viscometric results are compiled in Table 4.27. For

convenience, the ferrocene conjugates in this section and the forthcomings will be reported without the molar percentage in parenthesis.

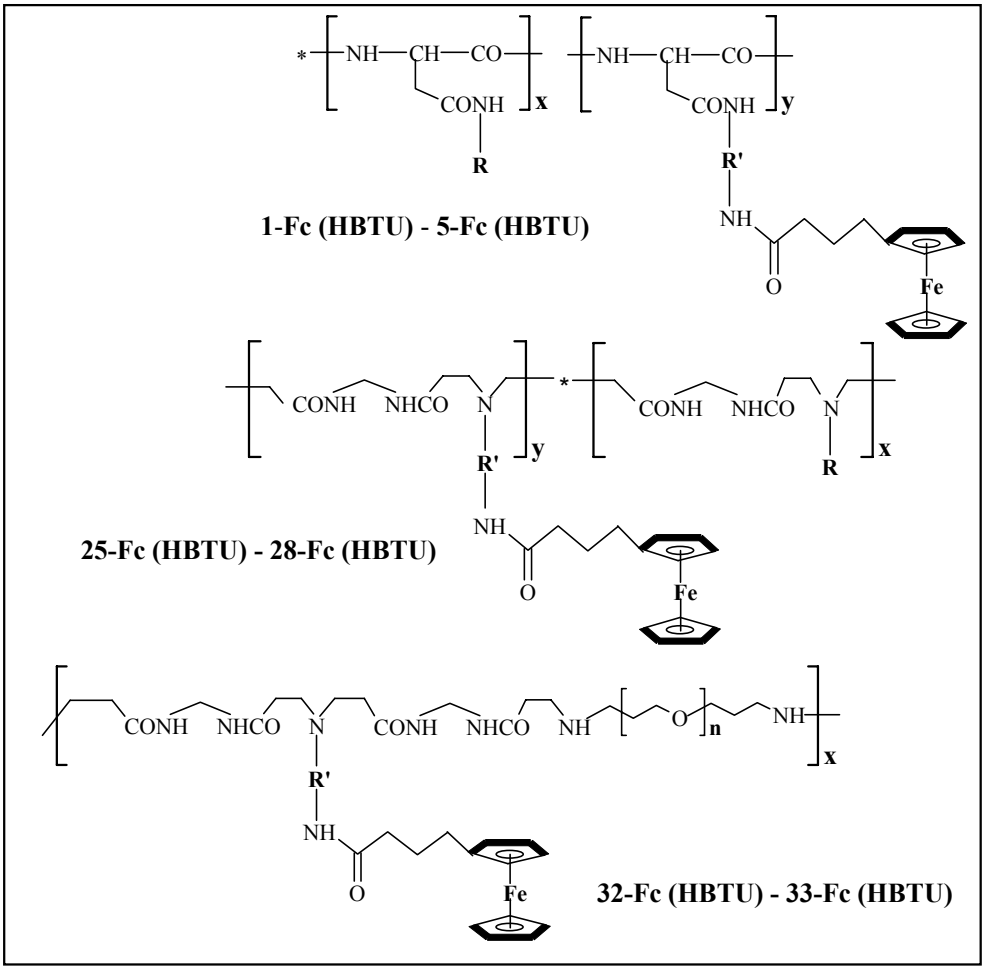


Scheme 4.10: Preparation of ferrocene-conjugates by HBTU-mediated coupling method



Scheme 4.10 continued

Table 4.25: Compostion of polymer-ferrocene conjugates prepared by HBTU–mediated coupling method



Carriers	R	R´	Conjugates designation
1 (90:10)	$-(CH_2)_3N(CH_3)_2$	$-(CH_2)_3-$	**1-Fc (HBTU)**
3 (90:10)	$-(CH_2)_3N(CH_3)_2$	$-(CH_2)_2NH(CH_2)_2-$	**3-Fc (HBTU)**
5 (90:10)	$-(CH_2)_3N(CH_3)_2$	$-(CH_2)_2O(CH_2)_2O(CH_2)_2-$	**5-Fc (HBTU)**
25 (80:20)	$-(CH_2)_2N(CH_3)_2$	$-(CH_2)_3-$	**25-Fc (HBTU)**
26(80:20)	$-(CH_2)_3N(CH_3)_2$	$-(CH_2)_3-$	**26-Fc (HBTU)**
27 (80:20)	$-(CH_2)_3N(CH_3)_2$	$-(CH_2)_2NH(CH_2)_2-$	**27-Fc (HBTU)**
28 (80:20)	$-(CH_2)_2N(CH_3)_2$	$-(CH_2)_2O(CH_2)_2O(CH_2)_2-$	**28-Fc (HBTU)**
32 (**n** = 3)		$-(CH_2)_3-$	**32-Fc (HBTU)**
33 (**n** = 32)		$-(CH_2)_3-$	**33-Fc (HBTU)**

Table 4.26: Reaction conditions for ferrocene conjugates prepared by HBTU-mediated coupling method

Reactants in feed				**Reaction conditions** [b]	**Fc (HBTU) conjugates**	
Carriers designation	**Coupling agent**	**Medium**	**Carrier : drug : coupling agent ratio** (mol-%) [a]		**Yield** (%) [c]	**Designation**
1 (90:10)	HBTU	DMF	1:1.2:1.1	3 h at RT	53	**1-Fc (HBTU)**
3 (90:10)	,,	,,	,,	,,	56	**3-Fc (HBTU)**
5 (90:10)	,,	,,	1:1.4:1.3	,,	64	**5-Fc (HBTU)**
25 (80:20)	,,	,,	1:1.2:1.1	,,	39	**25-Fc (HBTU)**
26 (80:20)	,,	,,	,,	,,	42	**26-Fc (HBTU)**
27 (80:20)	,,	,,	,,	,,	43	**27-Fc (HBTU)**
28 (80:20)	,,	,,	,,	,,	46	**28-Fc (HBTU)**
32 (**n** = 3)	,,	,,	,,	,,	72	**32-Fc (HBTU)**
33 (**n** = 32)	,,	,,	,,	,,	41	**33-Fc (HBTU)**

[a] Molar ratio of carrier repeating unit to ferrocenylbutanoic acid to coupling agent.

[b] RT= room temperature.

[c] Conjugate yield after size exclusion chromatography and ultimate (25 000 molecular weight-cut-off) dialysis.

Table 4.27: ^{1}H NMR and viscometric results for Fc (HBTU) conjugates

Conjugates designation	η_{inh} (mL g^{-1})	**x/y** [a]	**Base molecular mass** [b]	**% Fe** Calcd [c]	**% Fe** NMR [d]	**Protons counted** [e] (expected) [f] **chemical shift** (ppm) δ 4.8-4.5 [g]	δ 4.3-4.25	δ 3.8-3.5	δ 1.8-1.5
1-Fc (HBTU)	15.96	9	2218.6 (2218.6)	2.52	2.52		9 (9)		22 (22)
3-Fc (HBTU)	13.7	9	2247.6 (2247.6)	2.49	2.49		9 (9)		20 (20)
5-Fc (HBTU)	12.5	9.1	2290.1 (2292.7)	2.44	2.41		8.91 (9)		20 (20)
25-Fc (HBTU)	16.25	4	1451.6 (1451.7)	3.85	3.85	10 (10)	9 (9)		4 (4)
26-Fc (HBTU)	19.79	4	1507.8 (1507.8)	3.7	3.7	10 (10)	9 (9)		12 (12)
27-Fc (HBTU)	18.5	4	1535.8 (1535.8)	3.64	3.64	10 (10)	9 (9)		10 (10)
28-Fc (HBTU)	21.2	4	1525.8 (1525.8)	3.66	3.66	10 (10)	9 (9)	9 (8)	2 (2)
32-Fc (HBTU)	16.3		849.3 (856.9)	6.52	6.3	4 (4)	8.7 (9)	14 (12)	8 (8)
33-Fc (HBTU)	16.34		2109.0 (2134.4)	2.62	2.33	4 (4)	8 (9)	130 (128)	7 (8)

[a] Mole ratio of hydrosolubilizing to drug-anchoring groups after ^{1}H NMR integration.
[b] Molecular weight, actual. (in parenthesis, calculated for 100% acylation.)
[c] Mass percentage derived from 100% acylation.
[d] Mass percentage derived from ^{1}H NMR spectrum of conjugate (error limit ± 12%).
[e] In D_2O, pH 10-11, chemical shifts, δ/ppm, referenced against internal sodium 3-trimethylsilyl-2,2,3,3-d_4-propionate; integration error limits ± 12 %. Protons are calculated for structural representations in Table 4.25.
[f] Expected count for composition in accordance with recurring unit (see b).
[g] Proton assignment, δ/ppm: 4.8-4.5 (CONH*CH*$_2$HNCO); 4.3-4.25 (*CH* of ferrocenyl); 3.8-3.5 (O*CH*$_2$*CH*$_2$O); 1.8-1.5 (CH$_2$*CH*$_2$CH$_2$).

Table 4.28: Summary of analytical data for Fc (HBTU) conjugates

Conjugates designation	**η_{inh}** (mL g^{-1})	**% Fe** Calcd [a]	**% Fe** UV- ε_{440} [b]	**% Fe** NMR [c]	**NH_2 acylation** (%) UV [d]	**NH_2 acylation** (%) NMR [e]
1-Fc (HBTU)	15.96	2.52	2.45	2.52	98	100
3-Fc (HBTU)	13.7	2.49	2.48	2.49	100	100
5-Fc (HBTU)	12.5	2.44	2.39	2.41	98	99
25-Fc (HBTU)	16.25	3.85	3.82	3.85	~100	100
26-Fc (HBTU)	19.79	3.7	3.63	3.7	98	100
27-Fc (HBTU)	18.5	3.64	3.58	3.64	99	100
28-Fc (HBTU)	21.2	3.66	3.61	3.66	99	100
32-Fc (HBTU)	16.3	6.52	6.25	6.3	96	97
33-Fc (HBTU)	16.34	2.62	2.3	2.33	88	89

[a] Mass percentage calculated for 100% acylation.
[b] Mass percentage derived from UV-absorbance of bound Fc in H_2O at 440 nm using $\varepsilon = 100\ cm^{-1}M^{-1}$.
[c] Mass percentage derived from ^1H NMR spectrum of conjugate (error limit ± 12%).
[d] Ratio of b to a.
[e] Ratio of c to a.

The HBTU-mediated coupling method afforded ferrocene conjugates in yields of 39-72%, with inherent viscosities varying from 12 to 21 mL g^{-1}. These viscosities were higher when compared with those of the precursor carriers, in accordance with presence of drug molecules in the chains.

The solid-state IR spectra of these ferrocene conjugates retained the bands of the precursor carriers, notably the amide I band, in the 1680-1620 cm^{-1} region. The typical bands of the ferrocene system were buried in the underlying carrier bands.

The ^{1}H NMR spectra of the conjugates displayed the signals of the respective carriers and those of the incorporated ferrocenylation agent, especially the ferrocenyl (*C-H*) protons whose signal (4.3-4.25 ppm) was used for the assessment of the drug content in comparison with other prominent signals. For ferrocene conjugates **1-Fc (HBTU)**, **3-Fc (HBTU)** and **5-Fc (HBTU)** the prominent signal was that in the 1.8-1.5 ppm region, assigned to methylene ($CH_2CH_2CH_2$) protons. Thus, these conjugates were found to contain of 2.52, 2.49 and 2.41% of Fe by mass, respectively. This corresponds to 100, 100, and 99% of NH_2 acylation, respectively. Independent determination by UV spectroscopy using the molar extinction coefficient (ε = 100 $mol^{-1}cm^{-1}$) and the absorbance at λ = 440 nm in H_2O showed that these conjugates contain 2.45, 2.48, and 2.39% of Fe by mass, corresponding to 98, 100, and 98% extent of conjugation.

The assessment using the signal of methylene ($CONHCH_2NHCO$) protons (4.8-4.5 ppm) which belongs exclusively to the poly(amidoamine)-type carriers, showed the conjugates **25-Fc (HBTU)** to **32-Fc (HBTU)** to possess Fe contents in the 3.8-6.3% range, corresponding to conjugation extents in the range of 97 to 100%. This was confirmed by the UV spectroscopic analysis (see Table 4.28). These high degrees of conjugation, which were obtained in one step, proved the sufficiency of the molar feed ratio drug/polymer, which was in the 1.2-1.4 range. This finding contrasts somewhat with a reported investigation [170] where high conjugation (95-100%) was achieved by using a drug/polymer molar feed ratio of 1.8. In the present project, the high extent of conjugation could be due to the mode of reactant addition. Indeed, when the drug is allowed to react alone with

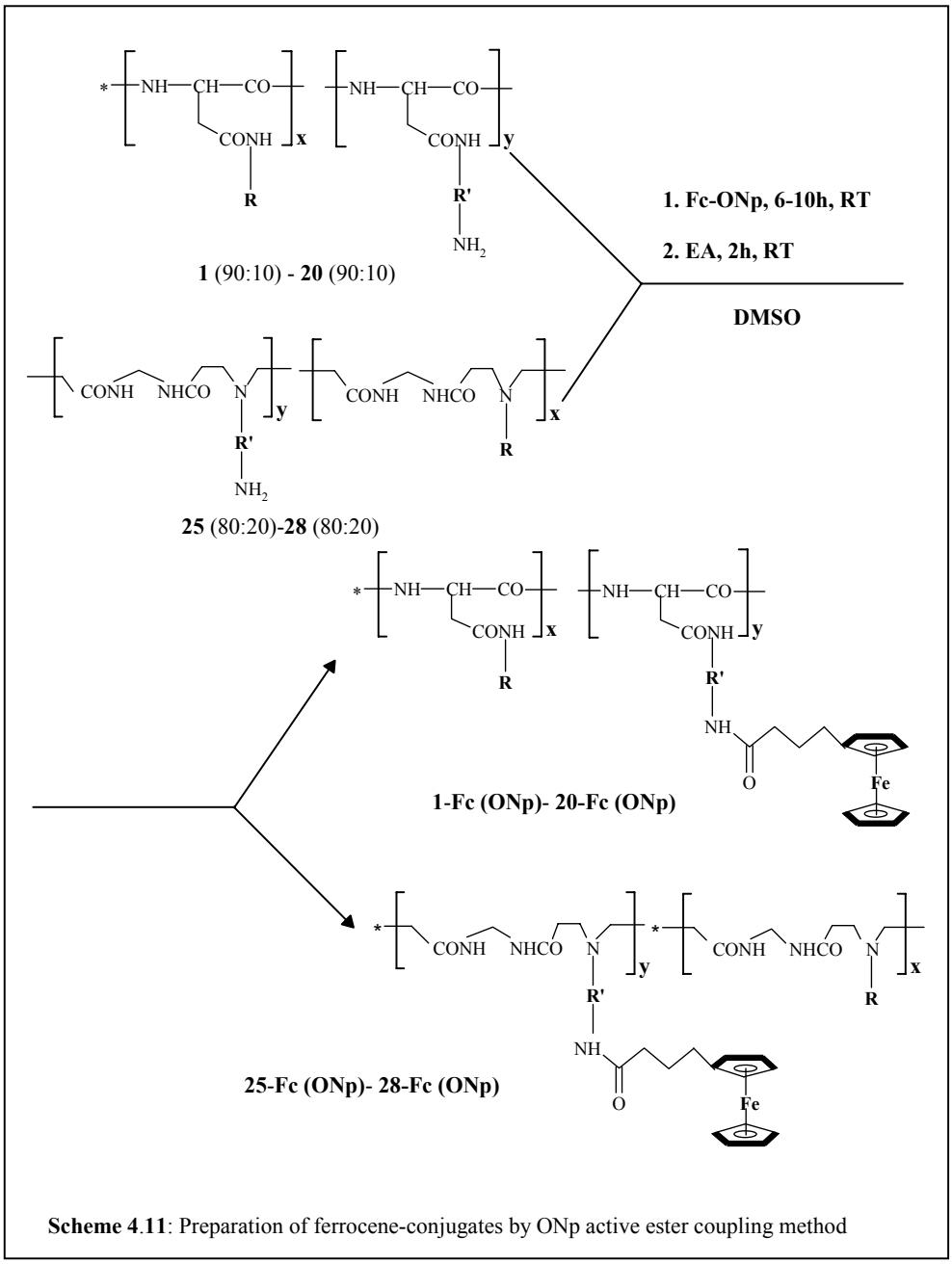
the coupling agent (HBTU) for an hour, this could favor the formation of active species which, when added to the predissolved polymer, could readily interact with the primary amino groups for a period of 2h. This finding requires re-investigation as it results from a small number of conjugates.

32-Fc (HBTU) (characterized by the presence of a short PEO segment with **n** = 3) was found to contain 6.4 and 6.25% of Fe by mass, which were determined by NMR and UV spectroscopy, respectively. These iron contents correspond to extents of conjugation of 95-97%. Conjugate **33-Fc (HBTU)** contains 2.38% of Fe (determined by NMR). This corresponds to drug incorporation of 89% level, and indicates low ferrocenylation of polymer **33**. The undersubstitution of this polymer could be due to lesser accessibility to the drug-anchoring site (possibly) caused by the long and flexible backbone (PEO, **n** = 32). However, more investigation will be required to elucidate this question.

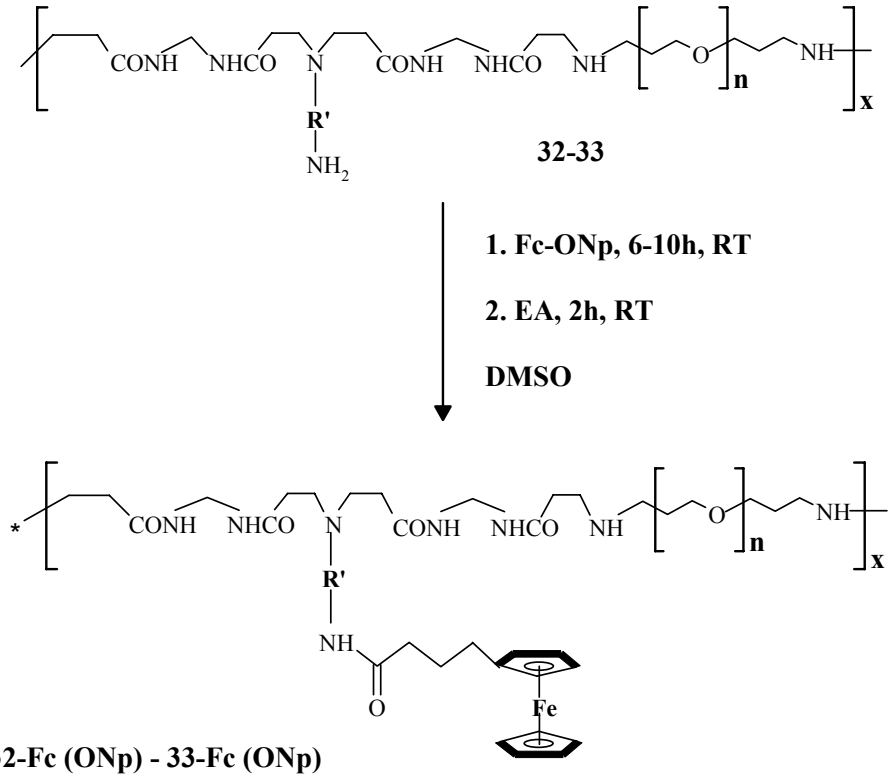
4.2.2.2 Polymer-ferrocene conjugation by active ester coupling method

A series of 32 screening experiments were performed in order to assess the coupling efficiency of the new active ester, *para*-nitrophenyl 4-ferrocenylbutanoate (Fc-ONp). This active ester was intended to act as an alternative to the extensively used N-succinimidyl 4-ferrocenylbutanoate (Fc-OSU) in this laboratory. These experiments involved the treatment of the Fc-ONp ester with selected carriers of polyaspartamide and poly(amidoamine) types in molar ester/carrier ratios of 1.2 as. Scheme 4.11 depicts their preparation.

The resulting water-soluble conjugates were purified by size exclusion chromatography and aqueous dialysis in a buffer medium as described for preceding ferrocene conjugates. The products were isolated in the solid state by freeze-drying.

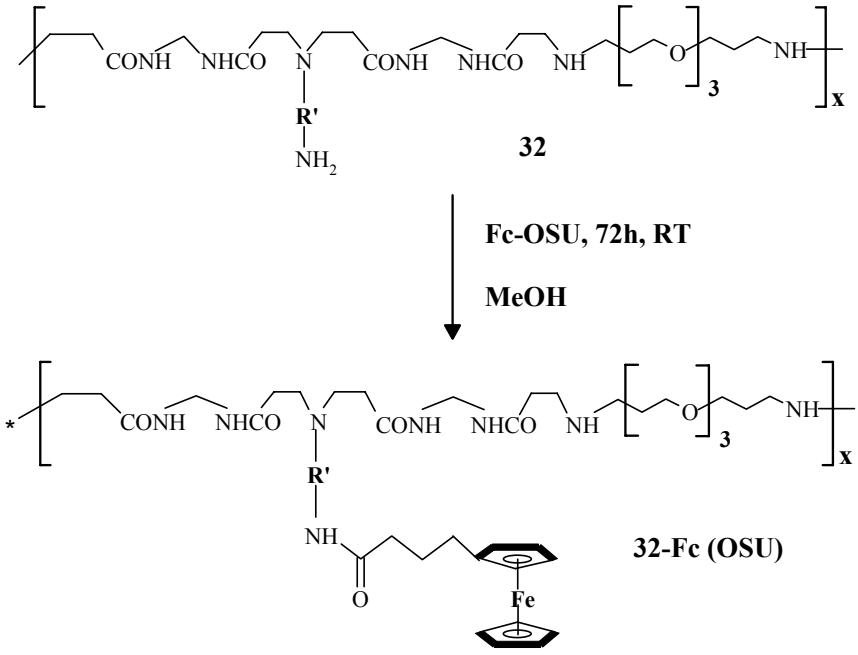


Scheme 4.11: Preparation of ferrocene-conjugates by ONp active ester coupling method



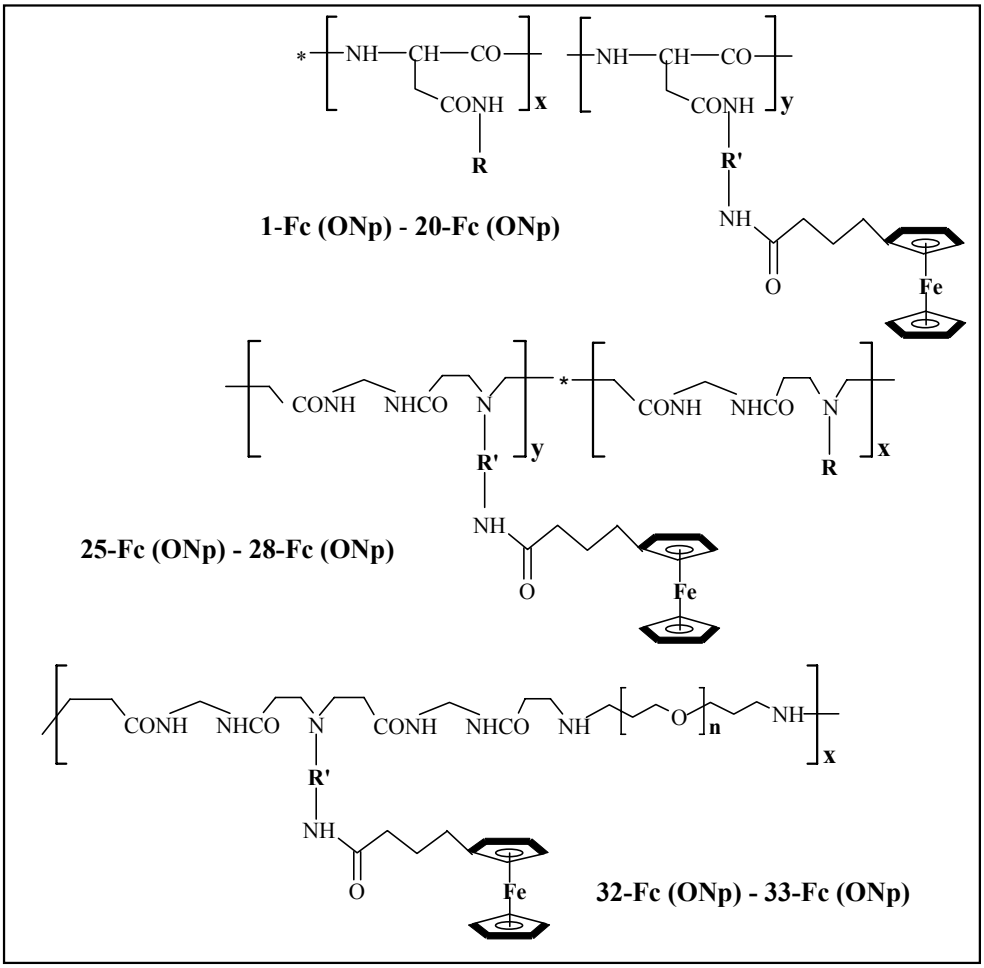
Scheme 4.11 continued

Polymer **32**, which features a short PEO solubilizing segment in the main chain, was treated with 1.3 equivalent of the active HSU ester (Fc-OSU) in methanolic medium. This was to test the coupling efficaciousness on replacing DMF with methanol. The resulting ferrocene conjugate was treated and isolated in a similar manner as described for the preceding conjugates.



Scheme 4.12: Preparation of poly(amidoamine)-ferrocene conjugate in methanol

Table 4.29: Composition of ferrocene conjugates prepared by the ONp active ester method



Carriers	R	R´	Conjugates designation
1 (90:10)	$-(CH_2)_3N(CH_3)_2$	$-(CH_2)_3-$	**1-Fc (ONp)**
2 (80:20)	$-(CH_2)_3N(CH_3)_2$	$-(CH_2)_3-$	**2-Fc (ONp)**
3 (90:10)	$-(CH_2)_3N(CH_3)_2$	$-(CH_2)_2NH(CH_2)_2-$	**3-Fc (ONp)**
4 (80:20)	$-(CH_2)_3N(CH_3)_2$	$-(CH_2)_2NH(CH_2)_2-$	**4-Fc (ONp)**
5 (90:10)	$-(CH_2)_3N(CH_3)_2$	$-(CH_2)_2O(CH_2)_2O(CH_2)_2-$	**5-Fc (ONp)**
7 (90:10)	$-(CH_2)_3N(CH_3)_2$	$-CH_2CHOHCH_2-$	**7-Fc (ONp)**

Table 4.29 continued

Carriers	R	R´	Conjugates designation
8 (90:10)	$-(CH_2)_2OH$	$-(CH_2)_2NH(CH_2)_2-$	**8-Fc (ONp)**
10 (90:10)	$-(CH_2)_2OH$	$-CH_2CHOHCH_2-$	**10-Fc (ONp)**
11 (90:10)	$-(CH_2)_2OH$	$-(CH_2)_3-$	**11-Fc (ONp)**
12 (90:10)	$-(CH_2)_2OH$	$-(CH_2)_2O(CH_2)_2O(CH_2)_2-$	**12-Fc (ONp)**
13 (90:10)	$-(CH_2)_2O(CH_2)_2OH$	$-(CH_2)_2NH(CH_2)_2-$	**13-Fc (ONp)**
14 (80:20)	$-(CH_2)_2O(CH_2)_2OH$	$-(CH_2)_2NH(CH_2)_2-$	**14-Fc (ONp)**
16 (90:10)	$-(CH_2)_2O(CH_2)_2OH$	$-CH_2CHOHCH_2-$	**16-Fc (ONp)**
17 (90:10)	$-(CH_2)_2OCH_3$	$-(CH_2)_2NH(CH_2)_2-$	**17-Fc (ONp)**
19 (90:10)	$-(CH_2)_2OCH_3$	$-(CH_2)_3-$	**19-Fc (ONp)**
20 (90:10)	$-(CH_2)_2OCH_3$	$-(CH_2)_2O(CH_2)_2O(CH_2)_2-$	**20-Fc (ONp)**
25 (80:20)	$-(CH_2)_2N(CH_3)_2$	$-(CH_2)_3-$	**25-Fc (ONp)**
27 (80:20)	$-(CH_2)_3N(CH_3)_2$	$-(CH_2)_2NH(CH_2)_2-$	**27-Fc (ONp)**
28 (80:20)	$-(CH_2)_2N(CH_3)_2$	$-(CH_2)_2O(CH_2)_2O(CH_2)_2-$	**28-Fc (ONp)**
32 (**n** = 3)		$-(CH_2)_3-$	**32-Fc (ONp)**
33 (**n** = 32)		$-(CH_2)_3-$	**33-Fc (ONp)**
32 (**n** = 3)		$-(CH_2)_3-$	**32-Fc (OSU)**

Tables 4.30 and 4.31 summarize the reaction conditions and ^{1}H NMR and viscometric results, respectively, while Table 4.32 shows the summary of all the analytical data.

Table 4.30: Reaction conditions for ferrocene conjugates prepared by the ONp active ester method

Reactants in feed				Reaction conditions	Fc (ONp) conjugates	
Carriers	**Drug active ester**	**Medium**	**Carrier : active ester** [a] (mol-%)		**Yield** (%) [b]	**Designation**
1 (90:10)	Fc-ONp	DMSO	1:1.2	12h, RT	55	**1-Fc (ONp)** [c]
2 (80:20)	,,	,,	,,	,,	55	**2-Fc (ONp)**
3 (90:10)	,,	,,	,,	,,	58	**3-Fc (ONp)** [d]
4 (80:20)	,,	,,	,,	,,	58	**4-Fc (ONp)**
5 (90:10)	,,	,,	,,	,,	55	**5-Fc (ONp)** [d]
7 (90:10)	,,	,,	,,	,,	59	**7-Fc (ONp)**
8 (90:10)	,,	,,	,,	,,	69	**8-Fc (ONp)** [c]
10 (90:10)	,,	,,	,,	,,	71	**10-Fc (ONp)**
11 (90:10)	,,	,,	,,	8h, RT	73	**11-Fc (ONp)** [d]
12 (90:10)	,,	,,	,,	,,	75	**12-Fc (ONp)** [d]
13 (90:10)	,,	,,	,,	10h, RT	75	**13-Fc (ONp)** [c]

Table 4.30 continued

Reactants in feed				Reaction conditions	Fc (ONp) conjugates	
Carriers	**Drug active ester**	**Medium**	**Carrier : active ester** (mol-%) [a]		**Yield** (%) [b]	**Designation**
14 (80:20)	Fc-ONp	DMSO	1:1.2	10h, RT	57	**14-Fc (ONp)**
16 (90:10)	,,	,,	,,	,,	46	**16-Fc (ONp)** [d]
17 (90:10)	,,	,,	,,	,,	74	**17-Fc (ONp)** [d]
19 (90:10)	,,	,,	,,	8h, RT	78	**19-Fc (ONp)**
20 (90:10)	,,	,,	,,	,,	50	**20-Fc (ONp)**
25 (80:20)	,,	,,	,,	10h, RT	51	**25-Fc (ONp)**
27 (80:20)	,,	,,	,,	,,	42	**27-Fc (ONp)**
28 (80:20)	,,	,,	,,	,,	42	**28-Fc (ONp)**
32	,,	,,	,,	,,	48	**32-Fc (ONp)**
33	,,	,,	,,	,,	44	**33-Fc (ONp)**
32	Fc-OSU	MeOH	1:1.3	72h, RT	40	**32-Fc (OSU)**

[a] Molar ratio of carrier repeating unit to Ferrocenylbutanoic acid active ester.

[b] Conjugate yield after size exclusion chromatography and ultimate (25 000 molecular weight cut-off) dialysis.

[c] Reaction performed in duplicate and data averaged.

[d] Reaction performed in triplicate and data averaged.

Table 4.31: ^{1}H NMR and viscometric results for all Fc (ONp) conjugates

Conjugates designation	η_{inh} (mL g^{-1}) [a]	**x/y** [b]	**Base molecular mass** [c]	**% Fe** Calcd. [d]	**% Fe** NMR [e]	**Protons counted** [f] (expected) [g] **chemical shift** (ppm) δ 4.8-4.5 [h]	δ 4.3-4.25	δ 3.8-3.5	δ 1.8-1.5
1-Fc (ONp)	15.92	9	2218.5 (2218.5)	2.52	2.52		9 (9)		22 (22)
2-Fc (ONp)	13.15	4.1	1214.7 (1222.3)	4.57	4.45		8.73 (9)		12 (12)
3-Fc (ONp)	13.25	9	2247.6 (2247.6)	2.49	2.49		9 (9)		20 (20)
4-Fc (ONp)	12.85	4	1251.4 (1251.4)	4.46	4.46		9 (9)		10 (10)
5-Fc (ONp)	11.95	9.3	2285.1 (2292.7)	2.44	2.37		8.7 (9)		20 (20)
7-Fc (ONp)	14.5	9.5	2221.9 (2234.6)	2.5	2.39		8.51 (9)		20 (20)
8-Fc (ONp)	17.75	9	1877.8 (1877.8)	2.97	2.97		9 (9)	18 (18)	
10-Fc (ONp)	13.75	9.3	1857.2 (1864.8)	3.0	2.92		8.73 (9)	19 (19)	
11-Fc (ONp)	13.5	9.2	1843.7 (1848.8)	3.02	2.97		8.79 (9)	18 (18)	
12-Fc (ONp)	14.28	9.3	1915.2 (1922.9)	2.9	2.83		8.75 (9)	26 (26)	
13-Fc (ONp)	15.25	9	2274.3 (2274.3)	2.46	2.46		9 (9)	54 (54)	
14-Fc (ONp)	13.50	4.2	1258.1 (1263.2)	4.42	4.35		8.82 (9)	24 (24)	
16-Fc (ONp)	12.86	9.2	2256.2 (2261.3)	2.47	2.43		8.82 (9)	55 (55)	
17-Fc (ONp)	18.5	9	2004.1 (2004.1)	2.79	2.79		9 (9)	45 (45)	
19-Fc (ONp)	16.89	9	1975.1 (1975.1)	2.83	2.83		9 (9)	45 (45)	2 (2)

Table 4.31 continued

Conjugates designation	η_{inh} (mL g^{-1})	**x/y** [a]	**Base molecular mass** [b]	**% Fe** Calcd [c]	**% Fe** NMR [d]	**Protons counted** [e] (expected) [f] **chemical shift** (ppm) δ 4.8-4.5 [g]	δ 4.3-4.25	δ 3.8-3.5	δ 1.8-1.5
20-Fc (ONp)	15.45	9.2	2044.1 (2049.1)	2.73	2.68		8.82 (9)	53 (53)	
25-Fc (ONp)	14.5	4	1451.7 (1451.7)	3.85	3.85	10 (10)	9 (9)		4 (4)
27-Fc (ONp)	17.05	4	1535.9 (1535.9)	3.64	3.64	10 (10)	9 (9)		10 (10)
28-Fc (ONp)	22.05	4	1525.8 (1525.8)	3.66	3.66	10 (10)	9 (9)	9 (8)	2 (2)
32-Fc (ONp)	15.75		854.4 (856.9)	6.52	6.45	4 (4)	8.9 (9)	13 (12)	9 (8)
33-Fc (ONp)	16.85		2126.8 (2134.4)	2.62	2.53	4 (4)	8.7 (9)	130 (128)	7 (8)
32-Fc (OSU)	15.05		839.1 (856.9)	6.52	6.08	4 (4)	8.4 (9)	14 (12)	10 (8)

[a] Mole ratio of hydrosolubilizing to drug-anchoring groups after ^{1}H NMR integration, given by the carrier.

[b] Molecular weight, actual. (in parenthesis, calculated for 100% acylation).

[c] Mass percentage of Fe calculated for 100% acylation.

[d] Mass percentage of Fe derived from ^{1}H NMR spectrum (error limit ± 15%).

[e] In D_2O, pH 10-11, chemical shifts, δ/ppm, referenced against internal sodium 3-trimethylsilyl-2,2,3,3-d_4-propionate; integration error limits ± 12 %. Protons are calculated for structural representations in Table 4.29.

[f] Expected count for composition in accordance with recurring unit (see b).

[g] Proton assignment, δ/ppm: 4.8-4.5 (CONH*CH*$_2$HNCO); 4.3-4.25 (*CH* of ferrocenyl); 3.8-3.5 (O*CH*$_2$*CH*$_2$O); 1.8-1.5 (CH$_2$*CH*$_2$CH$_2$).

Table 4.32: Summary of analytical results for all Fc (ONp) conjugates

Conjugates designation	**η_{inh}** (mL g^{-1})	**% Fe** Calcd [a]	**% Fe** UV- ε_{440} [b]	**% Fe** NMR [c]	**NH_2 acylation** (%) UV [d]	**NH_2 acylation** (%) NMR [e]
1-Fc (ONp)	15.92	2.52	2.48	2.52	99	100
2-Fc (ONp)	13.15	4.57	4.48	4.45	98	97
3-Fc (ONp)	13.25	2.49	2.46	2.49	99	100
4-Fc (ONp)	12.85	4.46	4.42	4.46	99	100
5-Fc (ONp)	11.95	2.44	2.39	2.37	99	97
7-Fc (ONp)	14.5	2.5	2.45	2.39	97	95
8-Fc (ONp)	17.75	2.97	2.94	2.97	99	100
10-Fc (ONp)	13.75	3.0	2.88	2.92	96	97
11-Fc (ONp)	13.5	3.02	2.98	2.97	99	98
12-Fc (ONp)	14.28	2.9	2.85	2.82	98	97
13-Fc (ONp)	15.25	2.46	2.41	2.46	98	100
14-Fc (ONp)	13.50	4.42	4.3	4.35	97	98

Table 4.32 continued

Conjugates designation	**η_{inh}** (mL g^{-1})	**% Fe** Calcd [a]	**% Fe** UV- ε_{440} [b]	**% Fe** NMR [c]	**NH_2 acylation** (%) UV [d]	**NH_2 acylation** (%) NMR [e]
16-Fc (ONp)	12.86	2.47	2.45	2.43	99	98
17-Fc (ONp)	18.5	2.79	2.73	2.79	98	100
19-Fc (ONp)	16.89	2.83	2.75	2.83	97	100
20-Fc (ONp)	15.45	2.73	2.70	2.68	99	98
25-Fc (ONp)	14.5	3.85	3.8	2.85	99	100
27-Fc (ONp)	17.05	3.64	3.57	3.64	98	100
28-Fc (ONp)	22.05	3.66	3.60	3.66	98	100
32-Fc (ONp)	15.75	6.52	6.54	6.45	100	99
33-Fc (ONp)	16.85	2.62	2.58	2.53	99	97
32-Fc (OSU)	15.05	6.52	6.01	6.08	92	93

[a] Mass percentage calculated for 100% acylation.

[b] Mass percentage derived from UV absorbance of bound Fc in H_2O at 440 nm; $\varepsilon = 100\ cm^{-1}M^{-1}$.

[c] Derived from ^1H NMR spectrum (error limit ± 12%).

[d] Ratio of b to a.

[e] Ratio of c to a.

The Fc (ONp) conjugates were obtained in yields that varied from 42 to 78%, and were characterized by inherent viscosities in the 12-22 mL g^{-1} range. The Fe content, which was calculated from the percentage of ferrocene incorporation, was found to be in the range of 2.4-6.5% by mass. Independent analysis by UV-vis absorption spectroscopy performed on these conjugates confirmed the above results of Fe content (see Table 4.32). These results show that under the experimental conditions, acylation of primary amines available in the carriers were achieved in the 97-100% range. The highest extent of undersubstitution was 3%. This allows the inference that the coupling method was efficient, and the molar feed ester/carrier ratio of 1.2 was sufficient to ensure high extent of drug incorporation. In light of the polyhomologous nature of the ferrocenylation reactions, the extent of ferrocene incorporation in the individual runs was not expected to be strictly reproducible. Therefore, some experiments were performed in duplicate or triplicate, and the tabulated data represent averages of the parallel runs.

The ONp ester coupling method affords high extents of conjugation without recourse to additional treatment. The active Fc-OSU ester provides acylation of same the magnitude upon forcing conditions, which include molar feed ester/carrier ratios of 1.8, a reaction period of 48h at room temperature and another 3h at 65^{o}C, and in some cases additional treatment with 0.5 equivalent of the ester [172]. These facts allow for preference of the active ONp ester over the active OSU ester coupling technique.

With the HBTU-mediated coupling, ferrocenylation levels in the order of 97-100% were achieved upon use of drug/carrier molar feed ratios of 1.2-1.4 and 1.1-1.3 equivalents of HBTU agent for a reaction period of 3h. The results of these screening experiments suggest active ONp ester and HBTU-mediated methods to be essentially of equivalent efficiency. However, in co-conjugation studies, the active ONp ester method would be preferred to the HBTU-mediated one, the latter being reported to cause main chain fragmentation [170], although such fragmentation

was not observed in the framework of this project for the nitrophenyl ester method.

The efficacy of the active ONp ester method was also shown with the poly(amidoamine) carriers **32** and **33**. The resulting ferrocene conjugates **32-Fc (ONp)** and **33-Fc (ONp)** were obtained in extents of ferrocenylation of 99 and 97% determined by NMR spectroscopy. These correspond to 6.45 and 2.53% of Fe by mass, respectively. UV-vis analysis confirmed these results (refer Table, 4.31 rows 9 and 10).

The active OSU ester method used in methanolic medium showed the treatment of poly(amidoamine) carrier **32** with the ester in molar feed ratio of ester/polymer repeat unit of 1.3 at RT for 72h to afford conjugate **32-Fc (OSU)** in yield of 40% with inherent viscosity 15.05 mL g^{-1}. The acylation of available primary amino groups was found by NMR spectroscopy to be 93%, corresponding to 6.08% Fe by mass. As this ferrocenylation experiment was intended to demonstrate the drug-binding potential of poly(amidoamine) carriers in media other than DMF, namely in alcoholic, no further attempt was made to achieve complete substitution of NH_2 groups by retreatment of the conjugate.

4.2.3 Polymer multidrug conjugation

As one of the tasks assigned to this project, the two anticancer compounds, MTX and ferrocene, were anchored to the same polymeric carrier backbone. The two drug systems operate by different cell killing mechanisms, and it was of interest here to establish potentiating or additive effects, if any, in subsequent bio-evaluation work. The conjugation was achieved by amide bond formation, resulting from reaction of acid group of the drugs with the amine function of the carriers. Also co-conjugated were the pairs MTX-folic acid and ferrocene-folic acid by the same method.

4.2.3.1 Synthesis of polyaspartamide-co-drug conjugates

The polyaspartamides **1**(90:10) and **3**(90:10), featuring tertiary amine-functionalized units as hydrosolubilizing and targeting moieties, were chosen to demonstrate the co-drug binding ability of these polymers. The choice was based on the report of cytotoxic activity performance of ferrocene conjugates against Colo 320 DM human colon cancer line [141] and current results (Section 4.2.1.4). Each carrier was conjugated to a pair of drug systems (MTX, Fc and FA), in a two-step procedure. Thus, the co-drug systems were symbolized by **FA/MTX**; **FA/Fc** and **MTX/Fc**, in reference to the following pairs; folic acid-methotrexate, folic acid-ferrocene, and methotrexate-ferrocene, respectively.

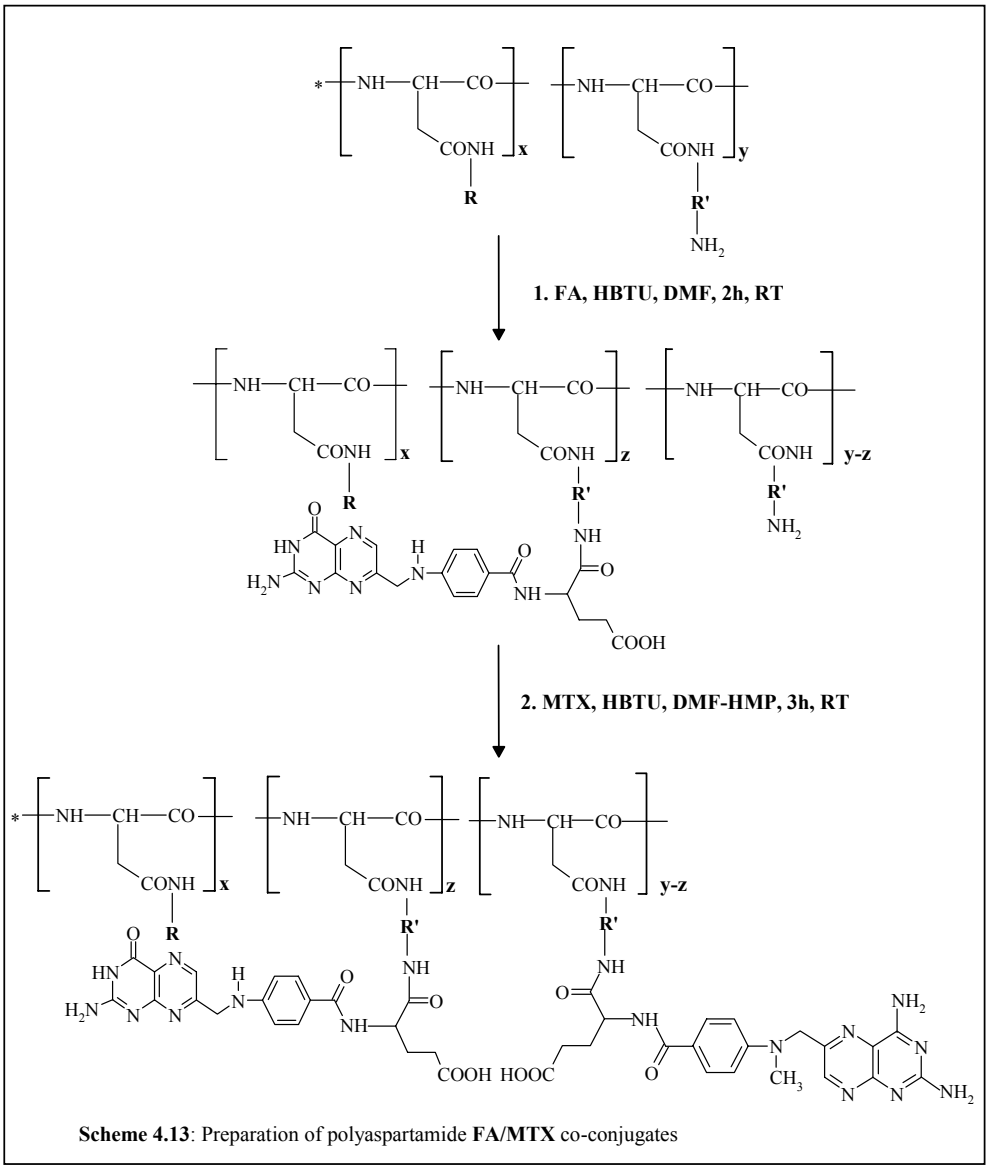
In the first two pairs, folic acid was used as an additional targeting moiety, given that the folate cellular uptake occurs by a natural endocytosis pathway mediated by folate receptor (FR), the latter being overexpressed on the surface of a variety of cancer cells including colon cancer [43]. Furthermore, since folate is an essential vitamin required in substantial quantities by virtually all dividing cells for purine, nucleotide, and DNA synthesis, one might speculate that folic acid would be avidly consumed, and hence required, by cancer cells. Consequently, the resulting co-conjugates, owing to the presence of the two targeting moieties *i.e.* the tertiary amine and folic acid, are expected to be more efficiently cell-selective in comparison with the conjugates possessing only the tertiary amine. Moreover, the presence of these entities suggests competitive mechanisms of cellular uptake, namely, folate receptor-mediated (folic acid) and adsorptive (tertiary amine) endocytosis. However, the fact that tertiary amine accounts for 90 mo-l% and folate at most 10 mol-% in the recurring unit, allows for speculation that the mechanism of cellular uptake of these co-conjugates would predominantly depend on cancer cell surface characteristics. In other words, since the FR is not a common characteristic of all cancerous cells, for those carrying negative surface charges, adsorptive endocytosis is expected to be the indicated mechanism of cell entry, while for others characterized by overexpressed FR, folate-mediated endocytosis would be the mechanism of cellular entry.

The simultaneous incorporation of MTX and ferrocene in these polymeric carriers, apart from exemplifying the co-drug conjugation ability, represents a tool for the delivery of two anticancer drugs with different mechanisms of biological activity. MTX is an antimetabolite and Ferrocene, an agent purportedly causing oxidative DNA damage. The **MTX/Fc** co-conjugates could be to be more efficient in cancer-cell killing than the individual drugs. The advantages of synergistic effects were reported by Buzdar and co-workers [144].

The first step leading to the formation of homoconjugate with desired 50% NH_2 acylation was generally HBTU-mediated. It involved the treatment of the carrier with 0.7-0.8 equivalents of the first drug and 0.6 equivalent of HBTU. After conventional work-up and isolation, the drug content was determined by spectroscopic analysis. In the second step, the homoconjugate was allowed to react with the second drug through either a second HBTU coupling or by the active ester method. Scheme 4.16 exemplifies the preparation of **FA/MTX** co-conjugate. Moreover, in all cases, either MTX or FA was anchored as the first drug to ensure incorporation *i.e.* 50% NH_2 acylation. With MTX or FA acid-bifunctionalized, there will be competitive reaction of the α and γ carboxylic groups of the glutamic moiety. Therefore, during the first step, characterized by more primary amino groups available for drug binding, the probability of MTX or FA drug loading up to the expected level will be increased.

In the cases of co-conjugation involving the ferrocene system, generally as the second drug, the active ester coupling was preferred over HBTU-mediated coupling to avoid main chain fragmentation.

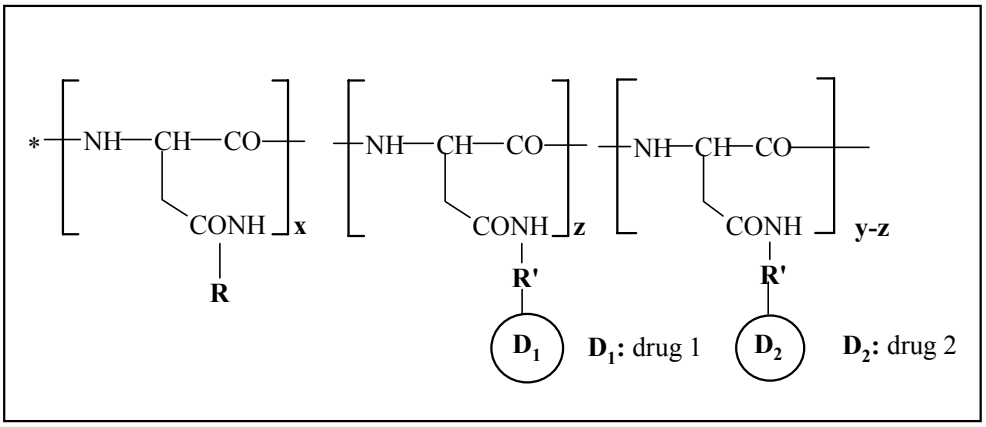
The water-soluble co-conjugates were precipitated from solution and, after fractionation and purification by size exclusion chromatography and aqueous dialysis, were isolated by freeze-drying. Drug contents, in percent by mass, were determined by various analytical methods, with inductively coupled plasma-optical emission spectroscopy (ICP-OES) used exclusively for iron. In cases of undersubstitution (*i.e.* below 95% of available primary amino groups), the co-conjugates were retreated with 0.8 equivalent of the second drug.



Scheme 4.13: Preparation of polyaspartamide **FA/MTX** co-conjugates

Tables 4.33 and 4.34 show the composition of these co-conjugates and the reaction conditions, respectively, whereas Table 4.35 reports the viscometric and ^{1}H NMR results, and Table 4.36 gives a summary of all analytical results.

Table 4.33: Composition of PAsA co-conjugates



Carriers	R	R'	x/y	D_1	D_2	Co-conjugates designation
1 (90:10)	$-(CH_2)_3N(CH_3)_2$	$-(CH_2)_3-$	9	FA	MTX	**1** (90:10)**-FA/MTX**
3 (90:10)	$-(CH_2)_3N(CH_3)_2$	$-(CH_2)_3N(CH_2)_2-$	9	FA	MTX	**3** (90:10)**-FA/MTX**
1 (90:10)	$-(CH_2)_3N(CH_3)_2$	$-(CH_2)_3-$	9	FA	Fc	**1** (90:10)**-FA/Fc**
3 (90:10)	$-(CH_2)_3N(CH_3)_2$	$-(CH_2)_3N(CH_2)_2-$	9	FA	Fc	**3** (90:10)**-FA/Fc**
1 (90:10)	$-(CH_2)_3N(CH_3)_2$	$-(CH_2)_3-$	9	MTX	Fc	**1** (90:10)**-MTX/Fc**
3 (90:10)	$-(CH_2)_3N(CH_3)_2$	$-(CH_2)_3N(CH_2)_2-$	9	MTX	Fc	**3** (90:10)**-MTX/Fc**

Table 4.34: Reaction conditions for all PAsA co-conjugates

Reactants in feed				**Reaction conditions** [b]	**PAsA co-conjugates**	
Carriers	**Drug (or) active ester /(coupling agent)**	**Carrier : drug (or active ester) : coupling agent ratio** (mol-%) [a]	**Medium**		**Yield** (%) [c]	**Designation**
1 (90:10)	Step 1: FA/HBTU Step 2: MTX/HBTU	Step 1: 1:0.7:0.6 Step 2: 1:0.8:0.5	Step 1: DMF Step 2: DMF-HMP	Step 1: 2h, RT Step 2: 3h, RT	53 [d]	**1** (90:10)**-FA/MTX**
3 (90:10)	´´	´´	´´	´´	65 [d]	**3** (90:10)**-FA/MTX**
1 (90:10)	Step 1: FA/HBTU Step 2: Fc-ONp	Step 1: 1:0.7:0.6 Step 2: 1:0.8	Step 1: DMF Step 2: DMSO	Step 1: 2h, RT Step 2: 10h, RT	75	**1** (90:10)**-FA/Fc**
3 (90:10)	´´	´´	´´	´´	62	**3** (90:10)**-FA/Fc**
1 (90:10)	Step 1: MTX/HBTU Step 2: Fc-ONp	Step 1: 1:0.8:0.7 Step 2: 1:0.8	´´	´´	75	**1** (90:10)**-MTX/Fc**
3 (90:10)	´´	´´	´´	´´	63	**3** (90:10)**-MTX/Fc**

[a] Molar ratio of carrier repeating unit to drug to coupling agent in step 1, and molar ratio of homoconjugate to drug (or active ester) (to coupling agent) in step 2.

[b] RT= room temperature.

[c] Co-conjugate yield (based on starting homoconjugate) after size exclusion chromatography and ultimate (25 000 molecular weight cut-off) dialysis.

[d] Yield (based on starting co-conjugate) after posttreatment.

Table 4.35: ^{1}H NMR and viscometric results for PAsA co-conjugates

Co-conjugates designation	**x**	**z** [a]	**y** [b]	**y-z** [c]	**% MTX** Found [d]	**% FA** Found [d]	**% Fe** Found [d]	**Protons counted** [e] (expected) [f] **chemical shift** (ppm) δ 8.5-6.5 [g]	δ 4.25-4.0	δ 3.5-3.0	δ 1.8-1.5
1 (90:10)**-FA/MTX**	90	5.8	9.7					4.83 (5)	-	23 (22)	20 (20)
3 (90:10)**-FA/MTX**	´´	4.3	9.6					4.8 (5)	-	22 (22)	18 (18)
1 (90:10)**-FA/Fc**	´´	5.8	10	4.9		9.38	1.2	2.6 (5)	4.4 (9)	21.7 (22)	21 (21)
3 (90:10)**-FA/Fc**	´´	4.6	9.8	5.3		8.57	1.28	2.3 (5)	4.8 (9)	21.5 (22)	19 (19)
1 (90:10)**-MTX/Fc**	´´	4.8	9.9	5.5	8.7		1.3	2.2 (5)	4.95 (9)	22 (22)	20.6 (21)
3 (90:10)**-MTX/Fc**	´´	4.3	9.8	5.6	8.23		1.35	2.1 (5)	5.1 (9)	22 (22)	19 (19)

[a] Mol-% of first drug derived from ^{1}H NMR after step 1.

[b] Total mol-% of drugs derived from ^{1}H NMR after step 2.

[c] Mol-% of second drug derived from ^{1}H NMR after step 2.

[d] Mass percentage of drug derived from ^{1}H NMR after step 2.

[e] In D_2O, pH 10-11, chemical shifts, δ/ppm, referenced against internal sodium 3-trimethylsilyl-2,2,3,3-d_4-propionate; integration error limits ± 12 %.
Protons are calculated for conjugate composition (Scheme 4.13).

[f] Expected count for composition in accordance with recurring unit (see b).

[g] Proton assignment, δ/ppm: 8.6-6.6 (aromatic and heteroaromatic *CH* of MTX and (or) FA); 4.3-4.25 (*CH* of ferrocenyl); 3.5-3.0 (CONH*CH_2*); 1.8-1.5 (CH_2*CH_2*CH_2).

Table 4.36: Summary of analytical data for all PAsA co-conjugates

Carriers designation	η_{inh} (mL g^{-1}) [a]		**y** [b]	**% MTX** UV [c]	**% MTX** NMR [d]	**% Fe** OES [e]	**% Fe** NMR [d]	**% FA** UV [c]	**% FA** NMR [d]	**NH_2 acylation** (%) [f]
	Homoconjugate (step 1)	Co-conjugate								
1 (90:10)-**FA/MTX**	15.05	16.01	9.7	8	7.45	-	-	-	11.58	97 [g]
3 (90:10)-**FA/MTX**	13.25	14.5	9.6	10.58	10.0	-	-	-	8.7	96 [g]
1 (90:10)-**FA/Fc**	18.0	19.75	10	-	-	1.25	1.2	9.55	9.8	100
3 (90:10)-**FA/Fc**	14.05	15.5	9.8	-	-	1.12	1.28	8.75	9.0	98
1 (90:10)-**MTX/Fc**	16.5	17.05	9.9	8.37	8.7	1.24	1.34	-	-	99
3 (90:10)-**MTX/Fc**	14.25	15.3	9.8	8.23	8.66	1.28	1.35	-	-	98

[a] At 30.0 ± 0.5 ^{o}C, in deionized H_2O; concentration c = 2 mg/mL.

[b] Total mol-% of drugs derived from ^{1}H NMR after step 2.

[c] Mass percentage calculated from UV absorbance of MTX and FA in H_2O at 370 nm using ε = 6500 $M^{-1}cm^{-1}$ and 6200 $M^{-1}cm^{-1}$, respectively.

[d] Mass percentage derived from ^{1}H NMR spectrum (error limit ± 12%) assuming no loss of first drug during step 2.

[e] Mass percentage of Fe obtained by ICP-OES.

[f] Derived from co-conjugate composition after step 2.

[g] In parallel experiments conducted under identical or modified conditions, percentage acylation ranged from 74-92%, requiring retreatment.

As can be seen in Table 4.33, the polyaspartamide co-drug conjugates were obtained in yields of 53-75%. They were characterized by inherent viscosities in the range of 16-20 mL g^{-1}. These were higher than those of the precursor carriers (11-12 mLg^{-1}) and the derived homoconjugates (13-18 mL g^{-1}). The **FA/Fc** and **MTX/Fc** co-drugs were incorporated into polymer in overall extents of 98-100% NH_2 whereas for **FA/MTX**, a posttreatment was required to achieve an extent of conjugation of 96-97%. The homoconjugates **1**(90:10)-**FA** and **3**(90:10)-**FA** resulting from the first step of the synthesis of **FA/MTX** co-conjugates showed extents of conjugation of 58 and 43%, respectively. These correspond to folate incorporation of 11.58 and 8.7 % FA by mass, respectively, determined by NMR spectroscopy (see Section 5.3.3.3). On balance, the undersubstitution observed with the co-conjugates **1**(90:10)-**FA**/**MTX** and **3**(90:10)-**FA**/**MTX** could reasonably be traced to the bifunctionality of MTX. Indeed, MTX being bifunctionlized doubles the probability of competitive reaction of the α and γ carboxylic groups of the glutamic moiety to the remaining free amino groups during the second step. The almost complete acylation observed with the **FA/Fc** and **MTX/Fc** co-conjugates involving Fc as second drug supports this argument because the ferrocene is monofunctionalized, and therefore no competitive reactivity occurs. For the **FA/MTX** co-conjugates, the exact MTX content by mass could not be assessed by NMR spectroscopy. This, because the spectra of FA and MTX are identical especially in the aromatic and heteroaromatic of 8.5-6.5 ppm region, of which peak integrals are commonly used for such determination (see Section 4.2.1.1). Thus, one had recourse to UV-vis spectroscopic analysis. The procedure is amply described in Section 5.3.4 (page 204). This analytical technique revealed the co-conjugates **1**(90:10)-**FA**/**MTX** and **3**(90:10)-**FA**/**MTX** to contain 8 and 10.58% MTX by mass, respectively. These MTX contents were in fair correspondence with those provided by NMR spectroscopy (*i.e.* 7.45 and 10%, respectively). The latter were obtained on assumption that no major loss of FA by cleavage occurred during the second step of this preparation.

For the determination of the exact **Fe** content by mass in the co-conjugates **1**(90:10)-**FA/Fc** to **3**(90:10)-**MTX/Fc**, the ICP-OES method was used as an alternative to NMR spectroscopy. Thus, the co-conjugates **1**(90:10)-**FA/Fc** and **3**(90:10)-**FA/Fc** were found to contain 1.25 and 1.12% Fe by mass, respectively. The co-conjugates **1**(90:10)-**MTX/Fc** and **3**(90:10)-**MTX/Fc** contained 1.24 and 1.28 % Fe by mass, respectively. On assumption that the homoconjugates were stable enough to survive the second step, the NMR spectroscopy confirmed these Fe contents.

Furthermore, the UV-vis spectra of Fc conjugates (Section 4.2.2.1) in H_2O revealed almost no Fc absorption in the region 370-380nm which occurred with **MTX**. Therefore, it appears reasonable to attribute the absorption at 370nm to bound **MTX** in the spectra of **MTX/Fc** co-conjugates. The UV-vis determination of MTX content using the molar extinction coefficient value, $\varepsilon = 6500\ mol^{-1}cm^{-1}$ and the absorbance at $\lambda = 370$ nm in H_2O, showed the co-conjugates **1**(90:10)-**MTX/Fc** and **3**(90:10)-**MTX/Fc** to contain 8.37 and 8.23% MTX by mass, respectively. On assumption of homoconjuagte stablility retained during the second step, one finds the co-conjugates to be loaded with 8.7 and 8.66% MTX by mass, determined by ^1H NMR.

The clear correspondence of drug contents in the co-conjugates determined by the different analytical methods demonstrates that the polyaspartamide-type polymers were effective co-drug carriers, although only a small number of carriers were investigated. These results also show that there was no major loss of either MTX or folic acid during the two steps of the co-conjugation process.

The IR spectra of these co-conjugates were dominated by the strong amide I and II bands at 1650 and 1540 cm^{-1}.

4.2.3.2 Cell culture testing

The antiproliferative activity of the polyaspartamide co-conjugates was also evaluated against HeLa (drug-sensitive) and Colo (strongly drug-resistant) cell lines. The procedure was identical to that employed in previous cell culture testing

experiments. The performance of the Fe containing conjugates was referenced against that of free cisplatin used as control, while the activity of free MTX served as reference for the MTX co-conjugates. The IC_{50} values derived from plots of cell growth relative to untreated control versus conjugate concentration (Figures 4.7 and 4.8), are compiled in Table 4.37 for both cell types. The table also comprises the IC_{50} data determined under the same conditions for free drugs (MTX and cisplatin) as well as the activity factors of the conjugates expressed in terms of IC_{50} (free drug)/ IC_{50} (co-conjugate). For comparison, data are also included for homoconjugates of MTX or ferrocene.

Let us first inspect the data for folate-**MTX** conjugates. An averaged activity factor of 1.09 derives from an averaged IC_{50} value (0.047 μg MTX/mL) against HeLa cells. Against the resistant cells, an averaged factor of 3.14 is found, which derives from an averaged IC_{50} value (0.7955 μg MTX/mL). Thus, these co-conjugates as a group are as active as free MTX against the sensitive line, and some 3-fold more active than the free drug against the strongly resistant cells. When comparing the activity factors of the homoconjugates with those of the folate-MTX co-conjugates, it can be seen that the folate by its presence reduces the cell-killing efficaciousness of the homoconjugates. Thus, these co-conjugates as group possess some 7- and 5-fold lower activity than homoconjugates as a group against HeLa and Colo cells, respectively. On comparing the performance of folate-**MTX** co-conjugates with their folic acid contents, there also appears a trend of decreasing activity with increased folate incorporation. Thus, by being less cytotoxic than the homoconjugates, the folate-**MTX** co-conjugates did not much improve the performance of MTX against the tested cells; hence, they do not represent an improvement of therapeutic effectiveness. This limits the utility of the simultaneous delivery of folic acid and its antagonist MTX.

Let us now proceed with Fe containing conjugates. The AF values reveal, on balance, all ferrocene samples to be less active than cisplatin as growth inhibitors against both cell lines. Averaged activity factors of 0.09 (from averaged IC_{50} value, 0.852 μg Fe/mL) and 0.2 (from averaged IC_{50} value, 0.5988 μg Fe/mL) are found against HeLa and Colo cells, respectively. Thus, as a group the ferrocene

samples are some 11- and 5-fold less effective than free cisplatin in killing the sensitive and resistant cells, respectively. However, the IC_{50} values in the range of 0.1-1.6 μg Fe/ml, are lower than previously reported values of 2-5 μg Fe/ml against HeLa cells [139] and 0.2-2 μg Fe/ml against Colo cells [141].

Moreover, the decrease of antiproliferative activity upon folic acid incorporation, encountered with MTX-homoconjugates, is also apparent with those of the ferrocene-type. Thus, the folate-**Fc** co-conjugates as group experience 3- and 10-times lower activity against the sensitive and resistant cells, respectively, in comparison to the homoconjugates. This loss of activity also increases with increasing incorporated folate.

When considering the IC_{50} values, one finds co-conjugate **1-FA/Fc** to be less active than **1-Fc** against Colo cells. However, the cell-killing efficacy is more pronounced with **1-FA/Fc** insofar as the ultimate extent of cell viability is concerned, with only 8% of cells surviving, whereas **1-Fc** forms an unexpected, even slightly increasing plateau at the concentration of ~0.2 μg Fe/mL corresponding to about 30% cells surviving (Fig. 4.8(d)). Thus, the folate incorporation had a beneficial effect in this case.

As folic acid incorporation did not improve significantly the cytotoxic activity of ferrocene against the sensitive cell line, the folate-ferrocene approach is not beneficial from a cancer therapeutic point of view. However, this approach could be an interesting route where the simultaneous delivery of folic acid and iron is needed. For pregnancy, where iron deficiency anaemia and folate deficiency macrocytic anaemia are the most encountered anaemias [174], there would be an appropriate case for the exploration of this approach.

In summary: the data indicated that the incorporation of folic acid, contrary to expectation, profoundly reduces the efficacy in killing cancer cells of the polymer-drug conjugate of both MTX and ferrocene types. One could speculate that since folate is a cellular nutrient, once within the cell, it induces cancer cell proliferation. However, the limited number of compounds investigated did not allow for drawing realistic conclusions. Therefore, more *in vitro* experiments will be required to elucidate the question of the reduction of cytotoxicity associated

with the folate-drug co-conjugates. As it stands, these preliminary results do not support the use of folic acid as a targeting moiety for the delivery of the drug systems herein investigated.

Table 4.37: Antiproliferative activity of polyaspartamide co-conjugates

Polyaspartamide co-conjugates				HeLa		CoLo	
Designation	% MTX by mass	% Fe by mass	% FA by mass	IC_{50} (μg MTX/mL)	AF [a]	IC_{50} (μg MTX/mL)	AF
1-MTX	18.52	-	-	0.013	3.92	0.196	12.4
3-MTX	18.7	-	-	0.0013	39.2	0.149	16.2
1-FA/MTX	7.45	-	11.58	0.054	0.94	1.426	1.7
3-FA/MTX	10.0	-	8.7	0.04	1.3	0.165	14.7
MTX	-	-	-	0.051	-	2.42	-
				IC_{50} (μg Fe/mL)	AF [c]	IC_{50} (μg Fe/mL)	AF
1-Fc	-	2.5	-	0.124	0.64	0.032	3.78
3-Fc	-	2.49	-	0.741	0.11	0.171	0.68
1-FA/Fc	-	1.2	9.8	1.648	0.05	1.5	0.08
3-FA/Fc	-	1.28	9.0	0.895	0.09	0.692	0.18
Cisplatin	-	-	-	0.079	-	0.121	-

[a] Activity factor defined as IC_{50} [fre MTX] : IC_{50} [conjugate].
[b] Resistance factor defined as IC_{50} [Colo] : IC_{50} [HeLa].[c] Activity factor defined as IC_{50} [free Cisp] : IC_{50} [conjugate].

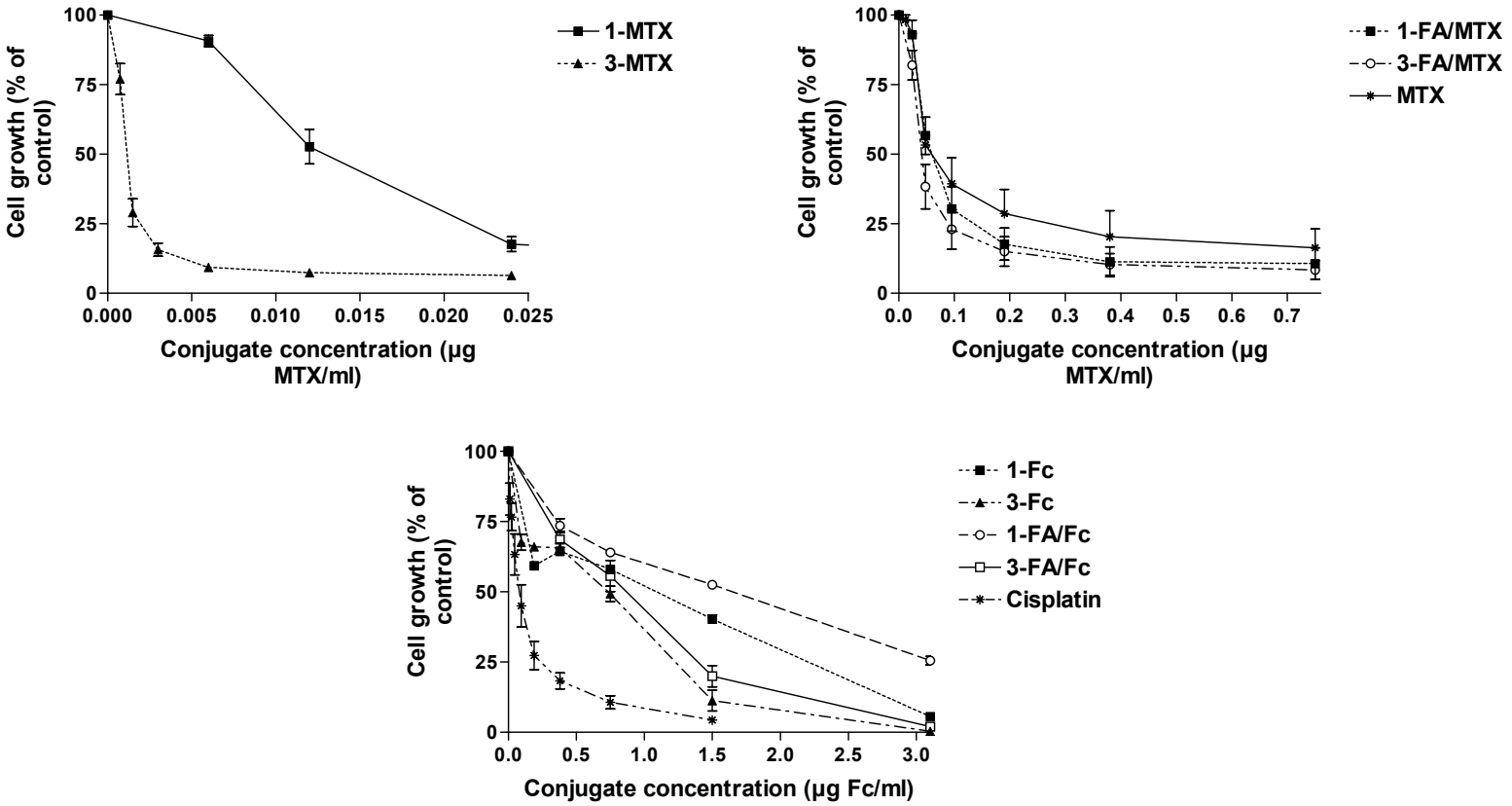


Figure 4.7: Antiproliferative activity of PAsA co-conjugates, free MTX, and free cisplatin against HeLa cells

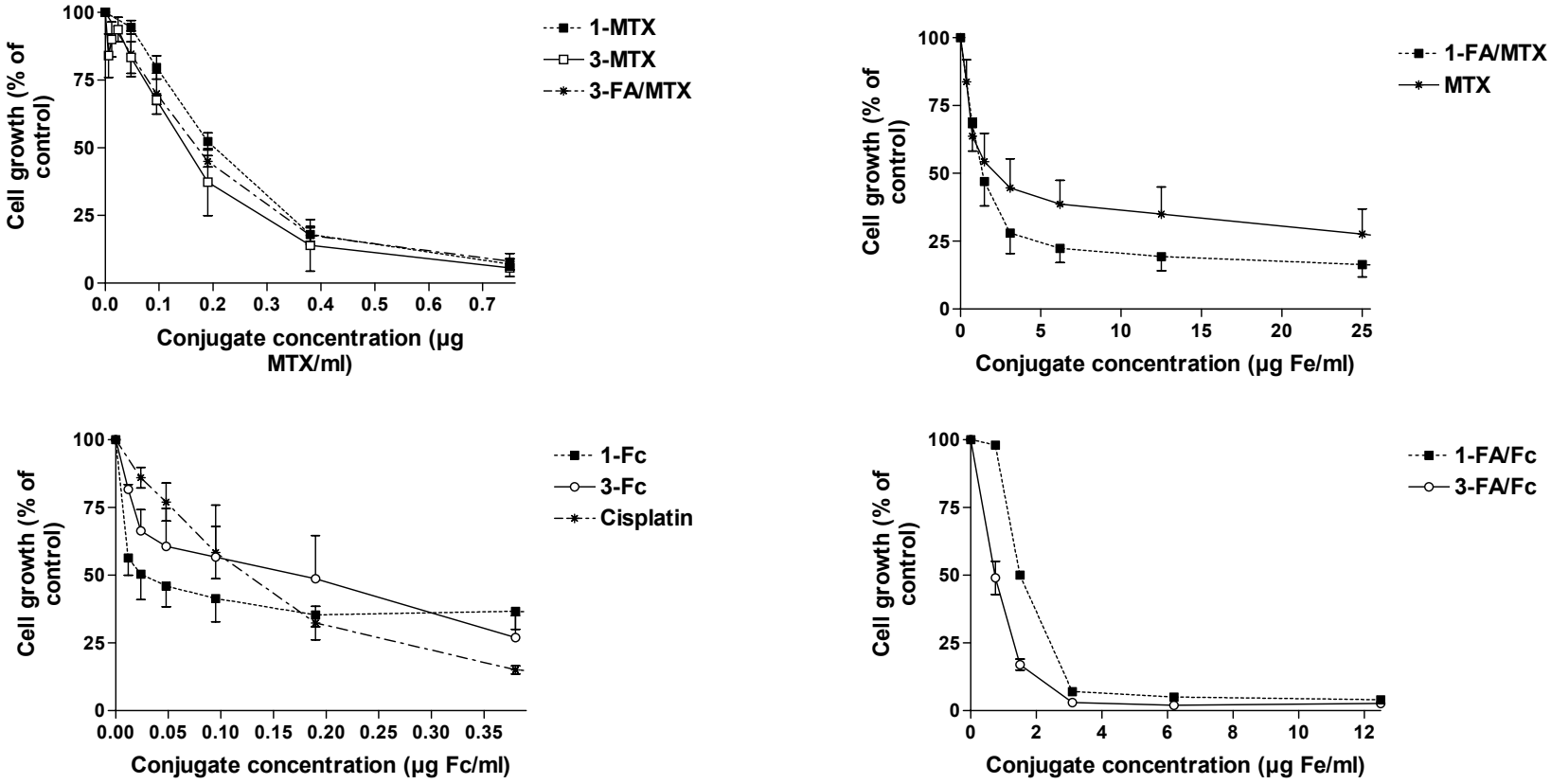


Figure 4.8: Antiproliferative activity of PAsA co-conjugates, free MTX, and free cisplatin against Colo cells

CHAPTER 5

EXPERIMENTAL SECTION

5.1 General Procedures

Solid-state Infrared (IR) spectra were recorded on KBr pellets over the region of 4000-600 cm^{-1}. However, only significant bands were cited in this thesis. ^{1}H-NMR spectra (in D_2O solutions) were obtained using BRUKER AVANCE 300 operating at 300 MHz; chemical shifts,δ in ppm, were referenced against sodium 3-(trimethylsilyl)-2,2,3,3-d_4-propionate ($\delta_{HOD} \approx 4.83$ ppm; integration error limit ± 12%). Immediately prior to recording, the pH was adjusted to 10 (NaOH) in order to eliminate potential protonation effects. The spectra of conjugates were scanned in *duplo* and the derived intensities averaged for proton count determination. Inherent viscosities, η_{inh}, were determined at 30.0 ± 0.5°C in Cannon-Fenske tubes. Deionized water and DMF were the solvents (c = 0.2 g/100 mL), and the results, obtained as the mean of triplicate determinations, were given in units of mL g^{-1}. Prior to dialysis, purification was performed by size exclusion chromatography on a 2.5 x 25 cm column loaded with Sephadex G-25 gel, eluted with distilled water.

Dialysis operations were performed against deionized water in cellulose tubing, Spectra/Por 4 and Spectra/Por 6 (Spectrum Industries, Los Angeles, CA), with weight-average molecular weight cut-off limits of 12000 - 14000, and 25000, respectively.

Aqueous polymer and conjugate solutions were freeze-dried in a VIRTIS Bench Top 3 freeze-drier operating at -30°C, 10-15 Pa. The freeze-dried polymers were routinely post-dried in a SARTORIUS Thermo Control infrared drying system.

Iron determinations were made by inductively coupled plasma-optical emission spectroscopy (ICP-OES) using a multi-standard solution calibrated at 0.5 ppm in water. UV spectroscopy was done on a HITACHI 2000 spectrophotometer, scan

speed 400nm/min; both analytical methods were performed in the School of Chemistry of this University.

The weight-average molecular weight (M_w) and number-average molecular weight (M_n) of final polymers and polymer-drug conjugates were determined by gel permeation chromatography (GPC) on Akta Explorer (Amersham, Pharmacia, Sweden) equipped with a 1.5 x 100 cm column packed with Sepharose 6 gel, at a flow rate of 0.5ml/min, refraction index detectors (7-15), using a buffer solution of 0.3 M sodium acetate containing 0.5 g NaN_3, pH 6.5., as mobile phase. These determinations were generously performed in the laboratory of medicinal chemistry, Institute of Macromolecular Chemistry, Academy of Science of the Czech Republic, Prague, and data forwarded back. Therefore no GPC chromatograms were available to be included in this thesis. Carbon, hydrogen, and nitrogen analyses (in triplicate, data averaged) were performed in the same institution.

5.2 Reagents, Reactants, and Solvents

The aprotic solvent, N,N-Dimethylformamide (DMF), was refluxed over phosphoric anhydride (P_2O_5), distilled under reduced pressure in a faint stream of N_2, and kept over molecular sieves 4A. All reactions involving its use were performed under anhydrous conditions. N-methylpyrrolidone (NMP) and hexamethylphosphoramide (HMP) were predried over molecular sieves 4A prior use. Dimethylsulfoxide (DMSO) was used as delivered. Deionized H_2O was used also for dialysis operations.

The hydroxyamines, mono- and diamines, and methoxyamine were commercial grades (Fluka Chemie AG, Aldrich Chemie G.m.b.H), and used as received. These included: 1, 3-propylenediamine (PDA); 2, 2'-(ethylenedioxy) diethylamine (EDDA); diethylenetriamine (DET), ethylenediamine (EDA), 2-methoxyethylamine (MEA); 1, 3-diamino-2-propanol (DAP). ethanolamine (EA), 2-(2-aminoethoxy)ethanol (AEE); 3-(N,N-dimethylamino)propylamine (DMP) and 3-(N,N-dimethylamino)ethylamine (DME) were also commercial grades

(Across Organics) and where used as received, and so was glacial acetic acid (Merck).

D,L-aspartic acid, N,N'-dicyclohexylcarbodiimide (DCC); 2-(1H-benzotriazol-1-yl)-1,1,3,3-tetramethyluronium fluorophosphate (HBTU); triethylamine (TEA), 4,7,10-trioxa-1,13-tridecanediamine(TRIA), O,O´-Bis(aminopropyl)poly(ethylene glycol) 1500, di-*tert*-butyldicarbonate $(Boc)_2O$, (Fluka Chemie AG, Aldrich Chemie G.m.b.H) were also used as delivered. The solid methylenebisacrylamide (MBA) was recrystallized from isopropanol in the presence of 2,6-di-*tert*-butyl-p-cresol (Fluka Chemie AG) prior to use. *p*-Nitrophenol was purchased from BDH Laboratory Reagents and used as delivered.

The following solvents, diethyl ether (Et_2O), acetone (Me_2CO), hexane (Hex.) were used as supplied. Ethyl acetate (EtAc) was distilled and dried over calcium chloride ($CaCl_2$) before use. Dioxan was distilled and kept over potassium hydroxide. Dichloromethane (DCM) was dried, distilled, and kept over calcium chloride ($CaCl_2$).

Methotrexate, MTX (Sigma), which contains 2.5 mol of water per mol of drug, and folic acid dihydrate, FA, purchased from Across Organics, were pre-dried in an Aberhalden tube for 24h at 50^{o}C before use for conjugation.

5.3 Experimental Procedures

5.3.1 Preparation of polymeric carriers

5.3.1.1 Polyaspartamide (PAsA) carriers

Poly-DL-succinimide (PSI): PSI was prepared by the method of Neri and Antoni [151]; products of approximately equal viscosity were pooled from several runs and thoroughly mixed to give a master batch with η_{inh} (determined in DMF) of 35 mL g^{-1}.

Polyaspartamide carriers (PAsA): These carriers were prepared according to a general procedure, which, has been amply used in this laboratory. However, a

major modification was introduced. This concerns the reaction time in each step, the sequence and methods of addition of the different reactants, as well as the work-up.

Polyaspartamide 1 (90:10)

Polysuccinimide (PSI) (6g, 60mmol) was dissolved in 60 mL of freshly distilled DMF with stirring. 3-(N,N-Dimethylamino)propylamine (DMP) (5.52g, 54mmol) was dissolved in 15 mL of DMF, and added in one dash to the stirred PSI stirring solution. The resulting solution was saturated with N_2, the flask tightly stoppered to preclude any moisture penetration, and stirring continued at room temperature for 10 h.

To 1,3-propylenediamine (PDA) (1.33g, 18mmol, 3-fold excess) predissolved in 25 mL of DMF and cooled in an ice bath, was added dropwise the PSI-DMP solution over 1h. The overall solution was N_2-resaturated, stirred in the ice bath for 4h, then at room temperature for 24h at RT. The solution volume was reduced to ¼ by rotatory evaporation under reduced pressure (bath temperature not exceeding 70 ^{o} C). The polymeric product was precipitated out with 150 mL of Et_2O-Me_2CO (2:1), thoroughly washed with precipitant to eliminate any unreacted diamine, dissolved in 100 mL of distilled water, and purified in a two-step dialysis process. Firstly, the solution was dialysed in Spectra/Por 4 tubing for 48h against distilled water, the outer batches being changed several times, and secondly, in Spectra/Por 6 tubing for another 48h. The retentate, pH~8, was free-dried to afford 6.25g (52%) of beige, water-soluble material; η_{inh}, 11.61 mL g^{-1}. Analysis by GPC revealed the following characteristics: M_w = 25 280; M_n = 12 330; I_n = 2.05 (Table 4.7 row 2).

^{1}H NMR (D_2O), δ/ppm: 4.75-4.5, 10H (expected: 10H, *CH* Asp); 3.5-3.0, 20H (expected: 20H, CONH-*CH_2*-); 2.9-2.0, 94H (expected: 94H, -CO-*CH_2*, *CH_2*N(*CH_3*)$_2$, *CH_2*NH_2); 1.8-1.5, 20H (expected: 20H, CH_2*CH_2*CH_2).

Polyaspartamide 2 (80:20)

Polymer **2** (a variant of **1**, see Table 4.2 row 4), was prepared analogously to **1**. Thus, PSI (2g, 20mmol), DMP (1.64g, 16mmol) and PDA (0.9g, 12mmol)

afforded polymer **2** in a yield of 2.85g (72%) as beige, water-soluble material; η_{inh}, 14.47 mL g^{-1}. Analysis of **2** by GPC revealed the following characteristics: M_w = 27 640; M_n = 12 230; I_n = 2.26 (Table 4.7 row 3).

^{1}H NMR (D_2O), δ/ppm: 4.75-4.5, 5H (expected: 5H, *CH* Asp); 3.5-3.0, 10H (expected: 10H, CONH*CH_2*); 2.9-2.0, 44H (expected: 44H, -CO-*CH_2*, *CH_2*N (*CH_3*)$_2$, *CH_2*NH_2); 1.8-1.5, 10H (expected: 10H, CH_2*CH_2*CH_2);

Polyaspartamides 3 (90:10) and 4 (80:20)

Polyaspartamides **3** and **4** were prepared by the procedure used to afford **1** and **2** respectively, 1, 3-propylenediamine (PDA) being replaced by diethylenetriamine (DET); the reactions conditions as well as molar ratio of reactants were maintained.

Polymer **3** was obtained as beige, water-soluble, and hygroscopic material in a yield of 52%; η_{inh}, 10.24 mL g^{-1}; it possessed the following characteristics: M_w = 22 560; M_n = 12 190; I_n = 1.85 (Table 4.7 row 4).

^{1}H NMR (D_2O), δ/ppm: 4.75-4.5, 10H (expected: 10H, *CH* Asp); 3.5-3.0, 20H (expected: 20H, CONH*CH_2*); 2.9-2.0, 98H (expected: 98H, -CO-*CH_2*, *CH_2*N (*CH_3*)$_2$, *CH_2*NH-); 1.8-1.5, 18H (expected: 18H, CH_2*CH_2*CH_2).

Polymer **4**, obtained in a yield of 59%, was also beige, showed water solubility and hygroscopicity; η_{inh}, 16.99 mL g^{-1}; M_w = 28 360; M_n = 11 340; I_n = 2.5 (Table 4.7 row 5).

^{1}H-NMR (D_2O), δ/ppm: 4.75-4.5, 5H (expected: 5H, *CH* Asp); 3.5-3.0, 10H (expected: 10H, CONH*CH_2*); 2.9-2.0, 48H (expected: 48H, -CO-*CH_2*, *CH_2*N (*CH_3*)$_2$, *CH_2*NH-); 1.8-1.5, 8H (expected: 8H, CH_2*CH_2*CH_2).

Polyaspartamide 5 (90:10)

The preparation procedure is similar to that leading to **1**. However, minor l modifications concerning the second step reaction time and in the work-up were introduced.

Thus, PSI (6g, 60mmol) was dissolved in 60 mL of freshly distilled DMF with stirring. DMP (5.52g, 54mmol) dissolved in 15 mL of DMF, was added in one dash to the stirred PSI solution. The resulting solution was saturated with N_2, the flask tightly stoppered to preclude any moisture penetration, and stirring was continued for 10 h at RT.

To 2,2'-(ethylenedioxy)diethylamine (EDDA) (2.68g, 18mmol, 3-fold excess), predissolved in 25 mL of DMF and cooled in an ice bath, was added dropwise the PSI-DMP solution over a period of 1h. The resulting solution was N_2-resaturated, stirred in the ice bath for 4h, and then at room temperature for 24h. The solution volume was reduced to ¼ by rotatory evaporation under reduced pressure (bath temperature not exceeding 70^{o}C). The polymeric product was precipitated out with 150 mL of Et_2O- Me_2CO (2:1), thoroughly washed with 3x15 mL of boiling toluene to remove efficiently the excess diamine (in previous experiments from this laboratory, washing with the precipitant showed inefficacy to remove the unreacted EDDA), dissolved in 100 mL of distilled water, and purified in a two-step dialysis process. Firstly, the solution was dialysed in Spectra/Por 4 tubing for 48h against distilled water, the outer batches being changed several times, and secondly, in Spectra/Por 6 tubing for another 48h. The retentate, pH~8.5, was free-dried to afford 7.85g (61%) of beige, water-soluble material; η_{inh}, 10.57 mL g^{-1}, it was characterized as follows: M_w = 24 480; M_n = 11 540; I_n = 2.12 (Table 4.7 row 6).

^{1}H NMR (D_2O), δ/ppm: 4.75-4.5, 9H (expected: 10H, *CH* Asp); 3.7-3.6, 9H (expected: 8H, *CH_2*O), 3.5-3.0, 20H (expected: 20H, CONH*CH_2*); 2.9-2.0, 94H (expected: 94H, -CO-*CH_2*, *CH_2*N (*CH_3*)$_2$, *CH_2*NH_2); 1.8-1.5, 18H (expected: 18H, CH_2*CH_2*CH_2); (Table 4.3 row 7).

Polyaspartamide 6 (80:20)

Polymer **6** (a variant of **5**, see Table 4.2 row 8), was prepared and worked up similarly to **5**. Thus, PSI (2g, 20mmol), DMP (1.64g, 16mmol) and EDDA (1.78g, 12mmol, 3-fold excess) afforded 2.41g (61%) of polymer **6** as beige, water-

soluble material, η_{inh}, 20.14 mL g^{-1}; with the following characteristics: M_w = 54 850; M_n = 30 470; I_n = 1.8 (see Table 4.7 row 7).

^{1}H NMR (D_2O), δ/ppm: 4.75-4.5, 4H (expected: 5H, *CH* Asp); 3.7-3.6, 7H (expected: 8H, CH_2O), 3.5-3.0, 11H (expected: 10H, CONHCH_2); 2.9-2.0, 43H (expected: 44H, -CO-CH_2, $CH_2N(CH_3)_2$, CH_2NH_2); 1.8-1.5, 8H (expected: 8H, $CH_2CH_2CH_2$); (Table 4.3 row 9).

Polyaspartamide 7 (90:10)

This polymer was prepared analogously to **1** (90:10) with a change in the amount polysuccinimide, and PDA being replaced by 1, 3-diamino-2-propanol (DAP). Thus, from PSI (3g, 30mmol), DMP (2.76g, 27mmol) and DAP (0.81g, 9mmol), it was obtained 3.19g (54%) of Polymer **7** as beige, fully water-soluble material.
η_{inh}, 13.25 mL g^{-1}, M_w = 17 860; M_n = 12 850; I_n =1.39 (Table 4.7 row 8).

^{1}H NMR (D_2O), δ/ppm: 4.75-4.5, 10H (expected: 10H, *CH* Asp); 3.7-3.6, 1H (expected: 1H, *CH*-OH), 3.5-3.0, 21H (expected: 20H, CONHCH_2); 2.9-2.0, 95H (expected: 94H, -CO-CH_2, CH_2-N(CH_3)$_2$, CH_2NH_2); 1.8-1.5, 18H (expected: 18H, $CH_2CH_2CH_2$).

Polyaspartamide 8 (90:10)

Polymer **8** was prepared in a two-step reaction procedure similarly to **1**. However, 3-(N,N-dimethylamino)propylamine (DMP) was substituted by ethanoamine (EA), and the first step consequently proceeded at a longer reaction time of 24h. PSI (3g, 30mmol) was used for the preparation and polymer **8** was obtained in a yield of 65%, and was characterized as follows: η_{inh}, 16.2 mL g^{-1}; M_w = 23 560; M_n = 28 280; I_n = 1.2 (Table 4.7 row 9)

^{1}H NMR (D_2O), δ/ppm: 4.75-4.5, 10H (expected: 10H, *CH* Asp); 3.7-3.6, 18H (expected: 18H, CH_2O), 3.5-3.0, 20H (expected: 20H, CONHCH_2); 2.9-2.0, 26H (expected: 26H, -CO-CH_2, CH_2NH-); (Table 4.6 row 3).

Polyaspartamide 9 (80:20)

Polymer **9** was obtained in an analogous procedure to the preparation of **8**. The reactants were the same. The only change concerned the molar ratios (refer to Table 4.5. row 4).

Polymer **9** was afforded as beige and water-soluble material in a yield of 68%, and possessed the following characteristics: η_{inh}, 14.02 mL g^{-1}; M_w = 54 000; M_n = 25 710; I_n = 2.1 (Table 4.7 row 10).

^{1}H NMR (D_2O), δ/ppm: 4.75-4.5, 5H (expected: 5H, *CH* Asp); 3.7-3.6, 8H (expected: 8H, *CH_2*O), 3.5-3.0, 10H (expected: 10H, CONH*CH_2*); 2.9-2.0, 16H (expected: 16H, -CO-*CH_2*, *CH_2*-NH-).

Polyaspartamide 10 (90:10)

Polymer **10** was obtained in a two-step reaction procedure similarly to **1**. However, 3-(N,N-dimethylamino)propylamine (DMP) was substituted by ethanoamine (EA), and the first step consequently proceeded at a longer reaction time of 24h. Diethylenetriamine (DET) in the second step was replaced by 1, 3-diamino-2-propanol (DAP).

Polymer **3** was obtained as beige, water-soluble, and hygroscopic material in a yield of 3.29g (68%) of as beige, and water-soluble material, η_{inh}, 18.43 mL g^{-1}; M_w = 31 070; M_n = 20 990; I_n = 1.48 (Table 4.7 row 11).

^{1}H NMR (D_2O), δ/ppm: 4.75-4.5, 10H (expected: 10H, *CH* Asp); 3.7-3.6, 55H (expected: 54H, *CH*-OH, *CH_2*O), 3.5-3.0, 20H (expected: 20H, CONH*CH_2*); 2.9-2.0, 22H (expected: 26H, -CO-*CH_2*, *CH_2*NH-); refer to Table 4.6 row 5.

Polyaspartamides 11 (90:10) and 12 (90:10)

These polymers were prepared similarly to the procedure that leading to polymer **10** with the exception that the diamine, DAP, in the second step, was replaced by PDA and EDDA for **11** and **12**, respectively.

Polymer **11** was also obtained as beige and fully water-soluble solid, in a yield of 2.5 g (74%), η_{inh}, 12.05 mL g^{-1}.

^{1}H NMR (D_2O), δ/ppm: 4.75-4.5, 10H (expected: 10H, *CH* Asp); 3.7-3.6, 18H (expected: 18H, *CH_2*O), 3.5-3.0, 20H (expected: 20H, CONH-*CH_2*); 2.9-2.0, 22H (expected: 26H, -CO-*CH_2*, *CH_2*NH); 1.8-1.5, 2H (expected: 2H, CH_2*CH_2*CH_2).

Polyaspartamide **12** obtained in yield of 2.25g (69%), was also found fully water - soluble, η_{inh}, 13.45 mL g^{-1}.

^{1}H NMR (D_2O), δ/ppm: 4.75-4.5, 10H (expected: 10H, *CH* Asp); 3.7-3.6, 24H (expected: 24H, *CH_2*O), 3.5-3.0, 20H (expected: 20H, CONH*CH_2*); 2.9-2.0, 22H (expected: 26H, -CO-*CH_2*, *CH_2*NH-); (Table 4.6 row 7).

Polyaspartamides 13 (90:10) and 14 (80:20)

The polyaspartamides **13** and **14** were obtained using a procedure analogous to that leading to polymers **8** and **9**. A minor modification was introduced by replacing ethanolamine (EA) by 2-(2-aminoethoxy)ethanol (AEE). Comparatively, polymer **14** is a variant of **13**, therefore, only the molar ratio of the reactants changes during the preparation.

Polymer **13** was afforded in a yield of 68% and possessed the following characteristics: η_{inh}, 11.54 mL g^{-1}; M_w = 54 480; M_n = 20 300; I_n = 2.71 (Table 4.7 row 12).

^{1}H NMR (D_2O), δ/ppm: 4.75-4.5, 10H (expected: 10H, *CH* Asp); 3.7-3.6, 54H (expected: 54H, *CH_2*O), 3.5-3.0, 20H (expected: 20H, CONH*CH_2*); 2.9-2.0, 26H (expected: 26H, -CO-*CH_2*, *CH_2*NH-); (Table 4.6 row 8).

Polymer **14** was afforded in a yield of 70%, and was characterized as follows: η_{inh}, 17.31 mL g^{-1}; M_w = 29 400; M_n = 15 550; I_n = 1.89 (Table 4.7 row 13).

^{1}H NMR (D_2O), δ/ppm: 4.75-4.5, 5H (expected: 10H, *CH* Asp); 3.7-3.6, 37H (expected: 36H, *CH_2*O), 3.5-3.0, 10H (expected: 10H, CONH*CH_2*); 2.9-2.0, 16H (expected: 16H, -CO-*CH_2*, *CH_2*-NH-); (Table 4.6 row 9).

Polyaspartamides 15 (90:10) and 16 (90:10)

The same experimental procedure leading to polymer **13** (90:10) was applied. However, the last diamine reactant, diethylenetriamine (DET) was replaced by 1, 3-propylenediamine (PDA) and 1,3-diamino-2-propanol (DAP) to afford **15** (90:10) and **16** (90:10) respectively. All the other variables were maintained (refer to Table 4.5 rows 10 and 11).

Polyaspartamide **15** (90:10) was obtained as beige, water-soluble and hygroscopic material in a yield of 62%, η_{inh}, 11.54 mL g^{-1}.

^{1}H NMR (D_2O), δ/ppm: 4.75-4.5, 9H (expected: 10H, *CH* Asp); 3.7-3.6, 55H (expected: 54H, *CH_2*O), 3.5-3.0, 20H (expected: 20H, CONH*CH_2*); 2.9-2.0, 24H (expected: 24H, -CO-*CH_2*, *CH_2*NH-); 1.8-1.5, 2H (expected: 2H, CH_2*CH_2*CH_2).

Polymer **16** (90:10) was also afforded as beige and possessed the water solubility property. The yield was 63% and the inherent viscosity**, η_{inh},** 11.28 mL g^{-1}.

^{1}H NMR (D_2O), δ/ppm: 4.75-4.5, 10H (expected: 10H, *CH* Asp); 3.7-3.6, 54H (expected: 55H, *CH_2*O, *CH*-OH), 3.5-3.0, 20H (expected: 20H, CONH*CH_2*); 2.9-2.0, 22H (expected: 22H, -CO-*CH_2*, *CH_2*-NH-); (Table 4.6 row 11).

Polyaspartamide 17 (90:10)

Polymer **17** was prepared in a two-step reaction procedure similarly to **1**. However, 3-(N,N-Dimethylamino)propylamine (DMP) was substituted by ethanoamine (MEA), and the first step consequently proceeded at a longer reaction time of 24h.

PSI (3g, 30mmol) afforded 2.9g (54%) polymer **17** of as beige, and water-soluble product, η_{inh}; 18.43 mL g^{-1}.

^{1}H NMR (D_2O), δ/ppm: 4.75-4.5, 10H (expected: 10H, *CH* Asp); 3.7-3.6, 45H (expected: 45H, *CH_2*O, O*CH_3*), 3.5-3.0, 20H (expected: 20H, CONH*CH_2*); 2.9-2.0, 25H (expected: 26H, -CO-*CH_2*, *CH_2*NH-); (Table 4.6 continued row 3).

Polyaspartamide 18 (80:20)

Polymer **18** (a variant of **17**, refer to Table 4.2…) was prepared analogously to **17**. From PSI (1g, 10mmol), it was obtained after work-up 1.2g (66%) polymer **18** of as beige, fluffy and water-soluble product, η_{inh}; 17.31 mL g^{-1}.

^{1}H NMR (D_2O), δ/ppm: 4.75-4.5, 5H (expected: 5H, *CH* Asp); 3.7-3.6, 20H (expected: 20H, CH_2O, OCH_3), 3.5-3.0, 10H (expected: 10H, $CONHCH_2$); 2.9-2.0, 16H (expected: 16H, -CO-CH_2, CH_2NH-); (Table 4.6 continued row 4).

Polyaspartamides 19 (90:10) and 20 (90:10)

Both polyaspartamides were prepared in an analogous fashion to polymer **17** (90:10) with minor modification. This concerns the replacement of diamine, DET, in the second step by PDA and EDDA, respectively.

Thus, polyaspartamide **19** (90:10) was isolated after work-up as beige and water-soluble solid in a yield of 71% with inherent viscosity, η_{inh}; 15.45 mL g^{-1}.

^{1}H NMR (D_2O), δ/ppm: 4.75-4.5, 10H (expected: 10H, *CH* Asp); 3.7-3.6, 45H (expected: 45H, CH_2O, OCH_3), 3.5-3.0, 20H (expected: 20H, $CONHCH_2$); 2.9-2.0, 22H (expected: 22H, -CO-CH_2, CH_2NH-); 1.8-1.5, 2H (expected: 2H, $CH_2CH_2CH_2$); see Table 4.6 continued row 5.

Polyaspartamide **20** (90:10) was obtained in yield of 55% as water-soluble material with inherent viscosity, η_{inh}; 14.85 mL g^{-1}.

^{1}H NMR (D_2O), δ/ppm: 4.75-4.5, 10H (expected: 10H, *CH* Asp); 3.7-3.6, 53H (expected: 53H, CH_2O, OCH_3), 3.5-3.0, 20H (expected: 20H, $CONHCH_2$); 2.9-2.0, 22H (expected: 22H, -CO-CH_2, CH_2NH-); refer to Table 4.6 row 6.

5.3.1.2 Poly(amidoamine) (PAA) Carriers

Mono-N-Boc-protected primary diamines

Compound 21, *N-(tert-butoxycarbonyl)1,2-diaminoethane (N-Boc-EDA)*
Di-*tert*-butyl dicarbonate, $(Boc)_2O$ (10.9g, 50mmol) was dissolved in 70 mL of dioxin and added dropwise over a period of 2h to 1,2-diaminoethane (EDA) (21g, 350mmol), predissolved in 60 mL of the same solvent. The mixture was stirred at ambient temperature for another 24h period, and the solvent, together with excess EDA, was distilled off by rotary evaporation at 50°C bath temperature. Upon addition of 50 mL of H_2O, a small portion of insoluble N,N´-bisprotected amine was removed by filtration, and the filtrate was extracted with several 40-mL portions of methylene chloride, leaving any residual unreacted diaminoethane as the most hydrophilic constituent in the aqueous phase. The combined extracts, dried over anhydrous $MgSO_4$ afforded N-Boc-EDA, **21**, after solvent removal as a yellow, oily liquid in a yield of 6.72g (93%). The compound gave a clean ^1H NMR spectrum.

^1H-NMR (D_2O), δ/ppm: 3.1 t, 2H (expected: 2H, CONHCH_2); 2.7 t, 2H (Expected: 2H, CH_2NH_2), 1.4 s, 9H (Expected: 9H, CH_3); see Table 4.9 row 3.

Compound 22, *N-(tert-butoxycarbonyl)1,3-diaminopropane (N-Boc-PDA):* In an analogous fashion to the above described procedure, N-(tert-butoxycarbonyl)1, 3-diaminopropane, N-Boc-PDA, **22**, was prepared from di-*tert*-butyl dicarbonate, $(Boc)_2O$, (10g, 45.8mmol) and, 1, 3-diaminopropane (PDA) (30.4g, 410mmol) in a total of 130 mL of dioxan. Work-up as in the preceding experiment afforded the crude mono-Boc-protected diamine **22** as an oily liquid in a yield of 7.05g (85%).

^1H-NMR (D_2O), δ/ppm: 3.1 t, 2H (expected: 2H, CONHCH_2); 2.65 t, 2H (Expected: 2H, CH_2NH_2), 1.6 m, 2H (Expected: 2H, $CH_2CH_2CH_2$); 1.45 s, 9H (Expected: 9H, CH_3); Table 4.9 row 4.

Compound 23, *N-(tert-butoxycarbonyl)-1,4,7-triaza-heptane (N-Boc-DET):* Di-*tert*-butyl dicarbonate, $(Boc)_2O$, (10g, 45.8mmol), and diethylenetriamine (DET) (32g, 310mmol), in 130 mL of dioxan, treated as in preceding experiments, gave 8.8g (92%) of N-Boc-DET, **23** as an oily liquid.

^{1}H-NMR (D_2O), δ/ppm: 3.2 t, 2H (expected: 2H, CONH*CH_2*); 2.6 m, 6H (Expected: 6H, remaining CH_2); 1.45 t, 9H (Expected: 9H, *CH_3*).

Compound 24, *N-(tert-butoxycarbony)-4,7-dioxa-1,10-diaza-decane (N-Boc-EDDA):* The preparation of N-(*tert*-butoxycarbonyl)-4,7-dioxa-1,10-diaza-decane, N-Boc-EDDA, **24**, from di-*tert*-butyl dicarbonate, $(Boc)_2O$, (15g, 68.7mmol), and 2,2'-(ethylenedioxy)diethylamine (EDDA) (69.3g, 468mmol) in 260 mL of dioxan follows the same basic procedure employed in preceding experiments. The mono-Boc-protected diamine, **24** was obtained in a yield of 15.6g (92%), and the ^{1}H NMR spectrum was very clean.

^{1}H-NMR (D_2O), δ/ppm: 3.7 s, 4H (Expected: 4H, O*CH_2CH_2*O); 3.6 m, 4H (Expected: 4H, N-CH_2*CH_2*O); 3.2 t, 2H (expected: 2H, CONH*CH_2*); 2.75 t, 2H (Expected: 2H, *CH_2*NH_2); 1.45 s, 9H (Expected: 9H, *CH_3*); see Table 4.9 row 6.

Preparation of poly(amidoamine) carriers: Amounts of polymeric educts and products are given as base moles and thus refer to the simplest recurring units, defined by structures **25-31** normalized to y = 1.

Copoly(amidoamine) 25 (80:20)

The detailed procedure given in the following for the synthesis of **25** is representative of the general method for the copolymerization of methylenebisacrylamide (MBA) with mono-Boc-protected diamines, and therefore will be used to afford all the other six target copolyamidoamine carriers, **26-31**.

Methylenebisacrylamide (MBA) (2.47g, 16mmol) was dissolved 15 mL of hot H_2O. Upon cooling, mono-Boc derivative **22** (0.6g, 3.2mmol) predissolved in 5 mL of H_2O was added in one dash. The N_2-saturated solution was stirred at ambient temperature for 24h then at 50^{o}C for another 24h.

2-(dimethylamino)ethylamine (DME) (1.13g, 12.8mmol) dissolved in 5 mL of H_2O, was added. Stirring of the solution, resaturated with N_2, was continued for 36h at 60^{o}C, and upon the addition of ethanolamine, EA (0.049g, 8mmol), for

another 2h at the same temperature. The last-named step served to eliminate terminal vinyl groups as potential causes of delayed crosslinking. The volatiles were now removed by rotating evaporation (60^{o}C bath temperature), and the residual intermediary polymer was treated with 5 mL of trifluoroacetic acid (TFA) for 1h at room temperature. Removal of the acid under reduced pressure at 30^{o}C bath temperature was followed by precipitation of the product polymer with Et_2O, which was thoroughly washed with boiling toluene, and redissolved in 20mL of H_2O. The pH was adjusted to 7 with NaOH, and the solution was purified by dialysis successively in Spectra/Por 4 tubing for 48h and for another 48h in Spectra/Por 6 tubing against distilled water. For the last 4h of this operation, the pH of the tube contents was raised to 8.5-9 with NH_4OH to eliminate protonation effects. The retentate, pH~8, was freeze-dried to afford 0.850 g (22.1%) of beige, crispy and water- and methanol-soluble **25**, η_{inh}, 24.29 mL g^{-1}; M_w = 65 360; M_n = 23 990; I_n = 2.73; Table 4.13 row 2.

^{1}H-NMR (D_2O), δ/ppm: 4.6-4.5, 10H (Expected: 10H, CONH*CH*$_2$HNCO), 3.0-2.8, 21H (Expected: 20H, -CO-*CH*$_2$), 2.7-2.0, 65H (Expected: 66H, *CH*$_2$N (*CH*$_3$)$_2$, *CH*$_2$-N (*CH*$_2$) (CH_2), *CH*$_2$-NH_2), 1.8-1.5, 2H (Expected: 2H, CH_2*CH*$_2$$CH_2$).

Copoly(amidoamine) 26 (80:20)

In the preparation of polymer **26**(80:20), 3-(dimethylamino)propylamine was employed *in lieu* of the ethylamine derivative serving as solubilizing factor. The adopted work-up gave 0.68g (16.8%) of water- and methanol-soluble solid **26** characterized as follows: η_{inh}, 17.5 mL g^{-1}; M_w = 11 020; M_n = 6 240; I_n = 1.72; Table 4.13 row 3.

^{1}H-NMR (D_2O), δ/ppm: 4.6-4.5, 10H (Expected: 10H, CONH*CH*$_2$HNCO), 3.0-2.8, 21H (Expected: 20H, -CO-*CH*$_2$), 2.7-2.0, 66H (Expected: 66H, *CH*$_2$N (*CH*$_3$)$_2$, *CH*$_2$-N (*CH*$_2$) (CH_2), *CH*$_2$-NH_2), 1.8-1.5, 10H (Expected: 10H, CH_2*CH*$_2$$CH_2$).

Copoly(amidoamine) 27 (80:20)

This polymer was prepared by reacting MBA (2.47g, 16mmol), N-Boc-derivative **23** (0.65g, 3.2mmol), and 3-(dimethylamino)propylamine (DMP) (1.31g,

12.8mmol) following the standard procedure. Polymer **27** was afforded as beige, crispy, water- and methanol-soluble solid in a yield of 0.72g (16.8%); η_{inh}, 16.86 mL g^{-1}; M_w = 13 210; M_n = 6 300; I_n = 2.09; see Table 4.13 row 4.

^{1}H-NMR (D_2O), δ/ppm: 4.6-4.5, 10H (Expected: 10H, CONH*CH*$_2$HNCO), 3.0-2.8, 22H (Expected: 20H, -CO-*CH*$_2$), 2.7-2.0, 70H (Expected: 68H, *CH*$_2$N (*CH*$_3$)$_2$, *CH*$_2$-N (*CH*$_2$) (CH_2), *CH*$_2$-NH_2), 1.8-1.5, 7H (Expected: 8H, CH_2*CH*$_2$$CH_2$).

Copoly(amidoamine) 28 (80:20)

By the basic procedure described for the synthesis of **25**, copoly(amidoamine) **26** was prepared from MBA (2.47g, 16mmol), mono-Boc-derivative **24** (0.7g, 3.2mmol), and 2-(dimethylamino)ethylamine (DME) (1.13g, 12.8mmol). Following the adopted work-up, the target polymer **28** was collected as water- and methanol-soluble solid in a yield of 0.636g (15.5%); it possessed the following characteristics: η_{inh}, 20.98 mL g^{-1}; M_w = 52 000; M_n = 24 760; I_n = 2.1; Table 4.13 row 5.

^{1}H-NMR (D_2O), δ/ppm: 4.6-4.5, 10H (Expected: 10H, CONH*CH*$_2$HNCO), 3.8-3.5, 8H (Expected: 8H, O*CH*$_2$*CH*$_2$O), 3.0-2.8, 22H (Expected: 20H, -CO-*CH*$_2$), 2.7-2.0, 66H (Expected: 66H, *CH*$_2$N (*CH*$_3$)$_2$, CH_2-N (CH_2) (CH_2), *CH*$_2$-NH_2).

Copoly(amidoamine) 29 (80:20)

The standard method was used for the preparation of **29**. The following amounts of reactants were used: MBA (2.47g, 16mmol), N-Boc-derivative **24** (0.7g, 3.2mmol), and 3-(dimethylamino)propylamine (DMP) (1.31g, 12.8mmol).

The water- and methanol-soluble polymer **29** was collected in a yield of 0.79g (18.4%); η_{inh}, 18.45 mL g^{-1}; M_w = 14 880; M_n = 5 590; I_n = 2.66.

^{1}H-NMR (D_2O), δ/ppm: 4.6-4.5, 10H (Expected: 10H, CONH*CH*$_2$HNCO), 3.8-3.5, 8H (Expected: 8H, O*CH*$_2$*CH*$_2$O), 3.0-2.8, 21H (Expected: 20H, CO*CH*$_2$), 2.7-2.0, 64H (Expected: 64H, *CH*$_2$N(*CH*$_3$)$_2$, *CH*$_2$-N(*CH*$_2$)(CH_2), *CH*$_2$-NH_2), 1.8-1.5, 8H (Expected: 8H, CH_2*CH*$_2$$CH_2$); Table 4.12 row 7.

Copoly(amidoamine) 30 (80:20)

This polymer was synthesized analogously to **25**, except that the ethylamine derivative, 2-(dimethylamino)ethylamine (DME) serving as solubilizing factor was replaced by 2-(2-aminoethoxy)ethanol (AEE) (1.35g, 12.8mmol). The target polymer was isolated as a water- and methanol-soluble solid in a yield of 0.625g (15.7%); η_{inh}, 20.1 mL g^{-1}.

^{1}H-NMR (D_2O), δ/ppm: 4.6-4.5, 10H (Expected: 10H, CONH*CH_2*HNCO), 3.8-3.5, 24H (Expected: 24H, O*CH_2CH_2*O), 3.0-2.8, 20H (Expected: 20H, -CO-*CH_2*), 2.7-2.0, 33H (Expected: 32H, *CH_2*-N(*CH_2*)(CH_2), *CH_2*-NH_2), 1.8-1.5, 2H (Expected: 2H, CH_2*CH_2*CH_2); Table 4.12 row 8.

Copoly(amidoamine) 31 (80:20)

Polymer **31** was prepared by reacting MBA (2.47g, 16mmol), N-Boc-derivative **24** (0.7g, 3.2mmol), and 2-(2-aminoethoxy) ethanol (AEE) (1.35g, 12.8mmol) following the standard procedure. The adopted work-up afforded 0.75g (18.4%) of **31** as a beige, crispy, water- and methanol-soluble solid; η_{inh}, 16.98 mL g^{-1}.

^{1}H-NMR (D_2O), δ/ppm: 4.6-4.5, 10H (Expected: 10H, CONH*CH_2*HNCO), 3.8-3.5, 31H (Expected: 32H, O*CH_2CH_2*O), 3.0-2.8, 20H (Expected: 20H, -CO-*CH_2*), 2.7-2.0, 33H (Expected: 32H, -*CH_2*N (*CH_3*)$_2$, *CH_2*-N (*CH_2*) (CH_2), *CH_2*-NH_2).

Poly(amidoamine) 32

MBA (1.25g, 16mmol) was dissolved in 5 mL of hot isopropanol-H_2O (4:1). The mono-Boc derivative **22** (0.7g, 4mmol) was dissolved in 1mL of isopropanol and was added to the MBA solution with stirring. Upon saturation with N_2, the resulting solution was stirred for 72h at ambient temperature.

Following solvent removal by rotary evaporation, the residual macromomonmer was redissolved in 40 mL of the same solvent blend, thus providing the high dilution ([MBA] = 0.2M) required for the second reaction step. After cooling in an ice bath, 4,7,10-trioxa-1,13-tridecanediamine, TRIA (0.88g, 4mmol), predissolved in 10 mL of the same solvent mixture, was added, followed by

triethylamine, TEA (0.41g, 4mmol), and stirring of the solution, resaturated with N_2, was continued for 24h at room temperature and another 48h at 60°C. The solvent was removed again under reduced pressure, 5 mL of trifluoroacetic acid was added, and stirring was continued for 1h at ambient temperature. The acid was removed under reduced pressure, and the residual material was washed with boiling toluene to remove traces of unreacted oligo (ethylene oxide). Polymer precipitation and further work-up was as described for polymer **25**. There was obtained 0.38g (16%) of water- and methanol-soluble **32**; η_{inh}, 15.58 mL g^{-1}; M_w = 28 830; M_n = 20 740; I_n = 1.39; Table 4.13 row 7.

^{1}H-NMR (D_2O), δ/ppm: 4.6-4.5, 4H (Expected: 4H, CONH*CH_2*HNCO), 3.8-3.5, 12H (Expected: 12H, O*CH_2CH_2*O), 3.0-2.8, 8H (Expected: 8H, -CO-*CH_2*), 2.7-2.0, 15H (Expected: 16H, -*CH_2*NH*CH_2*, *CH_2*-N(*CH_2*)(CH_2), *CH_2*-NH_2), 1.8-1.5, 6H (Expected: 6H, CH_2*CH_2*CH_2); Table 4.12 row 10.

Poly(amidoamine) 33

This polymer was prepared using the same procedure as in the preceding experiment, except that the trioxatridecanediamine (TRIA) was replaced by O,O´-bis(3-aminopropyl)poly(ethylene glycol) 1500 (PEO) (6g, 4mmol), and the solvent volume in the second reaction step was increased to 50 mL. The water- and methanol-soluble polymer **33** was isolated in yield of 1.75g (23%); η_{inh}, 14.17 mL g^{-1}; M_w = 23 440; M_n = 11 320; I_n = 2.07; Table 4.12 row 8.

^{1}H-NMR (D_2O), δ/ppm: 4.6-4.5, 4H (Expected: 4H, CONH*CH_2*HNCO), 3.8-3.5, 130H (Expected: 128H, O*CH_2CH_2*O), 3.0-2.8, 9H (Expected: 8H, -CO-*CH_2*), 2.7-2.0, 16H (Expected: 16H, *CH_2*NH*CH_2*, *CH_2*-N(*CH_2*)(CH_2), *CH_2*-NH_2), 1.8-1.5, 5H (Expected: 6H, CH_2*CH_2*CH_2); Table 4.12 row 11.

5.3.2 Polymer-MTX conjugates

The conjugation of methotrexate to amine-functionalized polymeric carriers was achieved by the HBTU coupling agent method, and the experimental details, which follow, illustrate the standard procedure adopted for the preparation of all

polymer-MTX conjugates herein investigated. These included polyaspartamide- and polyamidoamine-MTX conjugates.

5.3.2.1 Polyaspartamide-MTX conjugates

Hydrolytic stability test: In an attempt to test the hydrolytic stability of the polyaspartamide-MTX conjugates, polyaspartamides namely **3** (90:10) and **5** (90:10) were conjugated to folic acid, FA (chosen for its structural similarity to MTX). The conjugates were purified by both size exclusion chromatography and dialysis, isolated by freeze-drying, and characterized by ^{1}H NMR and UV-vis spectroscopy. The latter purification method was repeated once more, and FA content assessed again by both analytical methods.

Conjugate 3 (90:10)-FA

Polymer **3** (200mg, 0.1mmol) was dissolved in 7 mL of N-methylpyrrylidone (NMP). Folic acid (FA) (54mg, 0.12mmol) was added to the polymer solution with stirring. Upon rapid stirring, HBTU (43mg, 0.11mmol) predissolved in 2 mL of DMF, and then added dropwise over 20min, followed by the addition of triethylamine (TEA) (20mg, 0.2mmol). The resulting yellow solution was saturated with N_2 and stirred at ambient temperature for 2h and cooled at 5^{o}C for 1/2h. The polymeric conjugate was precipitated with 15 mL of Et_2O-hexane (2:1), isolated upon centrifugation, thoroughly washed warm Me_2CO and dissolved in 5 mL of H_2O. The pH adjustment to 10 using NaOH was followed by size exclusion chromatography on a 2.5 x 25 cm column packed with Sephadex G25 and eluted with distilled H_2O. The pH of the eluate was readjusted to 7 (glacial acetic acid) to prevent hydrolysis, and the solution dialyzed for 48h in Spectra/Por 6 tubing. The pH of the retentate was adjusted to 4 (HCl) to regenerate the unconjugated carboxyl group of FA from its salt. The aqueous solution was stirred at ambient temperature for 5min, then the pH re-adjusted to 6 (NH_4OH), and the dialysis in the same tubing was continued for another 8h with numerous changes of the aqueous outer phase for complete removal of inorganic salts. The retentate, pH~8, was freeze-dried to afford 120 mg (49%) of yellow, water-soluble conjugate **3**(90:10)-**FA**; η_{inh}, 12.15 mL g^{-1}.

^{1}H NMR (D_2O), δ/ppm: 8.5-6.5, 5H (Expected: 5H; aromatic and heteroaromatic *CH* of FA); 1.8-1.6, 18H (expected: 18H; $CH_2CH_2CH_2$). These data indicate 100% FA incorporation, corresponding to 18.26% by mass.

Determination of folate content in the conjugate by UV spectroscopy in H_2O (pH ~7, reference) using the absorbance at 363nm and the molar extinction coefficient value, $\varepsilon = 6200$ mol^{-1} cm^{-1}, revealed 18% by mass. [Found: FA, 18% (UV), 18.26% (NMR)]. This method was employed for all subsequent folate conjugates and co-conjugates.

120 mg of **3**(90:10)-**FA** were redissolved in 5mL of H_2O, pH adjusted to 7, and the solution redialyzed against distilled H_2O in Spectra/Por 6 tubing for another 48h, and the retentate pH~8 was freeze-dried again to give 110 mg (92%) of yellow water-soluble powder, η_{inh}, 12.05 mL g^{-1}. ^{1}H NMR spectrum showed 100% FA. [Found: FA, 17.98% (UV), 18.26% (NMR)].

Conjugate 5 (90:10)-FA

This conjugate was prepared in a similar fashion to **3**(90:10)-**FA**, except that **3** was replaced by **5**. Thus, the reaction of polymer **5** (200mg, 0.098mmol), FA (52mg, 0.118mmol), HBTU (40mg, 0.108mmol), and TEA (20mg, 0.196mmol), afforded 147mg (58%) of **5**(90:10)-**FA** as yellow water-soluble solid, η_{inh}, 15.85 mL g^{-1}.

^{1}H NMR (D_2O), δ/ppm: 8.5-6.5, 5H (Expected: 5H; aromatic and heteroaromatic *CH* of FA); 1.8-1.6, 18H (expected: 18H; $CH_2CH_2CH_2$). These data indicate FA incorporation to be 100% of available NH_2 anchoring group. [Found: FA, 17.9% (UV), 17.93% (NMR)].

147 mg of **5**(90:10)-**FA** were redissolved in 5mL of H_2O, pH adjusted to 7, and the solution redialyzed against distilled H_2O in Spectra/Por 6 tubing for another 48h, and the retentate pH~8.5 was freeze-dried again to give 110mg (75%) of yellow water-soluble powder, η_{inh}, 15.75 mL g^{-1}.

^{1}H NMR (D_2O), δ/ppm: 8.5-6.5, 5H (Expected: 5H; aromatic and heteroaromatic *CH* of FA); 1.8-1.6, 18H (expected: 18H; $CH_2CH_2CH_2$), indication of 100% of FA incorporation. [Found: FA, 17.85% (UV), 17.93% (NMR)].

Synthesis of polyaspartamide-MTX conjugates

Conjugate 1 (90:10)-MTX

This conjugate was obtained by using the standard procedure leading to **3**(90:10)-**FA** except that folic acid (**FA**) was replaced by methotrexate (**MTX**). Thus, the reaction of polymer **1** (200mg, 0.102mmol), MTX (56mg, 0.122mmol), HBTU (43mg, 0.112mmol), and TEA (21mg, 28μL, 0.204mmol), in a total of 7 mL of DMF, followed by the adopted work-up procedure afforded 150mg (61%) of yellow, water-soluble powder **1**(90:10)-**MTX**; η_{inh}, 16.15 mL g^{-1}; M_w = 26 350; M_n = 17 000; I_n = 1.55. Found: MTX, 18.3% (UV), 18.61% (NMR). Calcd. for $(C_{108}H_{186}N_{38}O_{24})_n$ (2400.9) $_n$ [**1**(90:10)-**MTX**]: MTX, 18.93%; refer to Table 4.17, row 2.

The MTX content in this conjugate and in the forthcomings involving this drug was determined by UV spectroscopy in H_2O (pH ~7, reference) using the molar extinction coefficient value, ε = 6500 mol^{-1} cm^{-1} and the absorbance at λ = 370 nm.

^{1}H NMR (D_2O), δ/ppm: 8.5-6.5, 4.9H (Expected: 5H; aromatic and heteroaromatic *CH* of MTX); 1.8-1.6, 20H (expected: 20H; $CH_2CH_2CH_2$), corresponding to 98% MTX incorporation.

Conjugate 2 (80:20)-MTX

For the preparation of this conjugate the basic procedure described for the synthesis of **1**(90:10)-**MTX** was used. However, carrier **2** replaced **1**. Polymer **2** (200mg, 0.207mmol) was treated with MTX (113mg, 0.249mmol), HBTU (86mg, 0.228mmol), TEA (42mg, 0.414mmol), in a total of 7 mL of DMF. After conventional work-up, a yield of 155mg (53%) of yellow fluffy water-soluble **2** (80:20)-**MTX** collected, and possessed the following characteristics:

η_{inh}, 19.95 mL g^{-1}; M_w = 32 200; M_n = 18 680; I_n = 1.74. Found: MTX, 30.75 % (UV), 31.68% (NMR). Calcd. for $(C_{63}H_{101}N_{23}O_{14})_n$ (1404.6) $_n$ [**2**(80:20)-**MTX**]: MTX, 32.36%; see Table 4.17, row 3.

^{1}H NMR (D_2O), δ/ppm: 8.5-6.5, 4.8H (Expected: 5H; aromatic and heteroaromatic *CH* of MTX); 1.8-1.6, 10H (expected: 10H; $CH_2CH_2CH_2$) corresponding to 96% MTX incorporation.

Conjugate 3 (90:10)-MTX

The general procedure leading to **1**(90:10)-**MTX** was used for the preparation of **3**(90:10)-**MTX** from carrier **3** (200mg, 0.1mmol), MTX (55mg, 0.12mmol), HBTU (41mg, 0.11mmol), TEA (21mg, 0.2mmol), in a total volume of 7 mL of DMF. After routine work-up, the conjugate was isolated in a yield of 125mg (53%) as yellow water-soluble solid.

^{1}H NMR spectrum revealed 80%MTX incorporation therefore the conjugate (120mg,~0.063mmol) was retreated with MTX (23mg, 0.05mmol), HBTU (12mg, 0.031mmol), and TEA (13mg, 0.125mmol), in a total of 6 mL of DMF-HMP (2:1), with the reaction period extended to 4h. The adopted work-up procedure afforded 90mg of the conjugate corresponding to an overall yield of 41%. The conjugate was characterized as follows:

η_{inh}, 16.75 mL g^{-1}; M_w = 28 250; M_n = 14 490; I_n = 1.95. Found: MTX, 18.36 % (UV), 18.7% (NMR). Calcd. for $(C_{109}H_{189}N_{39}O_{24})_n$ $(2429.9)_n$ [**3**(90:10)-**MTX**]: MTX, 18.7%; Table 4.17, row 4.

^{1}H NMR (D_2O), δ/ppm: 8.5-6.5, 5H (Expected: 5H; aromatic and heteroaromatic *CH* of MTX); 1.8-1.6, 18H (Expected: 18H; $CH_2CH_2CH_2$). MTX incorporation: 100%.

Conjugate 4 (80:20)-MTX

High MTX incorporation in this conjugate was afforded in a two-step process as in the preceding experiment. From carrier **4** (200mg, 0.201mmol), MTX (109mg, 0.241mmol), HBTU (84mg, 0.221mmol), TEA (41mg, 0.401mmol), **4** (80:20)-

MTX was afforded in a yield of 140mg (48%) as yellow, crispy, water-soluble solid; η_{inh}, 20.18 mL g^{-1}; M_w = 33 030; M_n = 15 300; I_n = 2.17. Found: MTX, 29.80% (UV), 30.81% (NMR). Calcd. for $(C_{64}H_{104}N_{24}O_{14})_n$ (1433.7)$_n$ [**4**(80:20)-**MTX**]: MTX, 31.7%.

^{1}H NMR (D_2O), δ/ppm: 8.5-6.5, 4.8H (Expected: 5H; aromatic and heteroaromatic *CH* of MTX); 1.8-1.6, 8H (Expected: 8H; $CH_2CH_2CH_2$). These data indicate 96% NH_2 acylation; Table 4.16, row 5.

Conjugate 5 (90:10)-MTX

For the preparation of this conjugate the two-step process was used as in the preceding experiments. Thus, the reaction of polymer **5** (200mg, 0.098mmol), MTX (54mg, 0.118mmol), HBTU (41mg, 0.108mmol), TEA (20mg, 0.196mmol), gave 105mg (43%) of **5**(90:10)-**MTX** as a yellow water-soluble solid. η_{inh}, 15.42 mL g^{-1}; M_w = 25 200; M_n = 15 270; I_n = 1.65. Found: MTX, 18.05 % (UV), 17.91% (NMR). Calcd. for $(C_{111}H_{192}N_{38}O_{26})_n$ (2475)$_n$ [**5**(90:10)-**MTX**]: MTX, 18.36%; Table 4.17, row 6.

^{1}H NMR (D_2O), δ/ppm: 8.5-6.5, 4.85H (Expected: 5H; aromatic and heteroaromatic *CH* of MTX); 1.8-1.6, 18H (Expected: 18H; $CH_2CH_2CH_2$), showing 97% MTX incorporation.

Conjugate 6 (80:20)-MTX

This conjugate was prepared in a similar fashion to **4**(80:20)-**MTX**. The reaction of carrier **6** (200mg, 0.192mmol), MTX (105mg, 0.23mmol), HBTU (80mg, 0.211mmol), TEA (39mg, 0.384mmol), afforded **6**(80:20)-**MTX** in a yield of 120mg (42%) as water-soluble solid. η_{inh}, 21.08 mL g^{-1}; M_w = 35 030; M_n = 18 070; I_n = 1.94. Found: MTX, 29.75% (UV), 30.08% (NMR). Calcd. for $(C_{66}H_{107}N_{23}O_{16})_n$ (1478.7)$_n$ [**6**(80:80)-**MTX**]: MTX, 30.7%; Table 4.17, row 7.

^{1}H NMR (D_2O), δ/ppm: 8.5-6.5, 4.85H (Expected: 5H; aromatic and heteroaromatic *CH* CH of MTX); 1.8-1.6, 18H (Expected: 18H; $CH_2CH_2CH_2$), indicating 97% of drug level incorporation.

Conjugate 7 (90:10)-MTX

The target conjugate was prepared using the basic procedure, in a one-step process, from carrier **7** (400mg, 0.202mmol), MTX (110mg, 0.242mmol), HBTU (82mg, 0.222mmol), TEA (41mg, 0.404mmol), in a total of 10 mL. The conjugate was collected as a yellow, fluffy, and water-soluble solid, in a yield of 360mg (74%). η_{inh}, 15.94 mL g^{-1}. Found: MTX, 18.2% (UV), 18.5% (NMR). Calcd. for $(C_{108}H_{186}N_{38}O_{25})_n$ $(2416.9)_n$ [**7**(90:10)-**MTX**]: MTX, 18.8%; Table 4.17, row 8.

^{1}H NMR (D_2O), δ/ppm: 8.5-6.5, 4.92H (Expected: 5H; aromatic and heteroaromatic *CH* of MTX); 1.8-1.6, 18H (Expected: 18H; $CH_2CH_2CH_2$). This data indicate 98% MTX incorporation.

Conjugate 8 (90:10)-MTX

The standard procedure leading to **7**(90:10)-**MTX** was applied for the preparation of this conjugate. Thus, using a molar feed ration MTX/NH_2 of 1.2., carrier **8** (200mg, 0.123mmol) was treated with MTX (67mg, 0.148mmol), HBTU (51mg, 0.136mmol), and TEA (25mg, 0.246mmol), in a total of 6 mL of DMF. After conventional work-up, the target conjugate was afforded as a deep-yellow, water-soluble solid, in a yield of 160mg (63%); η_{inh}, 18.66 mL g^{-1}; M_w = 31 860; M_n = 18 210; I_n = 1.75. Found: MTX, 20.85% (UV), 21.36 % (NMR). Calcd. for $(C_{82}H_{126}N_{30}O_{33})_n$ $(2060.1)_n$ [**8**(90:10)-**MTX**]: MTX, 22.06%; refer to Table 4.17, row 9.

^{1}H NMR (D_2O), δ/ppm: 8.5-6.5, 4.8H (Expected: 5H; aromatic and heteroaromatic *CH* of MTX); 3.8-3.5, 18H (Expected: 18H; CH_2-O). MTX incorporation: 96%.

Conjugate 9 (80:20)-MTX

The target conjugate was obtained under the experimental conditions affording **8**(80:20)-**MTX**, except that **8** was replaced by **9**, the molar feed ration of MTX/NH_2 being maintained to 1.2.The reaction of polymer **9** (200mg, 0.24mmol), MTX (131mg, 0.288mmol), HBTU (100mg, 0.264mmol), and TEA (49mg, 0.48mmol), in a total of 8 mL of DMF, gave after adopted work-up, 172mg (55%) of water-soluble solid **9**(80:20)-**MTX**; η_{inh}, 17.5 mL g^{-1}. Found: MTX, 33.02% (UV), 34.61% (NMR). Calcd. for $(C_{52}H_{76}N_{20}O_{18})_n$ $(1269.3)_n$ [**9**(80:20)-**MTX**]: MTX, 35.8%; Table 4.17, row 10.

^{1}H NMR (D_2O), δ/ppm: 8.5-6.5, 4.75H (Expected: 5H; aromatic and heteroaromatic *CH* of MTX); 3.8-3.5, 8H (Expected: 8H; CH_2-O), corresponding to 95% MTX incorporation.

Conjugate 10 (90:10)-MTX

The standard procedure was used for the preparation of this conjugate. However, minor modifications were introduced. Thus, to the rapidly stirred solution of carrier **10** (400mg, 0.248mmol) dissolved in 7 mL of DMF, MTX (135mg, 0.298mmol) dissolved in 2 mL, was added. With continued stirring, a solution of HBTU (101mg, 0.273mmol) in 1mL, was added dropwise over a 1/6h period, this was followed by the addition of TEA (37mg, 0.367mmol), and the yellow solution, N_2-saturated, was stirred at room temperature for an extended period of 3h then cooled at 5 ^oC for another 1/2h. The conjugate formed was precipitated with150 mL of Et_2O-Me_2CO (2:1), thoroughly washed with precipitant, further purified and isolated as described for **1**(90:10)-**FA**, yielding 380mg (74%) of yellow, water-soluble solid; η_{inh}, 16.5 mL g^{-1}. Found: MTX, 20.65% (UV), 21.31% (NMR). Calcd. for $(C_{81}H_{123}N_{29}O_{34})_n$ $(2047.0)_n$ [**10**(90:10)-**MTX**]: MTX, 22.2%; see Table 4.17 row 11.

^{1}H NMR (D_2O), δ/ppm: 8.5-6.5, 4.8H (Expected: 5H; aromatic and heteroaromatic *CH* CH of MTX); 3.8-3.5, 19H (Expected: 19H; CH_2-O, *CH*-OH), corresponding to 96% MTX incorporation.

Conjugate 13 (90:10)-MTX

Similarly to the preceding experiment, this conjugate was obtained from carrier **13** (400mg, 0.198mmol), MTX (108mg, 0.238mmol), HBTU (99mg, 0.218mmol), and TEA (40mg, 0.396mmol), in a total of 10 mL of DMF, as a yellow, fluffy, and water-soluble solid, in a yield of 350mg (71%); η_{inh}, 16.25 mLg^{-1}. Found: MTX, 18.25% (UV), 18.5% (NMR). Calcd. for $(C_{100}H_{162}N_{30}O_{42})_n$ $(2456.5)_n$ [**13**(90:10)-**MTX**]: MTX, 18.5%; refer to Table 4.17 continued row 2.

^{1}H NMR (D_2O), δ/ppm: 8.5-6.5, 5H (Expected: 5H; aromatic and heteroaromatic *CH* of MTX); 3.8-3.5, 54H (Expected: 54H; *CH_2*-O), showing the conjugate to contain MTX at the level of 100%.

Conjugate 14 (80:20)-MTX

This conjugate was obtained in a two-step process similar to that leading to **4**-**MTX**, except that polymer **14** was replaced **4**. **14**(80:20)-**MTX** was obtained from carrier **14**, MTX, HBTU, and TEA, in a molar feed ratio of 1:1.2:1.1:2. Thus, carrier **14** (200mg, 0.198mg) treated with MTX (108mg, 0.238mmol), HBTU (83mg, 0.218mmol), and TEA (40mg, 0.396mmol), in a total of 8 mL of DMF. Conventional work-up following the retreatment step, afforded the target conjugate as yellow, fluffy, and water-soluble solid, in the yield of 155mg (54%); it possessed the following the characteristics: η_{inh}, 15.95 mL g^{-1}. Found: MTX, 30.95% (UV), 31.4% (NMR). Calcd. for $(C_{60}H_{92}N_{20}O_{22})_n$ $(1445.5)_n$ [**14**(80:20)-**MTX**]: MTX, 31.14%; Table 4.17 continued row 3.

^{1}H NMR (D_2O), δ/ppm: 8.5-6.5, 5H (Expected: 5H; aromatic and heteroaromatic *CH* of MTX); 3.8-3.5, 24H (Expected: 24H; *CH_2*-O). These ^{1}H NMR data indicate 100% of drug incorporation.

Conjugate 15 (90:10)-MTX

For the preparation of this conjugate, no major changes were introduced in comparison with the basic procedure. The molar feed ratio of MTX/NH_2 was still 1.2. Thus, the reaction of carrier **15** (200mg, 0.101mmol), MTX (55mg,

0.121mmol), HBTU (41mg, 0.111mmol), TEA (20mg, 0.201mmol), in total of 8 mL volume of DMF, gave, after purification and freeze-drying, 160mg (65%); η_{inh}, 12.35 mL g^{-1}. Found: MTX, 17.41% (UV), 17.95% (NMR). Calcd. for $(C_{99}H_{159}N_{29}O_{42})_n$ $(2427.5)_n$ [**15**(90:10)-**MTX**]: MTX, 18.72%.

^{1}H NMR (D_2O), δ/ppm: 8.5-6.5, 4.75H (Expected: 5H; aromatic and heteroaromatic *CH* of MTX); 3.8-3.5, 54H (Expected: 54H; *CH_2*-O), corresponding to 95% NH_2 acylation; see Table 4.16 continued row 4.

Conjugate 16 (90:10)-MTX

Under the experimental conditions leading to **10**(90:10)-**MTX**, the reaction of carrier **16** (400g, 0.199mmol), MTX (109mg, 0.239mmol), HBTU (81mg, 0.219mmol), and TEA (40mg, 0.399mmol), afforded **16**(90:10)-**MTX**, isolated as yellow, fluffy, water-soluble, solid, in a yield of 390mg (80%), and possessing the characteristics: η_{inh}, 14.87 mL g^{-1}. Found: MTX, 18.04% (UV), 18.45% (NMR). Calcd. for $(C_{99}H_{159}N_{29}O_{43})_n$ $(2443.5)_n$ [**16**(90:10)-**MTX**]: MTX, 18.6%.

^{1}H NMR (D_2O), δ/ppm: 8.5-6.5, 4.95H (Expected: 5H; aromatic and heteroaromatic *CH* of MTX); 3.8-3.5, 19H (Expected: 55H; *CH_2*-O, *CH*-O), corresponding to 99% MTX incorporation; Table 4.16 continued row 5.

Conjugate 17 (90:10)-MTX

As in the preceding experiment, the basic procedure was used to synthesize this conjugate from carrier **17** (200mg, 0.114mmol), MTX (62mg, 0.137mmol), HBTU (48mg, 0.126mmol), and TEA (23mg, 0.229mmo), in a total of 7 mL of DMF. After the adopted work-up, the target conjugate was collected as yellow, crispy, water-soluble solid, in a yield of 195mg (77%); η_{inh}, 19.85 mL g^{-1}; M_w = 31900; M_n = 17060; I_n = 1.87. Found: MTX, 19.65 % (UV), 20.12% (NMR). Calcd. for $(C_{91}H_{144}N_{30}O_{33})_n$ $(2186.3)_n$ [**17**(90:10)-**MTX**]: MTX, 20.79%; Table 4.17 continued row 6.

^{1}H NMR (D_2O), δ/ppm: 8.5-6.5, 4.8H (Expected: 5H; aromatic and heteroaromatic *CH* of MTX); 3.8-3.5, 45H (Expected: 45H; CH_2OCH_3). MTX incorporation: 96%

Conjugate 18 (80:20)-MTX

Without major modification of the procedure affording the preceding compound, except 18 substituted that carrier 17, the target conjugate was obtained from carrier **18** (200mg, 0.225mmol), MTX (123mg, 0.270mmol), HBTU (94mg, 0.248mmol), TEA (46mg, 0.450mmol). The molar feed ratios of reactants were: 1:1.2:1.1:2. After purification as described in previous experiments, and freeze-drying, the target conjugate was collected as yellow powder, fully water-soluble, in a yield of 200mg (66%), and had the following characteristics: η_{inh}, 21.98 mL g^{-1}; M_w = 66 170; M_n = 31 880; I_n = 2.08. Found: MTX, 33.6 % (UV), 33.8% (NMR). Calcd. for $(C_{56}H_{84}N_{20}O_{18})_n$ $(1325.4)_n$ [**18**(80:20)-**MTX**]: MTX, 34.3%; see Table 4.17 continued row 7.

^{1}H NMR (D_2O), δ/ppm: 8.5-6.5, 4.95H (Expected: 5H; aromatic and heteroaromatic *CH* of MTX); 3.8-3.5, 20H (Expected: 20H; CH_2OCH_3). MTX incorporation: 99%.

5.3.2.3 Poly(amidoamine)-MTX conjugates

The basic procedure leading to the polyaspartamide-MTX conjugates was still valid for the preparation of the polyamidoamine-MTX conjugates investigated in this project.

Conjugate 25 (80:20)-MTX

This conjugate was synthesized from carrier **25** (200mg, 0.167mmol), MTX (91mg, 0.2mmol), HBTU (70mg, 0.183mmol), and TEA (34mg, 0.333mmol), in a total of 6 mL of DMF. After precipitation, purification, and freeze-drying, as described in preceding experiments, the conjugate **25**(80:20)-**MTX** was obtained as yellow, crispy, water-soluble solid in a yield of 124mg (45%), and

characterized as follows: η_{inh}, 25.09 mL g^{-1}; M_w = 86 600; M_n = 67 100; I_n = 1.29. Found: MTX, 27.74% (UV), 27.8% (NMR). Calcd. for $(C_{74}H_{128}N_{28}O_{14})_n$ $(1634.1)_n$ [**25**(80:20)-**MTX**]: MTX, 27.8%; refer to Table 4.21 row 2.

^{1}H NMR (D_2O), δ/ppm: 8.5-6.5, 5H (Expected: 5H; aromatic and heteroaromatic *CH* of MTX); 4.8-4.5, 10H (Expected: 10H, CONH*CH*$_2$HNCO). These ^{1}H NMR data indicate 100% MTX incorporation.

Conjugate 26 (80:20)-MTX

In a similar fashion to the preceding experiment, carrier **26** (200mg, 0.159mmol) treated with MTX (87mg, 0.191mmol), HBTU (67mg, 0.175mmol), TEA (32mg, 0.319mmol), in an overall of 6 mL of DMF, afforded, after conventional work-up, 136mg (50%) of water-soluble solid **26**(80:20)-**MTX**; η_{inh}, 19.35 mL g^{-1}; M_w = 15 050; M_n = 9 330; I_n= 1.61. Found: MTX, 26.09% (UV), 26.49% (NMR). Calcd. for $(C_{78}H_{136}N_{28}O_{14})_n$ $(1690.2)_n$ [**26**(80:20)-**MTX**]: MTX, 26.89%; see Table 4.21 row 3.

^{1}H NMR (D_2O), δ/ppm: 8.5-6.5, 4.9H (Expected: 5H; aromatic and heteroaromatic *CH* of MTX); 4.8-4.5, 10H (Expected: 10H, CONH*CH*$_2$HNCO), corresponding to 98% MTX incorporation.

Conjugate 27 (80:20)-MTX

This conjugate was synthesized under the experimental conditions leading to the compound **27**(80:20)-**MTX**. Thus, in the same molar feed ration of MTX/NH_2 of 1.2, carrier **27** (200mg, 0.155mmol), was treated with MTX (84mg, 0.186mmol), HBTU (65mg, 0.17mmol), and TEA (31mg, 0.309mmol), in DMF (6 mL). The work-up comprising precipitation, purification, and freeze-drying afforded 133mg (49%) of yellow solid **27**(80:20)-**MTX**, fully water-soluble; η_{inh}, 20.65 mL g^{-1}; M_w = 15 520; M_n = 10 250; I_n = 1.52. Found: MTX, 26.16% (UV), 26.25% (NMR). Calcd. for $(C_{79}H_{139}N_{29}O_{14})_n$ $(1719.2)_n$ [**27**(80:20)-**MTX**]: MTX, 26.4%; Table 4.21 row 4.

^{1}H NMR (D_2O), δ/ppm: 8.5-6.5, 4.95H (Expected: 5H; aromatic and heteroaromatic *CH* of MTX); 4.8-4.5, 10H (Expected: 10H, CONH*CH*$_2$HNCO), indication of 99% NH_2 acylation.

Conjugate 28 (80:20)-MTX

For the preparation of this conjugate, the standard procedure was employed without modification. The reactants were used in a molar feed ratio of 1:1.2:1.1:2.as previously. The polymer **28** (200mg, 0.156mmol) was allowed to react at room temperature for 2h, with MTX (85mg, 0.187mmol), HBTU (65mg, 0.171mmol), and TEA (32mg, 0.312mmol), in a total of 6 mL of DMF. The routine work-up including precipitation with Et_2O-Me_2CO (2:1), isolation upon centrifugation, dissolution in 5 mL of H_2O, purification by both size exclusion chromatography and dialysis, and freeze-drying, gave 120mg (44%) of yellow, crispy, fully water-soluble solid **28**(80:20)-**MTX**; η_{inh}, 22.05 mL g^{-1}; M_w = 60 800; M_n = 45 800; I_n = 1.33. Found: MTX, 25.0% (UV), 25.51% (NMR). Calcd. for $(C_{77}H_{134}N_{28}O_{16})_n$ $(1708.2)_n$ [**28**(80:20)-**MTX**]: MTX, 26.6%; see Table 4.21 row 5.

^{1}H NMR (D_2O), δ/ppm: 8.5-6.5, 4.8H (Expected: 5H; aromatic and heteroaromatic *CH* of MTX); 4.8-4.5, 10H (Expected: 10H, CONH*CH*$_2$HNCO), indicating 96% NH_2 acylation.

Conjugate 29 (80:20)-MTX

Analogously to the preparation of **28**(80:20)-**MTX**, with the exception that polymer **28** was replaced by **29**, the conjugate **29**(80:20)-**MTX** was synthesized from carrier **29** (200mg, 0.158mmol), MTX (86mg, 0.189mmol), HBTU (66mg, 0.174mmol), TEA (32mmg, 0.316mmol), in a total of 6 mL of DMF. It was obtained 127mg (48%) of yellow, fluffy, and water-soluble conjugate **29**(80:20)-**MTX**; η_{inh}, 21.08 mL g^{-1}; M_w = 18 660; M_n = 13 610; I_n = 1.37. Found: MTX, 25.0% (UV), 25.76% (NMR). Calcd. for $(C_{81}H_{142}N_{28}O_{16})_n$ $(1764.3)_n$ [**29**(80:20)-**MTX**]: MTX, 25.76%; refer to Table 4.21 row 6.

^{1}H NMR (D_2O), δ/ppm: 8.5-6.5, 5H (Expected: 5H; aromatic and heteroaromatic *CH* of MTX); 4.8-4.5, 10H (Expected: 10H, CONH*CH*$_2$HNCO), showing 100% MTX incorporation (see Table 4.20 row 6).

Conjugate 32-MTX

The standard procedure was used to afford this conjugate. However, the reaction period was extended to 3h. Thus, carrier **32** (200mg, 0.339mmol) treated with MTX (185mg, 0.407mmol), HBTU (138mg, 0.373mmol), and TEA (67mg, 0.678mmol), in a total of 6 mL, at room temperature for 3h. The routine work-up afforded 166mg (47%) of faint-yellow, fluffy conjugate **32-MTX**; η_{inh}, 21.95 mL g^{-1}; M_w = 26 090; M_n = 13 440; I_n = 2.47. Found: MTX, 40.1% (UV), 40.24% (NMR). Calcd. for $(C_{47}H_{74}N_{16}O_{11})_n$ $(1039.3)_n$ (**32-MTX**): MTX, 43.73%; Table 4.21 row 7.

^{1}H NMR (D_2O), δ/ppm: 8.5-6.5, 4.6H (Expected: 5H; aromatic and heteroaromatic *CH* of MTX); 4.8-4.5, 10H (Expected: 10H, CONH*CH*$_2$HNCO), MTX incorporation: 92% (see Table 4.20 row 7).

Conjugate 33-MTX

In the same fashion as described for the preparation of **32-MTX**, except that polymer **32** was replaced by **33**, the conjugate **33-MTX** was obtained by treating carrier 29 (200mg, 0.108mmol) with MTX (69mg, 0.151mmol), HBTU (49mg, 0.13mmo), and TEA (22mg, 0.216mmol), in 6 mL of DMF. It was obtained after routine work-up, 150mg(60%) of faint-yellow, water-soluble solid **33-MTX**, presenting the listed characteristics: $\boldsymbol{\eta_{inh}}$, 21.80 mL g^{-1}; M_w = 33 020; M_n = 14 490; I_n = 1.8. Found: MTX, 15.3% (UV), 16.69% (NMR). Calcd. for $(C_{105}H_{190}N_{16}O_{40})_n$ $(2316.8)_n$ [**33-MTX**]: MTX, 19.62%; see Table 4.21 row 8.

^{1}H NMR (D_2O), δ/ppm: 8.5-6.5, 4H (Expected: 5H; aromatic and heteroaromatic *CH* of MTX); 4.8-4.5, 4H (Expected: 4H, CONH*CH*$_2$HNCO), MTX incorporation: 80% (see Table 4.20 row 8).

An attempt to increase drug incorporation by retreating 50mg (~0.085mmol) of conjugate with MTX (31mg, 0.068mmol), HBTU (16mg, 0.042mmol), and TEA (17mg, 0.169mmol), in a total of 3 mL of DMF, at room temperature for a more extended reaction period of 4h, was unsuccessful, as the ^{1}H NMR spectrum revealed only 80% NH_2 acylation.

5.3.3 Polymer-ferrocene conjugates

5.3.3.1 Synthesis of ferrocenylbutanoic acid derivatives

Synthesis of ferrocenylbutanoic acid: This ferrocenylation agent was prepared according to the procedure described in the literature [167]. Several products of close melting points were thoroughly mixed to give a batch of mp: 116-119^{o}C (Lit.[170] 119-120^{o}C).

The solid-state IR spectrum showed a C=O band at 1705 cm^{-1} as well as CH out-of-plane bending (ferrocenyl) at 810 cm^{-1}.

Anal. Found: C, 61.60; H, 5.85%. Calcd. For $C_{14}H_{16}FeO_2$ (272.14): C, 61.79; H, 5.93%.

^{1}H-NMR ($CDCl_3$), δ/ppm: 4.25-4.1, 8.5H (expected: 9H, *CH* of ferrocenyl); 2.4-2.2, 4H (expected: 4H, $CH_2CH_2CH_2$); 1.9-1.7, 2H (expected: 2H, $CH_2CH_2CH_2$).

Synthesis of p-nitrophenyl 4-ferrocenylbutanoate (Fc-ONp):

4-Ferrocenylbutanoic acid (2.178g, 8mmol) and *p*-Nitrophenol, pNOH (1.35g, 9.6mmol) were dissolved in 20 mL of dry ethyl acetate, and stirred in an ice-water bath. Dicyclohexylcarbodiimide, DCC (1.62g, 7.92mmol) was added, in small portions. Stirring was continued for a period of 1/2h in the ice-water then at room temperature for another 2h. Dicyclourea was filtered off, and thoroughly washed with 36 mL of ethyl acetate used in several portions. The filtrate and washings were combined, and spun to dryness by rotating evaporation (40^{o}C bath temperature).The residue was recrystallized from hot 95% ethanol containing 1% acetic acid (to prevent hydrolysis of the ester). The recrystallization repeated once

more, afforded 2.04g (65%) of brownish material. Several products of close melting points were thoroughly mixed to give a batch of 4.8g; mp: 70-71 ^{0}C. Anal. Found: C, 60.98; H, 5.19; N, 3.54 %. Calcd. For $C_{20}H_{19}FeO_4N$ (393.22): C, 61.09; H, 4.87; N, 3.56%. R_f = 0.59 (silica gel, CH_2Cl_2: Hexane (2:1)).

^{1}H-NMR ($CDCl_3$), δ/ppm: 8.25-7.25, 4H (expected: 4H, *CH* of aromatic ring); 4.25-4.1, 9H (expected: 9H; *CH* of ferrocenyl); 2.4-2.2, 4H (expected: 4H, $CH_2CH_2CH_2$); 1.9-1.7, 2H (expected: 2H, $CH_2CH_2CH_2$).
p-nitrophenyl group; λ = 274nm ε = 9500mol^{-1}L cm^{-1} in DMSO.

Synthesis of N-succinimidyl 4-ferrocenylbutanoate (Fc-OSU):
This ferrocene derived active ester was prepared from 4-ferrocenylbutanoic acid and N-hydroxysuccinimide (HSU) as described below:
4-Ferrocenylbutanoic acid (2.72g, 10mmol) was dissolved in 50 mL of ethyl acetate upon heating. On cooling at ambient temperature, N-hydroxysuccinimide, HSU (1.38g, 12mmol) was added in small portions, and the solution stirred, then placed in an ice bath, with stirring continued. Dicyclohexylcarbodiimide, DCC (2.48g, 12mmol) predissolved in 5 mL of ethyl acetate was added dropwise over 0.5-1h period, and stirring continued in the ice bath for a period of 4h then at room temperature for another 48h. Afterwards, dicyclourea was filtered off, and thoroughly washed with 3 x 5 mL of ethyl acetate. The filtrate and washings were combined, spun to dryness by rotating evaporation (50^{o}C bath temperature), and the residue, recrystallized from isopropanol. The fractions of close melting point were collected to afford a batch of 3.15g (85%). mp: 67-70^{o}C.
Anal. Found: C, 58.5; H, 5.15; N, 3.8 %. Calcd. For $C_{18}H_{19}FeO_4N$ (369.2): C, 58.6; H, 5.19; N, 3.79%.

^{1}H-NMR ($CDCl_3$), δ/ppm: 4.25-4.1, 9H (expected: 9H, *CH* of ferrocenyl); 3.0-2.75, 4.1H (Expected: 4H, CH_2, succinimidyl), 2.4-2.2, 4.1H (expected: 4H, $CH_2CH_2CH_2$); 1.9-1.7, 2.1H (expected: 2H, $CH_2CH_2CH_2$).

5.3.3.2 Preparation of polymer-ferrocene conjugates

The incorporation of ferrocene into amine-functionalized carriers was achieved by amidation through two coupling methods. These included, first, direct free acid - primary amine coupling mediated by HBTU agent, *Method (1),* and, second, coupling *via* the *p*-Nitrophenol (HONp) active ester of ferrocenylbutanoic acid, *Method (2)*. In one case, the succinimide ester of the ferrocenylbutanoic acid was used to demonstrate the drug-binding potential of the poly(amidoamine) polymers on ferrocenylation in other organic solvents namely methanolic medium than dimethylformamide.

Conjugate 1-Fc (HBTU)

This conjugate was obtained using the *Method (1)* detailed below.

Carrier **1** (200mg, 0.102mmol) was dissolved in 5 mL of DMF with stirring. In a separate vessel, 4-ferrocenylbutanoic acid (33mg, 0.12mmol) and HBTU (42mg, 0.11mmol), dissolved in 2 mL of DMF, were stirred for a period of 1h at ambient temperature, protected from direct light, then added in one dash to the carrier solution, followed by the addition of TEA (21mg, 0.204mmol). The resulting brownish solution was saturated with N_2, and stirred at room temperature for another 2h, still protected from the light. Afterwards, the reaction vessel was cooled at 5^{o}C for 0.5h, then the conjugate was precipitated with 20 mL of Et_2O-hexane (2:1), isolated upon centrifugation, thoroughly washed with warm acetone, Me_2CO, and dissolved in 5 mL of H_2O. The pH was adjusted from ~9 to 10 upon NaOH addition, and the product was purified by size exclusion chromatography on 2.5 x 25 cm column packed with Sephadex G-25 and eluted with distilled H_2O. The pH of the eluate was readjusted to 7 (glacial acetic acid) to prevent hydrolysis, ~10mg of ascorbic acid was added to preclude ferrocene oxidation to ferricenium salts, and the solution was dialyzed for 48h in Spectra/Por 6 tubing. The retentate, pH~8, was freeze-dried to afford 120 mg (53%) of tan, fluffy, and water-soluble **1-Fc (HBTU)**, possessing the following characteristics: η_{inh}**,** 15.96 mL g^{-1}. Found: Fe, 2.45% (UV), 2.52% (NMR). Calcd. for $(C_{102}H_{180}N_{30}O_{21}Fe)_n$ $(2218.6)_n$ [**1-Fc (HBTU)**]: Fe, 2.52%. Refer to Table 4.27 row 2.

^{1}H NMR (D_2O), δ/ppm: 4.3-4.25, 9H (Expected: 9H; *CH* of ferrocenyl); 1.8-1.5, 22H (Expected: 22H, $CH_2CH_2CH_2$), indicating 100% NH_2 acylation.

The Fe content by mass of this conjugate (and the forthcomings) was derived from the ferrocene content UV spectroscopically determined in H_2O using the molar extinction coefficient value, $\varepsilon = 100$ mol^{-1} cm^{-1}, and the absorbance at $\lambda =$ 440 nm, of ferrocene proper.

Conjugate 1-Fc (ONp)

Method (2) was used to afford that conjugate. Thus, carrier **1** (200mg, 0.102mmol) and Fc-ONp (48mg, 0.122mmol) were dissolved in 2 mL of dry DMSO, protected from direct light, and the solution was stirred at room temperature; overnight then ethanolamine (EA) (8mg, 0.122mmol) was added to aminolyze the unreacted Fc-ONp. Stirring was continued at the stated temperature for another 3h. Thereafter, the polymeric conjugate was precipitated with 20 mL of Me_2CO:Et_2O (3:1), isolated upon centrifugation, thoroughly washed with 3x 5 mL of Me_2CO, dissolved in 5 mL of H_2O. The pH was adjusted from ~9 to 10 upon NaOH addition, and the product was purified by size exclusion chromatography on 2.5 x 25 cm column packed with Sephadex G-25 and eluted with distilled H_2O. The pH of the eluate was readjusted to 7 (glacial acetic acid) to prevent hydrolysis, ~10mg of ascorbic acid was added to preclude ferrocene oxidation, and the solution was dialyzed exhaustively for 48h in Spectra/Por 6 tubing. The retentate, pH~8, was freeze-dried to give 125 mg (55%) of **1-Fc (ONp)** as a tan-colored, fluffy, and water-soluble solid. η_{inh}, 15.92 mL g^{-1}.
Found: Fe, 2.48% (UV), 2.52% (NMR). Calcd. for $(C_{102}H_{180}N_{30}O_{21}Fe)_n$ $(2218.6)_n$ [**1-Fc (ONp)**]: Fe, 2.52%. Refer to Table 4.31 row 2.

^{1}H NMR (D_2O), δ/ppm: 4.3-4.25, 9H (Expected: 9H; *CH* of ferrocenyl); 1.8-1.5, 22H (Expected: 22H, $CH_2CH_2CH_2$). These ^{1}H NMR data showed 100% Fc incorporation.

Conjugate 2-Fc (ONp)

This conjugate was prepared analogously to **1-Fc (ONp)** by replacing carrier **1**(90:10) by its variant **2**(80:20). Thus, from carrier **2** (200mg, 0.21mmol), Fc-ONp (97mg, 0.248mmol) and EA (15mg, 0.248mmol), it was obtained after work-up 142mg (55%) of the target conjugate **2-Fc (ONp)** as tan-colored, fluffy and fully water-soluble material. η_{inh}, 13.15 mLg^{-1}. Found: Fe, 4.48% (UV), 4.55% (NMR). Calcd. for $(C_{57}H_{95}N_{15}O_{11}Fe)_n$ $(1222.3)_n$ [**2-Fc (ONp)**]: Fe, 4.57%). See to Table 4.31 row 3.

^{1}H NMR (D_2O), δ/ppm: 4.3-4.25, 8.73H (Expected: 9H; *CH* of ferrocenyl); 1.8-1.5, 12H (Expected: 12H, $CH_2\mathit{CH_2}CH_2$). These ^{1}H NMR data showed 97% Fc incorporation.

Conjugate 3-Fc (HBTU)

Similarly to the basic *Method (1)* leading to **1-Fc (HBTU)**, the conjugate **3-Fc (HBTU)** was obtained by treating carrier (200mg, 0.1mmol) with ferrocenylbutanoic acid (33mg, 0.11mmol), HBTU (42mg, 0.11mmol), TEA (20mg, 0.2mmol), in a total of 7 mL of DMF. After conventional work-up, it was obtained 125mg (56%) of tan-colored, water-soluble, solid **3-Fc (HBTU)**, characterized as follows: η_{inh}, 13.7 mL g^{-1}. Found: Fe, 2.48% (UV), 2.49% (NMR). Calcd. for $(C_{103}H_{183}N_{31}O_{21}Fe)_n$ $(2247.6)_n$ [**3-Fc (HBTU)**]: Fe, 2.49%; Table 4.27 row 3.

^{1}H NMR (D_2O), δ/ppm: 4.3-4.25, 9H (Expected: 9H; *CH* of ferrocenyl); 1.8-1.5, 20H (Expected: 20H, $CH_2\mathit{CH_2}CH_2$). These ^{1}H NMR data showed 100% Fc incorporation.

Conjugate 3-Fc (ONp)

For the preparation of this conjugate the standard procedure that afforded **1-Fc (ONp)** was used. Thus, the reaction of polyasparatamide **3** (200mg, 0.1mmol), Fc-ONp (47mg, 0.12mmol), and EA (7mg, 0.12mmol), in a total of 2 mL of DMSO, gave, after routine work-up, 130mg (58%) of fluffy, fully water-soluble

compound **3-Fc (ONp)**. η_{inh}, 13.25 mL g^{-1}. Found: Fe, 2.46% (UV), 2.49% (NMR). Calcd. for $(C_{103}H_{183}N_{31}O_{21}Fe)_n$ $(2247.6)_n$ [**3-Fc (ONp)**]: Fe, 2.49%; Table 4.31 row 4.

^{1}H NMR (D_2O), δ/ppm: 4.3-4.25, 9H (Expected: 9H; *CH* of ferrocenyl); 1.8-1.5, 20H (Expected: 20H, $CH_2CH_2CH_2$). These ^{1}H NMR data indicate 100% NH_2 acylation.

Conjugate 4-Fc (ONp)

This conjugate was obtained in a fashion similar to that leading to the preceding conjugate with the exception that carrier **3**(90:10) was replaced by **4**(80:20). Thus, the treatment of carrier **4** (200mg, 0.2mmol) with Fc-ONp (94mg, 0.241mmol) and EA (15mg, 0.241mmol) in a total of 2mL of DMSO, afforded after work-up 148mg (58%) of the target conjugate **4-Fc (ONp)** as tan-colored and water-soluble solid. η_{inh}, 12.85 mL g^{-1}. Found: Fe, 4.42% (UV), 4.45% (NMR). Calcd. for $(C_{58}H_{98}N_{16}O_{11}Fe)_n$ $(1251.4)_n$ [**4-Fc (ONp)**]: Fe, 4.46%; Table 4.31 row 5.

^{1}H NMR (D_2O), δ/ppm: 4.3-4.25, 9H (Expected: 9H; *CH* of ferrocenyl); 1.8-1.5, 10H (Expected: 10H, $CH_2CH_2CH_2$). These ^{1}H NMR data indicate 100% NH_2 acylation.

Conjugate 5-Fc (HBTU)

This conjugate was obtained by the direct coupling *Method (1)*. Thus, carrier **5** (200mg, 0.098mmol) treated with ferrocenylbutanoic acid (37mg, 0.137mmol), HBTU (45mg, 0.118mmol) and TEA (20mg, 0.196mmol), afforded 146mg (64%) of tan, fluffy and fully water-soluble solid. η_{inh}, 12.5 mL g^{-1}. Found: Fe, 2.39% (UV), 2.41% (NMR). Calcd. for $(C_{105}H_{186}N_{30}O_{23}Fe)_n$ $(2292.7)_n$ [**5-Fc (HBTU)**]: Fe, 2.44%; Table 4.27 row 4.

^{1}H NMR (D_2O), δ/ppm: 4.3-4.25, 8.91H (Expected: 9H; *CH* of ferrocenyl); 1.8-1.5, 20H (Expected: 20H, $CH_2CH_2CH_2$). These ^{1}H NMR data indicate 99% NH_2 acylation.

Conjugate 5-Fc (ONp)

For the preparation of this conjugate, the *Method (2)* was employed. Thus, 125mg (55%) of water-soluble solid were obtained from carrier **5** (200mg, 0.098mmol) and Fc-ONp (46mg, 0.118mmol), in a ratio NH_2: active ester of 1:1.2. The conjugate was found to possess the following characteristics: η_{inh}, 11.95 mL g^{-1}. Found: Fe, 2.39% (UV), 2.37% (NMR). Calcd. for $(C_{105}H_{186}N_{30}O_{23}Fe)_n$ $(2292.7)_n$ [**5-Fc (ONp)**]: Fe, 2.44%; Table 4.31 row 6.

^{1}H NMR (D_2O), δ/ppm: 4.3-4.25, 8.7H (Expected: 9H; *CH* of ferrocenyl); 1.8-1.5, 20H (Expected: 20H, $CH_2CH_2CH_2$), corresponding to drug incorporation of 97% level.

Conjugate 7-Fc (ONp)

Polymer **7** (400mg, 0.202mmol) and Fc-ONp (95mg, 0.242mmol) were reacted in DMSO solution for a period of 6h at RT followed by the addition of EA (15mg, 0.242mmol). The reaction was continued for another 2h at RT. The routine work-up comprising precipitation in non-solvent, isolation upon centrifugation, fractionation and purification by both size exclusion chromatography and exhaustive dialysis under pH control, and isolation in solid state by freeze-drying, afforded 270mg (59%) of the target conjugate as tan-colored and water-soluble compound. η_{inh}, 14.5 mL g^{-1}. Found: Fe, 2.42% (UV), 2.39% (NMR). Calcd. for $(C_{102}H_{180}N_{30}O_{22}Fe)_n$ $(2234.6)_n$ [**7-Fc (ONp)**]: Fe, 2.5%); see Table 4.31 row 7.

^{1}H NMR (D_2O), δ/ppm: 4.3-4.25, 8.51H (Expected: 9H; *CH* of ferrocenyl); 1.8-1.5, 20H (Expected: 20H, $CH_2CH_2CH_2$). This indicated the drug incorporation of 95% level.

Conjugate 8-Fc (ONp)

The *Method (2)* was employed for the obtaining of this conjugate. The reaction of carrier **8** (200mg, 0.123mmol) with Fc-ONp (58mg, 0.148mmol) and EA (9mg, 0.148mmol) in total of 2 mL of DMSO, at ambient temperature over a period of 10h, gave after adopted work-up 160mg (69%) of water-soluble solid **8-Fc**

(ONp); η_{inh}, 17.75 mL g^{-1}. Found: Fe, 2.94% (UV), 2.97% (NMR). Calcd. for $(C_{76}H_{120}N_{22}O_{30}Fe)_n$ $(1877.8)_n$ [**8-Fc (ONp)**]: Fe, 2.97%. See Table 4.31 row 8.

^{1}H NMR (D_2O), δ/ppm: 4.3-4.25, 9H (Expected: 9H; *CH* of ferrocenyl); 3.8-3.5, 18 (Expected: 18H, O*CH*$_2$OH). The spectroscopic results revealed the conjugation extent to be of 100%.

Conjugate 10-Fc (ONp)

In a fashion analogous to that leading to the preceding conjugate with the exception of carrier **8** being replaced by **10**, conjugate the target conjugate was obtained in a yield of 71% as faintly yellow solid from carrier **10** and Fc-ONp in ratio 1:1.2. The conjugate possessed full water-solubility. η_{inh}, 13.75 mL g^{-1}. Found: Fe, 2.88% (UV), 2.92% (NMR). Calcd. for $(C_{75}H_{117}N_{21}O_{31}Fe)_n$ $(1864.8)_n$ [**10-Fc (ONp)**]: Fe, 3.0%; Table 4.31 row 9.

^{1}H NMR (D_2O), δ/ppm: 4.3-4.25, 8.73H (Expected: 9H; *CH* of ferrocenyl); 3.8-3.5, 19H (Expected: 19H, *CH*-OH, O*CH*$_2$OH). These spectroscopic data indicated 97% NH_2 acylation.

Conjugate 11-Fc (ONp)

Polymer **11** (400mg, 0.25mmol) was treated with Fc-ONp (118mg, 0.3mmol) in DMSO medium for a period of 6h at ambient then EA (18mg, 0.3mmol) was added, and treatement continued for another 2h at the same temperature. After routine work-up, the target conjugate **11-Fc (ONp)** was isolated in yield of 340mg (73%) as tan-colored, fluffy and fully water-soluble solid. $\boldsymbol{\eta_{inh}}$, 13.5 mL g^{-1}. Found: Fe, 2.98% (UV), 2.97% (NMR). Calcd. for $(C_{75}H_{117}N_{21}O_{30}Fe)_n$ $(1848.8)_n$ [**11-Fc (ONp)**]: Fe, 3.02%); Table 4.31 row 10.

^{1}H NMR (D_2O), δ/ppm: 4.3-4.25, 8.79H (Expected: 9H; *CH* of ferrocenyl); 3.8-3.5, 18H (Expected: 18H, *CH*$_2$O); indicating the drug incorporation of the 98% level.

Conjugate 12-Fc (ONp)

The reaction of polymer **12** (400mg, 0.24mmol), Fc-ONp (113mg, 0.288mmol) and EA (18mg, 0.288mmol) in a total of 4 mL of DMSO, afforded after conventional work-up the conjugate **12-Fc (ONp)** as tan-colored water-soluble solid in a yield of 350mg (75%) with inherent viscosity, η_{inh}, 14.28 mL g^{-1}. Found: Fe, 2.85% (UV), 2.82% (NMR). Calcd. for $(C_{78}H_{123}N_{21}O_{32}Fe)_n$ $(1922.9)_n$ [**12-Fc (ONp)**]: Fe, 2.9%); Table 4.31 row 11.

^{1}H NMR (D_2O), δ/ppm: 4.3-4.25, 8.75H (Expected: 9H; *CH* of ferrocenyl); 3.8-3.5, 26H (Expected: 26H, CH_2O). These data indicated 97% of drug incorporation.

Conjugate 13-Fc (ONp)

The *Method (2)* was used for the preparation of this conjugate. Carrier **11** (200mg, 0.099mmol) was allowed to react with Fc-ONp (47mg, 0.119mmol) and EA (7mg, 0.119mmol), in a total volume of DMSO of 2 mL, over a period of 2h. The routinely work-up including purification by size exclusion chromatography and exhaustive dialysis, and freeze-drying, afforded 170mg (75%) of the target conjugate as a tan-colored and fully hydrophilic solid, possessing the following characteristics: η_{inh}, 15.25 mL g^{-1}. Found: Fe, 2.41% (UV), 2.46% (NMR). Calcd. for $(C_{94}H_{156}N_{22}O_{39}Fe)_n$ $(2274.3)_n$ [**13-Fc (ONp)**]: Fe, 2.46%; Table 4.31 row 12.

^{1}H NMR (D_2O), δ/ppm: 4.3-4.25, 9H (Expected: 9H; *CH* of ferrocenyl); 3.8-3.5, 18H (Expected: 19H, CH_2OCH_2OH). These data indicated 100% NH_2 acylation.

Conjugate 14-Fc (ONp)

Analogously to the preceding preparative experiment with exception of carrier **13** being replaced by its variant **14**, the target conjugate was obtained from carrier **14** and Fc-ONp in ratio of 1:1.2, in a yield of 57%, and was found to retain full water-solubility. η_{inh}, 13.5 mL g^{-1}. Found: Fe, 4.3% (UV), 4.35% (NMR). Calcd. for $(C_{54}H_{86}N_{12}O_{19}Fe)_n$ $(1263.2)_n$ [**14-Fc (ONp)**]: Fe, 4.42%); Table 4.31 row 13.

^{1}H NMR (D_2O), δ/ppm: 4.3-4.25, 8.82H (Expected: 9H; *CH* of ferrocenyl); 3.8-3.5, 24H (Expected: 24H, CH_2OCH_2OH), corresponding to drug incorporation level of 98%.

Conjugate 16-Fc (ONp)

The *Method (2)* was employed for the synthesis of conjugate **16-Fc (ONp)**. Thus, used in the similar (physical and stoichiometric) conditions as those leading to the preceding conjugate, carrier **16** (200mg, 0.1mmol) and with Fc-ONp (47mg, 0.12mmol) afforded after work-up, 105mg (46%) of the target conjugate as faint-yellow solid, fully hydrophilic. η_{inh}, 12.86 mL g^{-1}. Found: Fe, 2.45% (UV), 2.43% (NMR). Calcd. for $(C_{93}H_{153}N_{21}O_{40}Fe)_n$ $(2261.3)_n$ [**16-Fc (ONp)**]: Fe, 2.47%.

^{1}H NMR (D_2O), δ/ppm: 4.3-4.25, 8.82H (Expected: 9H; *CH* of ferrocenyl); 3.8-3.5, 55H (Expected: 55H, *CH*-OH, CH_2OCH_2OH), corresponding to drug incorporation level of 98%; Table 4.31 row 14.

Conjugate 17-Fc (ONp)

This conjugate was prepared in a fashion similar to that leading to the preceding conjugate with minor change concerning the replacement of carrier **16** by **17**. Thus, carrier **17** (200mg, 0.114mmol) treated with Fc-ONp (54mg, 0.137mmol) and EA (8mg, 0.137mmol), in total volume of DMSO of 2 mL, gave after work-up, 175mg (74%) of a tan-colored and water-soluble solid. η_{inh}, 18.5 mLg^{-1}. Found: Fe, 2.73% (UV), 2.79% (NMR). Calcd. for $(C_{93}H_{153}N_{21}O_{40}Fe)_n$ $(2003.1)_n$ [**17-Fc (ONp)**]: Fe, 2.79%; Table 4.31 row 15.

^{1}H NMR (D_2O), δ/ppm: 4.3-4.25, 9H (Expected: 9H; *CH* of ferrocenyl); 3.8-3.5, 45H (Expected: 45H, CH_2OCH_3). These data showed 100% NH_2 acylation

Conjugate 19-Fc (ONp)

For the preparation of this conjugate, the *Method (2)* was employed. Thus, the reaction of polymer **19** (400mg, 0.232mmol) with Fc-ONp (109mg, 0.278mmol) and EA (17mg, 0.278mmol) in DSMO medium at ambient temperature for a

period of 8h, afforded after routine work-up the target conjugate **19-Fc (ONp)** as water-soluble solid and characterized as follows: η_{inh}, 16.89 mL g^{-1}. Found: Fe, 2.75% (UV), 2.80% (NMR). Calcd. for $(C_{84}H_{136}N_{21}O_{30}Fe)_n$ $(1975.1)_n$ [**19-Fc (ONp)**]: Fe, 2.8%; Table 4.31 row 16.

^{1}H NMR (D_2O), δ/ppm: 4.3-4.25, 9H (Expected: 9H; *CH* of ferrocenyl); 3.8-3.5, 45H (Expected: 45H, CH_2OCH_3), indicating 100% NH_2 acylation.

Conjugate 20-Fc (ONp)

Polymer **20** (400mg, 0.223mmol) was allowed to react with Fc-ONp (105mg, 0.267mmol) and EA (16mg, 0.267mmol) in a similar fashion as that leading to the preceding conjugate. After work-up, the conjugate **20-Fc (ONp)** was isolated as tan-colored material possessing full water solubility and the following characteristics: η_{inh}, 15.45 mL g^{-1}. Found: Fe, 2.70% (UV), 2.68% (NMR). Calcd. for $(C_{84}H_{136}N_{21}O_{30}Fe)_n$ $(2049.1)_n$ [**20-Fc (ONp)**]: Fe, 2.73%.

^{1}H NMR (D_2O), δ/ppm: 4.3-4.25, 8.82H (Expected: 9H; *CH* of ferrocenyl); 3.8-3.5, 53H (Expected: 53H, CH_2O-, CH_2OCH_3). These data indicate the incorporation of drug of 98% level; Table 4.31 continued row 2.

Conjugate 25-Fc (HBTU)

This poly(amidoamine)-derived conjugate was obtained using the acylation *Method (1)* as described for **1-Fc (HBTU)**. In a molar feed ratio Fc/NH_2 of 1.2, poly(amidoamine) **25** (200mg, 0.167mmol), 4-ferrocenylbutanoic acid (68mg, 0.251mmol), HBTU (82mg, 0.217mmol), and TEA (34mg, 0.333mmol), in a total of 7 mL of DMF, afforded 95 mg (39%) of tan-colored, fully water soluble **25-Fc (HBTU)**. η_{inh}, 16.25 mL g^{-1}. Found: Fe, 3.82% (UV), 3.85% (NMR). Calcd. for $(C_{68}H_{122}N_{20}O_{11}Fe)_n$ $(1451.7)_n$ [**25-Fc (HBTU)**]: Fe, 3.85%. See Table 4.27 row 5.

^{1}H NMR (D_2O), δ/ppm: 4.8-4.5, 10H (Expected: 10H, CONHCH_2HNCO), 4.3-4.25, 9H (Expected: 9H; *CH* of ferrocenyl); 1.8-1.5, 4H (Expected: 4H, $CH_2CH_2CH_2$). These ^{1}H NMR data indicate 100% NH_2 acylation.

Conjugate 25-Fc (ONp)

Method (2) was applied for the preparation of this conjugate from carrier **25** (200mg, 0.167mmol), Fc-ONp (79mg, 0.2mmol), and EA (12mg, 0.2mmol), in 2 mL of DMSO. After work-up as described in the preceding experiments, it was obtained conjugate 2**5-Fc (ONp)** in a yield of 124mg (51%), tan-colored and water-soluble. $\boldsymbol{\eta_{inh}}$, 14.5 mL g^{-1}. Found: Fe, 3.8% (UV), 3.85% (NMR). Calcd. for $(C_{68}H_{122}N_{20}O_{11}Fe)_n$ $(1451.7)_n$ [2**5-Fc (ONp)**]: Fe, 3.85%.

^{1}H NMR (D_2O), δ/ppm: 4.8-4.5, 10H (Expected: 10H, CONH*CH*$_2$HNCO), 4.3-4.25, 9H (Expected: 9H; *CH* of ferrocenyl); 1.8-1.5, 4H (Expected: 4H, CH_2*CH*$_2$$CH_2$). Ferrocene incorporation: 100%; Table 4.31 continued row 3.

Conjugate 26-Fc (HBTU)

Using the *Method (1)* similarly to the synthesis of **25-Fc (HBTU)**, this polymeric drug conjugate was obtained from carrier **26** (200mg, 0.159mmol), ferrocenylbutanoic acid (65mg, 0.239mmol), HBTU (78mg, 0.208mmol), and TEA (32mg, 0.319mmol), in a total of 7 mL of DMF. The routine work-up afforded the target conjugate **26-Fc (HBTU)** in a yield of 100mg (42%) as tan-colored, water-soluble solid. It possessed the following characteristics:
η_{inh}, 19.79 mL g^{-1}. Found: Fe, 3.63% (UV), 3.7 (NMR). Calcd. for $(C_{72}N_{30}O_{11}Fe)_n$ $(1507.8)_n$ [**26-Fc (HBTU)**]: Fe, 3.7%. See Table 4.27 row 6.

^{1}H NMR (D_2O), δ/ppm: 4.8-4.5, 10H (Expected: 10H, CONH*CH*$_2$HNCO), 4.3-4.25, 9H (Expected: 9H; *CH* of ferrocenyl); 1.8-1.5, 12H (Expected: 12H, CH_2*CH*$_2$$CH_2$). Ferrocene incorporation: 100%.

Conjugate 27-Fc (HBTU)

This conjugate was prepared similarly to **25-Fc (HBTU)**, except that poly(amidoamine) **25** was replaced by **27**. Thus, carrier **27** (200mg, 0.155mmol), treated with 4-ferrocenylbutanoic acid (63mg, 0.233mmol), HBTU (77mg, 0.202mmol), TEA (31mg, 0.309mmol), in a total of 7 mL of DMF, gave 102mg (43%) of water-soluble solid **27-Fc (HBTU)**. η_{inh}, 18.5 mL g^{-1}. Found: Fe, 3.57%

(UV), 3.64% (NMR). Calcd. for $(C_{73}H_{132}N_{21}O_{11}Fe)_n$ $(1535.8)_n$ [**27-Fc (HBTU)**]: Fe, 3.64%. Refer to Table 4.27 row 7.

^{1}H NMR (D_2O), δ/ppm: 4.8-4.5, 10H (Expected: 10H, CONH*CH*$_2$HNCO), 4.3-4.25, 9H (Expected: 9H; *CH* of ferrocenyl); 1.8-1.5, 10H (Expected: 10H, CH_2*CH*$_2$$CH_2$), showing 100% NH_2 acylated.

Conjugate 27-Fc (ONp)

The basic procedure leading to **25-Fc (ONp),** was used for the preparation of this compound. Polymer **27** (180mg, 0.140mmol) was treated with Fc-ONp (66mg, 0.168mmol), and EA (10mg, 0.168mmol), in a total of 2 mL of DMSO. The routine work-up comprising precipitation, purification by both size exclusion chromatography, and freeze-drying, gave 90mg (42%) of water-soluble solid **27-Fc (ONp)**. η_{inh}, 17.05 mL g^{-1}. Found: Fe, 3.58% (UV), 3.64% (NMR). Calcd. for $(C_{73}H_{132}N_{21}O_{11}Fe)_n$ $(1535.8)_n$ [**27-Fc (ONp)**]: Fe, 3.64%.

^{1}H NMR (D_2O), δ/ppm: 4.8-4.5, 10H (Expected: 10H, CONH*CH*$_2$HNCO), 4.3-4.25, 9H (Expected: 9H; *CH* of ferrocenyl); 1.8-1.5, 10H (Expected: 10H, CH_2*CH*$_2$$CH_2$), showing 100% ferrocene incorporation; Table 4.31 continued row 4.

Conjugate 28-Fc (HBTU)

Method (1) was employed to afford this conjugate. Poly(amidoamine) **28** (200mg, 0.156mmol) treated ferrocenylbutanoic acid (64mg, 0.234mmol), HBTU (77mg, 0.203mmol), TEA (32mg, 0.312mmol), in a total of 7 mL of DMF, gave 120mg (43%) of water-soluble solid **28-Fc (HBTU)**, characterized as follows: η_{inh}, 21.2 mL g^{-1}. Found: Fe, 3.61% (UV), 3.66% (NMR). Calcd. for $(C_{71}H_{128}N_{20}O_{13}Fe)_n$ $(1525.8)_n$ [**28-Fc (HBTU)**]: Fe, 3.66%; Table 4.27 row 8.

^{1}H NMR (D_2O), δ/ppm: 4.8-4.5, 10H (Expected: 10H, CONH*CH*$_2$HNCO), 4.3-4.25, 9H (Expected: 9H; *CH* of ferrocenyl); 3.8-3.5, 9H (Expected: 8H,

O*CH*$_2$*CH*$_2$O); 1.8-1.5, 10H (Expected: 10H, CH$_2$*CH*$_2$CH$_2$), indicating 100% NH_2 acylation.

Conjugate 28-Fc (ONp)

In a similar fashion to that leading to the conjugate **27-Fc (ONp)**, from carrier **28** (130mg, 0.101mmol), Fc-ONp (48mg, 0.122mmol), and EA (8mg, 0.122mmol), it was obtained 65mg (42%) of the target conjugate **28-Fc (ONp)**, as tan-colored, fluffy, and water-soluble compound. η_{inh}, 22.05 mL g^{-1}. (Found: Fe, 3.60% (UV), 3.66% (NMR). Calcd. for $(C_{71}H_{128}N_{20}O_{13}Fe)_n$ $(1525.8)_n$ [**28-Fc (ONp)**]: Fe, 3.66%

^{1}H NMR (D_2O), δ/ppm: 4.8-4.5, 10H (Expected: 10H, CONH*CH*$_2$HNCO), 4.3-4.25, 9H (Expected: 9H; *CH* of ferrocenyl); 3.8-3.5, 9H (Expected: 8H, O*CH*$_2$*CH*$_2$O); 1.8-1.5, 10H (Expected: 10H, CH$_2$*CH*$_2$CH$_2$), indicating 100% NH_2 acylation; Table 4.31 continued row 5.

Conjugate 32-Fc (HBTU)

Similarly to the preparation of **1-Fc (HBTU)**, except that polyaspartamide **1** was replaced by poly(amidoamine) **32**, conjugate **32-Fc (HBTU)** resulted from the reaction of carrier **32** (100mg, 0.17mmol), ferrocenylbutanoic acid (56mg, 0.204mmol), HBTU (71mg, 0.187mmol), TEA (34mg, 0.34mmol), in a total of 7 mL of DMF. The adopted work-up afforded conjugate **32-Fc (HBTU)** in yield of 105mg (73%). It was found tan-colored and fully water-soluble. η_{inh}, 16.3 mL g^{-1}. Found: Fe, 6.25% (UV), 6.3% (NMR). Calcd. for $(C_{40}H_{66}N_8O_8Fe)_n$ $(856.9)_n$ [**32-Fc (HBTU)**]: Fe, 6.52%. See Table 4.27 row 9.

^{1}H NMR (D_2O), δ/ppm: 4.8-4.5, 4H (Expected: 4H, CONH*CH*$_2$HNCO), 4.3-4.25, 8.7H (Expected: 9H; *CH* of ferrocenyl); 3.8-3.5, 14H (Expected: 12H, O*CH*$_2$*CH*$_2$O); 1.8-1.5, 8H (Expected: 8H, CH$_2$*CH*$_2$CH$_2$). These ^{1}H NMR data indicate 97% NH_2 acylation.

Conjugate 32-Fc (ONp)

The reaction of carrier **32** (180mg, 0.339mmol), Fc-ONp (160mg, 0.407mmol) and EA (25mg, 0.406mmol) in DSMO medium afforded after conventional work-up 149mg (48%) of target conjugate conjugate **32-Fc (ONp)** as fully water-soluble solid which possessed the followings characteristics: η_{inh}, 15.55 mL g^{-1}. Found: Fe, 6.54% (UV), 6.45% (NMR). Calcd. for $(C_{40}H_{66}N_8O_8Fe)_n$ $(856.9)_n$ [**32-Fc (ONp)**]: Fe, 6.52%. Ree Table 4.31 continued row 6.

^{1}H NMR (D_2O), δ/ppm: 4.8-4.5, 4H (Expected: 4H, CONH*CH*$_2$HNCO), 4.3-4.25, 8.9H (Expected: 9H; CH of ferrocenyl); 3.8-3.5, 13H (Expected: 12H, O*CH*$_2$*CH*$_2$O); 1.8-1.5, 9H (Expected: 8H, CH_2*CH*$_2$$CH_2$). These ^{1}H NMR data indicate 99% NH_2 acylation.

Conjugate 33-Fc (HBTU)

The free acid HBTU mediated coupling *Method (1)* was applied. However, the molar feed ratio COOH/NH_2 was increased to 1.3 instead of 1.2 as for the preparation of **32-Fc (HBTU)**. Thus, from carrier **33** (200mg, 0.108mmol), ferrocenylbutanoic acid (35mg, 0.130mmol), HBTU (39mg, 0.119mmol), TEA (22mg, 0.216mmol), in a total of 7 mL of DMF, it was obtained 95mg (41%) of fully water-soluble conjugate **33-Fc (HBTU)** possessing the following characteristics: η_{inh}, 16.34 mL g^{-1}. Found: Fe, 2.3% (UV), 2.33% (NMR). Calcd. for $(C_{98}H_{182}N_8O_{37}Fe)_n$ $(2134.4)_n$ [**33-Fc (HBTU)**]: Fe, 2.62%; Table 4.27 row 10.

^{1}H NMR (D_2O), δ/ppm: 4.8-4.5, 4H (Expected: 4H, CONH*CH*$_2$HNCO), 4.3-4.25, 8.1H (Expected: 9H; *CH* of ferrocenyl); 3.8-3.5, 130H (Expected: 128H, O*CH*$_2$*CH*$_2$O); 1.8-1.5, 7H (Expected: 8H, CH_2*CH*$_2$$CH_2$). Ferrocene incorporation: 90%.

Conjugate 33-Fc (ONp)

The basic procedure affording conjugate **25-Fc (ONp)** was used for the preparation of the compound **33-Fc (ONp)** without major modification except **33** replaced that carrier **25**. The molar feed ratio of active ester/NH_2 remained 1.2.

Thus, carrier **33** (200mg, 0.108mmol) treated with Fc-ONp (51mg, 0.13mmol), and EA (8mg, 0.13mmol), in a total of 2 mL of DMSO, gave after conventional work-up, 100mg (44%) of light-brown, water-soluble solid **33-Fc (ONp)**. η_{inh}, 16.85 mL g^{-1}. (Found: Fe, 2.58% (UV), 2.53% (NMR). Calcd. for $(C_{98}H_{182}N_8O_{37}Fe)_n$ $(2134.4)_n$ [**33-Fc (ONp)**]: Fe, 2.62%; Table 4.31 continued row 7.

^{1}H NMR (D_2O), δ/ppm: 4.8-4.5, 4H (Expected: 4H, CONH*CH*$_2$HNCO), 4.3-4.25, 8.7H (Expected: 9H; CH of ferrocenyl); 3.8-3.5, 130H (Expected: 128H, O*CH*$_2$*CH*$_2$O); 1.8-1.5, 7H (Expected: 8H, CH_2*CH*$_2$$CH_2$). Ferrocene incorporation: 97%.

Conjugate 32-Fc (OSU)

For the preparation of this conjugate the active ester technique was used. However, major modifications were introduced. These concerned the active ester compound, the reaction medium as well as the molar feed ratio of reactants. Thus, contrarily to the preceding experiments, the Fc-ONp active ester was replaced by Fc-OSU, methanol was used instead of DMSO. Consequently, the reaction period was extended. The molar feed ratio of active ester/NH_2 was 1.3 rather than 1.2 as previously.

Thus, carrier **32** (180mg, 0.305mmol) and Fc-OSu (146mg, 0.396mmol) were dissolved in 5 mL of MeOH. The brown solution protected from direct light was stirred at room temperature for 72h. The solvent was completely removed upon rotary evaporation, and the polymeric residue, precipitated with 15 mL of Et_2O: Me_2CO (2:1) was dissolved in 5 mL of H_2O. The pH was adjusted from ~9 to 10 (NaOH) and the product was purified as routinely by size exclusion chromatography and dialysis. Freeze-drying of the retentate, pH~8.5, gave 102mg (40%) of light-brown, water-soluble solid **32-Fc (OSU)**. η_{inh}, 15.05 mL g^{-1}. Found: Fe, 6.01% (UV), 6.08% (NMR). Calcd. for $(C_{40}H_{66}N_8O_8Fe)_n$ $(856.9)_n$ [**32-Fc (OSU)**]: Fe, 6.52%; see Table 4.31 continued row 8.

^{1}H NMR (D_2O), δ/ppm: 4.8-4.5, 4H (Expected: 4H, CONH*CH_2*HNCO), 4.3-4.25, 8.4H (Expected: 9H; *CH* of ferrocenyl); 3.8-3.5, 14H (Expected: 12H, O*CH_2CH_2*O); 1.8-1.5, 10H (Expected: 8H, CH_2*CH_2*CH_2). These ^{1}H NMR data indicate 93% NH_2 acylation.

5.3.4 Polyaspartamide conjugates with two drug systems

These conjugates were synthesized in a two-step process combining both methods employed for the preparation of ferrocene conjugates. The first step consisting of binding of the first drug system to the polymeric carrier was achieved *via* coupling mediated by HBTU, and the anchoring of the second drug was brought about either by the preceding method or the active ester method.

Conjugate 1 (90:10)-FA/MTX

Step (1): Carrier **1** (600mg, 0.306mmol) and FA (95mg, 0.214mmol) were dissolved in 10 mL of NMP-HMP-DMF (4:3:3) upon heating. To this rapidly stirred solution at RT, was added dropwise over 0.5h period HBTU (70mg, 0.184mmol) predissolved in 2 mL of DMF. This was followed by the addition of TEA (62mg, 0.612mmol). The resulting yellow solution was saturated with N_2 and stirring was continued at RT for 2h, then cooled at 5^{o}C for another 0.5h. Thereafter, the routine work-up as in preceding experiments, gave 550mg (82%) of yellow, crispy, fully water-soluble material homoconjugate **1**(90:10)**-FA**, η_{inh}, 15.05 mL g^{-1}.

^{1}H NMR (D_2O), δ/ppm: 8.5-6.5, 2.9H (Expected: 5H; aromatic and heteroaromatic *CH* of FA); 1.8-1.6, 20H (expected: 20H; CH_2*CH_2*CH_2). These data indicate 58% FA incorporation. Found: FA, 11.05% (UV), 11.58% (NMR).

Step (2): The homoconjugate **1**(90:10)**-FA** (H) (200mg, 0.102mmol) and MTX (33mg, 0.072mmol) were dissolved in 8 mL of NMP-HMP (1:1) upon heating. On cooling and rapid stirring at RT, HBTU (23mg, 0.061mmol) predissolved in 2 mL of DMF, was added dropwise over 20min period followed by the addition of TEA

(21mg, 0.204mmol). The solution was saturated with N_2 and stirring was continued at RTfor 3h then cooled at 5^{o}C for another 0.5h.
The conventional work-up gave 150mg of co-conjugate **1**(90:10)**-FA/MTX** as a yellow material possessing full solubility; η_{inh}, 15.05 mL g^{-1}.

^{1}H NMR (D_2O), δ/ppm: 8.5-6.5, 4.58H (Expected: 5H; hetero- and aromatic CH of FA); 1.8-1.6, 20H (expected: 20H; CH_2*CH_2*CH_2), showing 92% (FA+MTX) incorporation.

In order to increase the drug incorporation, **1**(90:10)**-FA/MTX** (150mg, ~0.077mmol) was retreated with MTX (28mg, 0.061mmol), HBTU (15mg, 0.038mmol) and TEA (16mg, 0.153mmol), in a total of 7 mL of NMP-HMP (1:1), the reaction period being extended to 4h. After routine work-up, the co-conjugate was isolated in a total yield of 80mg (53%). η_{inh}, 16.01 mL g^{-1}.

^{1}H NMR (D_2O), δ/ppm: 8.5-6.5, 4.83H (Expected: 5H; hetero- and aromatic CH of FA); 3.5-3.0, 23H (Expected: 22H, CONH*CH_2*); 1.8-1.6, 20H (expected: 20H; CH_2*CH_2*CH_2). ^{1}H NMR data indicated the compound to contain (FA+MTX) at the level of 97%; see Table 4.35 row 2.

UV spectroscopy determination of MTX
As methotrexate and folic acid show identical ^{1}H NMR spectra, especially in the aromatic region, it was impossible to determine the exact content of drug (MTX) in the final compound by ^{1}H NMR spectroscopy. Therefore, UV spectroscopy was used to assess MTX content using the molar extinction coefficient value, ε = 6500 mol^{-1}cm^{-1} and the absorbance at λ = 370 nm. To this end, solutions of same concentration of both homo- and co-conjugate were prepared and absorbance at λ = 370 nm of the co-conjugate solution (reference, homoconjugate solution) read. The co-conjugate was found to contain 8% MTX by mass.

Assuming that no cleavage of folate occurred during the second step, 39% MTX incorporation, obtained by subtracting 58% FA from the count of 97%

(FA+MTX) established by NMR spectroscopy, was determined; this corresponded to 7.45% by mass. Found: FA, 11.05% (UV), 11.58% (NMR); MTX, 8% (UV), 7.45% (NMR).

Conjugate 3 (90:10)-FA/MTX

This co-conjugate was prepared similarly to the preceding except that carrier **3** replaced **1**. Thus, from carrier 3 (600mg, 0.3mmol), FA (93mg, 0.21mmol), HBTU (68mg, 0.18mmol), and TEA (61mg, 0.6mmol), it was obtained 580mg (87%) of water-soluble homoconjugate **3**(90:10)**-FA** (H). η_{inh}, 13.25 mL g^{-1}.

^{1}H NMR (D_2O), δ/ppm: 8.5-6.5, 2.16H (Expected: 5H; aromatic and heteroaromatic *CH* of FA); 1.8-1.6, 18H (expected: 18H; $CH_2\mathit{CH_2}CH_2$). These data indicate 43% FA incorporation. Found: FA, 8.2% (UV), 8.7% (NMR).

The reaction of **3**(90:10)**-FA** (H) (200mg, 0.1mmol) with MTX (32mg, 0.07mmol), HBTU (23mg, 0.06mmol), and TEA (20mg, 0.2mmol) afforded 105mg (47%) of yellow co-conjugate, showing 74% (FA+MTX) incorporation.

^{1}H NMR (D_2O), δ/ppm: 8.5-6.5, 3.75H (Expected: 5H; hetero- and aromatic CH of FA); 1.8-1.6, 18H (expected: 18H; $CH_2\mathit{CH_2}CH_2$).

The retreatment of this co-conjugate (100mg, ~0.05mmol) with MTX (18mg, 0.04mmol), HBTU (10mg, 0.025mmol), and TEA (10mg, 0.1mmol), gave after conventional work-up **3**(90:10)**-FA/MTX** as yellow, water-soluble solid, in an overall of 65mg (65%). η_{inh}, 14.5 mL g^{-1}.

^{1}H NMR (D_2O), δ/ppm: 8.5-6.5, 4.8H (Expected: 5H; aromatic and heteroaromatic *CH* of FA); 3.5-3.0, 22H (Expected: 22H, CONH$\mathit{CH_2}$); 1.8-1.6, 18H (expected: 18H; $CH_2\mathit{CH_2}CH_2$). These data indicate 96% (FA+MTX) incorporation. Found: MTX, 10.58% (UV), 10% (NMR); see Table 4.35 row 3. The % MTX (by NMR) in this co-conjugate was determined in the same fashion as for the preceding co-conjugate.

Conjugate 1 (90:10)-FA/Fc

Step (1): The reaction of carrier **1** (400mg, 0.204mmol) with FA (63mg, 0.143mmol), HBTU (46mg, 0.122mmol), and TEA (41mg, 0.408mmol), after worked-up in conventional fashion, gave a yellow, fully water-soluble, homoconjugate **1**(90:10)**-FA** (H) in a yield of 280mg (63%). η_{inh}, 16.75 mL g^{-1}.

^{1}H NMR (D_2O), δ/ppm: 8.5-6.5, 2.54H (Expected: 5H; aromatic and heteroaromatic *CH* of FA); 1.8-1.6, 20H (expected: 20H; $CH_2CH_2CH_2$). FA incorporation: 58%. Found: FA, 11.25% (UV), 11.58% (NMR).

Step (2): The target co-conjugate was obtained by reacting the homoconjugate with the ferrocene active ester. Thus, homoconjugate (200mg, 0.102mmol) treated with Fc-ONp (28mg, 0.072mmol), and EA (4mg, 0.072mmol), afforded **1**(90:10)**-FA/Fc** as fluffy, tan, water-soluble compound, in a yield of 150mg (70%), possessing the following characteristics: η_{inh}, 18 mL g^{-1}.

^{1}H NMR (D_2O), δ/ppm: 8.5-6.5, 2.57H (Expected: 5H; aromatic and heteroaromatic *CH* of FA); 4.3-4.25, 4.4 (Expected: 9H, *CH* of ferrocenyl); 3.5-3.0, 21.7H (Expected: 22H, CONHCH_2); 1.8-1.6, 21H (expected: 21H; $CH_2CH_2CH_2$), showing 51% FA and 49% Fc incorporation, corresponding to 100% NH_2 acylation.
Found: 9.55% (UV), FA, 9.8% (NMR); Fe, 1.25% (OES), 1.2% (NMR); Table 4.35 row 4.

Conjugate 3 (90:10)-FA/Fc

This co-conjugate was prepared similarly to the preceding without major change except that carrier **3** replaced **1**.
The first step afforded 200mg (60%) of water-soluble homoconjugate, η_{inh}, 14.05 mL g^{-1}, resulting from the reaction of carrier **3** (300mg, 0.150mmol) with FA (46mg, 0.105mmol), HBTU (34mg, 0.09mmol), TEA (30mg, 0.3mmol).

^{1}H NMR (D_2O), δ/ppm: 8.5-6.5, 2.3H (Expected: 5H; hetero- and aromatic CH of FA); 1.8-1.6, 18H (expected: 18H; CH_2*CH_2*CH_2). FA incorporation: 46%.
Found: FA, 8.95% (UV), 9.3% (NMR).

In the second step, the preceding homoconjugate (130mg, 0.065mmol), treated with Fc-ONp (20mg, 0.052mmol), and EA (3mg~5μL, 0.052mmol), in a total of 2 mL of DMSO, afforded the target co-conjugate **3**(90:10)**-FA/Fc** as water-soluble material in a yield of 80 m (58%). η_{inh}, 15.5 mLg^{-1}.

^{1}H NMR (D_2O), δ/ppm: 8.5-6.5, 2.28H (Expected: 5H; aromatic and heteroaromatic *CH* of FA); 4.3-4.25, 4.8 (Expected: 9H, *CH* of ferrocenyl); 3.5-3.0, 21.5H (Expected: 22H, CONH*CH_2*); 1.8-1.6, 19H (expected: 19H; CH_2*CH_2*CH_2), showing 45% FA and 53% Fc incorporation, corresponding to 98% NH_2 acylation.
Found: FA, 8.75% (UV), 9% (NMR); Fe, 1.12% (OES), 1.28% (NMR); refer to Table 4.35 row 5.

Conjugate 1 (90:10)-MTX/Fc
This conjugate was obtained by the two-step procedure leading the preparation of **1**(90:10)**-FA/Fc**. However, a major modification was introduced in the *step (1)* where FA was replaced by MTX.
Step (1): Carrier **1** (400mg, 0.204mmol) was reacted with MTX (65mg, 0.143mmol), HBTU (46mg, 0.122mmol), and TEA (41mg, 0.408mmol), in total volume of 10 mL, for 2h. The homoconjugate **1**(90:10)**-MTX** (H) worked-up in conventional fashion was found to be yellow, fully water-soluble, and in a yield of 290mg (65%). η_{inh}, 16.5 mLg^{-1}.

^{1}H NMR (D_2O), δ/ppm: 8.5-6.5, 2.4H (Expected: 5H; hetero- and aromatic CH of MTX); 1.8-1.6, 20H (expected: 20H; CH_2*CH_2*CH_2). These data indicate 48% MTX incorporation. Found: MTX, 9.25% (UV), 10% (NMR).

Step (2): The homoconjugate (200mg, 0.102mmol) and Fc-ONp (32mg, 0.082mmol) were dissolved in 2 mL of DMSO, and stirred at room temperature for 5h. EA (5mg, 0.082mmol) was added and stirring was continued at room temperature for another 3h. The routine work-up comprising precipitation, isolation upon centrifugation, purification by both size exclusion chromatography and aqueous dialysis, and freeze-drying afforded 150mg (70%) of tan-colored, fluffy, water-soluble solid **1-**(90:10)-**MTX/Fc**. η_{inh}, 17.05 mL g^{-1}.

^{1}H NMR (D_2O), δ/ppm: 8.5-6.5, 2.21H (Expected: 5H; aromatic and heteroaromatic *CH* of MTX); 4.3-4.25, 4.95 (Expected: 9H, *CH* of ferrocenyl); 3.5-3.0, 23H (Expected: 22H, CONH*CH_2*); 1.8-1.6, 20.6H (expected: 21H; CH_2*CH_2*CH_2). These data indicate 44% MTX and 55% Fc incorporation, corresponding to 99% NH_2 acylation. Found: MTX, 8.37% (UV), 8.7% (NMR); Fe, 1.24% (OES), 1.34% (NMR). Refer to Table 4.35 row 6.

Conjugate 3 (90:10)-MTX/Fc

In a fashion similar to that leading to **1**(90:10)-**MTX/Fc**, the target conjugate was synthesized in two steps.

In the first step, carrier **3** (400mg, 0.2mmol) treated with MTX (64mg, 0.14mmol), HBTU (46mg, 0.12mmol), and TEA (41mg, 0.4mmol), in a total volume of 10 mL, afforded 250mg (56%) of yellow, fully water-soluble, homoconjugate **3**(90:10)-**MTX** (H). η_{inh}, 14.25 mL g^{-1}.

^{1}H NMR (D_2O), δ/ppm: 8.5-6.5, 2.15H (Expected: 5H; hetero- and aromatic CH of MTX); 1.8-1.6, 18H (expected: 18H; CH_2*CH_2*CH_2) showing 43%NH_2 acylation. Found: MTX, 8.02% (UV), 8.96% (NMR).

In the second step, the homoconjugate (200mg, 0.1mmol) and Fc-ONp (31mg, 0.08mmol) were dissolved in 2 mL of DMSO, and stirred at room temperature for 10h. EA (5mg, 0.082mmol) was added and stirring continued at room temperature for another 3h. The routine work-up afforded 125mg (70%) of tan-colored, fluffy, water-soluble solid **3**(90:10)-**MTX/Fc**. η_{inh}, 15.3 mL g^{-1}.

^{1}H NMR (D_2O), δ/ppm: 8.5-6.5, 2.1H (Expected: 5H; hetero- and aromatic CH of MTX); 4.3-4.25, 5.1 (Expected: 9H, *CH* of ferrocenyl); 3.5-3.0, 23H (Expected: 22H, CONH*CH_2*); 1.8-1.6, 19H (expected: 19H; CH_2*CH_2*CH_2). These data indicate 42% MTX and 56% Fc incorporation, corresponding to 98% NH_2 acylation. Found: MTX, 8.23% (UV), 8.66% (NMR); Fe, 1.28% (OES), 1.35% (NMR). See Table 4.35 row 7.

CHAPTER 6

CONCLUSION AND PERSPECTIVE

The clinical usefulness of antitumor medicinal drugs has been severely limited by several factors such as poor water solubility, charge or polarity (which prevents cell entry by passive diffusion), lack of cell specificity, systemic toxicity, and a tendency to induce drug resistance. Among various strategies, the bioreversible binding of a medicinal drug to water-soluble and biocompatible carrier polymers represents an advanced technology that is designed to circumvent the critical pharmacological obstacles which the drug must clear for efficacious biological action. The polymer-drug conjugate resulting from the carrier-drug anchoring step acts as a prodrug which protects the active drug while in circulation and delivers it in free form at the target site. Carrier conjugation thus serves to enhance the drug's therapeutic effectiveness.

Two primary objectives motivated this research project. Firstly, the synthesis of water-soluble conjugates by bioreversible conjugation of the two selected anticancer drug models, methotrexate and the organoiron compound ferrocene, with water-soluble macromolecules. Secondly, evaluation of the antiproliferative activities of the synthesized conjugates and their comparison with those of the free drugs.

In order to fulfil these objectives, two macromolecular carrier types with suitable functionality for drug binding were synthesized. The first type comprised polyaspartamides, which were obtained in 52-74% yield by an aminolytic ring-opening process in polysuccinimide, and were characterized by inherent viscosities in the range of 10-20 mL g^{-1}. The weight-average molecular weight of these polymers (determined by gel permeation chromatography) was, for the most part, in the 20 000 - 30 000 range. This was sufficiently low to suppress inherent

polymer toxicity but high enough to retard renal clearance, and it showed no correlation with increasing viscosity.

The second type of carriers used for drug anchoring was based on poly(amidoamine) structures. These carriers obtained in yields of 15-23%, and possessing inherent viscosities in the 14-24 mL g^{-1}, were prepared in a two step-process. The first step comprised the Michael addition of mono-N-Boc-protected amine nucleophiles to bisacrylamide under careful control of experimental conditions, and the second step involved deprotection of the amino side group terminals so generated with trifluoroacetic acid to afford the appropriate functionality for drug binding.

Anchoring of methotrexate (MTX) to the primary amine-functionalized polymer of both types was brought about through formation of a biofissionable amide bond in a one-step coupling process. The resulting conjugates were purified by a combination of size exclusion chromatography and aqueous dialysis, and were isolated in the solid state in yields of 41-80%. In most cases a high extent of conjugation (95-100%) was reached, and the drug incorporation was 15-40% by mass. The weight-average molecular weight (25 000 – 86 000) of the conjugates increased as the inherent viscosity (12-25 mL g^{-1}) increased.

The water-soluble polymer-bound MTX conjugates were submitted for a preliminary biological activity assessment against various human cell lines, namely the human adenocarcinoma of the cervix (HeLa), the colorectal adenocarcinoma, (Colo 320 DM), and the human leukemic lymphoblast (CEM/S) and its resistant sub-line (CEM/E).

Overall, the *in vitro* tests revealed very promising cell growth-inhibitory activity, and the following conclusions were drawn:

(i) The polyaspartamide-MTX conjugates showed higher antiproliferative activity than free MTX against CEM/S and CEM/E cell lines. No distinct evidence of a structure-performance relationship was established.

(ii) There was a structure-performance relationship against HeLa and Colo cells lines. Thus, the *tert*-amine side chain terminals conjugates, irrespective of the carrier-type, were more effective than the free drug, while hydroxyl- or methoxy side chain terminals conjugates were found to be ineffective. The difference in cytotoxic performance suggested that the adsorptive pinocytotic mechanism of intracellular uptake, expected to occur with *tert*-amine functionalized conjugates, was more pronounced than the fluid-phase endocytosis by which other conjugates enter the intracellular compartment.

(iii) The *tert*-amine side chain terminals conjugates showed higher antiproliferative activities against the resistant cell line (Colo) than the sensitive one (HeLa).

(iv) The *tert*-amine side chain terminals conjugates of polyaspartamide-type showed higher cell growth-inhibitory activity than their counterparts of poly(amidoamine)-type.

(v) The poly(amidoamine)-MTX conjugates containing intrachain PEO segments, whether short or long, were found to be less effective than the free drug.

The results of this project showed the binding of methotrexate to the two water-soluble macromolecular carrier types to be a promising approach to enhance its *in vitro* cancer cell-killing efficacy. However, prior to *in vivo* testing, an effort will have to be made to firmly establish structure-cytotoxic performance relationships.

The investigation of the metal-containing drug model of the ferrocene type was narrowly focused on establishing the polymer-binding efficiency of two coupling methods. The primary amino group on selected carriers of both types was chosen as the cooperating functional group for reaction with the ferrocene-attached carboxylic acid group that allowed anchoring *via* the biofissionable amide bond.

Conjugations, achieved by either HBTU-mediated or ONp active ester processes, reached 98-100% extent of acylation and were therefore equivalent in efficiency.
The results of this study also showed the possibility of using not only the aprotic dimethylformamide, but also the protic methanol as a reaction medium in the conjugation of ferrocene, *via* 4-ferrocenylbutanoic acid, to poly(amidoamine)-type carriers.

Let us now conclude on the co-conjugation. Drug co-conjugation is a route for the simultaneous delivery of two or more anticancer compounds. The expected benefits are synergistic effects, which can potentially lead to reduction in doses and side effects caused by high dose of single drug, and the prevention of the development of multi-drug resistance.
Multidrug-binding ability of polyaspartamide-type carriers was demonstrated by the co-conjugation of methotrexate and ferrocene with selected carriers. Folic acid, a cell entry facilitator, was co-conjugated with methotrexate or ferrocene in a two-step process involving HBTU and active ester coupling methods. The resulting water-soluble folate-drug co-conjugates, obtained in yields of 53-75%., and characterized by inherent viscosities in the range of 16-20 mL g^{-1}, were screened against HeLa and Colo cell lines for antiproliferative activities.
The following preliminary conclusions were drawn from the *in vitro* tests.

(i) On the basis of the IC_{50} values, the presence of folate reduced the cytotoxicity of polymer-drug conjugate. This was more pronounced with folate-ferrocene co-conjugates than with folate-methotrexate co-conjugates.

(ii) The cytotoxicity decreases as the percentage of incorporated folate increases.

Future research should be focused on investigating a considerably larger number of folate-drug co-conjugates in order to draw realistic conclusions regarding the impact of folic acid incorporation on the cytotoxic performance of polymer-bound

methotrexate or ferrocene. Cytotoxicity of ferrocene-methotrexate co-conjugates should be investigated in order to evaluate the advantages associated with the co-conjugation of these two drug models. This would open up the possibility of extending the multidrug co-conjugation approach to other anticancer compounds.

REFERENCES

1. Sitas, F.; Canc. S. Africa, 1992 (1997).

2. Ligtenberg, M.; Hergervorst, F.; Van't Veer, L; et al. *J. Cancer* **79** (1999) 1475-1478.

3. Easton, D.F.; Bishop, D.T.; Ford, D.; Crocford, B.P; *Am. J. Hum. Genet*. **52** (1993) 678-701.

4. Friedman, L.S.; Ostermeyer, E.A.; Szabo, C.I.; Dowd, P.; Lynch, E.D.; Rowell, S.E.; King, M.C.; *Nat. Genet*. **8** (1994) 399-404.

5. Lenhard, R. E.; Osteen, R. T.; Gansler, T.; eds. *Clinical Oncology*. Atlanta, GA: American Cancer Society, 2001.

6. Pazdur, R.; Coia, L. R.; Hoskins, W. J.; Wagman, L. D.; eds. *Cancer Management*: A Multidisciplinary Approach, Medical Surgical and Radiation Oncology. Huntington: NY, PRR, 1996.

7. Eyre, H. J.; Lange, D.; Morris, L. B.; in *Informed Decisions*. 2nd Ed. Atlanta, GA: American Cancer Society, 1996.

8. Chabner, B.; in *Pharmacologic Principles of Cancer Treatment*, W.B. Saunders Co., Philadelphia, 1982.

9. Chabner, B.A.; Long, D.L.; in *Cancer Chemotherapy and Biotherapy*, 2nd Edn. , Eds., Lippincott-Raven Publ., Philadelphia, 1996.

10. Foye, W.D.; in *Cancer Chemotherapeutic Agents*, Ed., Am. Chem. Soc., Washington, DC, 1995.

11. Lowenthal, R.M.; Eaton, K.; *Oncol. Clin. North Am.* **10** (1996) 967-990.

12. Kartner, N.; Ling, V.; *Sci. Am.* **260** (1989) 26.

13. Arcamone, F.; Animati, F.; Capranico, G.; Lombardi, P.; Praseti, G.; Manzini, S.; *et. al. Pharmacol. Therapeutics* **76** (1997) 117-124.

14. Aubel-Sadron, G.; Londos-Gagliardi, D.; *Biochemie **66*** (1984) 333-352.

15. Arcamone, F.; in *Doxorubicin Anticancer Antibiotics*; Academic Press: NY, (1981) Chp. II.

16. Minko, T.; Kopečkova, P.; Pozharov, V.; Kopeček, J.; *J. Control. Release* **54** (1998) 223-233.

17. Embleton, M. J.; and Garnett, M.C.; in *Monoclonal antibodies for cancer detection and therapy* (R. W. Baldwin, and V. S. Byers, Eds.), Academic Press, London, 1985, pp 317-344,

18. Karber, S.; Diamond, L. K.; Mercer, R. D.; Sylvester, R. F.; Woly, J. A.; *N. Engl. J. Med.* **238** (1940) 787.

19. Ward, J. R.; *J. Rheumatol*. **12** (1985) 3-6.

20. Kremer, J. M.; *J. Rheumatol*. **44** (1996) 34-37.

21. Moss, R. B.; *Chest* **107** (1995) 817-825.

22. Feagan, B. G.; Rochon, J.; Fedorak, R. N.; Irvine, E. J.; Wild, G.; Sutherland, L.; *et. al. N. Engl. J. Med.* **332** (1995) 292-297.

23. Leeman, L. M.; Wendland, C. L.; *Arch. Fam. Med*. **9** (2000) 72-77.

24. Marin, M. G.; *Chest* **112** (1997) 29-33.

25. Lichtman, S. M.; Brody, J.; Kaplin, M. H.; Susin, M.; Kodro, P.; Goh, J. C.; *Leuk. Lymphoma* **9** (1993) 393.

26. Walsh, C.; Wernz, J. C.; Levine, A.; Rarick, M.; Wilson, E.; *et. al. J. Acquir. Immune Defic. Syndr.* **6** (1993) 265.

27. Panozzo, J.; Panozzo, J.; Akan, E.; Libertin, C.; Woloschak, G. E.; *Leukemia Research*, **20** (1996) 309-317.

28. Stolink, S.; Illum, L.; Davis, S.S.; *Adv. Drug. Deliv. Rev.* **16** (1995) 195-214.

29. Maeda, H.; Seymour, L. M.; Miyamoto, Y.; *Bioconjug. Chem*. **3** (1992) 351-362.

30. Duncan, R.; Seymour, L.C.W.; Scarlett, L.; Lloyd, J.B.; Rejmanova, P.; Kopececk, J.; *Biochem. Biophys. Acta* **880** (1986) 62-71.

31. Mathews, D. A.; Alden, R. A.; Bolin, J. T.; Freer, S. T.; *et. al. Science* **197** (1977) 452.

32. Jolly, L. E.; Fletcher, H. P.; *Toxicol. Appl. Pharmacol*. **39** (1977) 23-32.

33. Bertino, J. R.; Ed. *Ann. N.Y. Acad. Sci*. **186** (1971).

34. Bertino, J. R.; and Johns, D. G.; In: *Cancer Chemotherapy*, Brodsky, I., Ed., Grune & Straton, New York, N.Y., **2** (1971) 9-22.

35. Newell, D. R.; *Semin. Oncol*. **26** (1999) 74.

36. Jodrell, D. I.; Newell, D. R.; Gibson, W.; Hughes, L. R.; Calvert, A. H.; *Cancer Chemother. Pharmacol*. **28** (1991) 331.

37. Marshall, J. L.; DeLap, R. J.; *Clin. Pharmacokinet*. **26** (1994) 190.

38. Reynolds, J. E. F.; Parfitt, K.; Parsons, A. V.; Sweetman, S. C.; *The royal Pharmaceutical Society* **19** (1996) 1361-1362.

39. Lewisohn, R.; Leuchtenberger, C.; Leuchtenberger, R.; and Keresztezy, J. C.; *Science* **104** (1946) 436.

40. Butterworth C. E. Jr.; *Ann NY Acad Sci*; **669** (1992) 293-299.

41. Kulier, R.; De Onis, M.; Gulmezoglu, A. M.; Viallr, J.; *Gynaecol. Obstet*. **63** (1998) 231-246.

42. WHO Technical Report Series, **452**, Geneva, 1970.

43. Anderson, R. G. W.; Kamen, B. A.; Rothberg, K. G.; *Science* **255** (1992) 410-411.

44. Ross, J. F.; Chaudhuri, P. K.; Ratnam, M.; *Cancer* **73** (1994) 2432-2443.

45. Köpf-Maier, P.; *Eur. J. Clin. Pharmacol*. **47** (1994) 1.

46. Wilkinson, G.; Rosenblum, M.; Whiting, M. C.; Woodward, R. B.; *J. Am. Chem. Soc.* **74** (1952) 2123-2124.

47. Köpf-Maier, P.; Köpf, H.; *Struct. Bonding* **70** (1998) 103.

48. Neuse, E. W.; Kanzawa, F.; *Appl. Organomet. Chem*. **4** (1990) 19.

49. Neuse, E. W.; Mbonyana, C. W. N.; In: Inorganic and *Metal-Containing Polymeric Materials*, Sheats, J., et al. Eds., Plenum Press, New York, 1990, p.139.

50. Kovjazin, R.; Eldar, T.; Patya, M.; Vanichkin, A.; Lander, H. M.; Nogogrodsky, A.; *FASEB J*. **17** (2003) 467-469.

51. Tappero, J. W.; Conant, M., A.; Wolfe, S. F.; Berger, T. G.; *Am. Acad. Dermatatol.* **28** (1993) 371.

52. Ravindranth, M. H.; Morton, D. L.; In: Bast, R. C.; Kufe, D. W.; Pollock, R. E.; Weichselbaum, R. R.; Holland, J. F.; Frei, E.; eds. *Cancer Medicine*. 5th ed. Baltimore, MD: Williams and Wilkins; (2000) 800-814.

53. Skladanowski, A.; and Konopa, J.; *Br. J. Cancer* **82** (2000) 1300.

54. Sandmaaier, J. M.; Oparin, D. V.; Holmberg, L. A.; Reddish, M. A.; MacLean, G. D.; Longenecker, B. M.; *J. Immunother*. **22** (1999) 54-66.

55. Hsueh, E. C.; Nathanson, L.; Foshag, L. J.; *et. al. Cancer* **85** (1999) 2160-2169.

56. Hadden, J. W.; *Int. J. immunopharmacol*. **21** (1999) 79-101.

57. Scappaticci, F. A.; *J. Clin. Oncol*. **20** (2002) 3906-3927.

58. Smith, A.E.; *Annu. Rev. Microbiol*. **49** (1995) 807-838.

59. Ahn, C.-H.; Chae, S.Y.; Bae, Y.H.; Kim, S.W.; *J. Controlled Release* **80** (2002) 273-282

60. Reschel, T.; Koňák, Č.; Oupicky, D.; Seymour, L.W.; Ulbrich, K.; *J. Controlled Release* **81** (2002) 201-217.

61. Dumitriu, S.; and Dumitriu, M.; in *Polymeric Biomaterials* (S. Dumitriu, Ed.) marcel Dekker, New york, 1994.

62. Dunn, L.; and Ottenbrite, R. M.; Eds, in *Polymeric drug and Drug Delivery Systems*, ACS Symp.; Ser. 469; 1991.

63. Takura, Y.; and Hashida, M.; *Crit. Rev. Oncol. Hematol*. **18** (1995) 207-231.

64. Pietersz, G. A.; *Bioconjugate Chem*. **1** (1990) 89-95.

65. Ouchi, T.; and Ohya, Y.; *Prog. Polym. Sci*. **20** (1995) 211-257.

66. Gabison, A.; In: Roerdink, F.H.D.; and Kroon, A.M.; Eds., *Drug carrier systems*, John Wiley, New York, **9** (1989) 185-212.

67. Brannonpeppas, L.; *Int. J. Pharm*. **116** (1995)1-9.

68. Kerr, D.J.; and kaye, S.B.; *CRC Crit. Rev. Ther. Drug Carrier Sys.* **8** (1991) 19-39.

69. Yang, M.B.; Tamargo, R.J.; and Brem, H.; *Cancer Res***. 49** (1989) 5103-5107.

70. Springer, C. J.; Bagshawe, K. D.; Sharma, S.K.; Searle, F.; Sherwood, R. F.; and Melton, R. G.; *Eur. J. Cancer* **27** (1991) 1361-1366.

71. Duncan, R.; and Kopeček, J.; *Adv. Polym. Sci.* **57** (1984) 53-101.

72. Harris, J. M. J.; in *Macromol. Sci. Rev. Macromol. Chem. Phys*., 1985, Chp. 25, p. 325.

73. Davidson, R. L.; O'Malley, K. A.; and Wheeler, T. B.; *Somatic Cell Genetics* **2** (1976) 271.

74. Abuchowski, A.; Van Es, T.; Plozuk, N. C.; and Davis, F. F.; *J. Biol. Chem.* **252** (1977) 3578.

75. Lee, R. J.; and Low, P. S.; *J. Biol. Chem.* **269** (5) (1994) 3198.

76. Hirano, T.; Klesse, W.; Ringsdorf, H.; *Makromol. Chem*. **180** (1979) 1125.

77. Ohaya, Y.; Nakao, T.; Ouchi, T.; *J. Macromol. Sci. Pure Appl. Chem.* A **29** (1992) 325.

78. Katayose, S.; Kataoka, K.; *J. Pharm. Sci*. **97** (1998) 160.

79. Rejmanová, P.; Kopeček, J.; Duncan, R.; Lloyd, J. B.; *Biomaterials* **6** (1985) 45-48.

80. Kopeček, J.; *Biomaterials* **5** (1984) 19-25.

81. Krinick, N. L.; Říhová, B.; Ulbrich, K.; Strohalm, J.; Kopeček, J.; *Makromol. Chem*. **191** (1990) 839.

82. McCormick, L. A.; Seymour, L. C. W.; Duncan, R.; Kopeček, J.; *J. Bioact. Comp. Polym.* **1** (1986) 4.

83. Ohkawa, K.; Hatano, T.; Tsukada, Y.; Matsuda, M.; *Br. J. Cancer* **67** (1993) 274.

84. Song, Y.; Onishi, H.; Nagai, T.; *Biol. Pharm*. *Bull*. **16** (1993) 48.

85. Noguchi, A.; Takahashi, T.; Yamaguchi, T.; Kitamura, K.; Takakura, Y.; Hashida, M.; Sezaki, H.; *Bioconjuagte Chem*. **3** (1992) 132.

86. Goddard, P.; Petrak, K.; *J. Bioact. Compat. Polym*. **4** (1989) 372.

87. McGuire, J. J.; Russell, C. A.; *Leukemia* **4** (1990) 48.

88. Saiki, I.; Murata, K.; Matsuno, K.; Ogawa, R.; Nishi, N.; Tokura, S.; Azuma, I.; *Jpn J. Cancer Res.* **81** (1990) 660.

89. Seymour, L. W.; *J. Bioact. Compat. Polym*. **6** (1991) 178.

90. Thomas, H.; *Drugs of today* **28** (1992) 311.

91. Ringsdorf, H.; *J. Polym. Sci. Polym. Symp.* **51** (1975) 135-153.

92. Bovarnick, M.; Fieber, S.; Bovarnick, M. R.; and Kozlowski, J.; *Proc. Soc. Exp. Biol. Med.* **83** (1953) 253.

93. Kessler, B. J.; Di Grado, C. G.; Benante, C.; Bovarnick, M.; Sieber, R. H.; and Zambito, A. J.; *ibid*. **88** (1955) 651.

94. Loebl, W. Y.; Ulimann, T. D.; Yaron, A.; Sela, M.; Berger, A.; and Katchalski, E.; *ibid*. **108** (1961) 661.

95. Blout, E. R.; Farber, S.; Fasman, G. D.; Klein, E.; and Narrod, M.; In: *Proceedings of the international Symposium of Polyamino Acids and Proteins* (Stahmann, M. A.), Ed., University of Wisconsin Press, Madison, Wis., 1962, p. 379.

96. Gerola, A.; Antoni, G.; Benvenuti, F.; Cocola, F.; and Neri, P.; In: *Shock: Biochemical, Pharmacological and Clinical Aspects*, Plenum Press, New York, N. Y., 1970, p. 329.

97. Gruber, U. F.; In: *Blood Replacement*, Springer-Verlag, Berlin-Heidelberg-New York, 1969, p. 51.

98. Antoni, G.; Neri, P.; Sclavo, I. S. V. T.; *Biopolymers* **13** (1974) 1721-1729.

99. Giammona, G.; Carlisi, B.; Cavallaro, G.; Pitarresi, G.; and Spampinato, S.; *J. Controlled Release* **29** (1994) 63-72.

100. Filipovic-Grcic, J.; Maysinger, D.; Zorc, B.; *Int. J. Pharm*. **116** (1995) 39-44.

101. Byron, P. R.; Sun, Z.; Katayama, H.; *Pharm. Res*. **11** (1994) 221-225.

102. Lu, Z.-R.; Yu, J.-H.; Zhuo, R.-X.; Wang, X.-L.; Yang, F.-H.; *Chem. J. Chin. Univ.* **19** (1998) 817-821.

103. Caliceti, P.; Quarta, S. M.; Veronese, F. M.; Cavallaro, G.; Pedone; E.,Giammona, G.; *Biochem. Biophys. Acta* **1528** (2001) 177-186.

104. Danusso, F.; Ferruti, P.; *Polymer* **11** (1970) 88-113.

105. Ferruti, P.; Marchisio, M. A.; Barbucci, R.; *Polymer* **26** (1985) 1336-1348.

106. Hill, I. R. C.; Garnett, M. C.; Bignotti, F.; Davis, S. S.; *Biochem. Biophys. Acta* **1427** (1999) 161-174.

107. Ranucci, E.; Spagnoli, G.; Ferruti, P.; Sgouras, D.; Duncan, R.; *J. Biomat. Sci. Polym*. **2** (1991) 313-315.

108. Ferruti, P.; Barbucci, R.; *Adv. Polym. Sci*. **58** (1984) 55-92.

109. Ferruti, P.; Danzo, N.; Oliva, L.; Barbucci, R.; Barone, V.; *J. Chem. Soc.* Dalton Trans.; 1981, pp. 539-542.

109. Caldwell, G.; Neuse, E. W.; *S. Afr. Chem.* **45** (1992) 93.

110. Malgesini, B.; Verpilio, I.; Duncan, R.; Ferruti, P.; *Macromol. Biosci*. **3** (2003) 59-66.

111. Ferruti, P.; Marchisio, M. A.; Duncan, R.; *Macromol. Rapid Commun*. **23** (2002) 332-355.

112. Ferruti, P. et al.; *Macromolecules* **33** (21) (2000) 7793-7800.

113. Giammona, G.; Puglisi, G.; Cavallaro, G.; Spadaro, A.; and Pitarresi, G.; *J. Controlled Release* **33** (1995) 261-271.

114. De Marre, A.; Seymour, L.; and Schacht, E.; *J. Controlled Release* **3** (1994) 189-197.

115. Giammona, G.; Cavallaro, G.; Fontana, G.; Pitarresi, G.; and Carlisi, B.; *J. Controlled Release* **54** (1998) 321-331.

116. Bouhadir, K. H.; Alsberg, E.; Mooney, D. J.; *Biomaterials* **22** (2001) 2625-2633.

117. Etrych, T.; Chytil, P.; Jelínková, M.; Říhová, B.; Ulbrich, K.; *Macromol. Biosci*. **2** (2002) 43-52.

118. Hamann, P. R.; Hinman, L. M.; Beyer, C. F.; Lindh, D.; *et. al*. *Bioconjuagte Chem*. **13** (2002) 40-46.

119. Duncan, R.; Dimithjevic, S.; and Evagorou, E. G.; *STP Pharma Sci.* **6** (1996) 234-263.

120. Maeda, H.; In: *Polymeric Site-Specific Pharmacotherapy* (A. J. Domb, Ed.), John Wiley and Sons Ltd, 1995, pp. 95-116

121. Duncan, R.; In Robinson, J. R.; and Lee, V. H.; (eds.) *Controlled Drug Delivery: Fundamentals and Applications*, 2nd ed., 1987, pp. 581-607.

122. Duncan, R.; Cable, H.C.; Rejmanová, P.; Kopeček, J.; Lloyd, J.B.; *Biochem. Biophys. Acta* **799** (1984) 1.

123. Kulkarni, P. N.; Blair, A. H.; and Ghose, T. I.; *Cancer Res*. **41** (1981) 2700-2706.

124. Upeslacis, J.; Hinman, L.; In: *Annual reports in Medical Chemistry* (N. Saltzman, Ed.), Academic Press, New York, 1988, pp 151-160.

125. Garnett, M. C.; Baldwin, R. W.; *Cancer Res*. **46** (1986) 2407-2412.

126. Bures, I.; Lichy, A.; Bostik, J.; Spundova, M.; *Neoplasma* **37** (1990) 225-231.

127. Chakraborty, P.; Bhaduri, A. N.; Das, P. K.; *Biochem. Biophys. Res. Commun.* **166** (1990) 404-410.

128. Sanzgiri, Y.; Blaton, C. D.; Gallo, J. M.; *Pharm. Res*. **7** (1990) 418-421.

129. Caldwell, G.; Meirim, M. G.; N'Da, D. D.; Neuse, E. W.; submitted for publication.

130. Meirim, M. G.; Neuse, E. W.; N'Da, D. D.; *J. Appl. Polym. Sci.* **82** (2001) 1844-1849.

131. Kono, K.; Liu, M.; Fréchet, J. M. J.; *Bioconjugate Chem*. **10** (1999) 1115-1121.

132. Okamoto, C. T.; *Adv. Drug Del. Rev.* **29** (1998) 215-228.

133. Wang, S.; Luo, J.; Lantrip, D. A.; Waters, D. J.; Low, P. S.; *et. al. Bioconjuagte Chem*. **8** (1997) 673-679.

134. Sudimack, J.; Lee, R. J.; *Adv. Drug Delivery Rev.* **41** (2000) 147-162.

135. Coney, L. R.; Tomasetti, A.; Carayannopoulos, L.; Frasca, V.; Kamen, B. A.; *et. al. Cancer Res.* **51** (1991) 6125-6132.

136. Leamon, C. P.; Parker, M. A.; Vlahov, I. R.; Xu, L.-C.; Reddy, J. A.; Vetzel, M; Douglas, N.; *Bioconjuagte Chem*. **13** (2002)1200-1210.

137. Anderson, K. E., Stevenson, B. R., Rogers, J. A. (1999) *J. Controlled Release* **60**, 189-198.

138. Caliceti, P.; Salmaso, S.; Semenzato, A.; Carofiglio, T.; Fornasier, R.; Fermeglia, M.; *et. al. Bioconjuagte Chem*. **14** (2003) 899-908.

139. Neuse, E. W., *Macromol. Symp.* **172** (2001) 127-138.

140. Neuse, E. W.; Meirim, M. G.; N'Da, D. D.; Caldwell, G.; *J. Inorg. Organometal. Polym.* **9** (1999) 221-230.

141. Jonhson, M. T.; Kreft, E.; N'Da, D. D.; Neuse, E. W.; van Rensburg, C. E. J.; *J. Inorg. Organometal. Polym.* **13** (2003) 225.

142. Ikeda, M.; Okada, S.; Ueno, H.; Okusaka, T.; Tanaka, N.; Kuriyama, H.; Yoshimori, M.; *Hepato-Gastroenterology* **47** (2000) 862-865.

143. Presant, C. A.; Wolf, W.; Walush, V.; Wiseman, C. L.; Weitz, I.; Shani, J.; *J. Clin. Oncol*. **18** (2000) 255-261.

144. Buzdar, A. U.; Hortobagyi, G. N.; *Sem. Oncol*. **26** (1999) 21-27.

145. Von Minckwitz, G.; Costa, S. D.; Eiermann, W.; Blohmer, J. U.; Tulusan, A. H.; Jackish, C.; Kaufmann, M.; *J. Clin. Oncol*. **17** (1999) 1999-2005.

146. Narayani, R.; Rao, P.; *Intern. J. Pharm.* **138** (1996) 121-124.

147. Coessens, V.; Schacht, E.; Domurado, D.; *J. Control. Release* **38** (1996) 141-150.

148. Etrych, T.; Jelínková, M.; Říhová, B.; Ulbrich, K.; *J. Control. Release* **73** (2001) 89-102.

149. Drobník, J.; Kalal, J.; Dabrowska, L.; Praus, R.; Vachova, M.; Elis, J.; *Polym. Sci., Polym. Symp*., **66** (1975) 75.

150. Kricheldorf, H. R.; in: *α-amino acid N-carboxyanhydride and related heterocycles*, Springer-Verlag, 1987, pp. 3-58.

151. Neri, P.; and Antoni, G.; *Macromol. Synt*., **8** (1982) 25.

152. Tomida, M.; Nakato, T.; Matsunami, S.; Kakuchi, T.; *Polymer* **38** (1997) 4733-4736.

153. Machado, M. De L.; Neuse, E. W.; Perlwitz, A. G.; (*Die Angewandte Makromolekulare Chemie* **195** (1992) 35-56.

154. Shen, W.-C.; Ballou, B.; Ryser, H. J.-P.; Hakala, T. R.; *Cancer Res.* **46** (1986) 3912.

155. Vlasak, J.; Rypacek, F.; Drobnik, J.; Saudek, V.; *J. Polym. Sci. Polym. Symp.* **66** (1979) 59-64.

156. Caldwell, G.; Neuse, E. W.; and Stephanou, A.; *J. Appl. Polym. Sci.* **50** (1993) 393.

157. Komane, L. L.; N'Da, D. D., and Neuse, E. W.; submitted for publication.

158. Pandey, G.; Bagul, T. D.; Sahoo, A. K.; *J. Org. Chem*. **63** (1998) 760-768.

159. Ferruti, P., Marchisio, M. A. In: *Biomedical and Dental Applications of Polymers*, Gebelein, C. G., Koblitz, F. F., eds., Plenum Press, New York, 1981, p.39.

160. Jonhson, M. T.; Neuse, E. W.; Kreft, E.; van Rensburg, C. E. J.; *J. Inorg. Organometal. Polym.* **13** (2003) 55.

161. Pytela, J.; Kotva, R. and Rypaček, F.; *J. Bioact. Comp. Polym*. **13** (1998) 199.

162. Hudecz, F.; Clegg, J. A.; Kajár, J.; *et. al. Bioconjugate Chem*. **4** (1993) 25-33.

163. Arnold, L. J.; Dagan, A.; and Kaplan, N. O.; In: *Targeted Drugs*, Goldberg, E.P., Ed., Wiley, New York, 1983, Chp. 5.

164. Bolin, J.; Filman, D. J.; Matthews, D. A.; Hamlin, R. C.; and Kraut, J.; *J. Biol. Chem*. **257** (1982) 13650.

165. Li, Y.; Kwon, G. S.; *Colloids& Surfaces B: Biointerfaces* **16** (1999) 217-226.

166. van Rensburg, C. E. J., van Staaden, A. M., Anderson, R., *Cancer Res*. **53** (1993) 318.

167. Veronese, F. M.; Morpurgo, M.; *Il Farmaco* **54** (1999) 497.

168. Maeda, H.; Wu, J.; Sawa, T.; Matsumura, Y.; Hori, K.; *J. Control. Release* **65** (2000) 271.

169. Styring, M. G. ans Hamiele, A. E.; *Determination of Molecular weight*. Cooper, A. R., Ed., Wiley, New York, 1989, p. 263.

170. Swarts, J. C.; Neuse, E. W.; and Lamprecht, G. J.; *J. Inorg. Organomet. Polym.* **4** (1994) 143.

171. Blom, N. F.; Neuse, E. W.; and Thomas, H. G.; *Transition. Met. Chem.*,**12** (1987) 301.

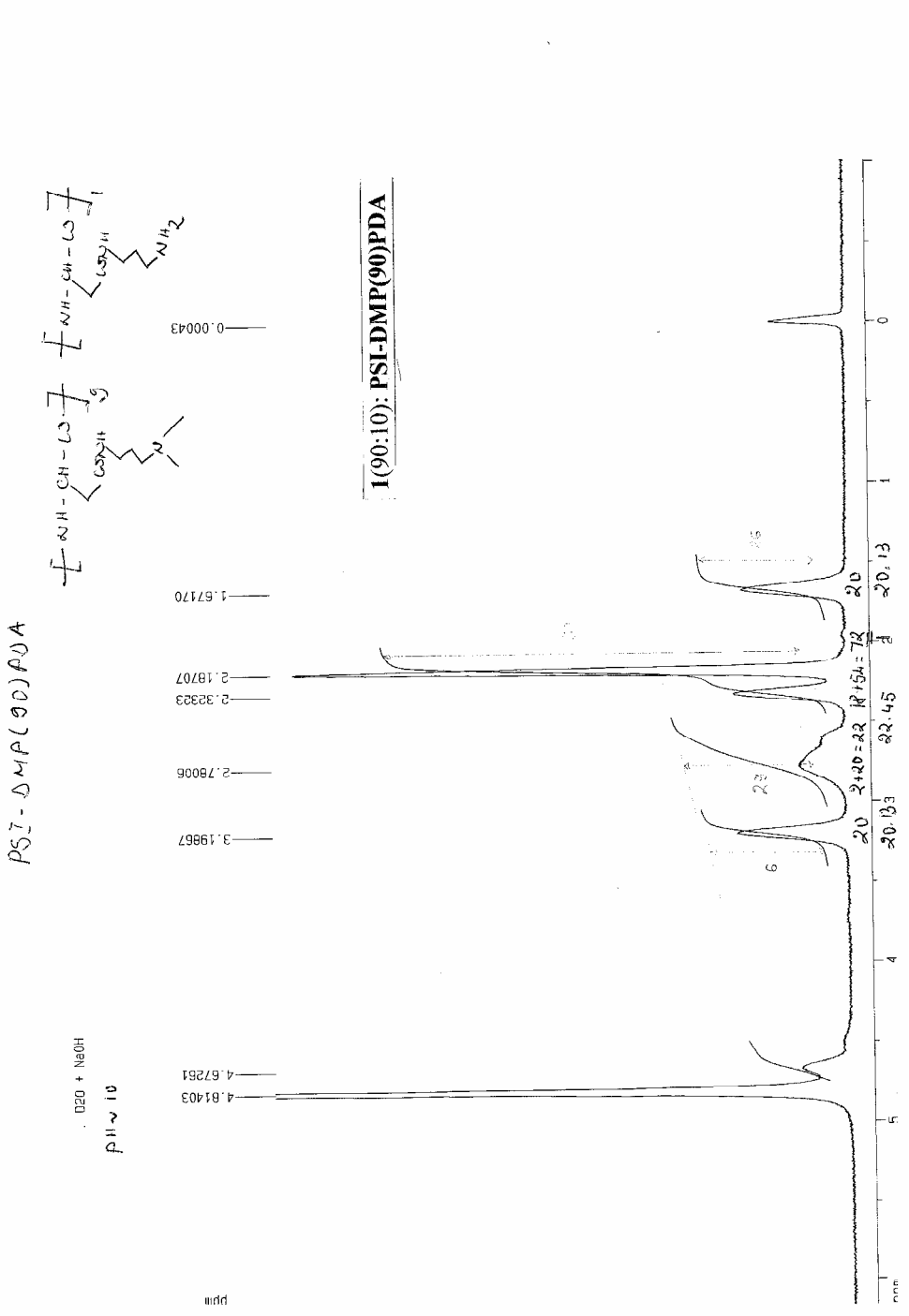
172. Meirim; M. G.; Neuse, E. W.; and Caldwell, G. A.; *J. Inorg. Organomet. Polym.* **7** (1997) 71.

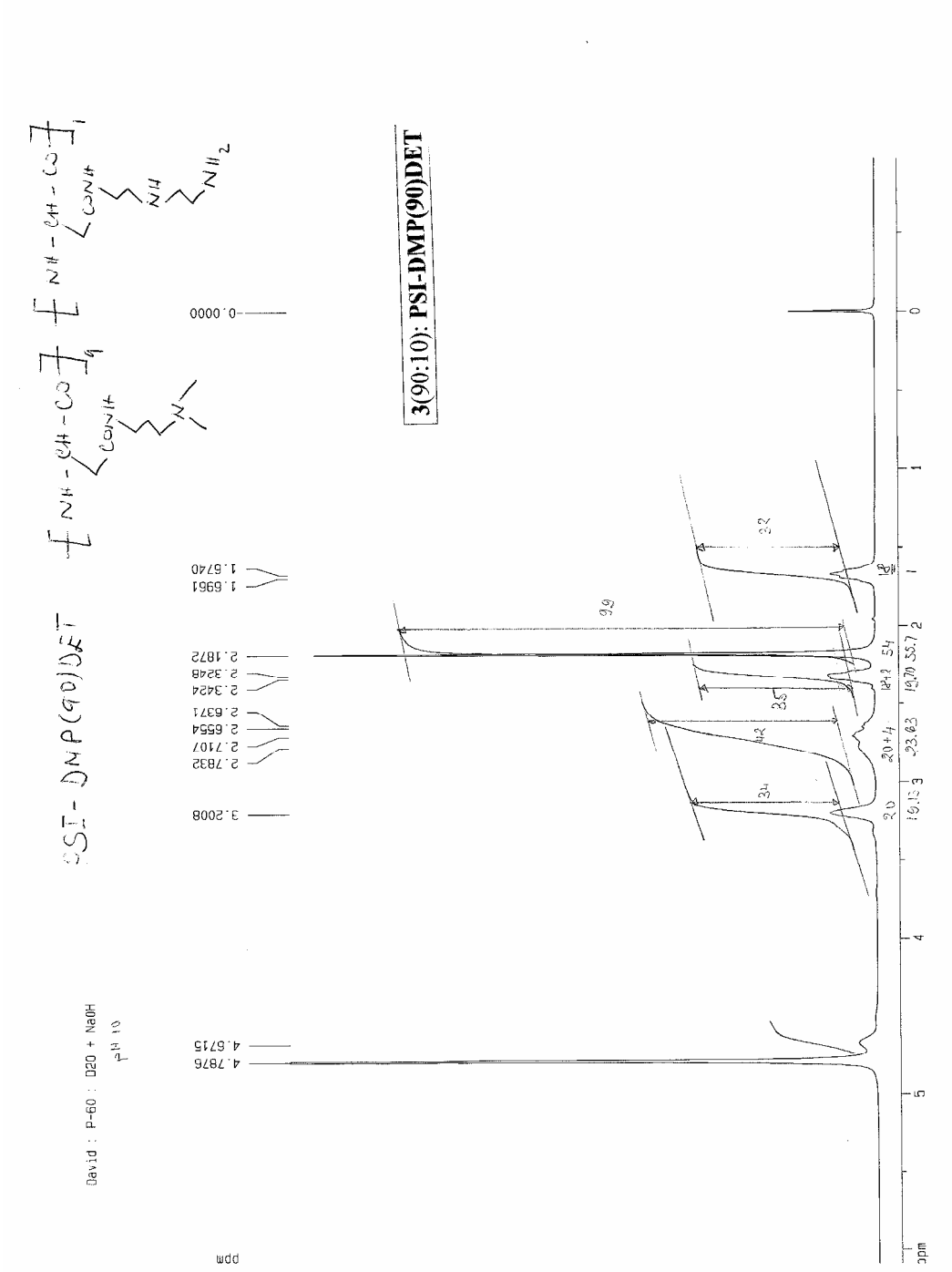
173. Bodansky, M.; and Bodansky, A.; In: *The practice of peptide synthesis*, 2nd rev. ed. p.cm. Springer-Verlag Berlin Heidelberg, 1994, p. 97.

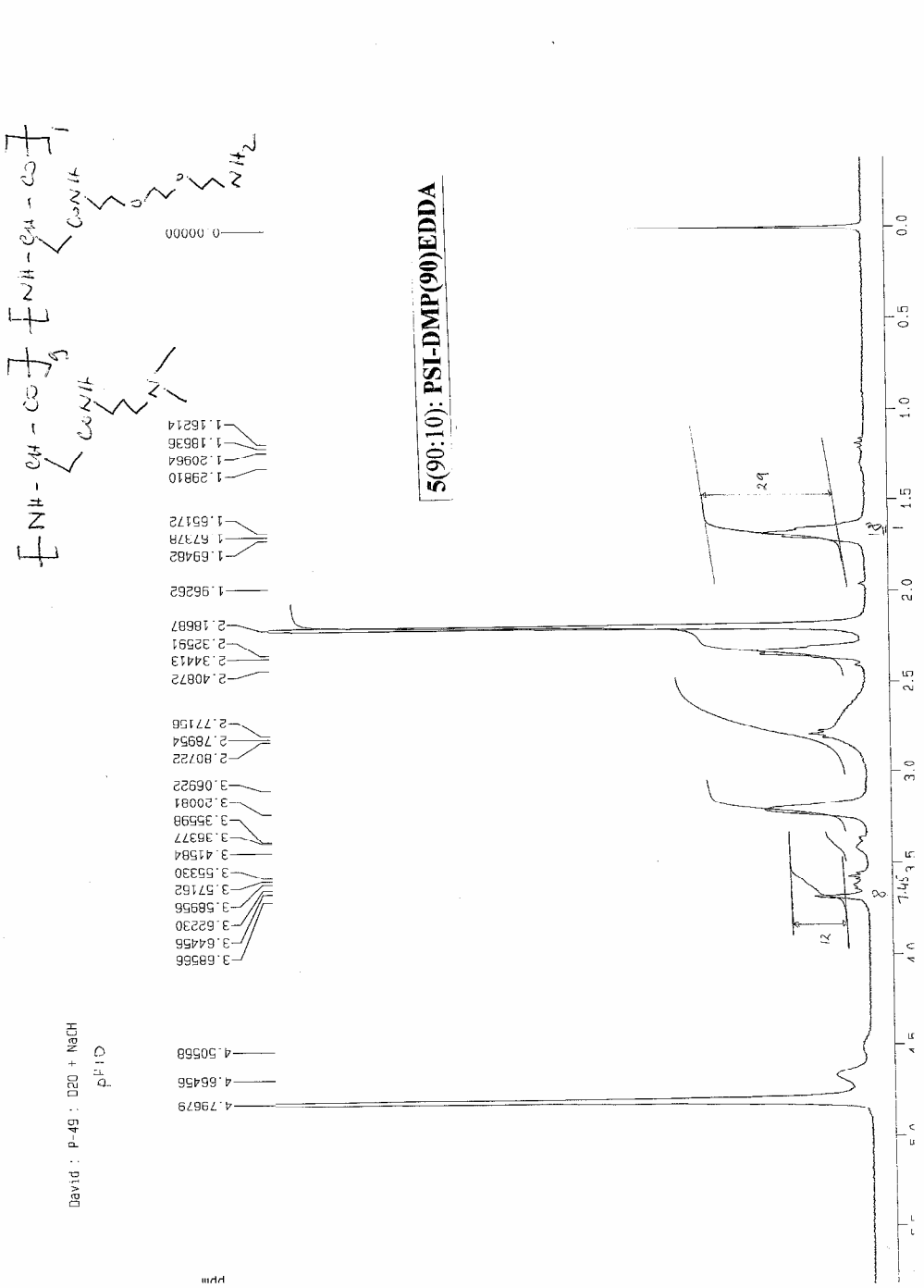
174. Hazra, A.; Tripathi, S. K.; *Indian J. Pharma.* **33** (2001) 322-342.

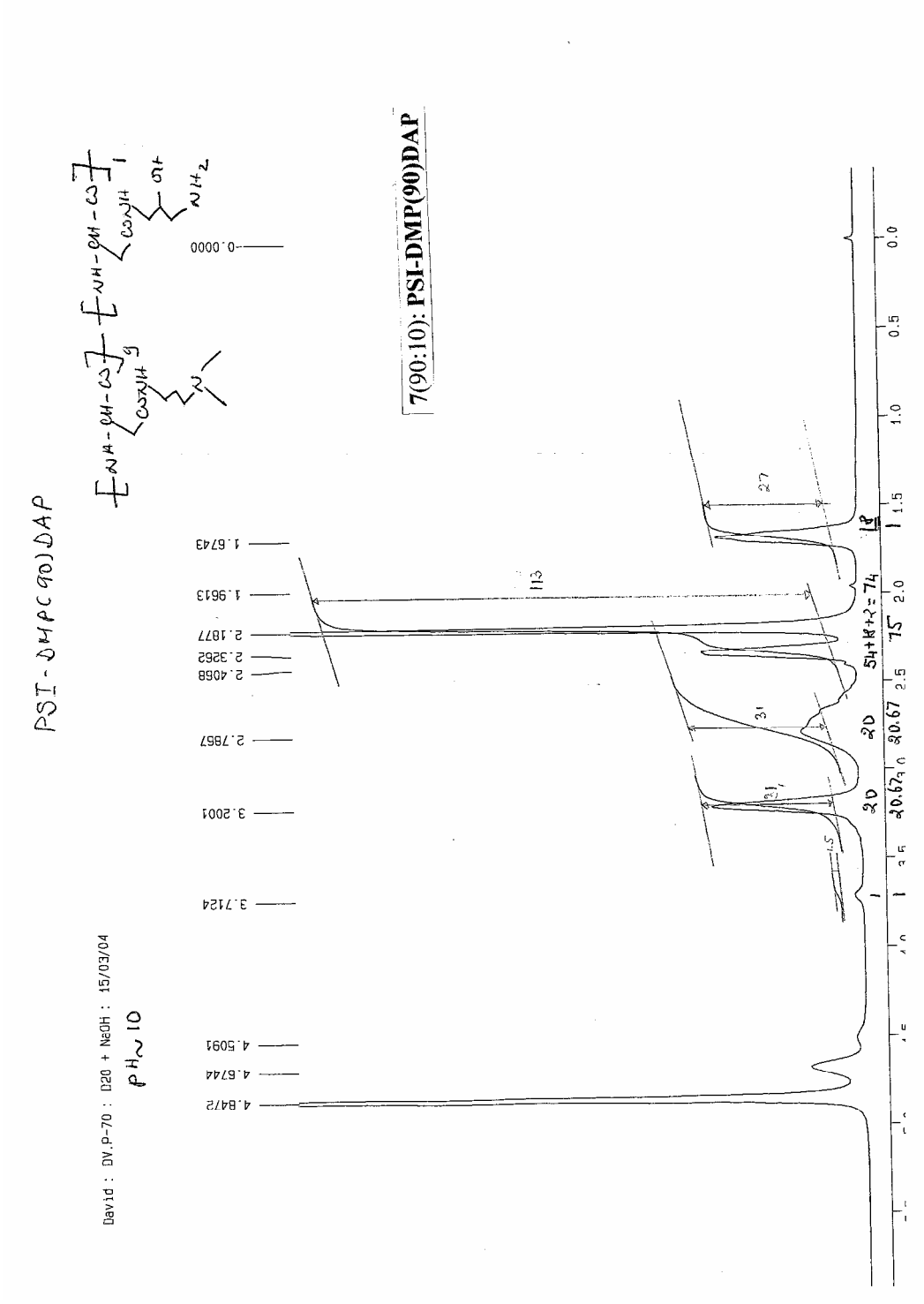
APPENDIX:

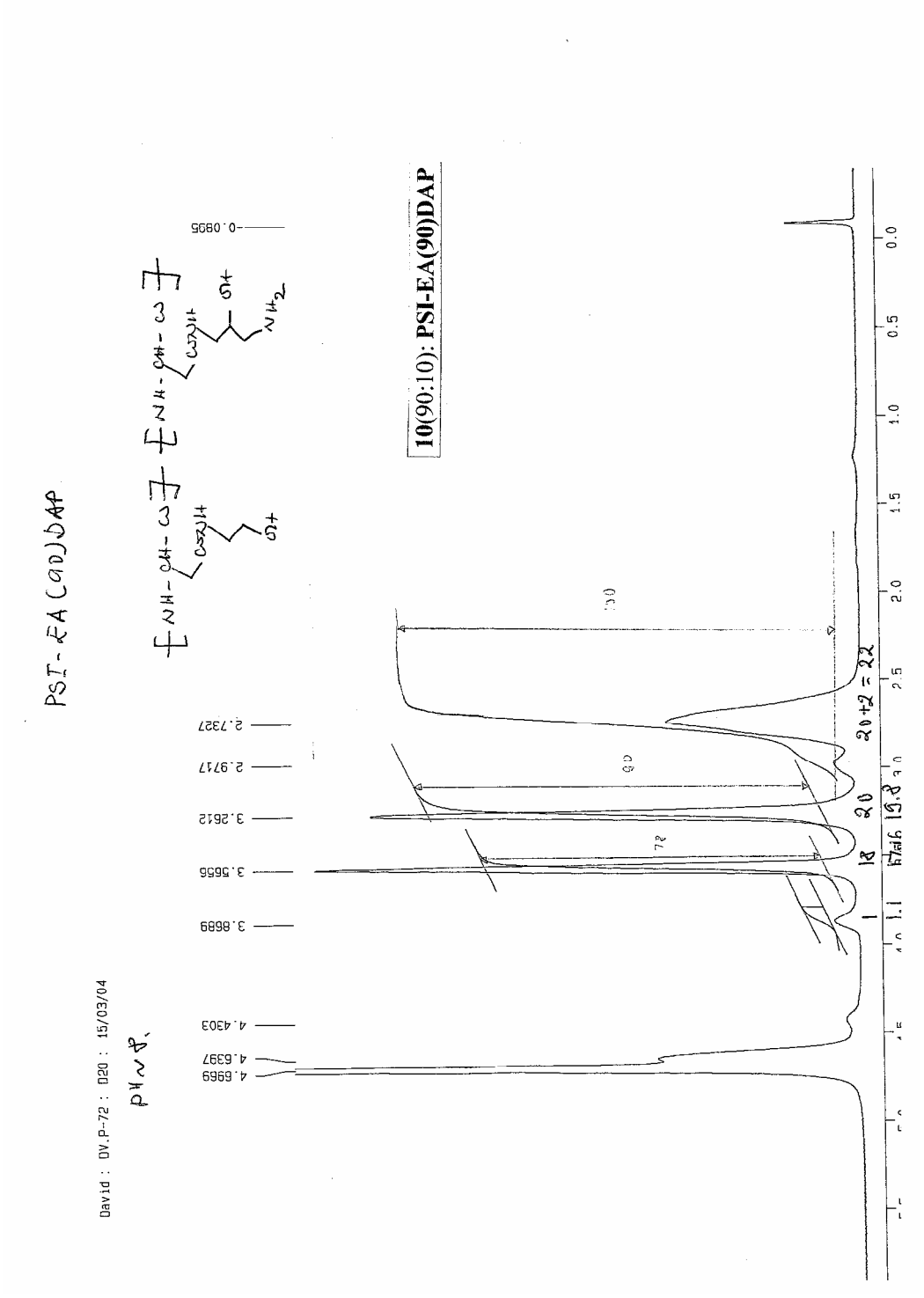
^{1}H NMR SPECTRA

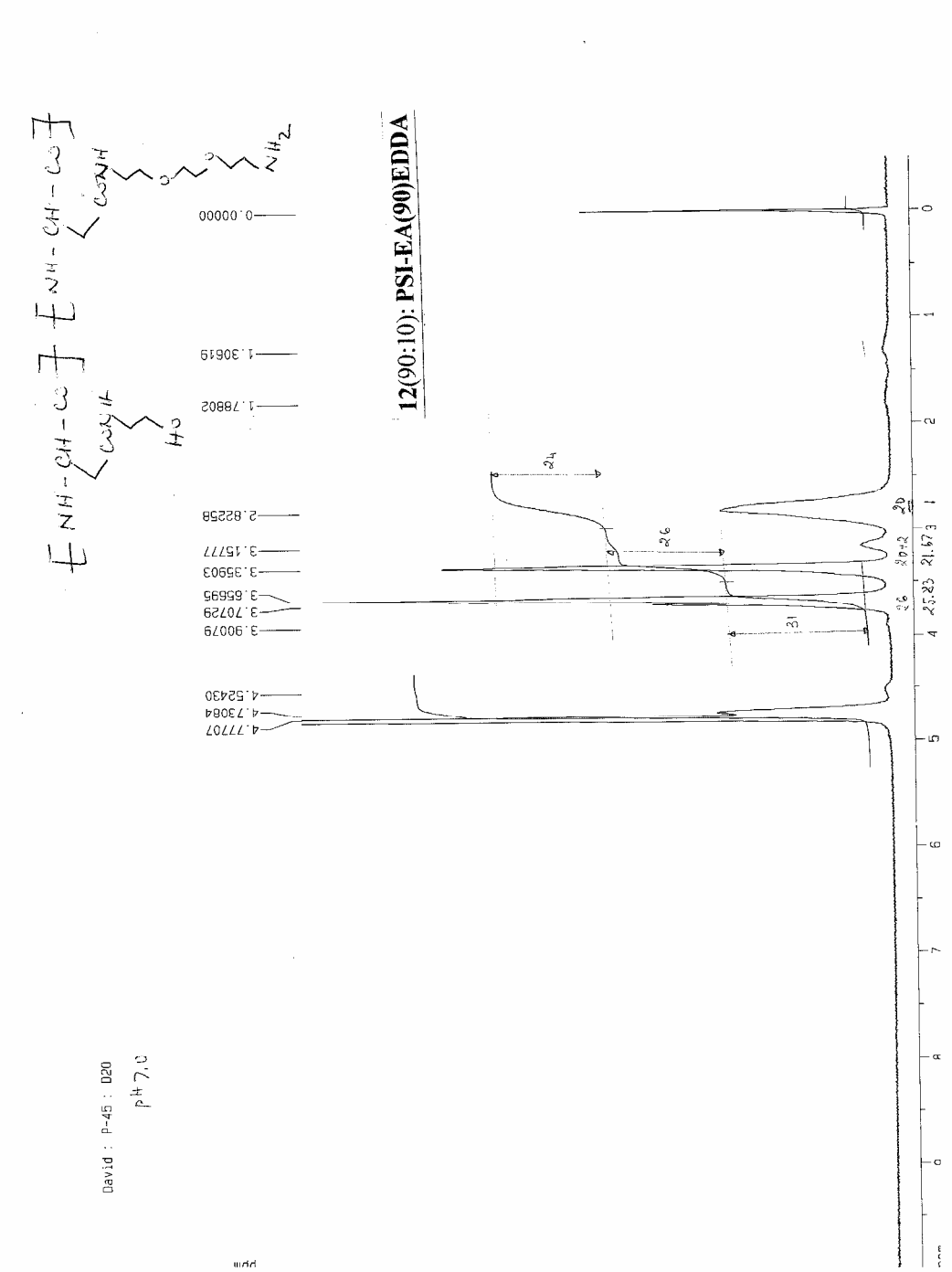

1(90:10): PSL-DMP(90)PDA
PSL-DMP(90)PDA
pH ~ 10
D2O + NaOH
4.81403
4.67261
3.19867
2.78006
2.32323
2.18707
1.67170
0.00043
ppm
20
2+20=22
22.45
20.13
20
20.13


3(90:10): PSI-DMP(90)DET
PSI-DMP(90)DET
David : P-60 : D2O + NaOH
4.7876
4.5715
3.2008
2.7832
2.7107
2.6554
2.6371
2.3424
2.3248
2.1872
1.6951
1.6740
0.0000
9.9
2.2
3.5
4.2
3.4
2.0
ppm

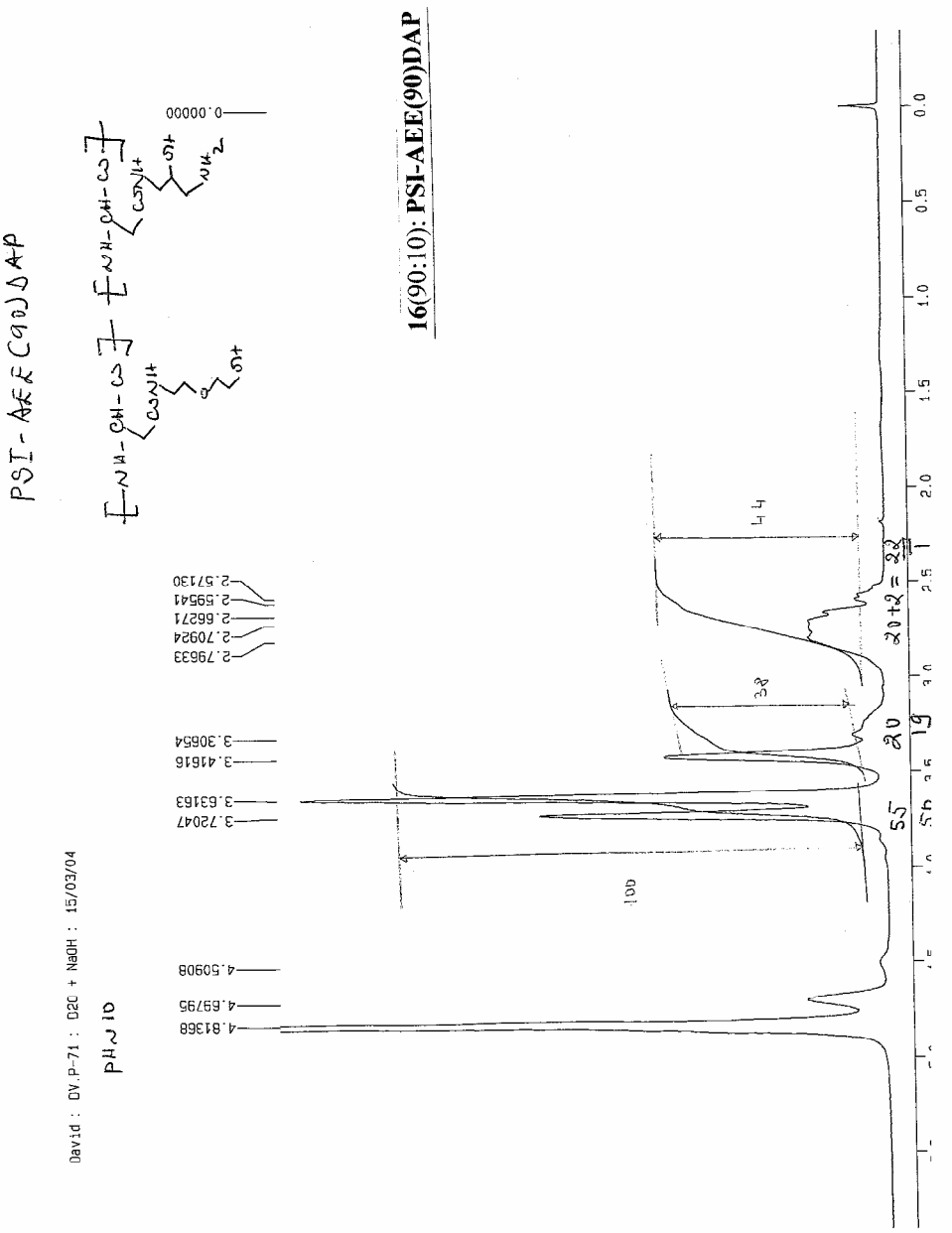

5(90:10): PSI-DMP(90)EDDA
David : P-49 : D2O + NaOH
pH d
ppm


PSI-DMP(90)DAP
7(90:10): PSI-DMP(90)DAP
David : DV.P-70 : D2O + NaOH : 15/03/04
pH ~ 10
4.8472
4.5744
4.5091
3.7124
3.2001
2.7857
2.4068
2.3262
2.1877
1.9613
1.6743
0.0000
113
31
27
54+14+2=74
75
20
20
20.67
20.67
20.67

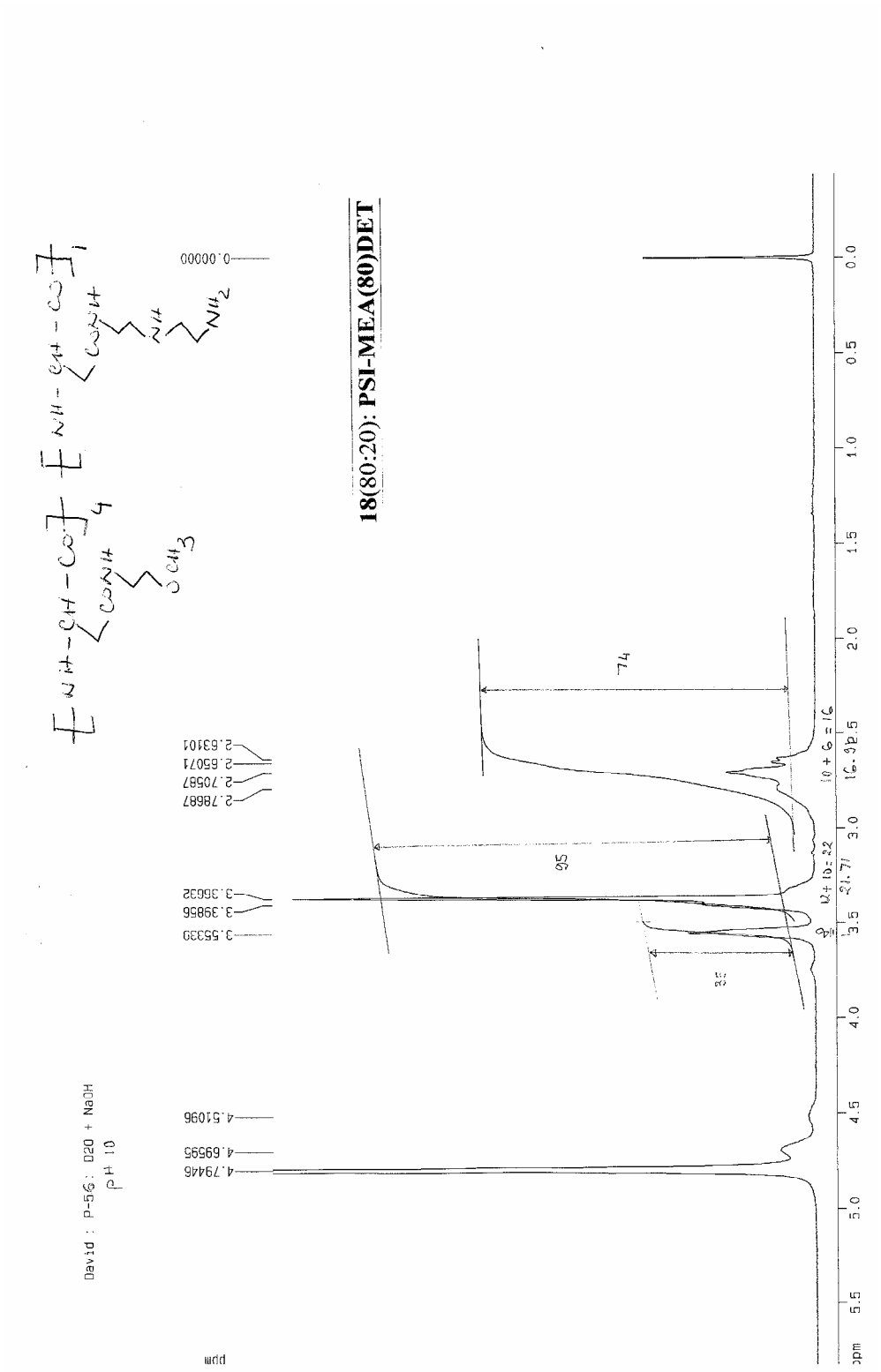

10(90:10): PSI-EA(90)DAP
David : DV.P-72 : D20 : 15/03/04
4.6969
4.6397
4.4303
3.8689
3.5656
3.2612
2.9717
2.7327
-0.0805

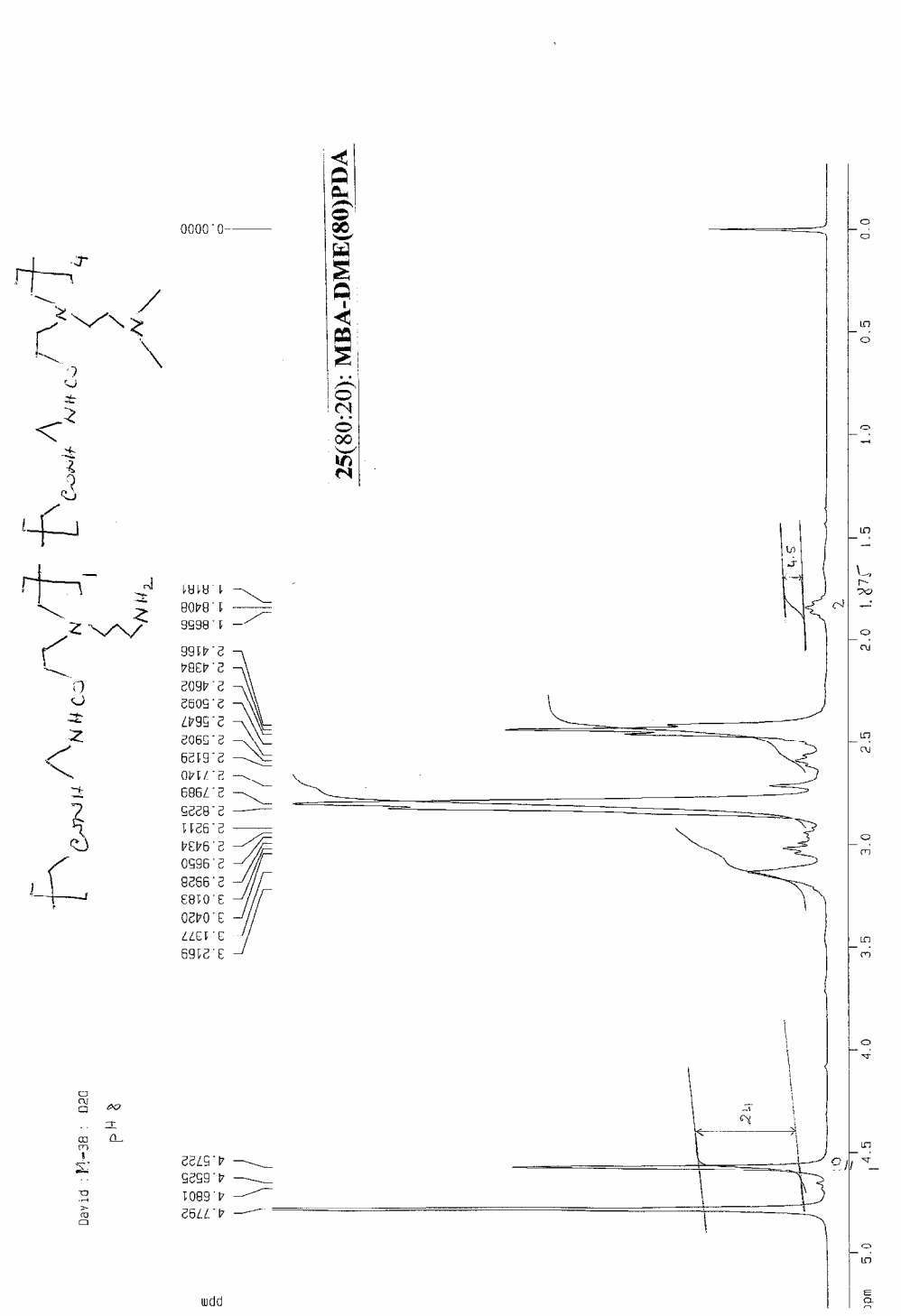

12(90:10): PSI-EA(90)EDDA
David : P-45 : D20
pH 7.0
0.00000
1.30619
1.78802
2.82258
3.15777
3.35903
3.65695
3.70729
3.90079
4.52430
4.73084
4.77707
24
26
31
25.83
21.67

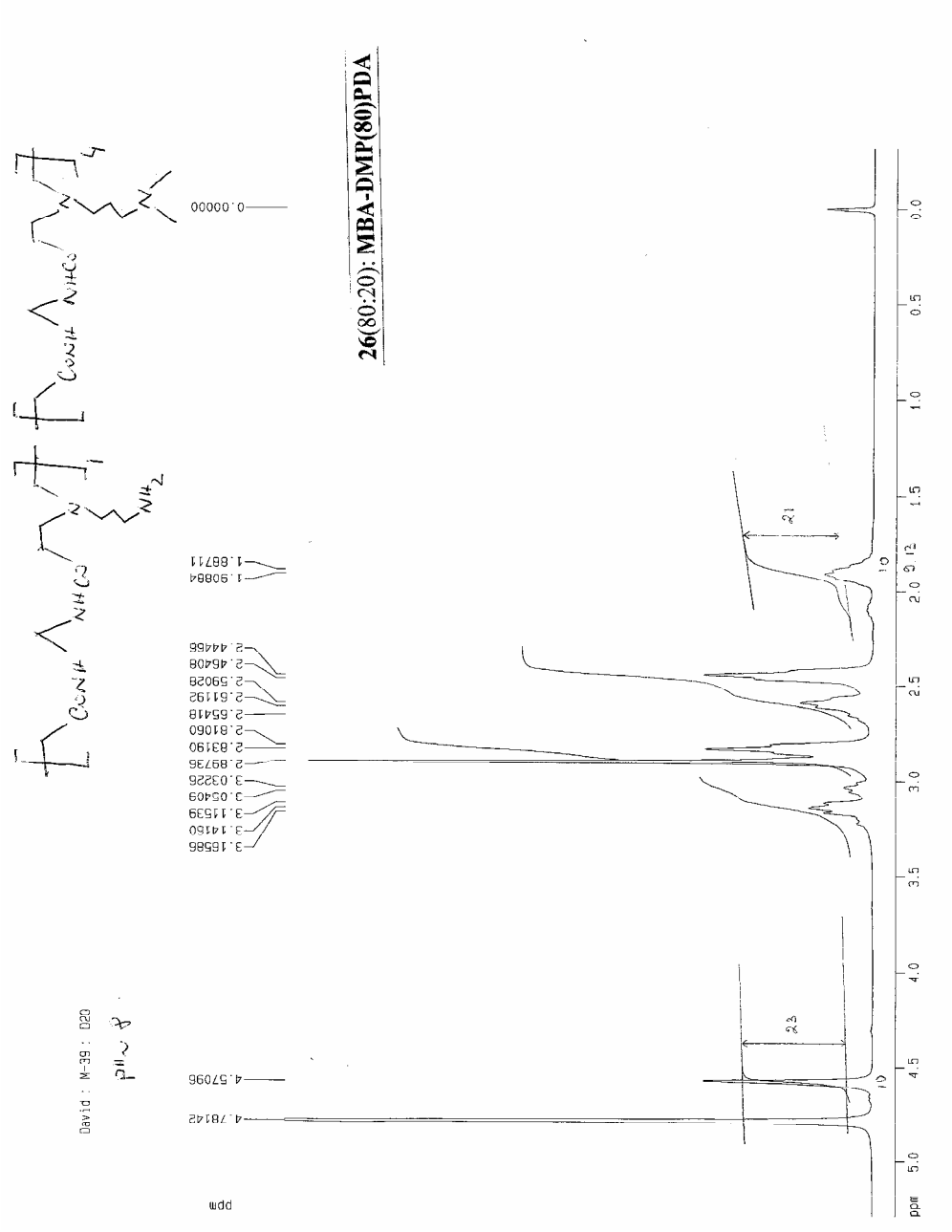
16(90:10): **PSI-AEE(90)DAP**

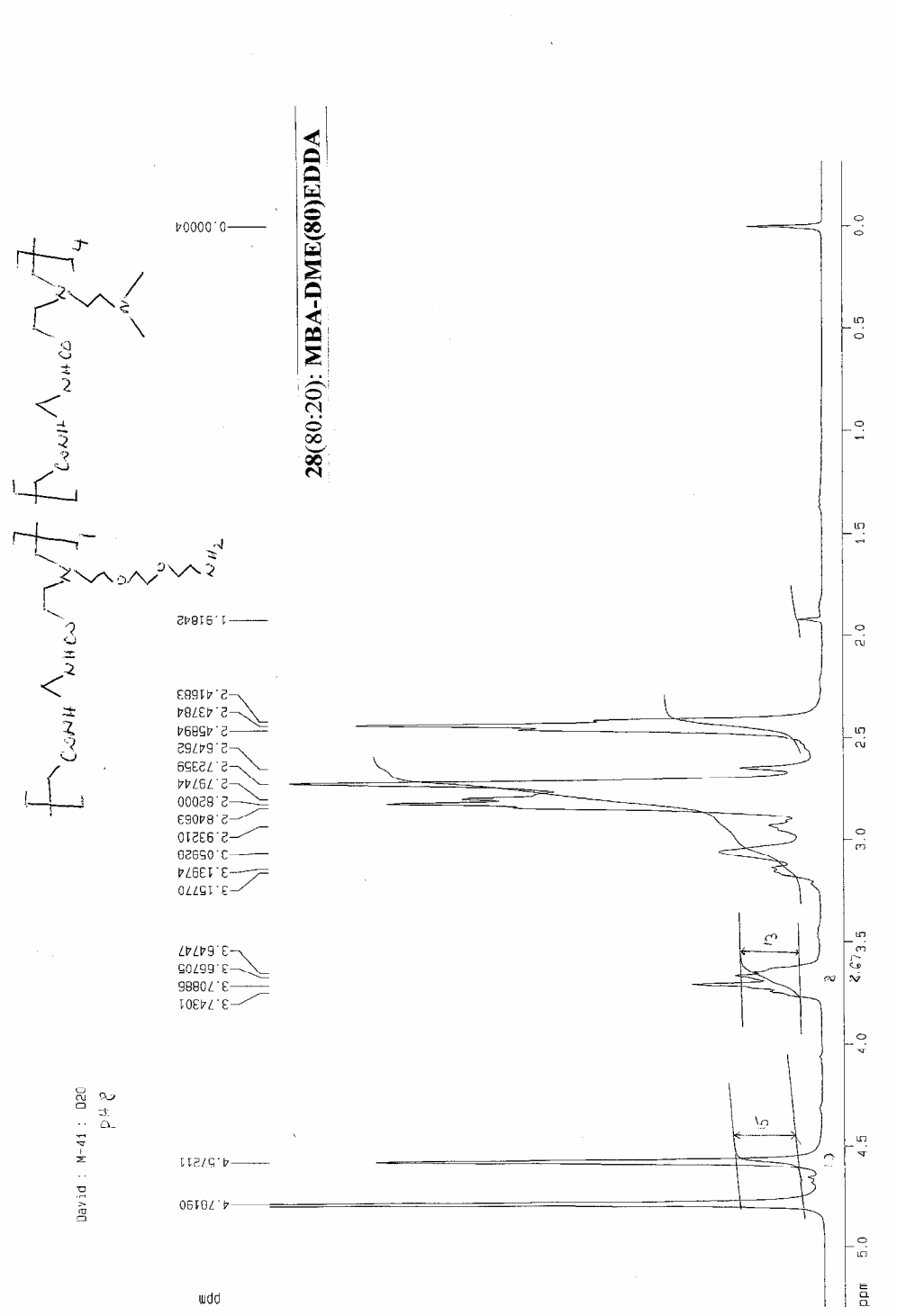


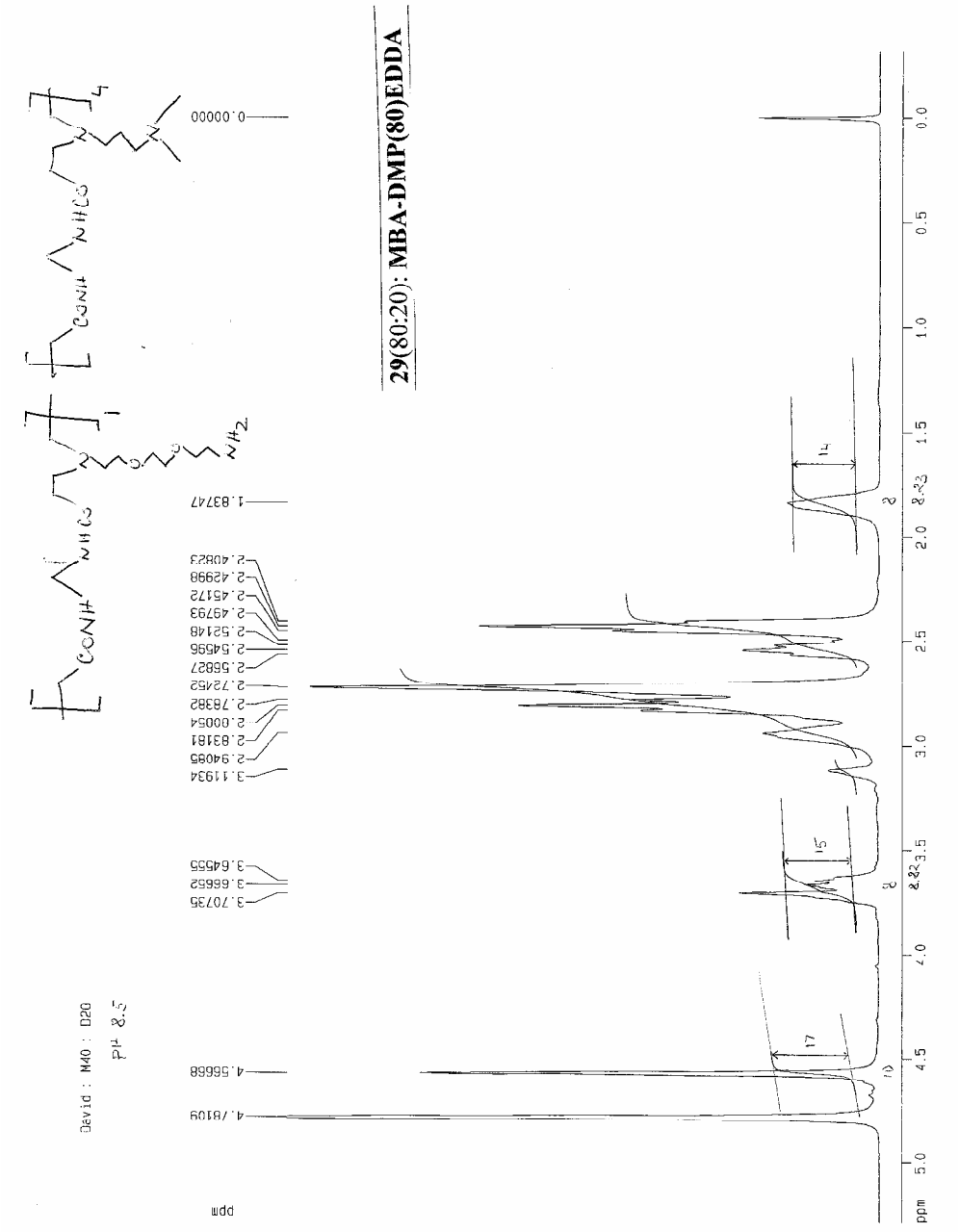
18(80:20): **PSI-MEA(80)DET**

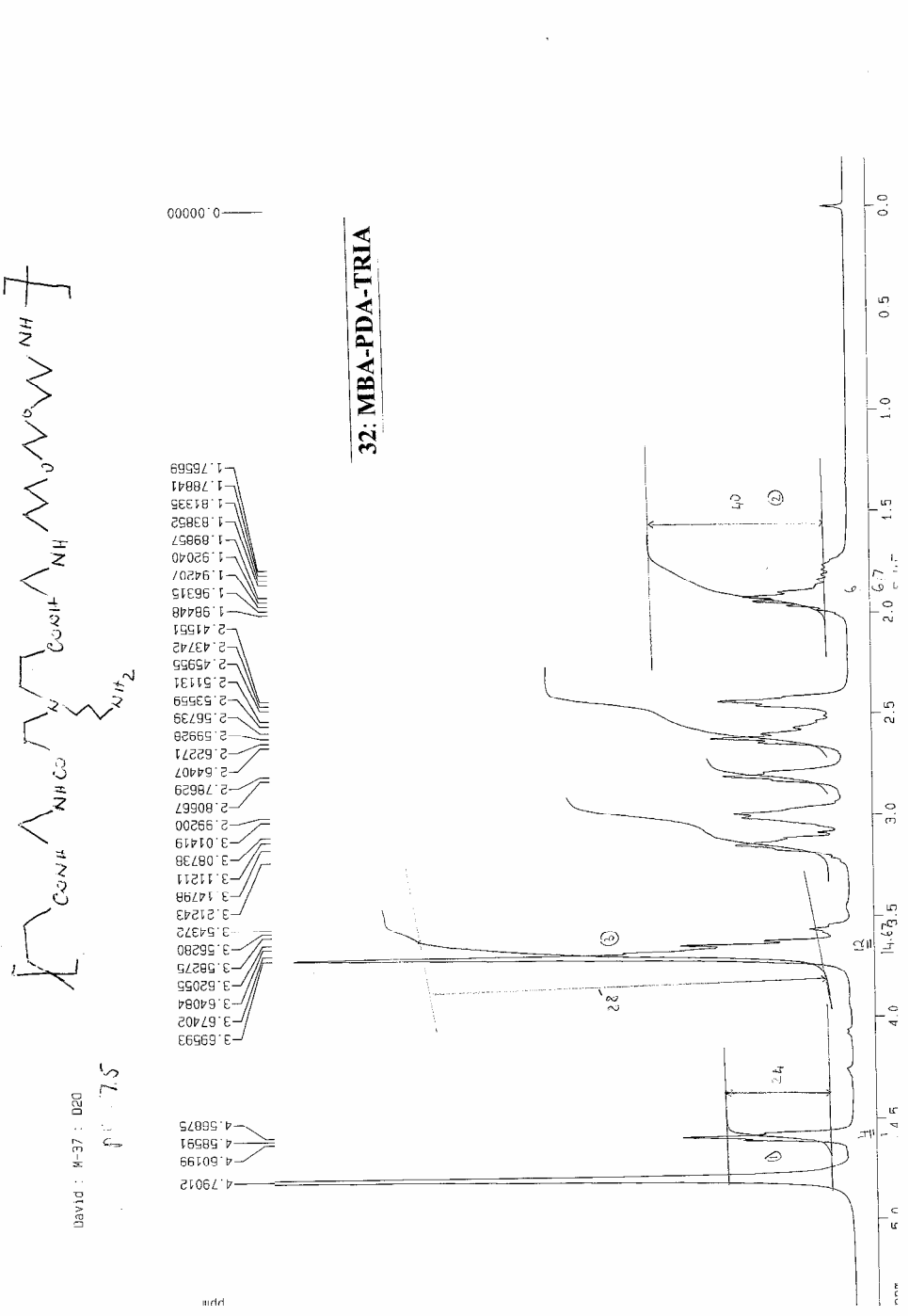


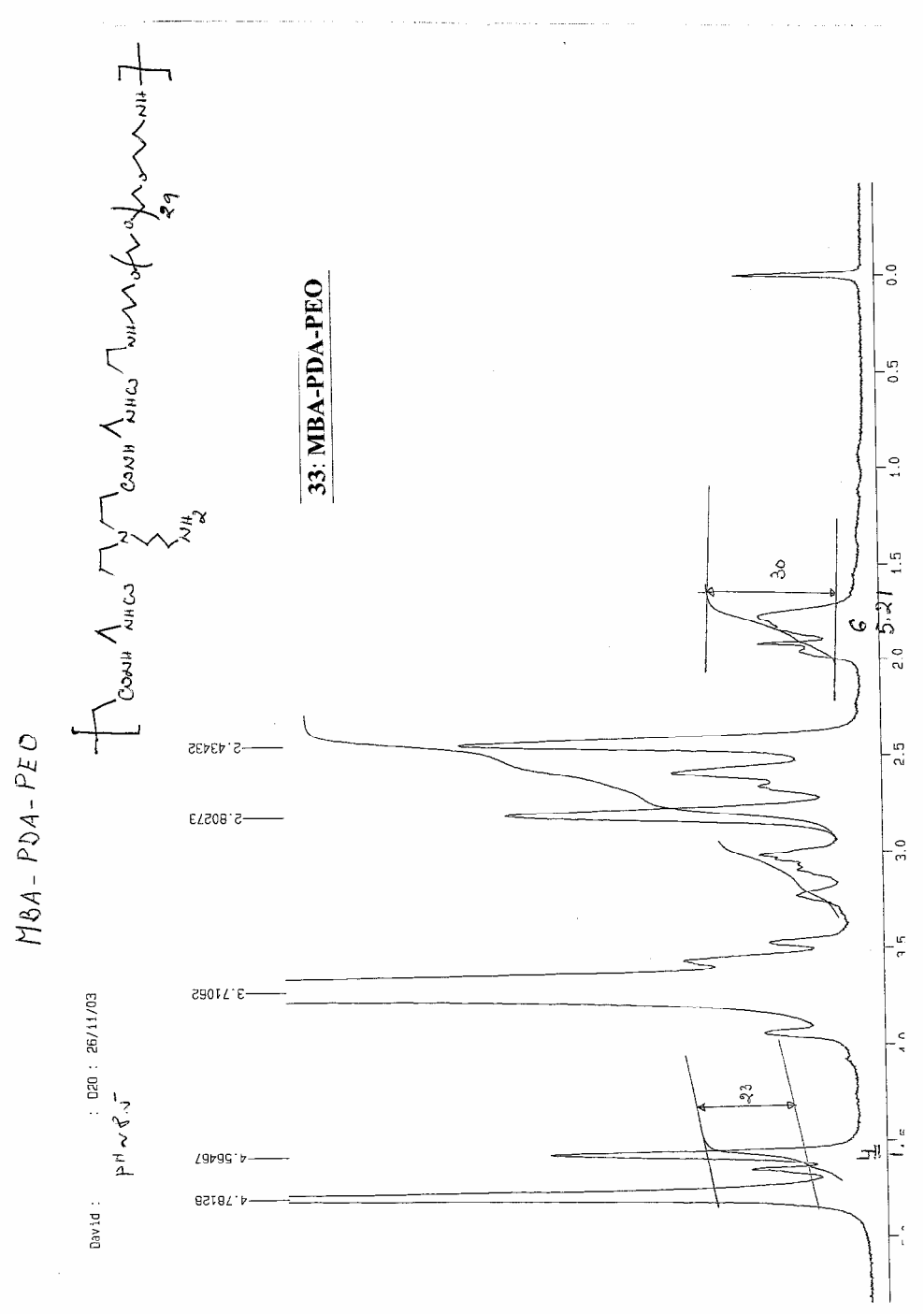

25(80:20): MBA-DME(80)PDA
David : M-38 : D2O
pH 8
ppm
4.7792
4.6801
4.5725
4.5722
3.2169
3.1377
3.0420
3.0183
2.9928
2.9650
2.9434
2.9211
2.8225
2.7989
2.7140
2.6129
2.5902
2.5647
2.5092
2.4602
2.4384
2.4166
1.8656
1.8408
1.8181
0.0000
2.1
4.5
1.87
1
2
5.0
4.5
4.0
3.5
3.0
2.5
2.0
1.5
1.0
0.5
0.0

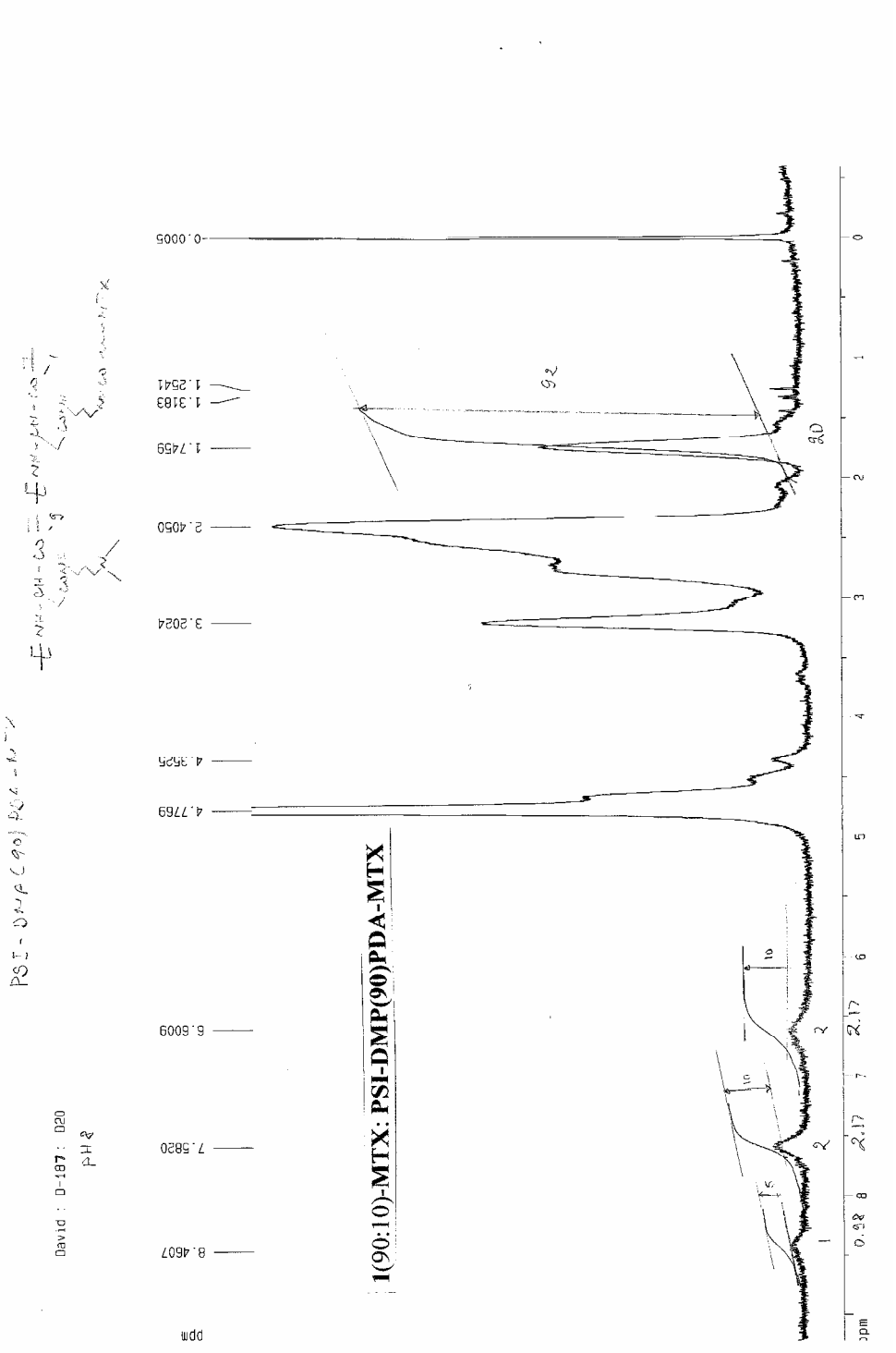

26(80:20): MBA-DMP(80)PDA
David : M-39 : D2O
ppm
4.78142
4.57096
3.16586
3.14160
3.11539
3.05409
3.03226
2.89736
2.83190
2.81060
2.65418
2.61192
2.59028
2.46408
2.44466
1.90884
1.88711
0.00000
2.3
2.1
1.0
5.0
4.5
4.0
3.5
3.0
2.5
2.0
1.5
1.0
0.5
0.0

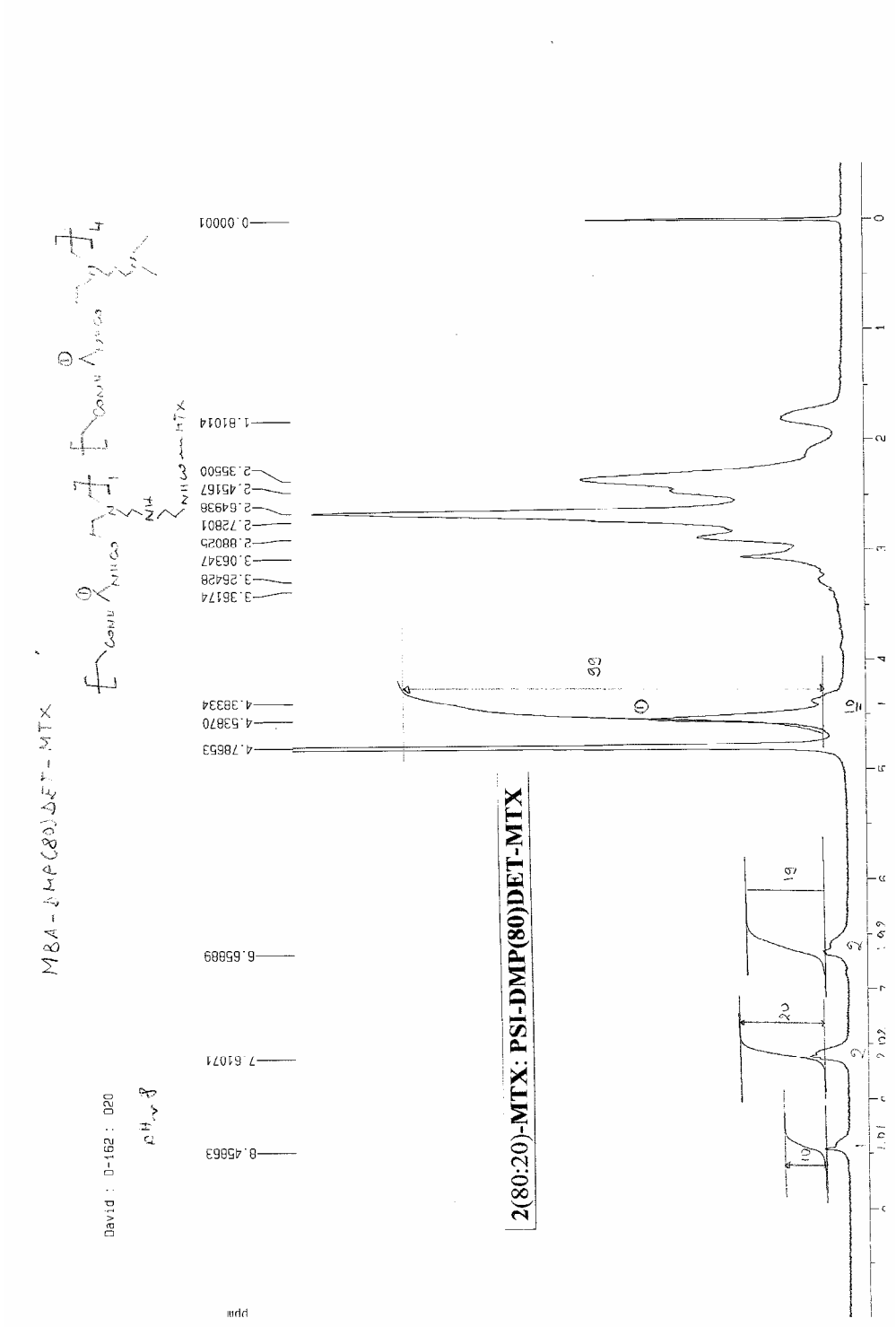

28(80:20): MBA-DME(80)EDDA
David : M-41 : D20
p4 2
0.00004
1.91842
2.41683
2.43784
2.45894
2.54762
2.72359
2.79744
2.82000
2.84063
2.93210
3.05920
3.13974
3.15770
3.64747
3.65705
3.70886
3.74301
4.57211
4.70190
ppm
5.0
4.5
4.0
3.5
3.0
2.5
2.0
1.5
1.0
0.5
0.0

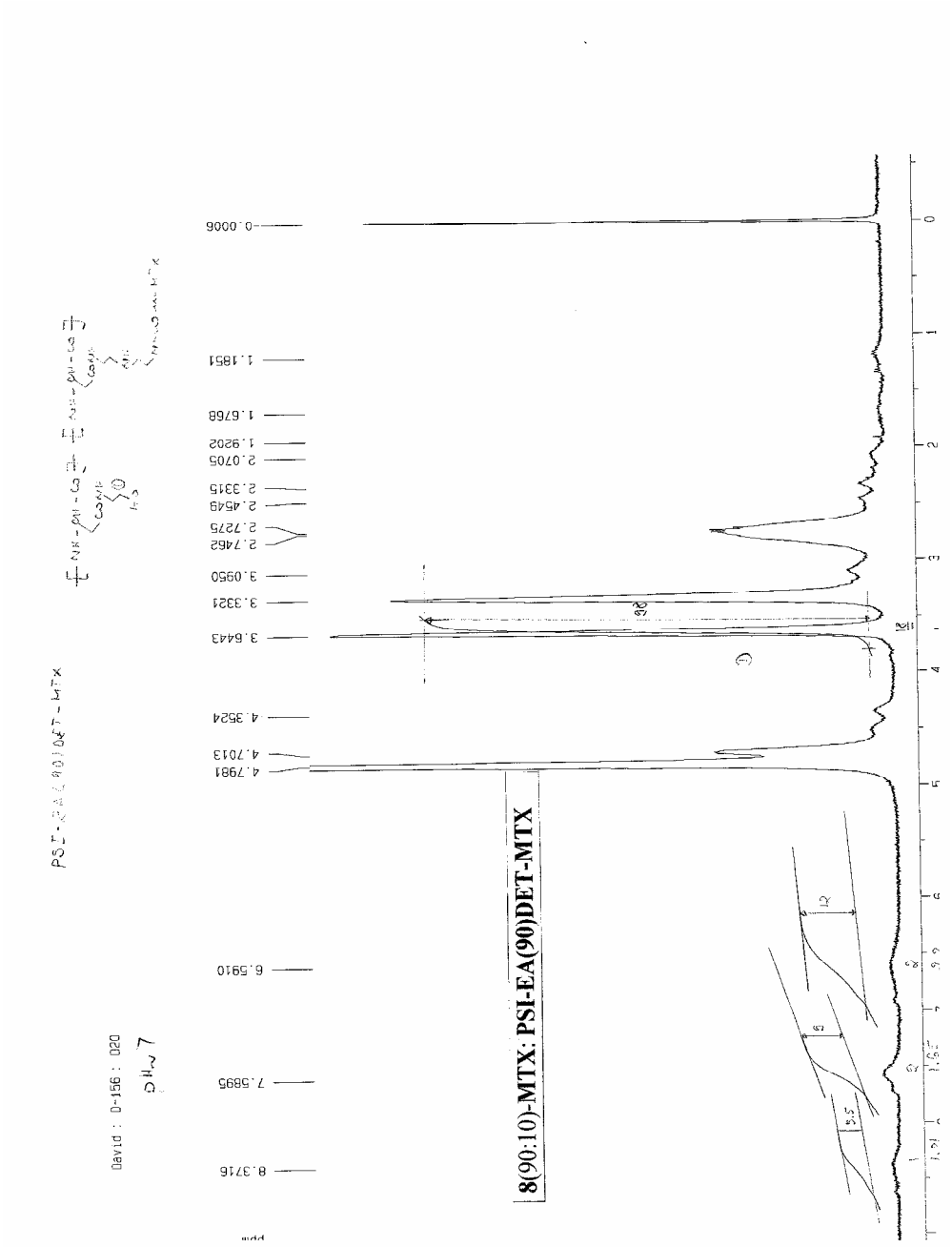

29(80:20): MBA-DMP(80)EDDA
David : M40 : D20
PH 8.5
ppm
4.87109
4.56668
3.64555
3.66652
3.70735
3.11934
2.94085
2.83181
2.78382
2.72452
2.56827
2.54596
2.52148
2.49793
2.45172
2.42998
2.40823
1.83747
0.00000
17
15
14
8.33
8.32
5.0
4.5
4.0
3.5
3.0
2.5
2.0
1.5
1.0
0.5
0.0

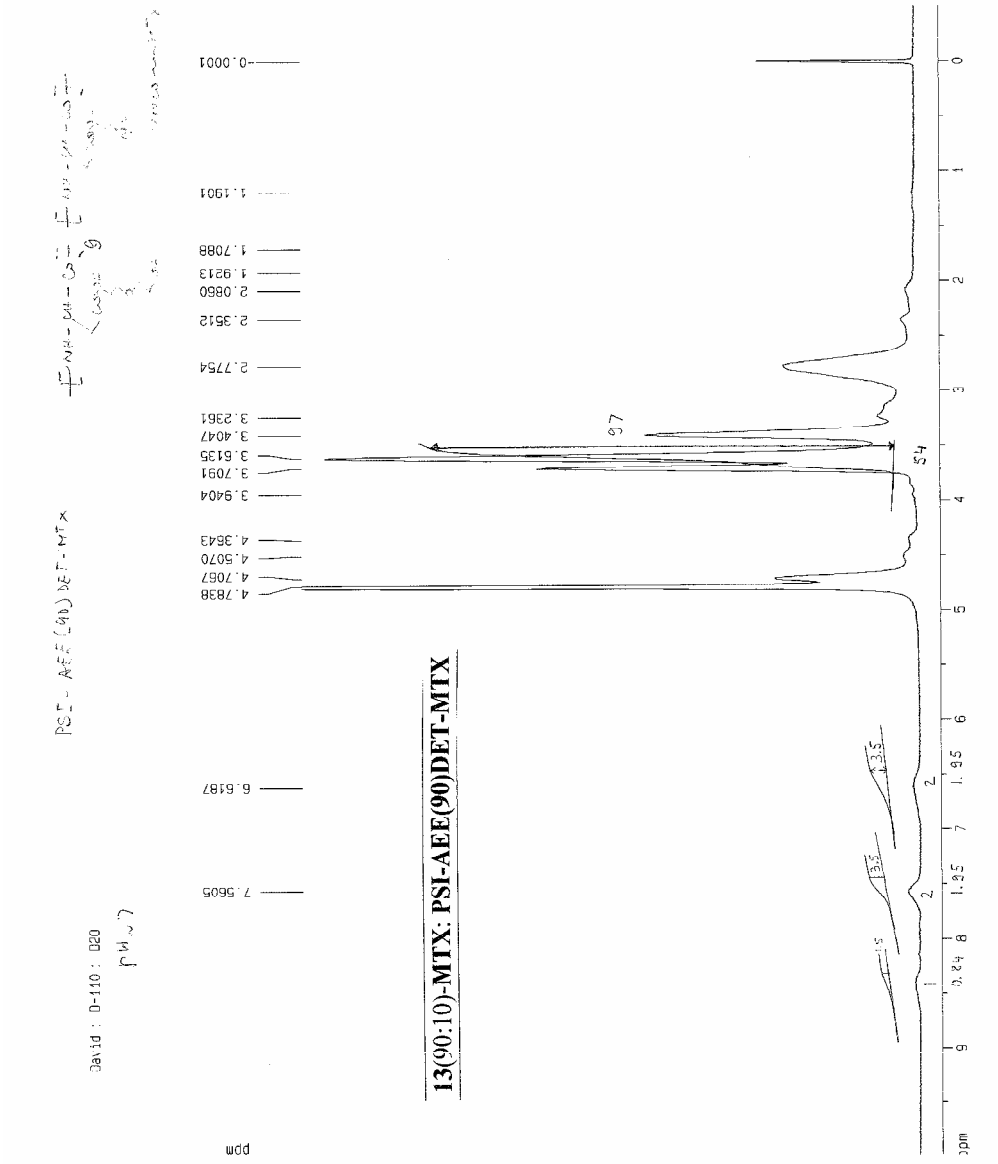

32: MBA-PDA-TRIA

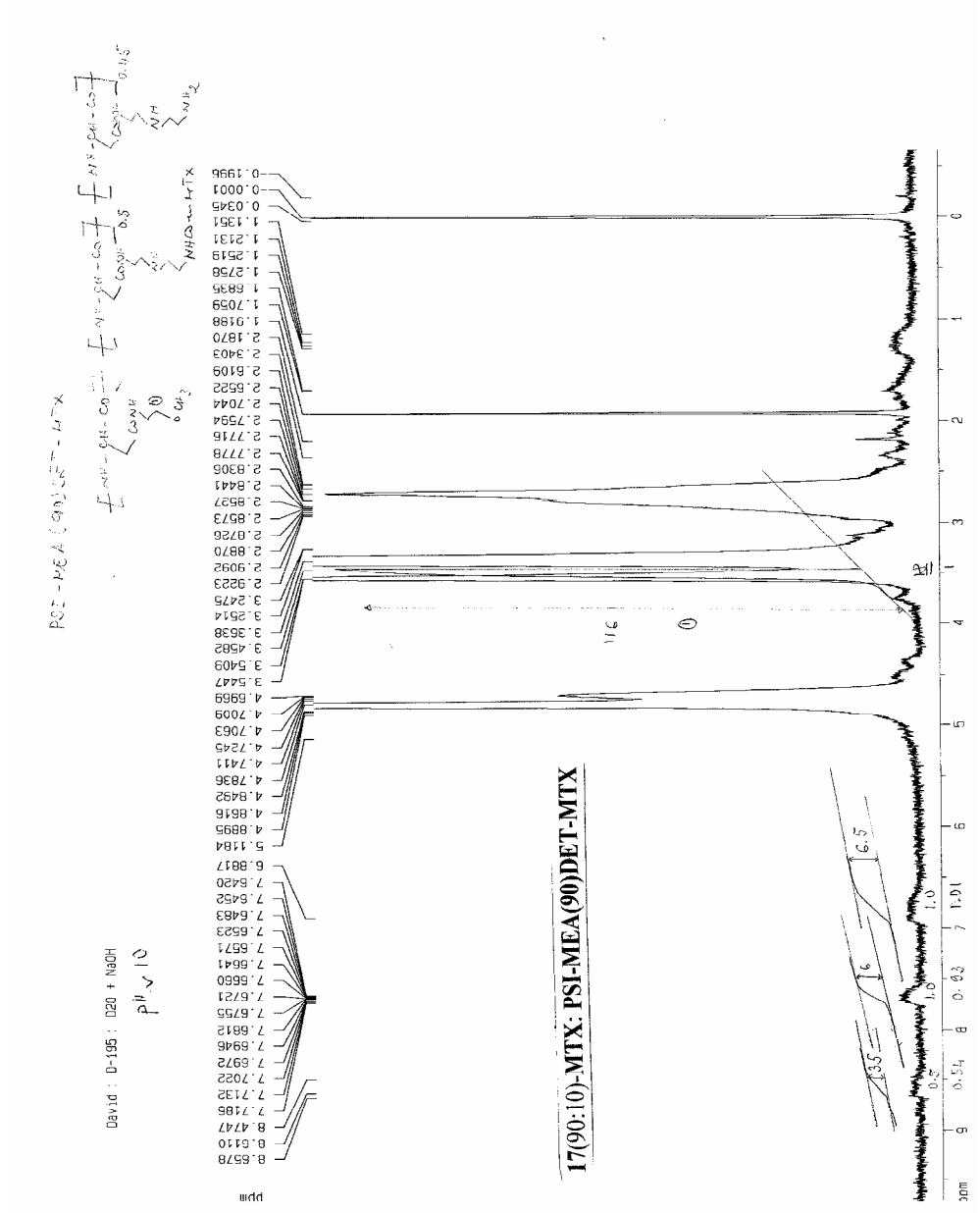

MBA-PDA-PEO
David : 020 : 26/11/03
pH ~ 8.5
33: MBA-PDA-PEO
4.78128
4.56467
3.71052
2.80273
2.43432
23
30
5.21


1(90:10)-MTX: PSI-DMP(90)PDA-MTX
David : D-187 : D20
pH 8
ppm
8.4607
7.5820
6.5009
4.7769
4.3525
3.2024
2.4050
1.7459
1.3183
1.2541
0.0005
2.17
2.17
0.98
1
2
2
1
2
1
2

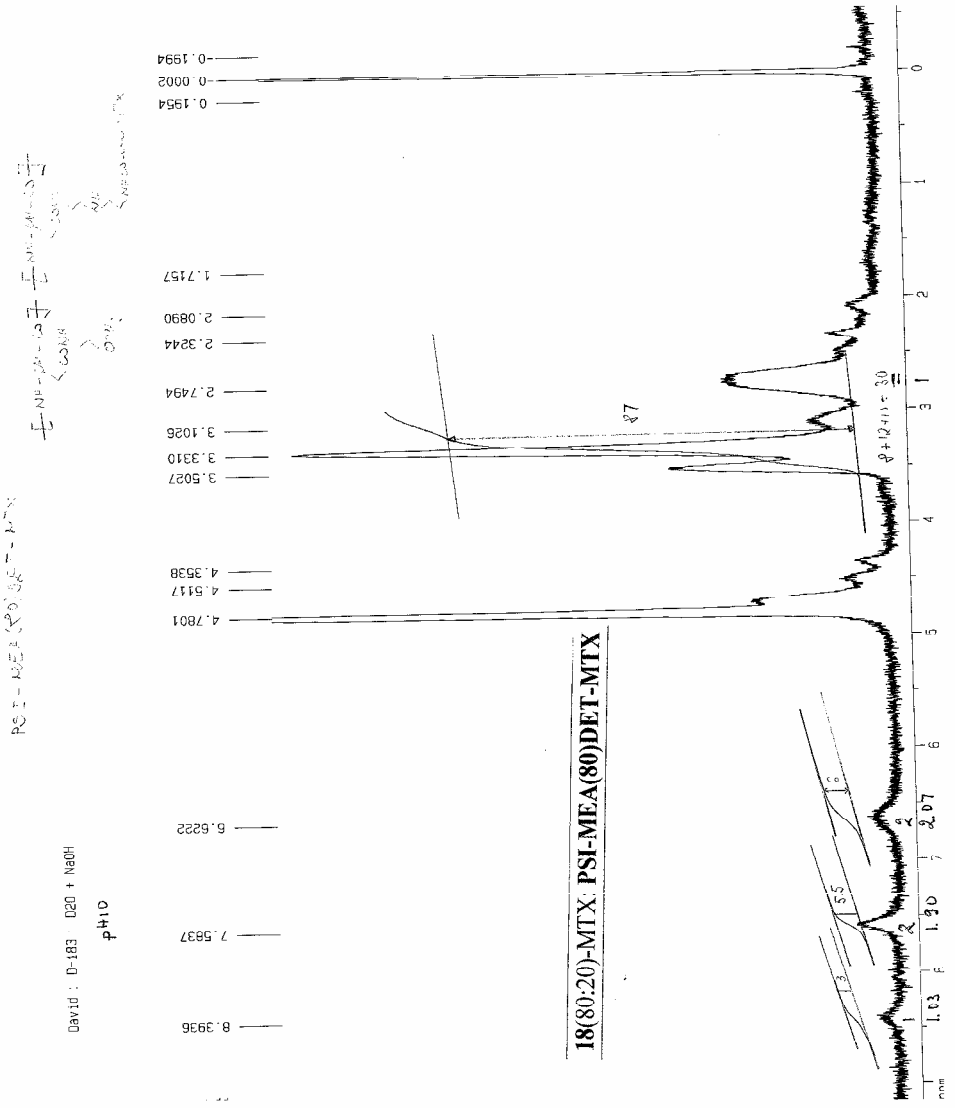

MBA-DMP(80)DET-MTX
David : D-162 : 020
ppm
0.00001
1.81014
2.35500
2.45167
2.64938
2.72801
2.88025
3.06347
3.25428
3.36174
4.38334
4.53870
4.78653
6.65889
7.61071
8.45863
2(80:20)-MTX: PSI-DMP(80)DET-MTX

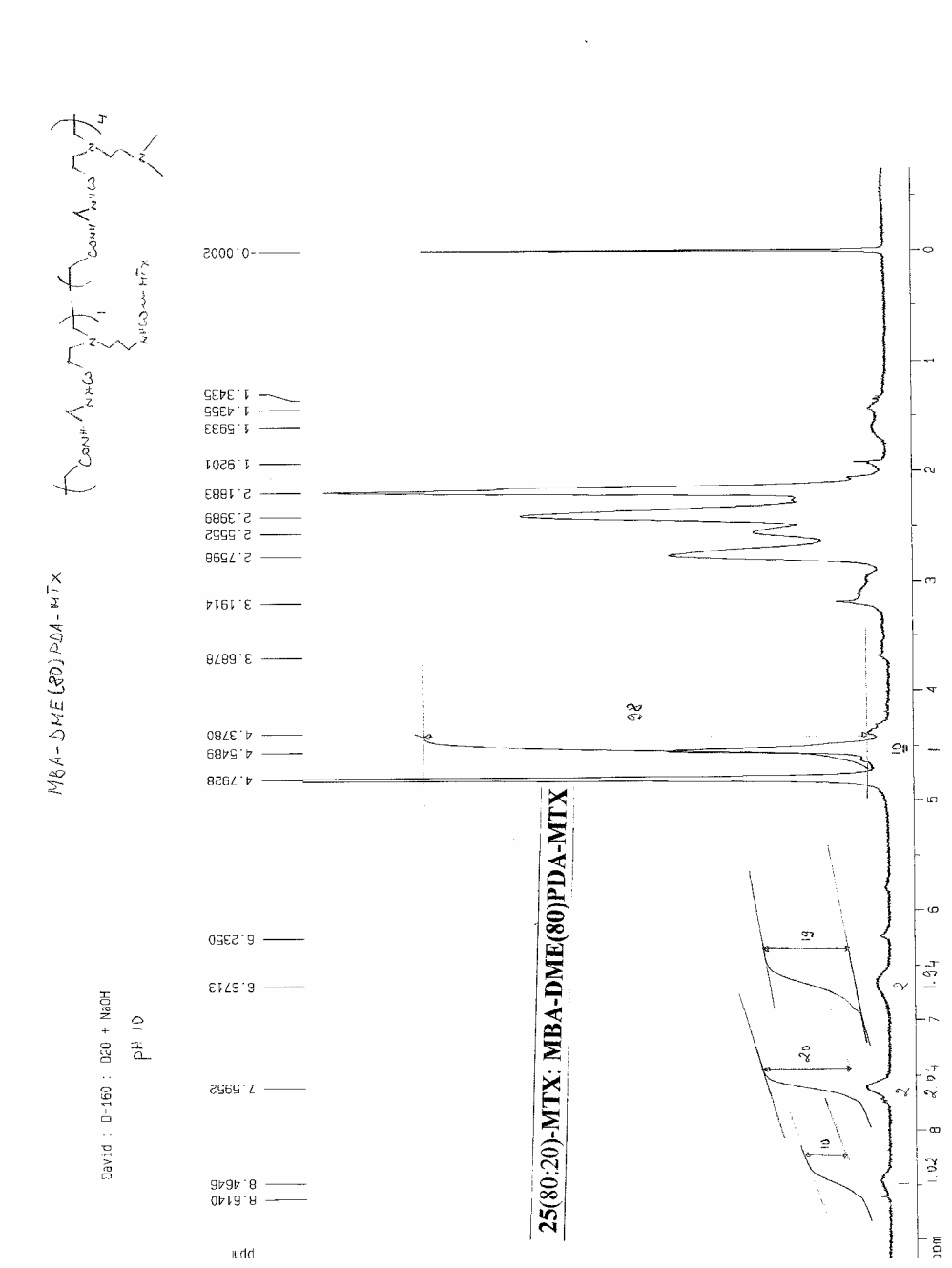

8(90:10)-MTX: PSI-EA(90)DET-MTX

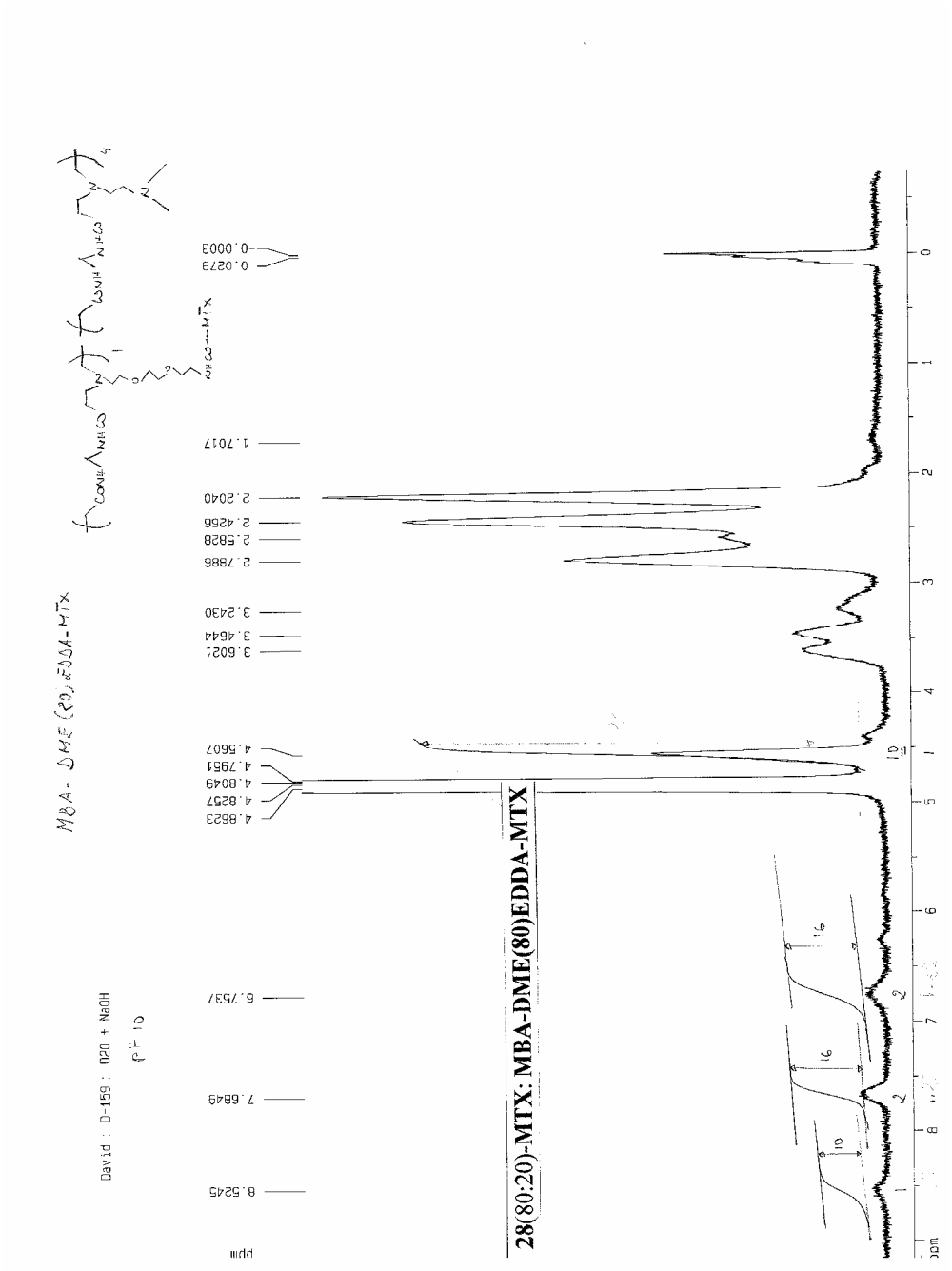

13(90:10)-MTX: PSI-AEE(90)DET-MTX
ppm
6.6187
7.5605
4.7838
4.7067
4.5070
4.3643
3.9404
3.7091
3.6135
3.4047
3.2361
2.7754
2.3512
2.0860
1.9213
1.7088
1.1901
0.0001
97
54
13.5
13.5
2
2
1
0.24
8
1.25
7
1.95
6
5
4
3
2
1
0
ppm

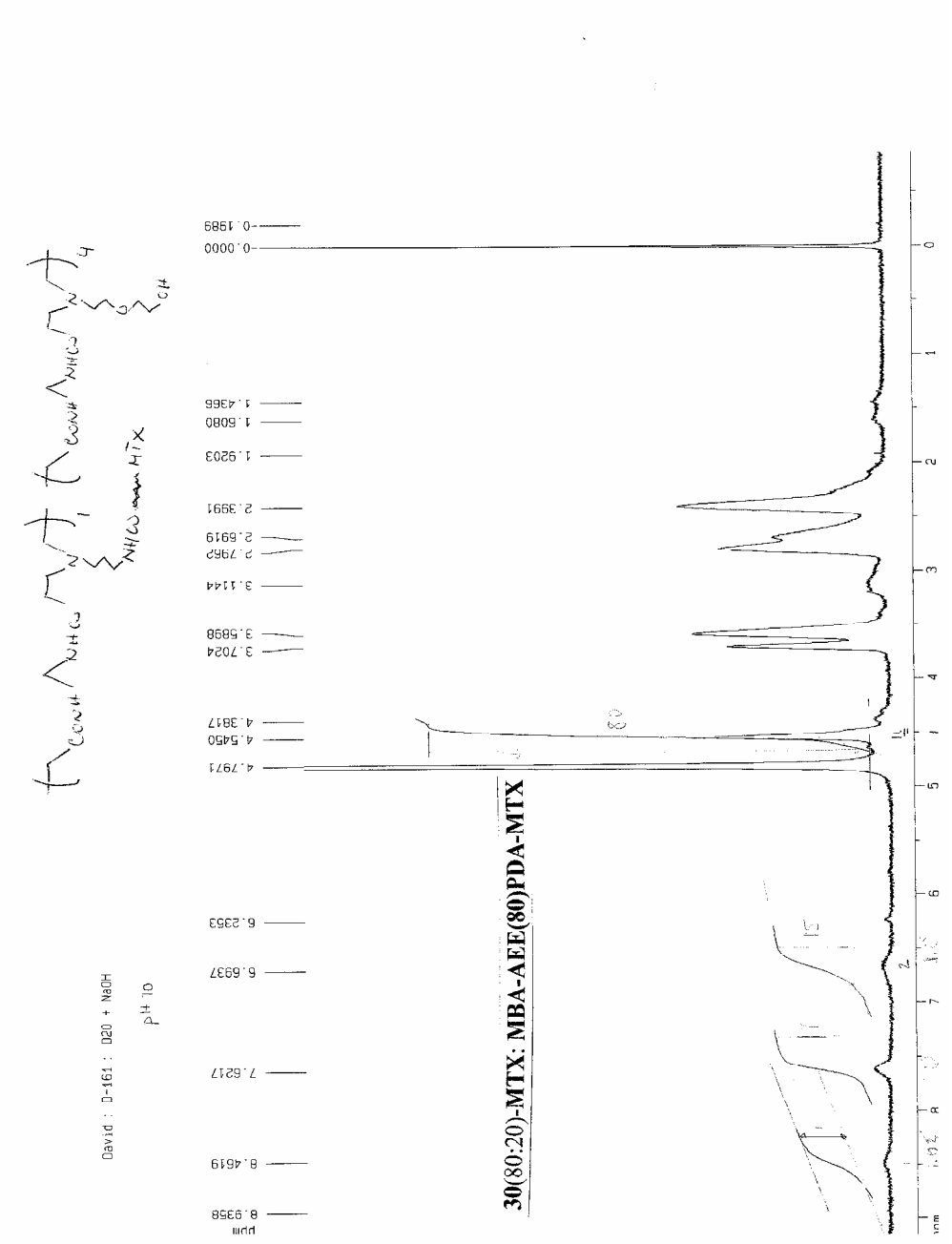


17(90:10)-MTX: PSI-MEA(90)DET-MTX

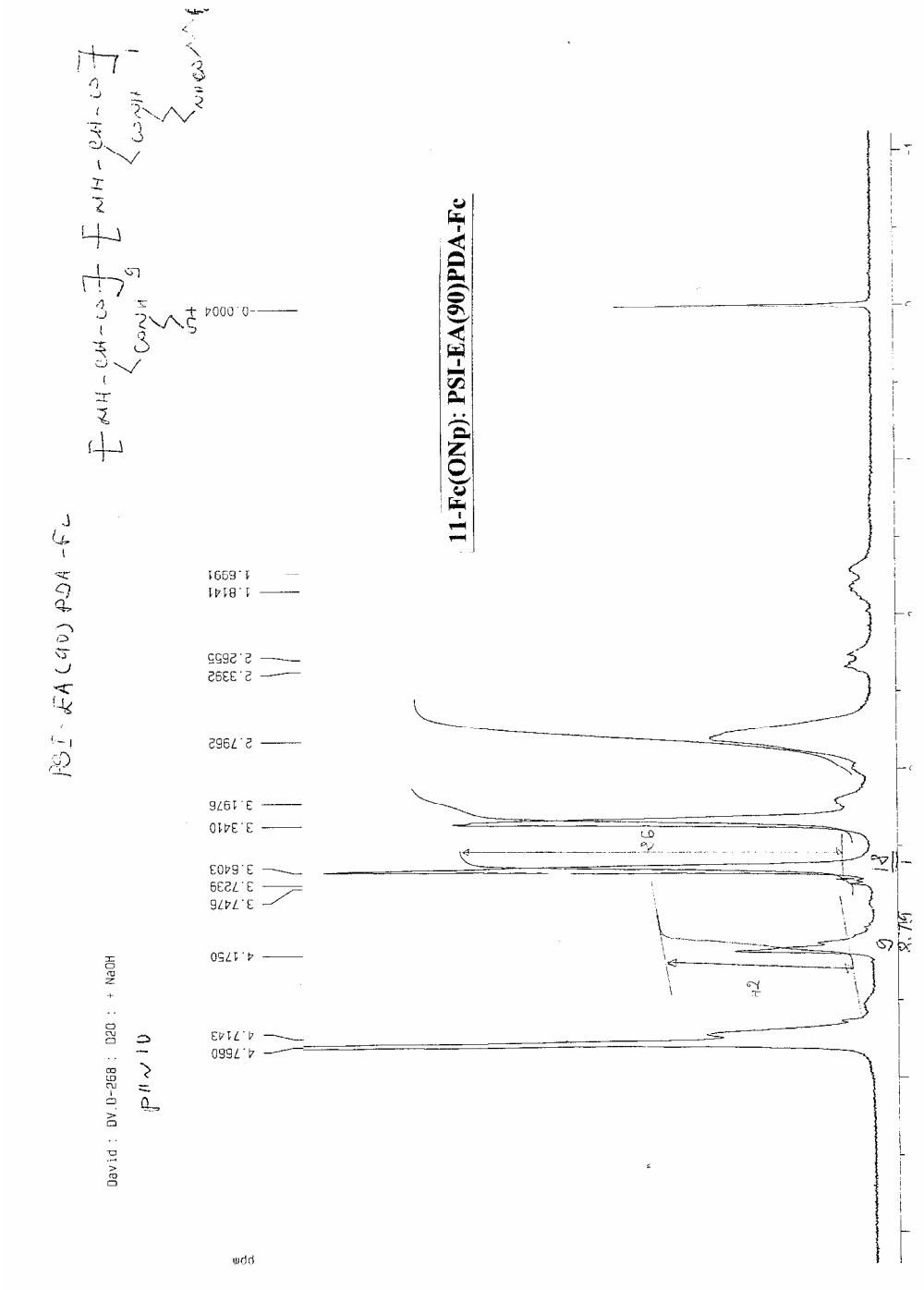

18(80:20)-MTX: PSI-MEA(80)DET-MTX
David : D-183 D2O + NaOH
pH10
8.3936
7.5837
6.6222
4.7801
4.5117
4.3538
3.5027
3.3310
3.1026
2.7494
2.3244
2.0890
1.7157
0.1994
0.0002
0.1954
ppm

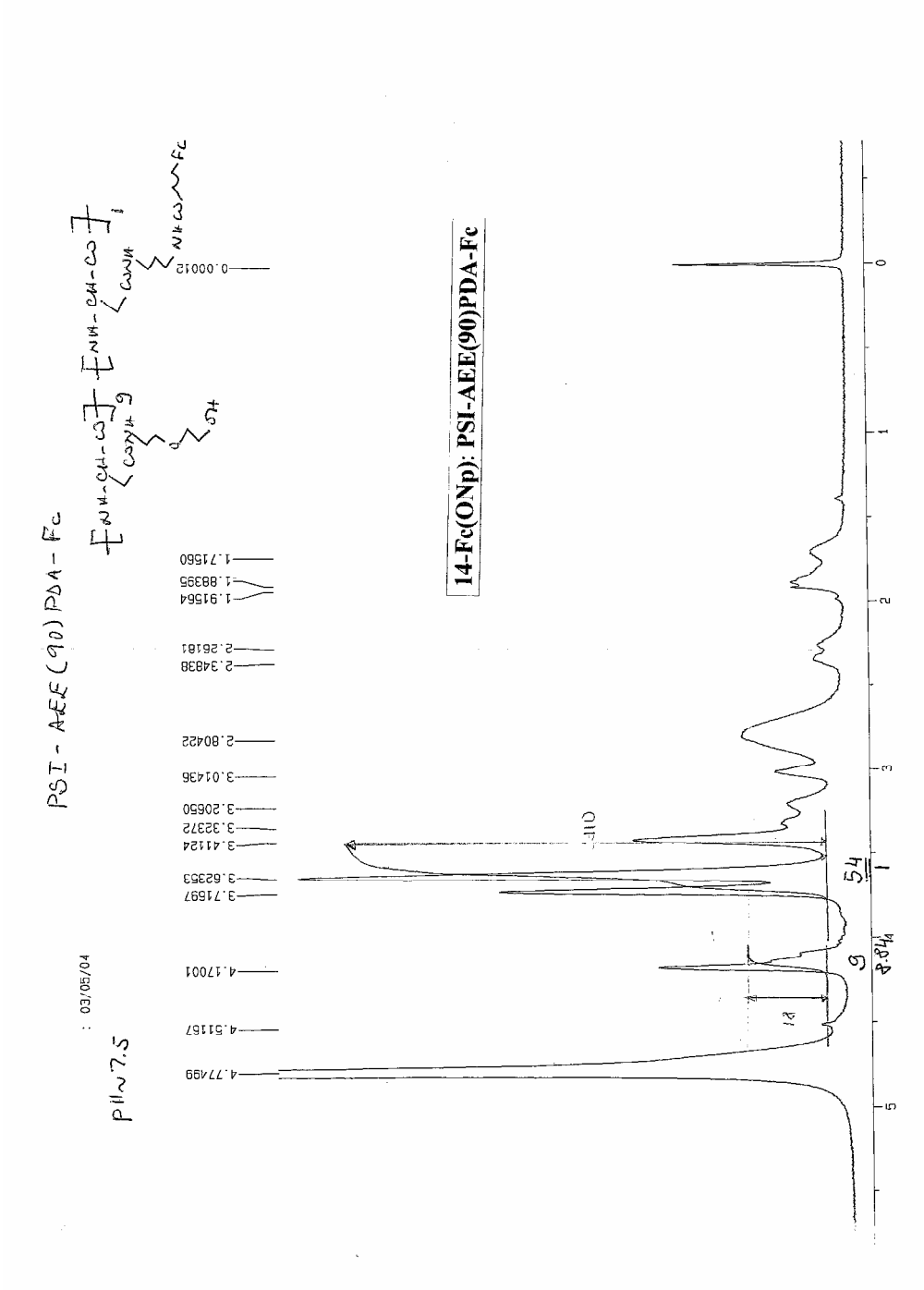

MBA-DME(80)PDA-MTX
David : D-160 : D20 + NaOH
pH 10
ppm
8.4646
8.4140
7.5952
6.8713
6.2350
4.7928
4.5489
4.3780
3.6878
3.1914
2.7598
2.5552
2.3989
2.1883
1.9201
1.5933
1.4355
1.3435
0.0002
25(80:20)-MTX: MBA-DME(80)PDA-MTX

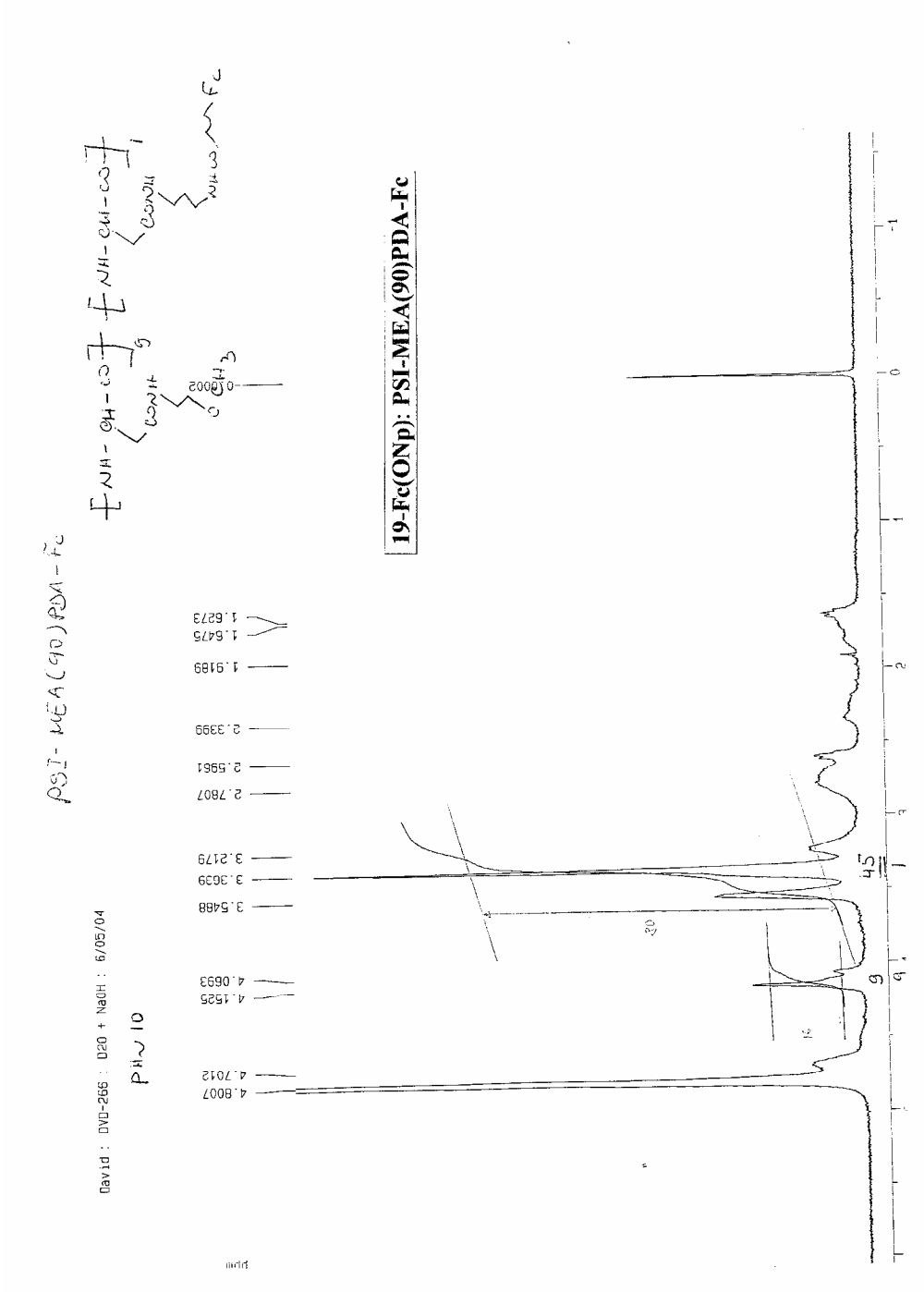

MBA-DME(80)EDDA-MTX
David : D-159 : D2O + NaOH
pH 10
ppm
8.5245
7.6849
6.7537
4.8623
4.8257
4.8049
4.7951
4.5607
3.6021
3.4644
3.2430
2.7886
2.5828
2.4266
2.2040
1.7017
0.0279
0.0003
28(80:20)-MTX: MBA-DME(80)EDDA-MTX

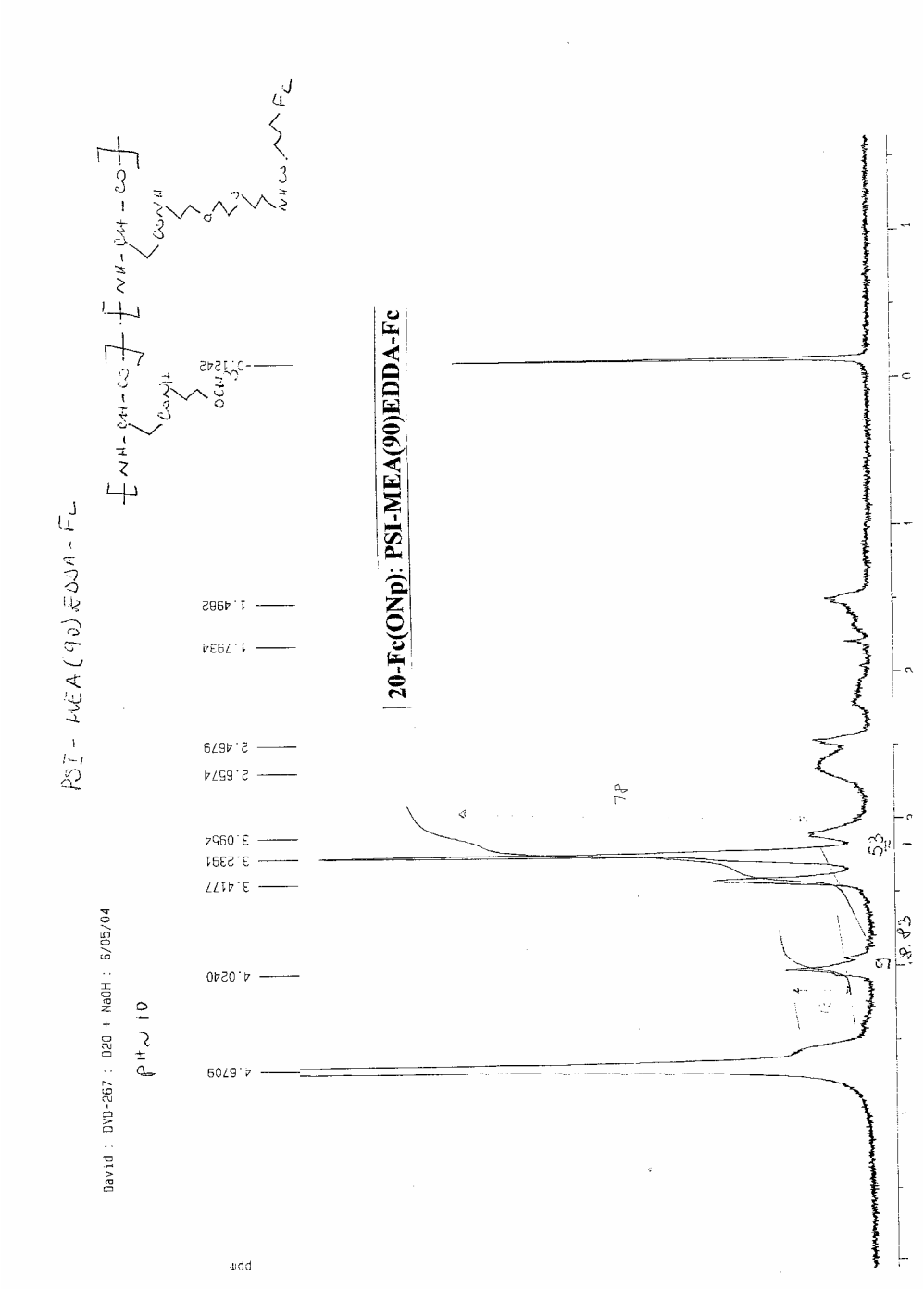


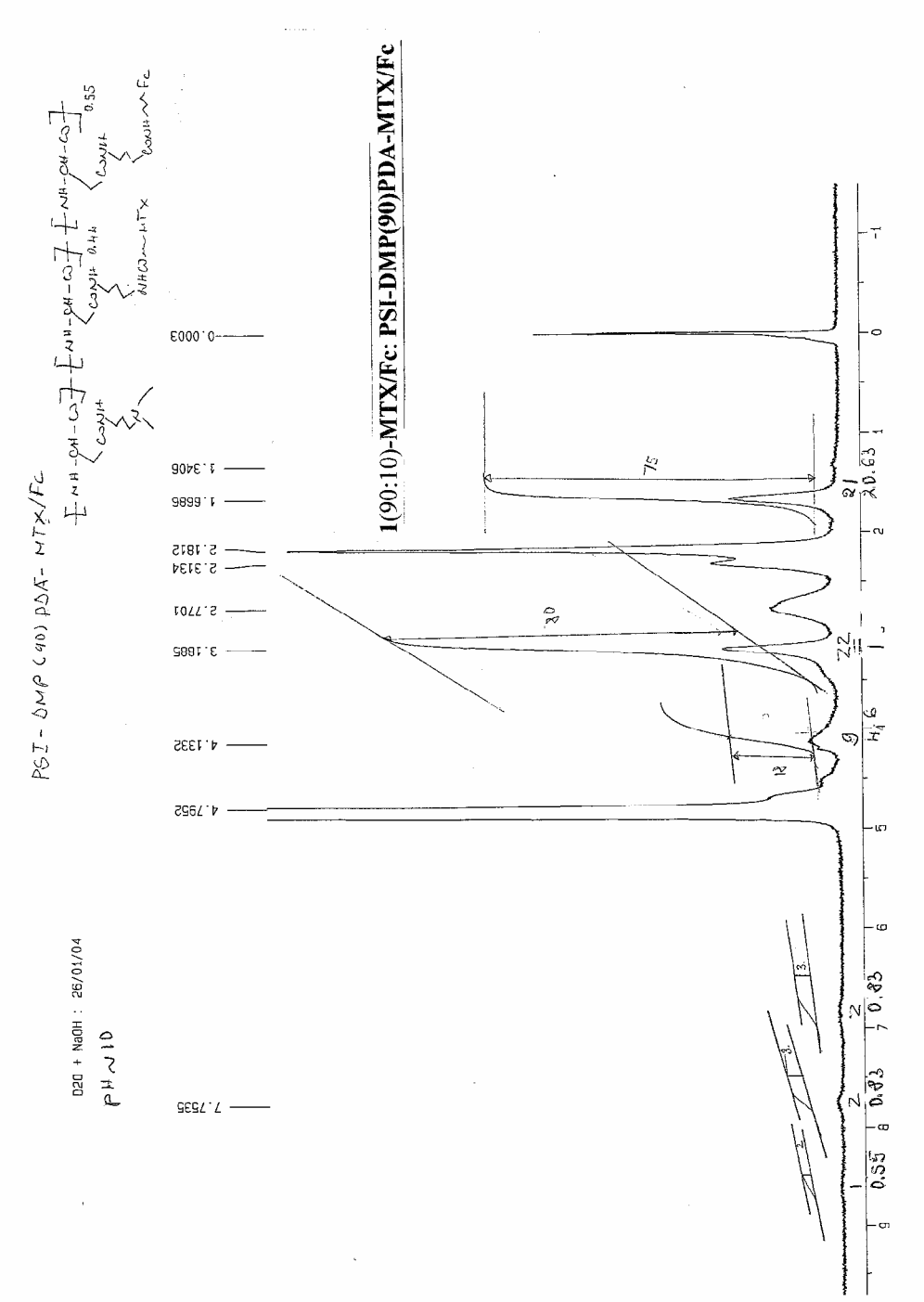
30(80:20)-**MTX**: **MBA-AEE(80)PDA-MTX**

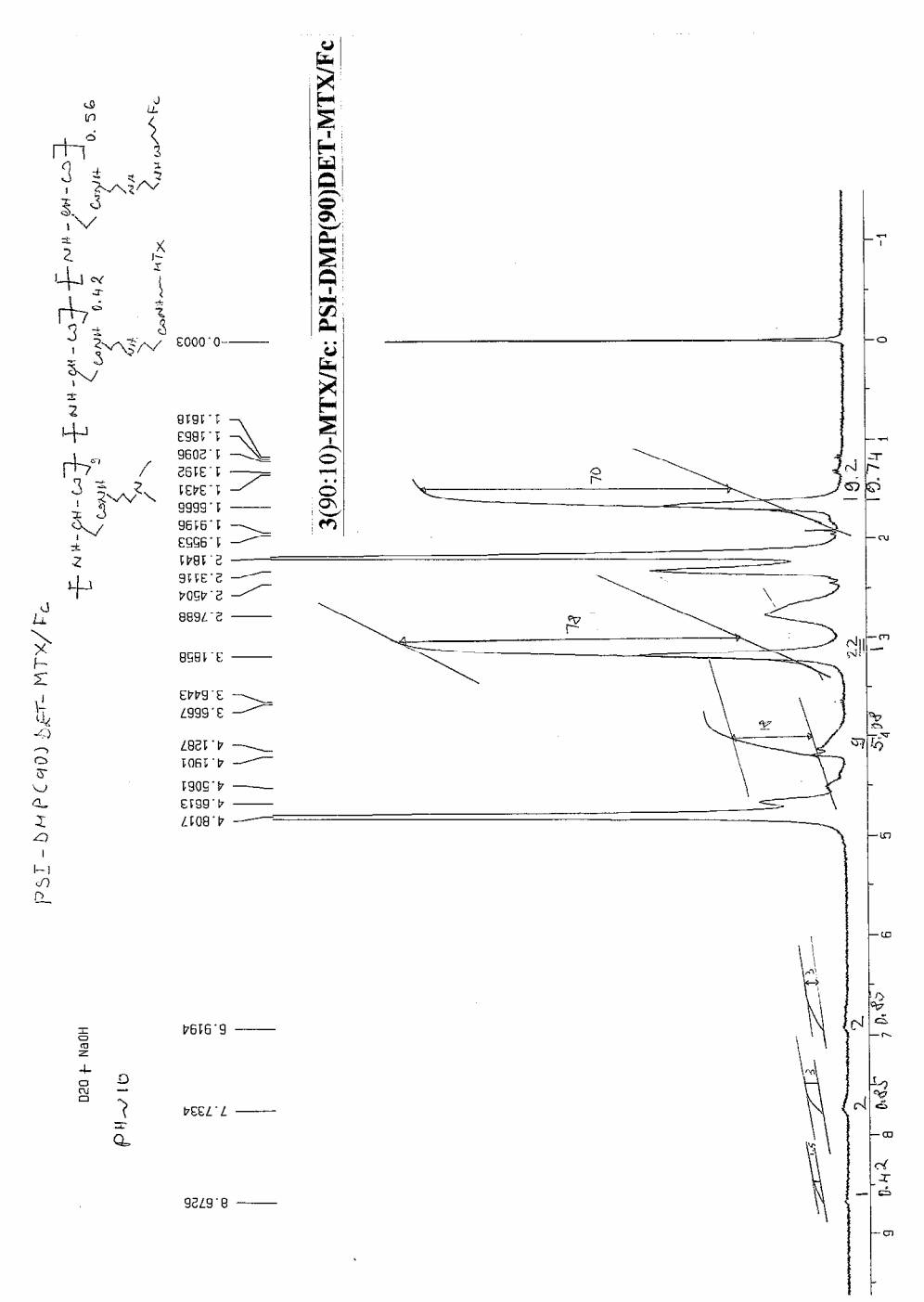

11-Fc(ONp): PSI-EA(90)PDA-Fc
David : DV 0-268 : D2O : + NaOH
PSI-EA(90)PDA-Fc
4.7660
4.7143
4.1750
3.7476
3.7239
3.6403
3.3410
3.1976
2.7962
2.3392
2.2655
1.8141
1.6991
-0.0004
ppm


14-Fc(ONp): PSI-AEE(90)PDA-Fc
PST - AEE (90) PDA - Fc
pH~7.5
: 03/05/04
4.77499
4.51167
4.17001
3.71597
3.62353
3.41124
3.33372
3.20650
3.01436
2.80422
2.34838
2.26181
1.91564
1.88395
1.71560
0.00012
DIP
54
9
12


19-Fc(ONp): PSI-MEA(90)PDA-Fc
David : DVD-266 : D2O + NaOH : 6/05/04
PH~ 10
4.8007
4.7012
4.1525
4.0693
3.5488
3.3639
3.2179
2.7807
2.5961
2.3399
1.9189
1.6475
1.6273


20-Fc(ONp): PSI-MEA(90)EDDA-Fc
David : DVD-267 : D2O + NaOH : 5/05/04
pH ~ 10
4.6709
4.0240
3.4177
3.2391
3.0954
2.6574
2.4879
1.7934
1.4982
ppm


1(90:10)-MTX/Fc: PSI-DMP(90)PDA-MTX/Fc
PST - DMP (90) PDA - MTX/Fc
D2O + NaOH : 26/01/04
pH ~ 10
7.7535
4.7952
4.1332
3.1885
2.7701
2.3134
2.1812
1.6886
1.3406
0.0003
0.55
0.83
0.83
0.63
30
75
12
22
21


3(90:10)-MTX/Fc: PSI-DMP(90)DET-MTX/Fc
PSI-DMP(90)DET-MTX/Fc
D2O + NaOH
pH ~ 10
8.6726
7.7334
6.9194
4.8017
4.6813
4.5061
4.1901
4.1287
3.6687
3.6443
3.1858
2.7688
2.4504
2.3116
2.1841
1.9553
1.9196
1.5666
1.3431
1.3192
1.2096
1.1863
1.1618
0.0003
0.42
0.56
19.2
20.74